Silicon and Neodymium Isotope Constraints on Biogeochemical Cycles and Water Mass Mixing in the Eastern Equatorial Pacific

Dissertation

Zur Erlangung des Doktorgrades

Dr. rer. nat.

der Mathematisch-Naturwissenschaftlichen Fakultät

der Christian-Albrechts Universität

vorgelegt von

Patricia Grasse

Kiel, 2012

Referent:	Prof. Martin Frank
Koreferent:	Prof. Anton Eisenhauer

Eingereicht am:	5.01.2012
Tag der mündlichen Prüfung:	8.02.2012

Zum Druck genemigt:

Gez. (Titel, Vor-und Zuname), Dekan

Erklärung

Hiermit versichere ich an Eides statt, dass ich diese Dissertation selbständig und nur mit Hilfe der angegebenen Quellen und Hilfsmittel erstellt habe. Ferner versichere ich, dass der Inhalt dieses Dokumentes weder in dieser, noch in veränderter Form einer weiteren Prüfungsbehörde vorliegt. Die Arbeit ist unter Einhaltung der Regeln guter wissenschaftlicher Praxis der Deutschen Forschungsgemeinschaft entstanden.

Kiel, den 5.01.2012

_____

-Dipl.-Biol. Patricia Grasse-

Contents

Abstract

Stable and radiogenic isotope systems are powerful tools to investigate biogeochemical processes, nutrient cycling and water mass mixing in the ocean. Here a comprehensive study of the stable isotopes of silicon (Si) and the radiogenic isotope composition of the Rare Earth Element (REE) neodymium (Nd) is presented for the Eastern Equatorial Pacific (EEP), where one of the globally largest Oxygen Minimum Zones (OMZs) is located. The two isotope systems are used to investigate biogeochemical cycling and water mass mixing processes, which are the key factors controlling the oxygen content and the extent of the OMZ. Silicic acid ($Si(OH)_4$), besides Nitrate (NO_3^-), is a main nutrient for diatoms, which are the dominant phytoplankton group in upwelling areas and therefore play a major role in controlling CO_2 exchange between the ocean and the atmosphere. Si isotopes in seawater are mainly influenced by uptake of silicic acid by diatoms, whereas the Nd isotopes are independent of biological fractionation and can be used as water mass tracer. A comprehensive data set for the dissolved Si and Nd isotope distribution, as well as concentrations in the Peruvian upwelling area were obtained on samples collected during Meteor cruises M77-3 and M77-4 between December 2008 and February 2009. The main goal was to characterize the Si and Nd isotope composition of water masses, in detail of the supply pathways of oxygen and to better understand the processes controlling biogeochemical cycling in the highly productivity upwelling region. These findings also contribute to a more reliable application of the two isotope systems as a proxy for past silicic acid utilization and water mass mixing in the EEP.

In a first step a detailed comparison between the dissolved Si isotope composition ($\delta^{30}Si(OH)_4$) in the water column along the Peruvian shelf and isotopic analyzes of biogenic silicate ($\delta^{30}Si_{bSiO2}$) and hand-picked diatoms ($\delta^{30}Si_{diatom}$) extracted from the underlying surface sediments was carried out. Under strong upwelling conditions surface waters were found only weakly fractionated in Si isotopes compared to the source waters of the coastal upwelling. Consistent with the $\delta^{30}Si(OH)_4$ distribution in the surface waters the

diatoms extracted from the sediment showed the lowest $\delta^{30}Si_{diatom}$ values in the main upwelling region.

Furthermore a direct comparison between the distribution of $\delta^{30}Si(OH)_4$ and the nitrogen (N) isotope composition of dissolved nitrate ($\delta^{15}NO_3^-$) was conducted to investigate the biogeochemical processes controlling nutrient cycling in the OMZ. During strong upwelling near the shelf, low $\delta^{30}Si(OH)_4$ signatures correspond to rather high $\delta^{15}NO_3^-$ because the source waters are influenced by dissolution of $bSiO_2$ and N-loss processes, which occur under suboxic conditions due to denitrification and/or anammox processes. During the time of sampling a large mesoscale eddy developed near the coast and moved through the study area, which had a major influence on the distribution of nutrients and their stable isotope compositions.

Besides, a characterization of deep water masses in the study area were conducted. Previous studies showed that different deep water masses show distinct Si isotope values. The data obtained in this study for water masses below 2000m show lower $\delta^{30}Si(OH)_4$ compared to the Central Pacific and higher values compared to the North Pacific. A comparison of the available data for the Pacific Ocean show no clear correlation between silicic acid concentrations or distinct water masses and $\delta^{30}Si(OH)_4$. Thus it is suggested that the distribution of distinct $\delta^{30}Si(OH)_4$ signatures in deep waters of the Pacific are a consequence of a combination of the relatively sluggish deep water circulation and remineralization processes.

In the last chapter the first full water column data set of dissolved Nd isotope compositions and Nd concentrations in the EEP is presented. Near surface zonal current bands, such as the Equatorial Undercurrent (EUC) and the Subsurface Countercurrent (SSCC), which supply oxygen-rich water to the OMZ are characterized by radiogenic Nd isotope signatures (ε_{Nd} = -2). Even though distinct water masses could be distinguished, the water masses show also clear evidence for non-conservative effects. Surface water masses show a trend towards more radiogenic values in the north coupled to higher Nd concentrations, which is most likely caused by particle exchange. Unexpectedly low Nd concentrations and radiogenic Nd isotope signatures in deep water

masses, indicates that particle scavenging, downward transport and release processes play also an important role.

Kurzfassung

Stabile und radiogene Isotopensysteme sind wichtige Werkzeuge zur Untersuchung biogeochemischer Prozesse, Nährstoffzyklen und Wassermassenmischung. Im folgenden wird eine umfangreiche Studie über das stabile Isotop Silizium (Si) und das radiogene Isotop Neodym (Nd) im östlich äquatorialem Pazifik vorgestellt, wo sich eine der weltweit größten Sauerstoffminimumzonen befindet. Biogeochemische Prozesse, Primärpoduktion und Wassermassenmischung sind wichtigen Faktoren, die den Sauerstoffgehalt und die Ausdehnung der Sauerstoffminimumzonen beeinflussen. Silikat ($Si(OH)_4$) ist neben Nitrate (NO_3^-) ein Hauptnährstoff für Diatomeen (Kieselalgen), welche die dominante Phytoplanktongruppe in Auftriebsgebieten sind und damit auch eine wichtige Rolle bei dem Austausch von CO_2 zwischen dem Ozean und der Atmosphäre spielen. Die Si Isotopensignaturen im Meerwasser sind hauptsächlich kontrolliert durch die Silikataufnahme von Diatomeen, wohingegen Nd Isotope nicht durch biologische Prozesse fraktioniert werden und zur Bestimmung der Herkunft von Wassermassen genutzt werden können. Ein umfangreicher Datensatz für gelöste Si und Nd Isotopen Messungen, wie auch für Konzentrationen wurde während der Meteor Ausfahrten M77-3 und M77-4 zwischen Dezember 2008 und Februar 2009 vor der Ecuadorianischen and Peruanischen Küste genommen. Das Hauptziel der Arbeit war die Charakterisierung der Wassermassen und im besonderen der Zulieferungswege für Sauerstoff. Ein weiteres Ziel war es ein besseres Verständnis über die biogeochemischen Prozesse zu erlangen, die die Isotopensignaturen beeinflussen. Die hierbei gewonnen Ergebnisses tragen auch für ein bessere Verständnis bei der Paläo-Rekonstruktion von Nährstoffnutzung und Wassermassenmischung bei.

Zunächst wurde ein detaillierter Vergleich zwischen gelösten Si Isotopen ($\delta^{30}Si(OH)_4$) in der Wassersäule und biogenem Silicat ($\delta^{30}Si_{bSiO2}$), beziehungsweise der Diatomeen Fraktion ($\delta^{30}Si_{diatom}$) aus dem darunter liegenden Sedimenten durchgeführt. Bereiche, die durch einen starken Auftrieb

gekennzeichnet waren, zeigten schwach fraktionierte Werte im Oberflächenwasser in Bezug zu der Quellsignatur. Die aus dem Sediment gewonnen Diatomeen spiegelten die Wasserdaten in sofern wider, dass die niedrigsten Werte ($\delta^{30}Si_{diatom}$) in den Bereichen des stärksten Auftriebs zu finden waren.

Des Weiteren wurde ein direkter Vergleich von Si Isotopen mit Nitrat (N) Isotopen ($\delta^{15}NO_3^-$) durchgeführt, um die biogeochemischen Prozesse zu untersuchen, die die Nährstoffkreislaufe kontrollieren. Bei starkem Auftrieb nahe der Küste waren die Wasseroberflächen durch niedrige $\delta^{30}Si(OH)_4$ Werte und relative hohe $\delta^{15}NO_3^-$ Werte charakterisiert. Gründe hierfür sind die partielle Auflösung von biogenem Silikat, wodurch Wassermassen mit einem niedrigerem $\delta^{30}Si(OH)_4$ an die Oberfläche gebracht werden, wohingegen Denitrifizierung und/oder Anammox Prozesse, die zum Verlust von Nitrat innerhalb der Sauerstoffminimumzone führen, höhere $\delta^{15}NO_3^-$ Werte hervorrufen. Ein großer Eddy, der sich zur Zeit der Probennahme von der Küste weg bewegte, hatte ebenfalls einen wichtigen Einfluss auf die Nährstoffverteilung und die entsprechenden stabilen Isotopensignaturen.

Außerdem wurde eine Charakterisierung der Si Isotopensignaturen im Tiefenwasser des Untersuchungsgebietes durchgeführt. Vorherige Studien hatten gezeigt, dass unterschiedliche Wassermassen durch distinkte Si Isotopensignaturen gekennzeichnet sind. Die in dieser Studie gewonnen Daten für Wassermassen unterhalb von 2000m zeigten niedrigere $\delta^{30}Si(OH)_4$ im Vergleich zu einer Studie aus dem Zentralen Pazifik und höhere Werte im Vergleich zum Nordpazifik. Der Vergleich der Daten zeigt keinen klaren Zusammenhang zwischen Silikatkonzentrationen oder unterschiedlichen Wassermassen und $\delta^{30}Si(OH)_4$, woraus sich schließen lässt, dass das Isotopensignal sowohl von einer trägen Mischung des Tiefenwassers als auch von Remineralisierungsprozessen beeinflusst ist.

Im letzten Kapitel präsentiere ich die ersten Daten für gelöste Nd Isotopensignaturen und Konzentrationen im Auftriebsgebiet vor Ecuador und Peru. Zonale Strömungsbänder, wie der “Equatorial Undercurrent“ oder der “Subsurface Countercurrent”, die Sauerstoff angereichertes Wasser zur

Sauerstoffminimumzone transportieren, konnten durch eindeutige Isotopensignaturen bestimmt werden (ε_{Nd} = -2). Obwohl anhand der Nd Isotopensignatur Wassermassen unterschieden werden können, zeigen die gewonnenen Daten auch den Einfluss nicht konservativer Effekte. Die Daten im Oberflächenwasser zeigen einen Trend zu radiogenen Werten im Norden, gekoppelt mit höheren Nd Konzentrationen, was mir großer Wahrscheinlichkeit durch Austausch mit Partikeln hervorgerufen wird. Überraschend niedrige Nd Konzentrationen und radiogene Nd Isotopensignaturen im Tiefenwasser ließen sich nicht durch reine Wassermassenmischung erklären. Grund hierfür könnten zum Beispiel „scavenging“ Prozesse sein, wobei das Nd an biogene Partikel gebunden wird.

Danksagung

Vor allem danke ich meinem Betreuer Martin Frank, der mir auch in den stressigsten Zeiten immer mit Rat und Tat zur Seite stand. Besonders in den Zeiten großer Frustration, wenn Messungen mal wieder nicht so funktioniert haben, wie sie sollten. Martin, du bist ein großartiger Betreuer, ich hätte sicherlich keinen besseren haben können.

Großer Dank geht auch an Claudia. Ich denke nur zusammen konnten wir es schaffen letztendlich doch noch vernünftige Daten für Silizium Isotope zu gewinnen. Außerdem hat das Zusammenarbeiten mit dir immer viel Spaß gemacht. Ich werde unsere gemeinsamen Silizium „Sessions“ sicherlich vermissen.

Lieber Torben und Roland, hättet ihr mir am Anfang nicht so viel im Labor gezeigt und mir jede meiner Fragen zu Neodym beantwortet hätte, würde ich wohl heute noch nicht wissen, was es mit diesen radiogenen Isotopen auf sich hat. Vor allem hätte ich ohne Roland nie soviel Wasser aus dem Pacific sammeln können. Unvergessen bleibt natürlich auch der ein oder andere Abend auf dem Glühweinmarkt mit euch.

Generell vielen Dank an die großartige Arbeitsgruppe von Martin (Clauschi, Steffi, Moritz, Ed, Anne, Tianyu, Fuqing, Mario, Nabil). Ich hoffe ich habe keinen vergessen! Man konnte sich immer auf euch verlassen und vor allem viel Spaß mit euch haben.

Besonderer Dank geht auch an Jutta, die immer für einen da war, einem all die Dinge besorgt hat, die man gerade so brauchte und mich in akuten Notfällen auch mit Koffein oder Keksen versorgte.

Dank auch an Greg de Souza und Ben Reynolds, die all unsere Fragen rund um Silizium beantwortet haben und jeden Missmut rund um dieses „schreckliche“ Element vollkommen verstehen konnten.

All die Probleme, die vor allem am Anfang immer wieder an der Nu aufgetreten sind, hätten wir wohl nie ohne Jan Fietzke lösen können. Sicherlich hätte ich ohne Jan auch nie soviel über die Nu gelernt.

Dank auch an die all die netten Menschen vom Westufer, die ich während der Meteorausfahrt kennen lernen durfte. Jassi, Leni, Nuño, Anna, Christian, Tobi, Harald, Tim, Sergio, Gaute und so vielen andere. Ihr habt mich immer wieder unglaublich zum Lachen gebracht. Besonders danke ich aber auch Harry und Tobi, ohne euch, die Pisco Sour und die NoXcuse hätte ich wohl oft nicht die Entspannung nach der Arbeit gefunden, die mir jeder Segelausflug mit euch beschert habt.

Ein großer Dank geht auch an all die anderen Freunde und auch meine Familie, die ich sicherlich gerade in dem letzten Jahr sehr vernachlässigt habe, immer mit der „Ausrede“, ich hätte zu viel bei der Arbeit zu tun. Ich versuche mich in Zukunft zu bessern.

Vor allem danke ich auch Brad, der vor allem in den letzten zwei Monaten meine zweitweise schlechten Launen aushalten musste und mich immer wieder aufgeheitert hat.

CHAPTER 1
Introduction

1.1 Motivation and Objectives

Isotopes are powerful tools to investigate biogeochemical processes, nutrient cycling and water mass mixing in the present and past ocean. In this study comprehensive investigations of the stable isotopes of silicon (Si) and the radiogenic isotope composition of neodymium (Nd) are presented from the Eastern Tropical Pacific (EEP) off the Ecuadorian and Peruvian coast, where one of the globally largest Oxygen Minimum Zones (OMZs) is located. The two isotope systems are used to investigate biochemical cycling and water mass mixing processes, which are the key factors controlling the oxygen content and the extent of the OMZ. So far only a few studies of dissolved Si isotopes and Nd isotopes are available from the Pacific Ocean and none from the upwelling area off Peru. The aim of this study was to characterize the Si and Nd isotope composition of water masses in the EEP and to better understand the biogeochemical processes, in particular those influencing the Si isotopes. The characterization of the isotope distribution in the water column should furthermore help to understand Si and Nd isotope data extracted from sediment cores, which can be used for the reconstruction of past water mass mixing and nutrient utilization.

This study was part of the SFB 754 (Climate – Biogeochemistry Interactions in the Tropical Ocean, www.sfb754.de) funded by the Deutsche Forschungsgemeinschaft. The aim of the SFB754 project is to understand the complex mechanisms controlling the OMZ in the present, as well as in the past in order to enable reliable predictions for the future. This study was conducted within subproject A5 “Water Mass structure in the Eastern Tropical Pacific: Relationship to Oxygen Variability and Geochemical Properties”.

The first chapter of this thesis will give an overview of previous work, will show the importance of OMZs, describe the water masses influencing the study area, and will give insights into biogeochemical cycling and primary productivity

in the area. Furthermore I will introduce the isotope systems used and their applications in marine systems.

1.2 Study area

1.2.1 Oxygen Minimum Zones

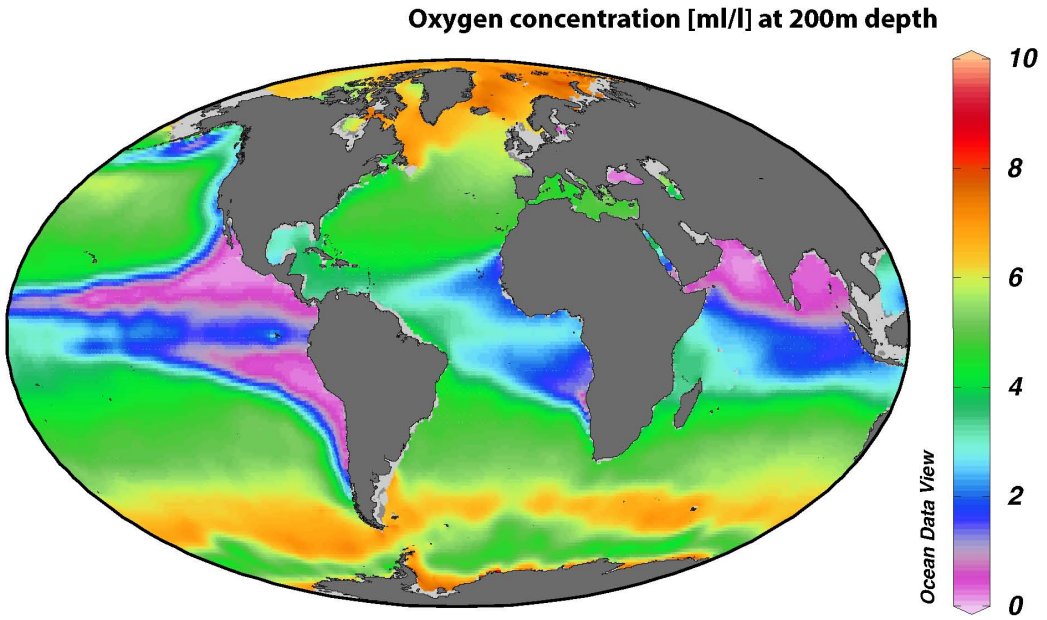

Fig.1.1: Oxygen concentration [ml/l] in the global ocean at 200m depth using the World Ocean Atlas 2009 (annual mean) created with ODV (Schlitzer, 2009).

Oxygen Minimum Zones are areas in the ocean where the oxygen concentrations are close to zero (Fig. 1.1). One of the globally largest OMZs is located at the South American coast off Equator, Peru and Chile. The extent of the OMZ ranges between 100m to 900m water depth with oxygen levels below 5 µmol/kg (suboxic) at a core depth between 300m and 500m (Karstensen et al., 2008). The oxygen content is mainly controlled by ventilation of water masses supplying oxygen and biogeochemical processes consuming the oxygen (Morales et al., 1999; Stramma et al., 2010) and has been sensitive to decadal and longer term climatic changes (Deutsch et al., 2011). Recently investigations have shown that the oxygen content of the global ocean is decreasing and OMZs are expanding (Stramma et al., 2008). This may lead to major shifts in nutrient cycling, e.g due to redox-dependent processes. A

decrease in oxygen concentrations in particular regions of the world and an increase of the extent of the OMZs may have a major impact on marine ecosystems (Vaquer-Sunyer and Duarte, 2008; Keeling et al., 2010). Furthermore most organisms are intolerant to anoxic conditions and an extension of OMZs could reduce their habitats (Stramma et al., 2011). Considering global warming and anthropogenic climate change which most likely will exert major influence on ocean circulation, it is of great importance to investigate low oxygen areas and the mechanisms controlling strength and extent of OMZs.

1.2.2 The global termohaline circulation and the water masses in the Eastern Equatorial Pacific

1.2.2.1 Global thermohaline circulation

The global thermohaline circulation (Fig. 1.2) also referred as “thermohaline conveyor belt” or “global conveyor belt” displays a simplified heat, density and wind driven circulation of water masses around the globe (Broecker,1991). Whereas deep water circulation is mainly driven by temperature and salinity, surface currents are mainly advected due to wind stress. Deep water formation occurs in polar regions by subduction of dense and cold surface water masses.

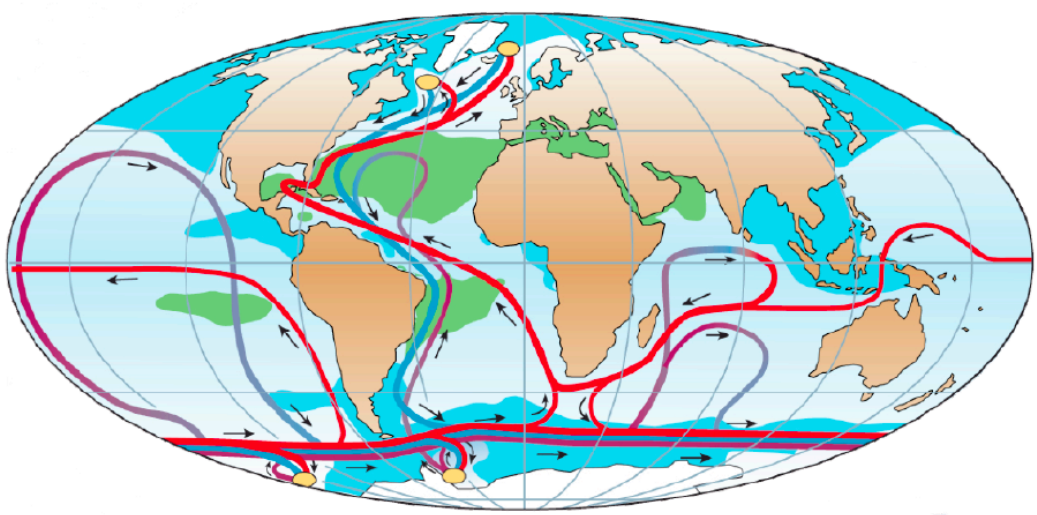

Fig. 1.2: Schematic map of the global thermohaline circulation with surface currents (red), deep water currents (blue) and bottom water currents (purple). Yellow circles in the polar regions indicate locations of deep water formation (adapted from Rahmstorf, 2002).

North Atlantic Deep Water (NADW) is formed by saline surface water that mainly originates from waters of the Caribbean warm-pool which are transported northward by the Gulf Stream system. The NADW flows southward along the South American Continent, where it is partly feeding the Antarctic Circumpolar Current (ACC) that is forming the Circumpolar Deep Water (CDW) and is flowing eastward around the Antarctic continent (e. g. Stramma and England, 1999). The CDW can be subdivided into Lower Circumpolar Deep Water (LCDW) and Upper Circumpolar Deep Water (UCDW) due to the inflow of NADW. Unlike the Atlantic Ocean, the Pacific Ocean has no high-latitude northern source of deep water and the densest water mass in the Pacific basin is LCDW (Wijffels et al., 1996). The LCDW transforms into North Pacific Deep Water (NPDW) by mixing with other water masses, which is again modified by admixture of UCDW near the Hawaiian Islands. From there NPDW broadly flows southward along the continental slope of Central and South America and contributes to the mixture of deep water masses off Peru (Wijffels et al., 1996; Kawabe and Fujio, 2010). Along this pathway the deep waters become enriched in major nutrients including silicic acid and nitrate (see also Fig. 1.10), which can also be used for the distinction of deep water masses such as NPDW and LCDW in addition to their temperature and salinity properties. Sea floor morphology divides the Pacific basin into several sub basins, which does essentially not allow the LCDW to reach the Peru Basin directly (Johnson and Toole, 1993; Kawabe and Fujio 2010).

1.2.2.2 Upwelling and water masses of the Eastern Equatorial Pacific

At the continental margins off Peru and Equator easterly trade and alongshore winds produce offshore Ekman transport of surface waters, which is replaced by upwelled nutrient-rich subsurface water. The main water mass supplying the Peruvian upwelling system is the southward flowing Peru-Chile Undercurrent (PCUC) (Figs. 1.3 & 1.4,), which prevails between 50m and 150m water depth (Brink et al., 1983, Huyer et al., 1987; Karstensen and Ulloa, 2008). This current is partly fed by the eastward flowing highly saline and oxygen-rich waters of the Equatorial Undercurrent (EUC, Lukas, 1986; Penven et al., 2005;

Kessler, 2006) and the Southern Subsurface Countercurrent (SSCC), both originating from the central Pacific (Brink et al., 1983; Toggweiler et al., 1991). The EUC originates at the Papua New Guinea slope, where it is derived from the New Guinea Coastal Undercurrent (Fig. 1.4, McGregor et al., 2008 and references therein). The offshore reach of the upwelling varies with latitude from 60km at 18°S to 270km at 4°S (Barber & Smith 1981). Chavez & Barber (1987) calculated a total upwelling area for the Peruvian margin of $1.82*10^{11}m^2$

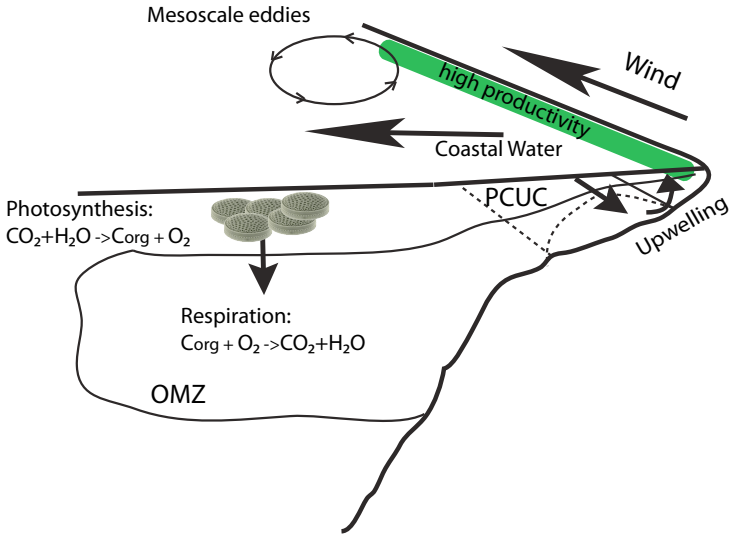

Fig. 1.3: Schematic view of the hydrography in the upwelling area off Peru. The extension of the OMZ is influenced by ventilation processes and the distribution and formation of organic matter (Corg), which is produced in the euphotic zone and is respired (remineralized) within the OMZ by bacteria under oxygen consumption. In addition, mesoscale eddies can influence the water mass distribution in the EEP.

The upwelling undergoes strong seasonal variations and is generally more intense in winter and also shows a large interannual variability due to the El Niño/ Southern Oscillation (ENSO, Brainard and McLain, 1987). The ENSO propagates via atmospheric or oceanic pathways into other areas of the world and can exert major influence on global climate and also has socioeconomic consequences (Karstensen and Ulloa 2008). During El Niño events less upwelling leads to a deepening of the thermocline, which is the reason for decreased nutrient supply and lower primary productivity.

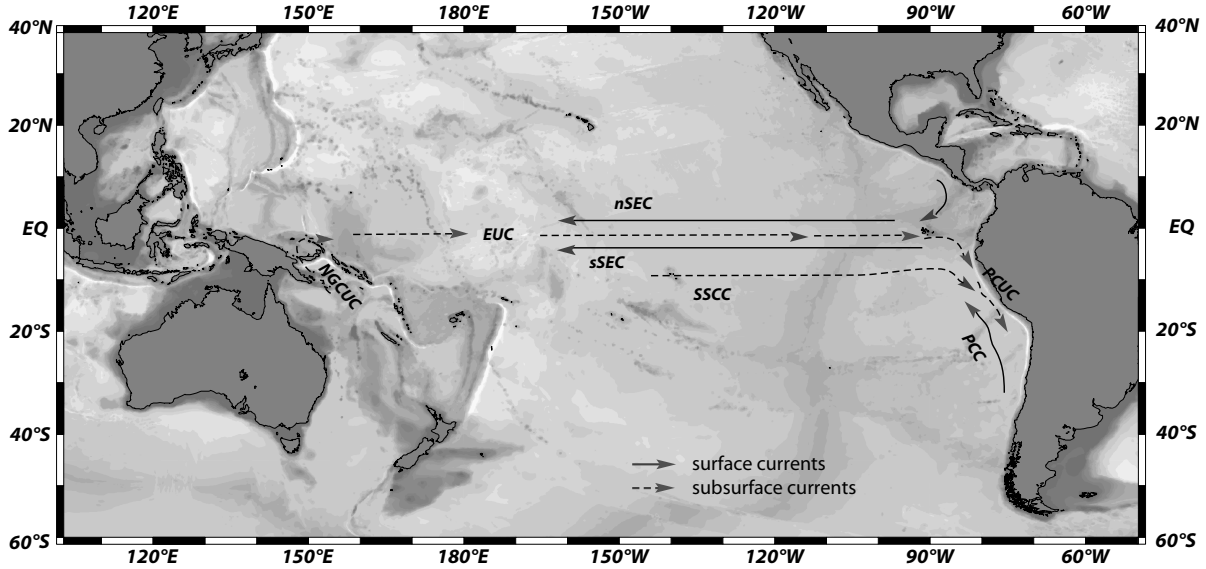

Fig. 1.4: Generalized circulation pathways of currents influencing the Eastern Equatorial Pacific (after Kessler, 2006; Penven et al, 2005, McGregor at al., 2008 and references therein). Surface currents (solid line): nSEC: northern South Equatorial Current, sSEC: southern South Equatorial Current, PCC: Peru-Chile Current (also called Humboldt Current), subsurface currents (dashed line): EUC Equatorial Undercurrent, SSCC: Southern Subsurface Countercurrent, PCUC Peru-Chile Undercurrent, NGCUC: New Guinea Coastal Current. A more detailed view of the surface and subsurface current system of the Eastern Equatorial Pacific can be found in Chapter 3.

The primary phytoplankton productivity off Peru, dominated by large diatoms and dinoflagellates can therefore be reduced by 50% during El Niño events (Chávez et al. 1989; Ocho et al., 1985; Rojas de Mendiola et al., 1985). In contrast La Niña events are characterized by very intense trade winds and therefore stronger upwelling (Carr et al., 2002 and references therein).

In addition, mesoscale eddies are a common feature in the upwelling areas (Leth and Middleton, 2004, Chaigenau et al. 2009) and can have a major influence on the distribution and dynamics of marine ecosystems (Ganachaud et al., 2011). On the one hand the eddies transport nutrients offshore and thus influence primary productivity, as well as pelagic fisheries further offshore (Hormazabal et al., 2004, Correa-Ramirez et al., 2007). On the other hand they can have a direct influence on thermocline depth and therefore on the nutrient supply to the euphotic zone (Fig. 1.5, Sarmiento and Gruber 2006; Ganachaud et al., 2011)

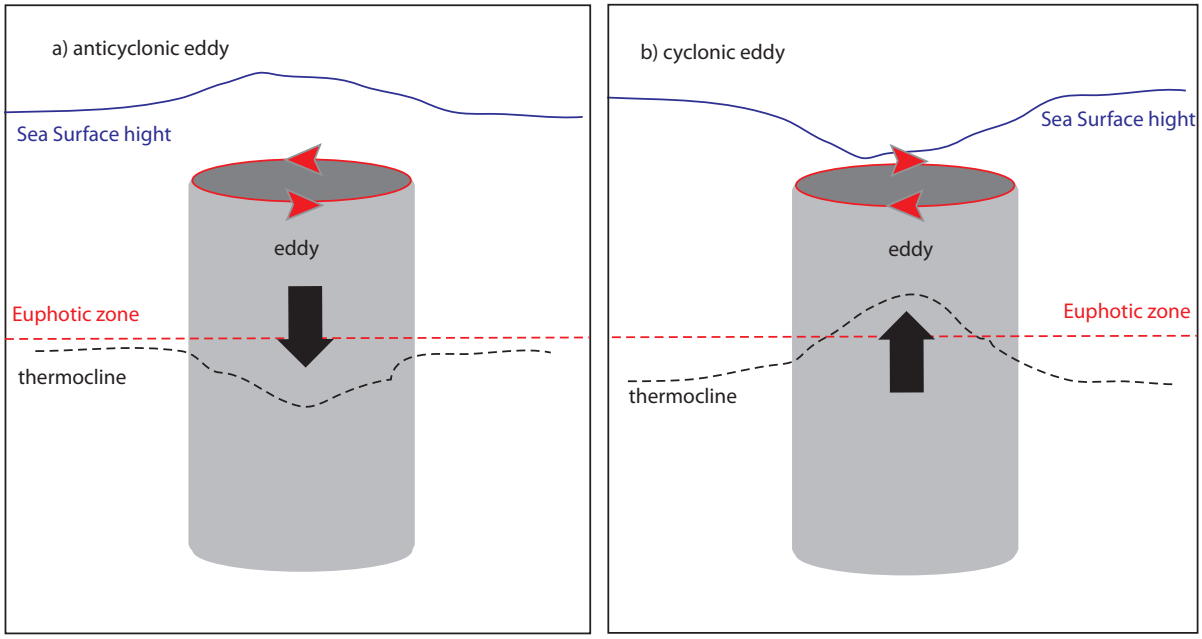

Fig. 1.5: Schematic picture of a) an anticyclonic eddy (counterclockwise) and b) a cyclonic eddy (clockwise) in the southern hemisphere showing the effects of the eddy structure on thermocline depth (dashed black line). A counterclockwise eddy pushes the thermocline downwards and the sea surface (solid blue line) is slightly raised within the eddy as it propagates westward. In contrast, a clockwise eddy raises the thermocline depth, which results in a higher nutrient availability in the euphotic zone (modified after Sarmiento and Gruber (2006) and Ganachaud et al. (2011). The dashed red line marks the boundary of the euphotic zone.

1.2.3 Primary productivity and nutrient cycling

The Peru upwelling is known as one of the most productive marine ecosystems of the global ocean (Barber and Smith, 1981; Carr, 2002) sustaining intensive pelagic fisheries (Alheit and Bernal, 1993; Bruland et al., 2005). The EEP accounts for up to 10% of the global oceanic primary production and the Peruvian upwelling is by far the richest coast in terms of chlorophyll concentrations (Pennington et al. 2006). Even though the high primary productivity in the EEP would suggest high carbon sequestration rates, these regions are considered a source for CO_2 and upwelling intensity is strongly linked to the amount of outgassing CO_2 (Friedrich et al., 2008). The organic matter (C_{org}) that is mainly produced by phytoplankton in the euphotic zone sinks into deeper waters where it is respired by bacteria under consumption of oxygen (Fig 1.3). The breakdown of organic matter and the remineralization of nutrients within the OMZ in turn stimulate primary productivity, in particular near the coast, when the nutrients are upwelled. The

main upwelling occurs between 10°S to 15°S, where major nutrients like silicic acid ($Si(OH)_4$), nitrate (NO_3^-) and phosphate (PO_4^{3-}) are never limited in surface waters near the coast (Fig. 1.6).

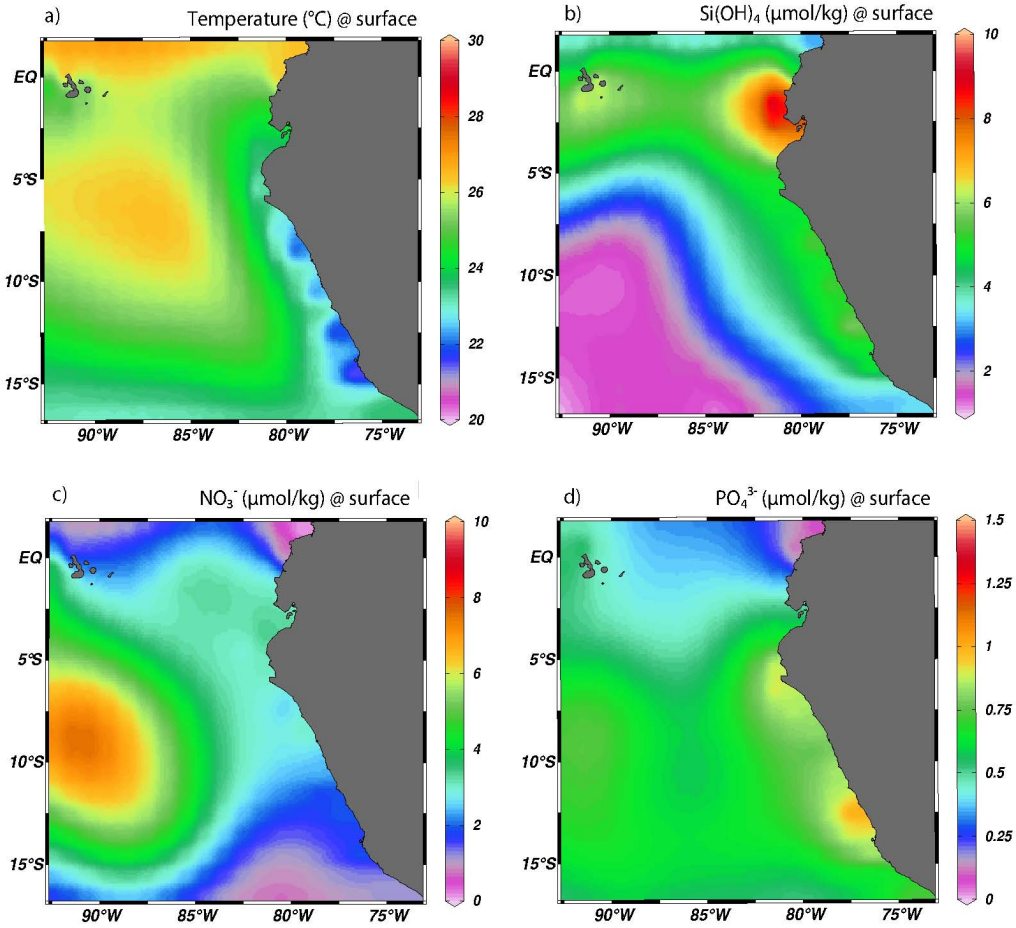

Fig. 1.6: Upwelling intensity off Ecuador and Peru is reflected by a) the sea surface temperature (°C) together with nutrient concentrations of b) silcic acid (µmol/kg), c) nitrate (µmol/kg) and d) phosphate (µmol/kg) in surface water. Plots were created with ODV (Schlitzer, 2009) using data from the World Ocean Atlas 2009

Within the OMZ, at oxygen concentrations below 5 µmol/kg nitrate concentrations are diminished due to N-loss processes, such as denitrification ($NO_3^-\rightarrow NO_2^-\rightarrow NO\rightarrow N_2O\rightarrow N_2$) and/or the more direct anammox process ($NH_4+NO_2^-\rightarrow N_2$) (Codispodi, 2007; Lam et al., 2009), which is the reason for nitrate limited surface waters south off 15°S.

The most dominant phytoplankton species in upwelling regions are diatoms (Smetacek, 1985, Estrada and Blasco, 1985; Abrantes et al., 2007), which require silicic acid to build their shells, also called valves or frustules

(Lewin, 1961). Diatoms, belonging to the Bacillariophyta group are so-called "bloomers" and dominate under eutrophic upwelling conditions (Quigg et al., 2003). Depending on climatic and oceanographic settings different diatoms assemblages prevail. Under equatorial upwelling conditions mainly *Chaetoceros* and *Thalassionema* dominate the phytoplankton regime, whereas *Thalassiosira* and *Azpetia nodulifera* are more prevalent when upwelling is weak such as during El Niño events (Abrantes et al., 2006). In warm High-Nutrient Low-Chlorophyll (HNLC) waters the microphytoplankton assemblage thus can be dominated by lightly silicified diatom species (Goméz et al., 2007). Other diatom taxa observed in the study area are *Nitzschia* spp, *Rhizosolena* spp, *Planktoniella* sol., *Skeletonema* (Marshall, 1970; Brodie and Kemp, 1994). Induced by stress, e.g. limited by light or $Si(OH)_4$, diatoms form so-called "resting spores" which are metabolically inactive and sink to the bottom (Fig. 1.7b). Triggered by more favorable growth conditions the resting spores can become active again and change to normal cell function (Round et al., 1990).

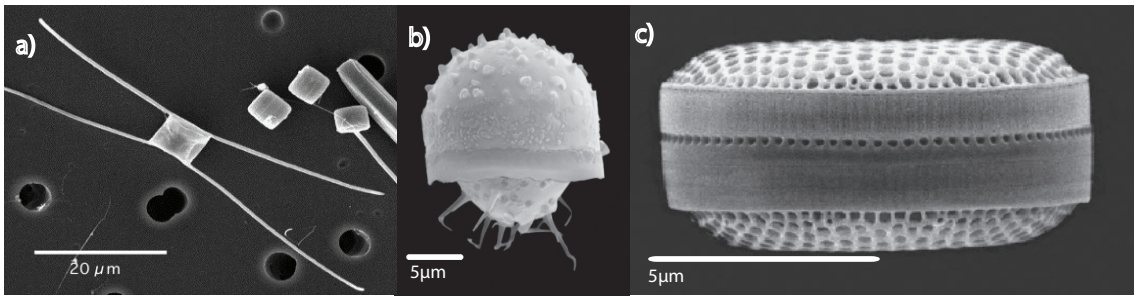

Fig. 1.7: REM modified images of a) Chaetoceros sp. b) a Chaetoceros sp. spore and Thalassiosira sp. (from Paul Harngraves, adapted from the Smithsonian Marine Station website (www.sms.si.edu/IRLSPEC/Phyl_Chryso1.htm)

1.2.3.1 The marine silicon cycle

The dissolved silicic acid concentrations of different water masses of the global ocean reflect a complex interaction between physical mixing and biogeochemical processes. $Si(OH)_4$ is mainly introduced to the ocean via riverine input, which accounts for approximately 5 Tmol Si yr^{-1}, whereas aeolian input, seafloor weathering and hydrothermal input together only account for 1.1 Tmol Si yr^{-1} (Tréguer et al., 1995). The utilization of silicic acid by phytoplankton,

mainly diatoms in the euphotic zone leads to a pronounced depletion in surface waters with concentrations normally less than 1µmol/kg. In general, the $Si(OH)_4$ concentrations in surface water are highest in the Southern Ocean, and the North and Eastern Pacific Ocean. The silicic acid concentrations in deep waters show a large gradient with low concentrations in the North Atlantic (~10µmol/kg) and high concentrations in the North Pacific (up to 170µmol/kg) roughly corresponding to the ages of water masses along the global thermohaline circulation (Fig. 1.2 and Fig. 1.8).

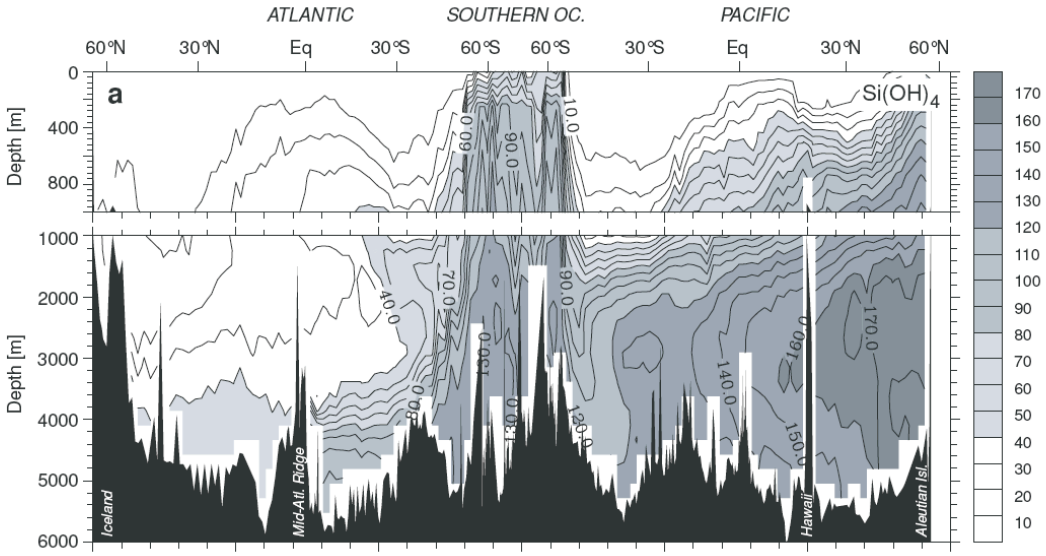

Fig. 1.8: Composite vertical section of dissolved silicic acid (µmol/kg) across the Pacific, Southern Ocean and the Atlantic (from Sarmiento and Gruber, 2006)

Approximately 50% of the biogenic silicate produced is already remineralized in the upper ocean (Demarest et al., 2011) and only 3% are ultimately buried on the ocean floor (Nelson et al., 1995). The dissolution of $bSiO_2$ is strongly influenced by physical parameters, such as temperature and pH (Lewin, 1961), but bacterial activity leads to higher dissolution rates (Bidle and Azam, 1999; Bidle et al., 2002). The high remineralization rate of $bSiO_2$ in the upper water column (Demarets et al., 2011) results in a relatively long average oceanic residence time for $Si(OH)_4$ of 15,000 years (Tréguer et al., 1995).

1.3 Applied Isotope Proxies

1.3.1. General

Isotopes are atoms of an element that have the same number of protons but differ in their number of neutrons, which leads to different masses. The differences in the masses of the isotopes result in different behavior during chemical and physical reactions and cause a mass-dependent fractionation, which means that the lighter, respectively the heavier isotope is preferentially released or incorporated during a reaction or process.

1.3.2 Stable Silicon Isotopes

Silicon has three stable isotopes with the atomic masses ^{28}Si, ^{29}Si and ^{30}Si, whereby ^{28}Si is the most abundant with 92.23% compared to ^{29}Si (4.67%) and ^{30}Si (3.1%) (Rosman and Taylor, 1998). Silicon isotope ratios are given in the delta notation, which is the deviation of the ^{30}Si/^{28}Si ratio in a measured sample from that of the standard reference material NBS28, expressed in parts per thousand:

$$\delta^{30}Si(‰) = \left(\frac{\left({}^{30}Si/{}^{28}Si \right)_{sample}}{\left({}^{30}Si/{}^{28}Si \right)_{NBS28}} - 1 \right) * 1000$$

whereas positive δ^{30}Si values show an enrichment in heavy silicon isotopes and negative values a depletion in heavy isotopes. In some publications the silicon isotope ratios are given as δ^{29}Si values, which corresponds to the deviation of the ^{29}Si/^{28}Si ratio in a measured sample from that of the standard reference material NBS28. The δ^{30}Si value can than be calculated from δ^{29}Si by multiplication with 1.93 because the fractionation of Si isotopes is strictly mass dependant (De La Rocha et al., 2002, Cardinal et al., 2005). The δ^{29}Si has been used to avoid interference problems with molecules such as ^{14}N^{16}O on mass 30 during mass spectrometry but these interferences are also excluded at mass resolutions above 2000.

Differences in the isotope ratio (R) between the product (P) and the substrate (S) are described by fractionation factor α, which is defined as

$$\alpha = R_P / R_S$$

Often the fractionation factor is also given as ε, the so-called “per mil enrichment factor”, which is defined as

$$\varepsilon \approx 1000 \ln \alpha \quad \text{or} \quad \varepsilon \approx (\alpha - 1) * 1000$$

if α is constant during a reaction the stable silicon isotope composition of the product is a linear function of ln(f) and the enrichment factor ε corresponds to the slope of the straight line which passes through the origin, respectively the source (Mariotti et al., 1981, see also the following description of the Raleigh type model).

To calculate the fractionation factor ε in a natural system two different models can describe the evolution of the $\delta^{30}Si$ composition of surface waters during biologically induced fractionation: a steady-state model, wherein a continuous supply of nutrients causes a dynamic equilibrium of the $Si(OH)_4$ content, and a Rayleigh-type model, in which no additional nutrients are newly supplied to the system (Mariotti et al., 1981, De La Rocha et al., 1997; Cardinal et al., 2005; Reynolds et al., 2006). The two models can be described and approximated by simple equations:

Steady-state system:

$$\delta^{30}Si_{Si(OH)_4\,obs} = \delta^{30}Si_{Si(OH)_4\,init} - \varepsilon * (1 - f)$$

$$f = Si(OH)_{4\,obs} / Si(OH)_{4\,init}$$

Rayleigh-type system:

$$\delta^{30}Si_{Si(OH)_4\,obs} = \delta^{30}Si_{Si(OH)_4\,init} + \varepsilon * (\ln f)$$

$$\delta^{30}Si_{diatom_{inst}} = \delta^{30}Si_{Si(OH)_4\,obs} + \varepsilon$$

$$\delta^{30}Si_{diatom_{acc}} = \delta^{30}Si_{Si(OH)_4\,init} - \varepsilon * (f \ln f / 1 - f)$$

where $\delta^{30}Si_{Si(OH)4\ init}$ is the Si isotope composition of $Si(OH)_4$ in the surface water before biological utilization starts to fractionate the Si isotopes, $\delta^{30}Si_{Si(OH)4\ obs}$ is the Si isotope composition measured in the surface water, *f* is the depletion factor describing the fraction of the initial $Si(OH)_4$ concentration that remains, ε is the fractionation factor between the $Si(OH)_4$ and the diatoms produced, $\delta^{30}Si_{diatom\ inst}$ is the Si isotope composition of the instantaneously produced diatoms at any time and $\delta^{30}Si_{diatom\ acc}$ is the silicon isotope

composition of the diatoms that accumulated and thus integrate the fractionation process over time. Both models assume a constant fractionation factor ε. The Si isotope fractionation factor ε for the formation of diatom silica from seawater assessed by culture experiments is -1.1‰ in $\delta^{30}Si$ (De La Rocha et al., 1997). The value of ε is given by the slope of the linear regression between $\delta^{30}Si_{Si(OH)4\ obs}$ and *f* for the steady-state model, and between $\delta^{30}Si_{Si(OH)4\ obs}$ and ln*f* for the Rayleigh-type system model (Fig. 1.9)

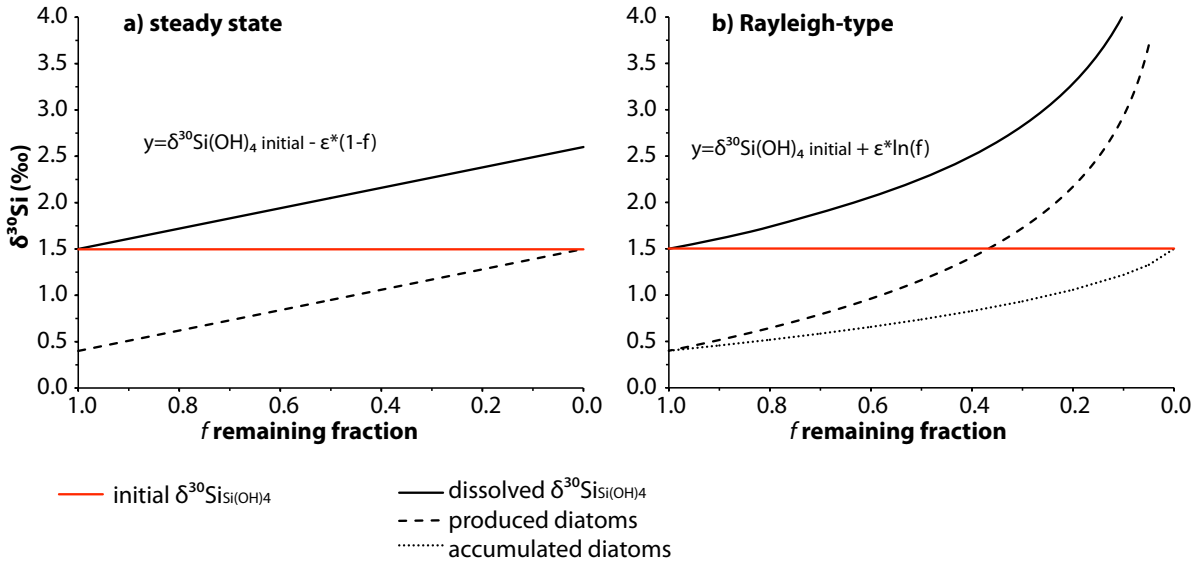

Fig.1.9: a) Steady State model for a) an open system(steady state) and b) a closed system (Raleigh-type model). Dissolved $Si(OH)_4$ (solid black line), produced bSi, respectively diatoms (dashed black line), accumulated diatoms (dotted black line) an the initial $\delta^{30}Si_{Si(OH)4}$ (solid red line). The remaining fraction f is calculated by the deviation of $Si(OH)_4$ in surface water from the $Si(OH)_4$ concentration in the source water. The regression lines derived from the two systems represent the fractionation factor ε and their intersection with the y-axis denotes the $\delta^{30}Si_{Si(OH)4}$ of the source.

1.3.2.1 Distribution of silicon isotopes in natural systems

The $\delta^{30}Si$ composition of terrestrial material, seawater and river water varies between -6‰ and +3.5‰, whereby clays and soils are characterized by the most negative $\delta^{30}Si$ values. The most positive $\delta^{30}Si$ values occur in marine and freshwater systems. The $\delta^{30}Si$ of organisms that utilize Si(OH)4, such as diatoms, radiolaria, sponges and silicoflagellates ranges between +3‰ and -3‰. The lightest $\delta^{30}Si$ of up to - 3‰ are observed in sponges and radiolaria, a unicellular phytoplankton group (Douthitt, 1982; De La Rocha, 2003; Wille et al., 2010), which show also a larger range in isotopic fractionation, dependent on

habitat depth and the surrounding silicic acid concentrations (Willet e al., 2010). The $\delta^{30}Si$ signature in diatoms ranges from +0.5‰ to +2‰ (De La Rocha et al., 2003; Cardinal et al., 2007).

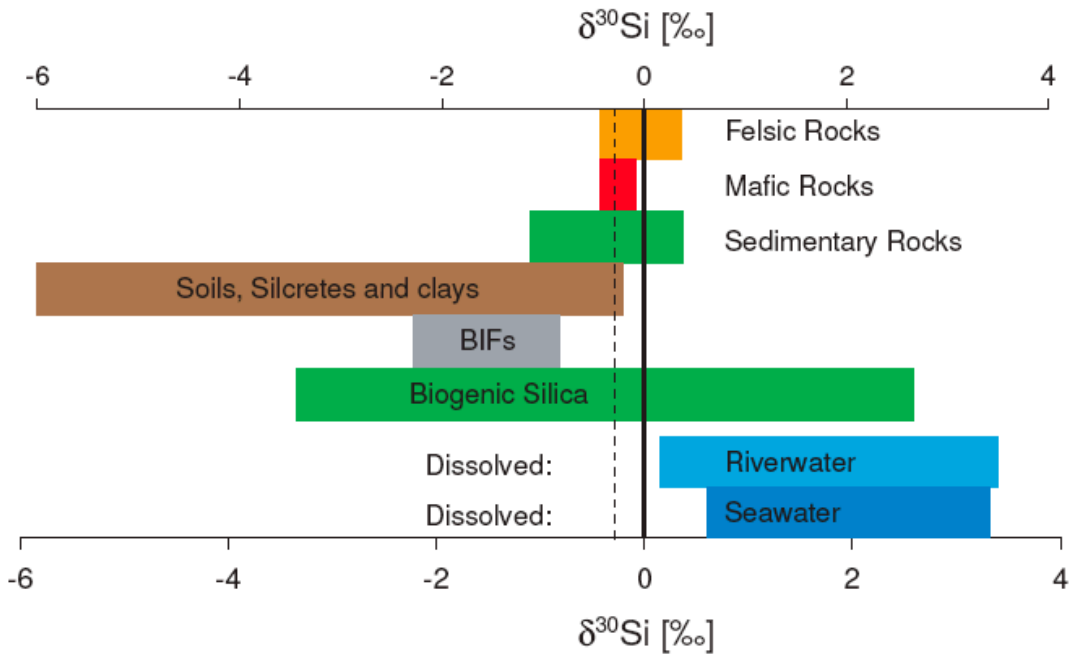

Fig.1.10: Variation of $\delta^{30}Si$ in different natural materials and solutions (from Reynolds, 2011). BIF: Banded iron formations. Biogenic silica represents diatoms, radiolaria, silicoflagellates, and sponges.

1.3.3 Neodymium Isotopes

The radiogenic isotope composition of the Rare Earth Element (REE) neodymium (Nd) is a powerful water mass tracer for the present and past ocean. Nd is produced by α-decay of Samarium (Sm) to Nd ($^{147}Sm \rightarrow {}^{143}Nd$) with a half-life time of 106 Gyrs. The radiogenic Nd isotope composition is generally expressed as

$$\varepsilon Nd = \left(\frac{\left({}^{143}Nd/{}^{144}Nd \right)_{sample}}{\left({}^{143}Nd/{}^{144}Nd \right)_{CHUR}} - 1 \right) * 10{,}000$$

with the Chondritic Uniform Reservoir (CHUR) having a $^{143}Nd/^{144}Nd=0.512638$ (Jacobsen and Wasserburg, 1980).

The Nd isotope composition of water masses is primarily controlled by the isotopic composition of the surrounding landmasses at their origin.

Weathering of young mantle-derived rocks surrounding the Pacific Ocean leads to more radiogenic values compared to the Atlantic Ocean with its margin predominantly composed of old continental crust (Fig. 1.11).

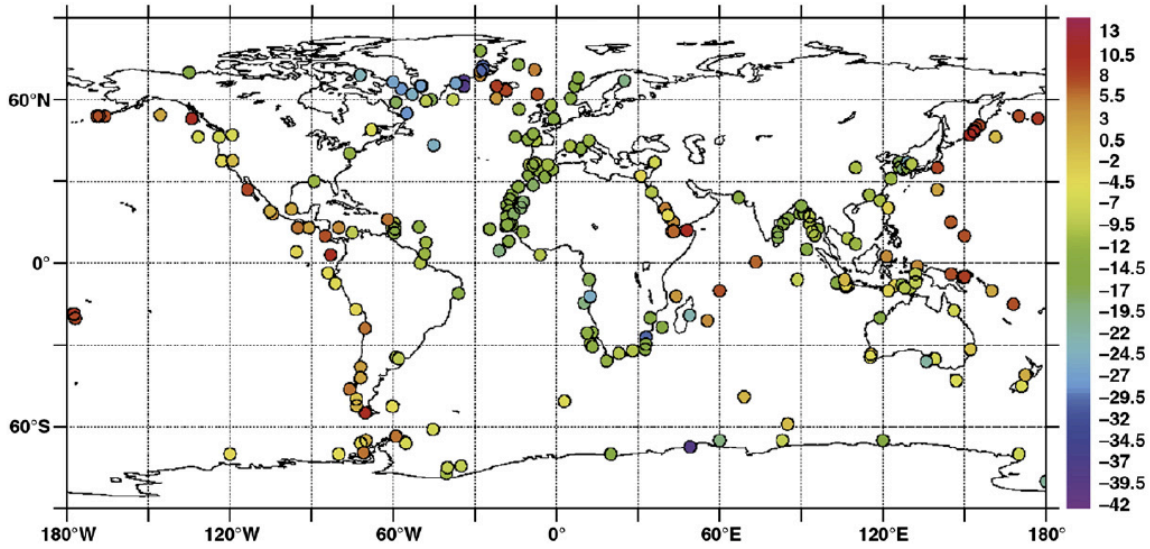

Fig.1.11: Nd isotope distribution in sediment core tops (Compilation study from Jeandel et al., 2007).

The exact input mechanisms and the influence of weathering processes on the Nd isotope composition and Nd concentration of seawater are not yet fully understood but it has become clear that besides eolian and riverine inputs (Goldstein et al., 1984; Goldstein & Jacobsen, 1988; Elderfield et al., 1989; Henry et al., 1994, Sholkovitz et al., 1999) also processes at the continent-seawater interface, so called “boundary exchange” must play an important role or may even dominate the inputs (Lacan & Jeandel, 2005; Arsouze et al., 2007, 2009). In contrast, the contribution of Nd to the ocean via hydrothermal inputs has been suggested to be negligible. In fact, hydrothermal vents rather have to be considered a sink of REEs in the global ocean budget together with particle scavenging processes (German et al., 1990; Klinkhammer et al., 1983; Halliday et al., 1992). The importance of particle scavenging and release processes is most notably documented by the nutrient-like vertical distribution of the concentrations of most REEs (e.g. Elderfield and Greaves, 1982). This phenomenon has been named the “Nd paradox” (Jeandel et al., 1995; Tachikawa et al., 1999; Siddall et al., 2008, which describes the decoupling of

the Nd isotope composition and the Nd concentrations. To better understand the processes influencing the isotope composition as well as the concentration gradients in the ocean, several modeling studies were conducted (Tachikawa et al., 2003; Arsouze et al., 2007, 2009; Jones et al., 2008; Siddall et al., 2008; Oka et al., 2009).

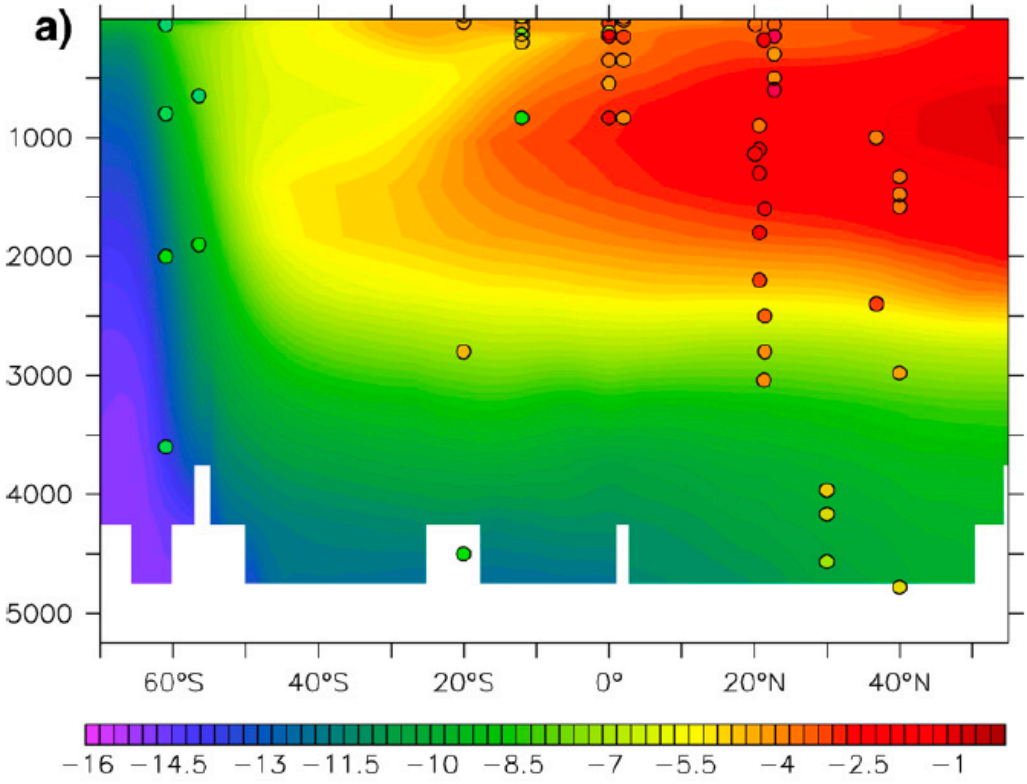

Fig. 1.12: Modeled ε_{Nd} distribution for a composite N-S Pacific section between 120°W and 160°W. Warm colours indicate radiogenic water masses from the north, cold colors indicate unradiogenic signatures originating in the south. Together with the modeled data, available ε_{Nd} measurements are plotted (dots, adapted from Arsouze et al., 2007)

Given that the factors influencing the Nd budget are not fully understood the global average residence time is also still under debate and estimations range between 390 and 1900 years (Piepgras at al., 1979; Jeandel et al., 1995; Frank, 2002; Tachikawa et al., 2003; Arsouze et al., 2007, 2009). This is in the range of the global ocean turnover time of about 1500 years (Broecker and Peng, 1982), which prevents complete homogenization of Nd isotope compositions and makes it possible to distinguish between different water masses. Numerous studies have demonstrated that particular water masses are clearly labeled Nd isotopes that can be followed across entire ocean basins. Thus water masses

from the northern Pacific and from the Southern Ocean are distinct in their Nd isotope compositions (Fig. 1.12).

1.4 Application of Si and Nd isotopes as paleo proxies in marine systems

De La Rocha (1997) showed that the fractionation between dissolved silicic acid in seawater and diatoms is -1.1‰, which is the basis for the use of silicon isotopes for reconstruction of past silicic acid utilization (De La Rocha et al., 1998; Reynolds et al., 2008; Pichevin et al., 2009; Brzezinski). However, the $\delta^{30}Si$ values recorded by the diatoms are not only controlled by $Si(OH)_4$ utilization but are also strongly influenced by surface water mass advection (Reynolds et al., 2006; Beucher et al., 2011), two processes that are difficult to disentangle in the paleo-record. Several studies demonstrated that Nd isotopes in paleo archives, such as ferromanganese (Fe-Mn) crusts, deep water corals, foraminifera, and fish teeth are powerful tools to reconstruct past ocean circulation (Frank et al. 2002; Vance et al. 2004; Martin and Scher, 2004; Van de Flierdt et al., 2010). The information on past changes in water mass advection and vertical mixing can be therefore gained from Nd isotopes. A combination of silicon isotopes, obtained from diatoms, respectively $bSiO_2$ from sediment cores and neodymium isotopes from foraminifera and Fe-Mn coatings can therefore be used to disentangle both processes. A study by Ehlert (2011) in the upwelling area off Peru was conducted to investigate the processes of silicic acid utilization and water mass mixing controlling the OMZ over the last 20,000years.

1.5 Previous work

1.5.1 Silicon isotopes

De La Rocha et al. (1997) showed that diatoms fractionate dissolved silicate in seawater during utilization in a way that they “preferentially” incorporate the lighter isotopes to build their frustules. Therefore, the isotopic signal in seawater and extracted from diatoms can be used to obtain information about the degree of utilization of the available silicic acid pool. A “first look at the stable isotope distribution in natural waters” was presented by De La Rocha (2000) and showed the range of silicon isotopes in different

marine and freshwater systems. Since then several studies were conducted to investigate the silicon isotope distribution in seawater and to understand the controlling processes including water mass mixing, utilization by diatoms and dissolution of biogenic silicate (Varela et al., 2004; Cardinal et al., 2005; Reynolds et al., 2006; Demarest et al., 2008; Beucher et al., 2008, Fripiat et al., 2011). So far only a few studies in the Pacific have been conducted. The two most important ones for the data obtained in this study were conducted in the North Pacific and in the Central Pacific. A study by Reynolds et al. (2006) in the north Pacific compared the Si isotope distribution in the Pacific oligotrophic subtropical gyre to the more eutrophic subantarctic gyre, whereas Beucher et al., (2008) characterized the water masses in the Central Pacific at 140°W. If $Si(OH)_4$ is limited as under oligotrophic conditions and the utilization of the available pool is high, the $\delta^{30}Si(OH)_4$ in surface waters are strongly fractionated (~3‰), whereas low utilization lead to less fractionated surface waters (~1.5‰). Furthermore these studies showed that the silicon isotope distribution in deep water masses of the Pacific can be distinguished in the way that North Pacific deep water show lower $\delta^{30}Si$ values (~0.7‰) compared to the Central Pacific (1.3‰). A larger data set of Si isotope distribution in deep water masses is therefore of interest to better understand the processes, like remineralization and water mass mixing influencing isotopic signal.

1.5.2. Neodymium isotopes

Previous studies have shown that neodymium isotopes are a powerful water mass tracer given that the Nd isotope composition of seawater reflects the isotopic fingerprint of its source and thus water masses can be clearly distinguished (see for example Frank, 2002). Most of the currently existing water column isotope and concentration data are available for the Atlantic Ocean (e.g. Piepgras and Wasserburg, 1983; Spivack and Wasserburg; 1988, Lacan and Jeandel, 2005, Rickli et al., 2008), whereas data for the Pacific are still scarce (Piepgras and Wasserburg, 1982; Piepgras and Jacobsen, 1988; Shimizu et al., 1994; Amakawa et al., 2000, 2004, 2009; Lacan & Jeandel, 2001; Vance et al., 2004). Most of the Pacific Ocean data were obtained in the

North Pacific (e.g. Amakawa et al., 2000, 2004, 2009) and the Central Pacific (e.g. Lacan and Jeandel, 2001). A study by Lacan and Jeandel (2001) at 140°W showed that the Equatorial Undercurrent, which is supplying oxygen-rich water to the OMZ of the Peruvian Upwelling is characterized by a distinct radiogenic Nd isotope signature (ε_{Nd}= -1.6). Additionally, water masses in the EEP are mainly influenced by water masses from the Northern Pacific (ε_{Nd}= -3 to ε_{Nd}= -5, Piepgras and Jacobsen, 1988; Amakawa et al., 2004; 2009) and water masses originating in the Southern Ocean (ε_{Nd}= -8 to ε_{Nd}= -9, Piepgras and Wasserburg, 1982; Stichel et al., 2011). Despite the fact that the Nd isotope compositions is a powerful water mass tracer, there is also clear evidence for non-conservative effects, which is shown by the nutrient-like distribution of Nd concentrations in the water column. This is the so-called Nd paradox and can be explained by scavenging and release processes influencing the Nd concentration. So far no data was obtained in highly productivity and therefore areas with high particle density like the Peruvian Upwelling.

1.6 Outline

The thesis is divided into 6 chapters. In the following chapter sample collection and the applied methods are explained in detail for Si and Nd isotope compositions, as well as the concentration measurements. The 3rd, 4th and 5th chapters deal with the Si isotope distribution in the Eastern Equatorial Pacific. In the 3rd chapter the dissolved $\delta^{30}Si(OH)_4$ in the water column and the underlying core top sediment data along the Ecuadorian and Peruvian shelf are discussed. This chapter represents a colaborative study with Claudia Ehlert who analyzed the silicon isotope composition of biogenic opal and the hand-picked diatom fraction, extracted from surface sediments. In the 4th chapter the dissolved Si isotope compositions measured on a 10°S transect perpendicular to the Peruvian coast are presented and compared to available nitrogen isotope data of dissolved nitrate provided by Evgenia Ryabenko. This chapter mainly investigated the upper 500m of the water column to better understand the biogeochemical cycling of silicic acid and nitrate. Subject of chapter 5 is the Si isotope distribution in deep water profiles further offshore and a comparison of

these data to available Si isotope data for the entire Pacific Ocean. Furthermore I analyzed the first water column Nd isotope data set for the Eastern Tropical Pacific in chapter 6, which represent the first available systematic data set for an upwelling system. Finally I provide a synthesis of the obtained data and will give an outlook for possible studies in the future.

Chapter 2

Methodology

2.1 Study area and sampling

The samples were collected during two cruises (M77/3 & 4) with the German research vessel RV Meteor between December 2008 and February 2009 in the frame of the Collaborative Research Centre (SFB) 754. All stations are located in the Eastern Equatorial Pacific between 2°N and 18°S off the Ecuadorian and Peruvian Coast (Fig. 2.1).

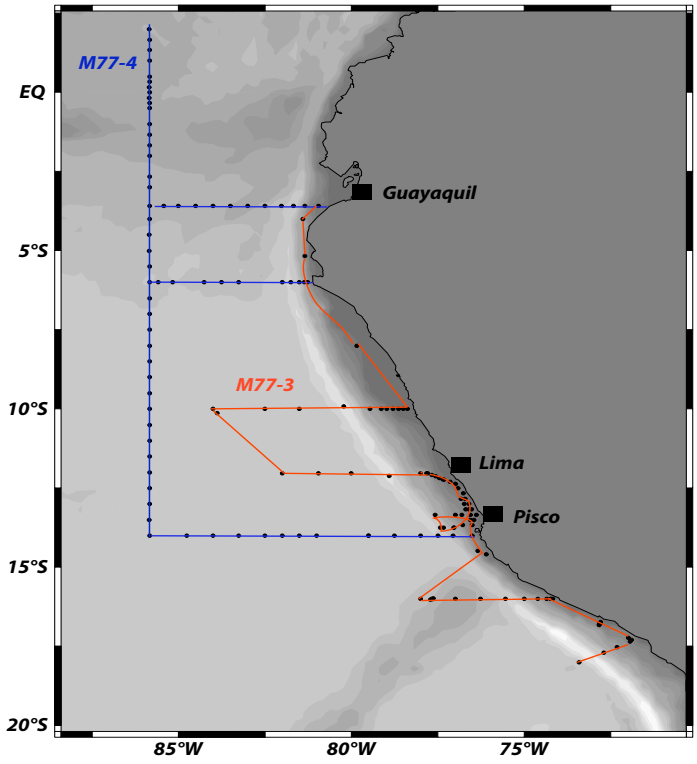

Fig. 2.1: CTD stations off Ecuador and Peru occupied during R/V Meteor cruises M77-3 (red line) & M77-4 (blue line) between December 2008 and February 2009.

.

All water samples for silicon (Si) and neodymium (Nd) isotopes, as well as for concentration measurements were collected using a rosette with 24 Niskin bottles (10L each), which was equipped with a SeaBird CTD (conductivity, temperature, depth/pressure) system and supplemented by an additional oxygen sensor.

Samples for nutrient analyzes (silicate, phosphate, nitrate, nitrite and ammonium) were taken for each station and water depth. During cruise M77/3 the samples were frozen (-20°C) onboard immediately after sampling. The nutrient measurements were carried out afterwards at the Max-Planck Institute (MPI) for Marine Microbiology in Bremen, Germany. $Si(OH)_4$ concentrations of frozen samples were compared to silicate concentrations of selected filtered and acidified (non-frozen) seawater samples taken at the same stations and water depths. The reproducibility between both approaches was within 5 to 10% (no systematic variations). The nutrient samples of cruise M77/4 were measured onboard. All nutrient concentrations were determined photometrically following (Grasshoff et al., 1999) with an analytical uncertainty of approximately 4.5%. Oxygen concentrations were measured with the CTD sensor and were afterwards calibrated to oxygen concentration analyses obtained by onboard Winkler titrations (Winkler, 1888). Particulate biogenic silicate concentrations were measured onboard, as well as at IFM-GEOMAR in Kiel by Jasmin Franz. For these analyses the biogenic silica, mainly consisting of diatom frustules, was sampled by filtration through cellulose acetate filters (0.65 µm pore size; 25 mm diameter) at low vacuum pressure (< 200 mbar) onboard and stored frozen at -20°C until further treatment. For analysis, the sample filters were immersed each with 25 ml NaOH (0.1 M) in Nalgene® bottles at 85°C in a shaking water bath for 2h 15 min. After cooling of the immersed samples, analysis was conducted according to the method for determination of inorganic silicate by Hansen & Koroleff (1999).

2.2. Silicon isotopes

2.2.1 Preconcentration of Si from seawater

For determination of the dissolved silicon isotope composition 500 to 2000 ml of seawater were sampled from the Niskin bottles. Samples were immediately filtered through nitro-cellulose acetate filters (Millipore®, 0.45 µm) to avoid further uptake of silicic acid by phytoplankton in the sample container. The filters were dried at 40°C and stored. In a next step the samples were acidified to pH 2 with concentrated subboiled HCl (1 mL HCl per liter of

seawater). The sample volume required for isotope measurements ranges from 5 to 300 ml depending on the concentration of silicic acid. A much larger volume of seawater was sampled to allow replicate measurements.

Tab. 2.1: Reagents used for measurements of silicon isotopes and silicic acid concentrations.

Chemical	Grade	Usage
Milli-Q water (MQ)	*>18MΩ (Co. Millipore)*	*Chromatography, sample dilution*
HCl	*32%, subboiled*	*Chromatography, acidification*
HNO_3	*65%, subboiled*	*Chromatography, acidification*
NaOH	*liquid, suprapure grade*	*brucite-coprecipitation*
NaOH	*pellets, p.a.*	*Standard fusion*
Ammonium heptamolybdate	*solid, p.a*	*$Si(OH)_4$ concentration measurements*
Ascorbic acid	*solid, p.a*	*$Si(OH)_4$ concentration measurements*
Oxalic acid	*solid, p.a*	*$Si(OH)_4$ concentration measurements*
H_2SO_4	*4.5M, p.a*	*$Si(OH)_4$ concentration measurements*
Si standard	*Merck® Titrisol (36 mmol/l)*	*Si calibration curve*

In the clean laboratory of IFM-GEOMAR silicon was preconcentrated using a brucite-coprecipitation method modified from Reynolds et al. (2006), which follows the so-called MAGIC method by Karl and Tien (1992) for the preconcentration of phosphate from seawater. Thereby Si is adsorbed onto the surface of brucite ($Mg(OH)_2$) and already separated from most of the remaining seawater matrix elements. A successful coprecipitation requires in total two full days. In a first step the acidified sample is neutralized with 1M NaOH (semiconductor grade, Sigma Aldrich®) by adding approximately 11% of the seawater volume (110 µl 1M NaOH per 10ml of seawater, 1.1 v/v % 1M NaOH). The samples have to be acidified at least 24h before the coprecipitation starts. After adjusting the sample to an alkaline pH 9 to 10 a milky-white brucite precipitate is formed, wherein approximately 10% of the total Mg content of the seawater samples precipitates. The samples were then shaken for 1 hour and left over night. On the next day the samples were centrifuged for 15 minutes at 2500 rpm (Heraeus Megafuge 1.0) and a second precipitation step was conducted by adding 1.1 v/v % 1M NaOH (Fig. 2.2) and again leaving the

samples over night. On the following day a subsample of 500µl was taken from the supernatant and the $Si(OH)_4$ concentration was measured. The recovery was carefully checked after the second precipitation step and only samples with more than 97% yield were used for isotopic measurements. After successful precipitation the supernatant was discarded and the precipitate containing the $Si(OH)_4$ was dissolved in 6M HCl. The sample solution was then diluted to a concentration of 35 to 70µmol/kg (1 to 2 ppm) and was ready for ion exchange chromatrography.

A 2-step brucite-coprecipitation was performed to separate all $Si(OH)_4$ from the seawater, given that incomplete precipitation would lead to fractionation of the silicon isotopes in the sample. Depending on the silicic acid concentration of the sample 5 to 300mL of seawater was precipitated. Water samples with concentrations below 10µmol/L $Si(OH)_4$ were preconcentrated through additional precipitation steps, applying the brucite-coprecipitation described above, means the 2-step precipitation was performed twice in total four times. After the second precipitation step, the milky-white precipitate was redissolved in HCl and then the additional 2-step precipitation was conducted. This minimized the amount of precipitated magnesium in the sample, as only 10% of the redissolved magnesium is again precipitated in the following step. To minimize the added volume of chemicals, we used concentrated HCl as well as concentrated NaOH (see also Reynolds et al., 2006).

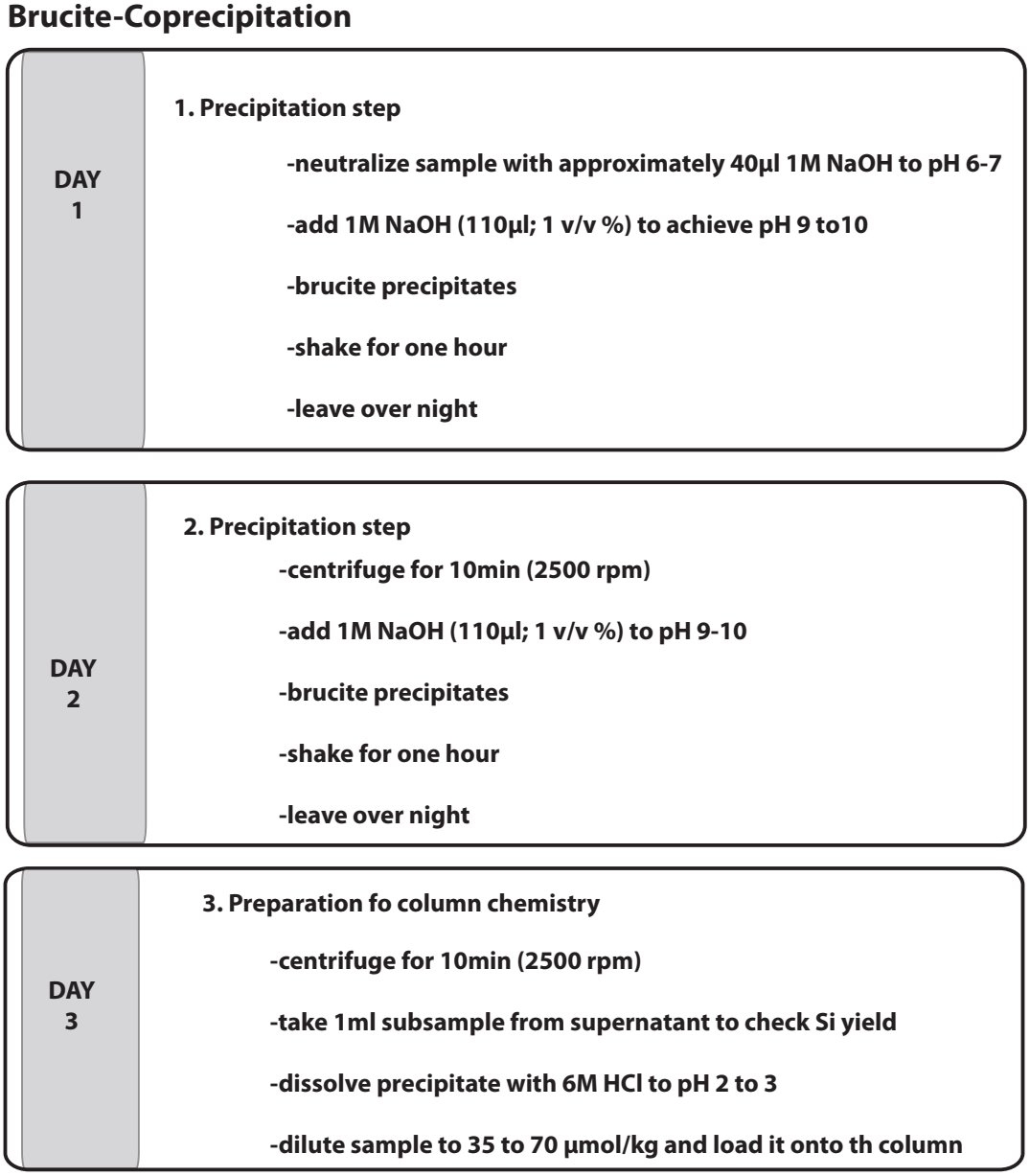

Fig. 2.2: Steps for brucite coprecipitation of silicon from an acidified 10ml seawater sample (pH 2). The sample has to be acidified at least 24h before the precipitation starts.

2.2.2 Ion exchange chromatography for separation and purification of Si

Immediately after the last precipitation step the sample (1ml) was loaded on a column containing 1ml AG50W-X8 resin (Biorad®, 200-400 mesh) according to a modified method by Georg et al. (2006). This is different to the method by Georg et al. (2006) who used an AG50W-X12 resin (Biorad®, 200-400 mesh) for Si separation and shortens the required time for chromatography by about 25% (pers. communication G. de Souza, ETH Zurich). The column

chemistry starts with cleaning of the resin with 6M HCl, respectively 3M HCl and conditioning with concentrated HNO_3. In the next step the cation exchange columns were rinsed at least three times with MQ water. The pH was carefully checked because the acidified Si sample in its uncharged orthosilicic acid ($H_4Si(OH)_4$) form has to be loaded onto a neutral column (pH 6-7). The silicon was collected directly and was completely eluted from the columns and diluted with MQ. Si isotope measurements on the *NuPlasma* MC-ICPMS were performed on the same day as the column chemistry. The used cation exchange resin was discarded after every sample because a complete cleaning of the resin is difficult. For a detailed description of the column chemistry see Tab. 2.2. Applying this method, it is not possible to separate matrix anions like Cl^- and SO_4^{2-} from the purified Si sample solution, but this does not seems to have any significant effect on the reproducibility and accuracy of the measurements (De Souza, 2011).

$Si(OH)_4$ concentrations were controlled before, during and after column chemistry. For this purpose 500µl of a subsample were diluted with 2500µl MQ and 200µl of a Ammonioheptamolybdate solution were added, shaken and after 30 min 200 µl oxalic acid and subsequently 200µl ascorbic acid were added. After 30 minutes, the absorption of the sample was measured photometrically at 810 nm. Samples with $Si(OH)_4$ concentrations below 1ppm were measured undiluted.

Tab.2.2: Ion exchange chromatography for silicon isotopes (1ml Biorad® AG50W-X8).

Step	Volume (ml)	acid	comment
Cleaning	*2*	*3M HCl*	
Cleaning	*2*	*6M HCl*	
Conditioning	*0.1*	*conc. HNO3*	
Cleaning	*2*	*3M HCl*	
Cleaning	*2*	*6M HCl*	
Cleaning	*2*	*3M HCl*	
Cleaning	*2*	*6M HCl*	
Cleaning	*2*	*3M HCl*	
Rinsing	*2*	*3 x MQ*	*to pH 6 (neutral)*
Loading	*1*	*sample (pH 2-3)*	*collect sample*
Wash out sample	*1*	*MQ*	*collect sample*

2.2.3 Silicon isotope measurements on the *NuPlasma* MC-ICPMS

The silicon isotope compositions were measured on a *NuPlasma* MC-ICPMS (Nu instruments) at IFM-GEOMAR in Kiel. The sample and standard solutions were introduced into the plasma via a Cetac Aridus II desolvator equipped with a PFA nebulizer with an uptake rate of 60 to 80 µL/min (Tab. 2.3).

Tab.2.3: Instrument setup for the MC-ICP-MS (Nu instruments).

Parameter	*Nu plasma* MC-ICP-MS
RF power	1300 W
1st acceleration potential	4 kV
torch	semi-demountable sapphire torch or glass torch
Sampler cone	common Ni cone
Skimmer cone	common Ni cone
Coolant flow rate (Ar)	13 l/min
Auxiliary flow rate (Ar)	1 to 1.1 l/min
Nebulizer	PFA
Nebulizer Uptake rate	60 to 80µl/min
Mass-resolution	> 2500
Cup configuration	H6 (^{30}Si), Ax (^{29}Si), L5 (^{28}Si)
Desolvator	Cetac Aridus II
Entrance slit	medium (pseudo-high resolution) position

Measurements were carried out using a standard-sample-standard bracketing method (Albarède et al., 2004) and each sample was measured three to five times within one run. Each measurement was integrated over 3 blocks of 10 cycles each. Because the silicon isotope measurement applying the standard-sample-standard bracketing method is time consuming, which can lead to effects of variations of the stability of the instrument it was attempted to reduce integration time, as well as the duration of the wash cycles as much as possible. On the silicon masses 28, 29, and 30 a constant instrument/desolvator blank, as well as a measurable blank originating from the HNO_3 and MQ prevailed during the measurements. The blanks were thus monitored during the measurements and should not be higher than 1% of the sample intensity. Normally the blank intensity ranged between 0.03V and 0.07V on mass 28

during the sessions depending on the instrument's sensitivity, whereas isotope measurements were performed at 3V to 6V on mass 28. A blank measurement (MQ) was conducted before each isotope measurement and then subtracted from the intensity of the sample (OnPeakZero method). Sample and standard solutions were adjusted to the same concentration within a possible 10% error of the voltages. This is important because differences in concentrations can lead to slightly different fractionation within the plasma given that it has to be assumed that the standard is fractionated in the same way as the sample. In addition, the correction for molecular interferences cannot be achieved at differences in concentrations between sample and standards.

The silicon isotope measurements are potentially biased by different mass interferences derived from molecular reactions of the sample carrier solution within the plasma. Possible molecular interferences are $^{14}N_2$ and $^{12}C^{16}O^+$ on ^{28}Si, $^{15/14}N_2$ on ^{29}Si, and $^{14}N^{16}O^+$, $^{15}N_2$ on ^{30}Si. These interferences need to be minimized by adjusting the mass resolution of the mass spectrometer to higher values. This is achieved with a narrower opening of the entrance slit (pseudo high resolution mode) and the α-slits. While the entrance slit separating is adjusted mechanically, the α-slits are adjusted electronically between 0 and 0.7mm using a "muscle wire" (Fig 2.3). The collector slits were not used. As a complete separation of the interference masses is not possible with the used *NuPlasma* MC-ICPMS, the Si measurements were integrated at the lower mass end of the peak plateau (Fig. 2.4).

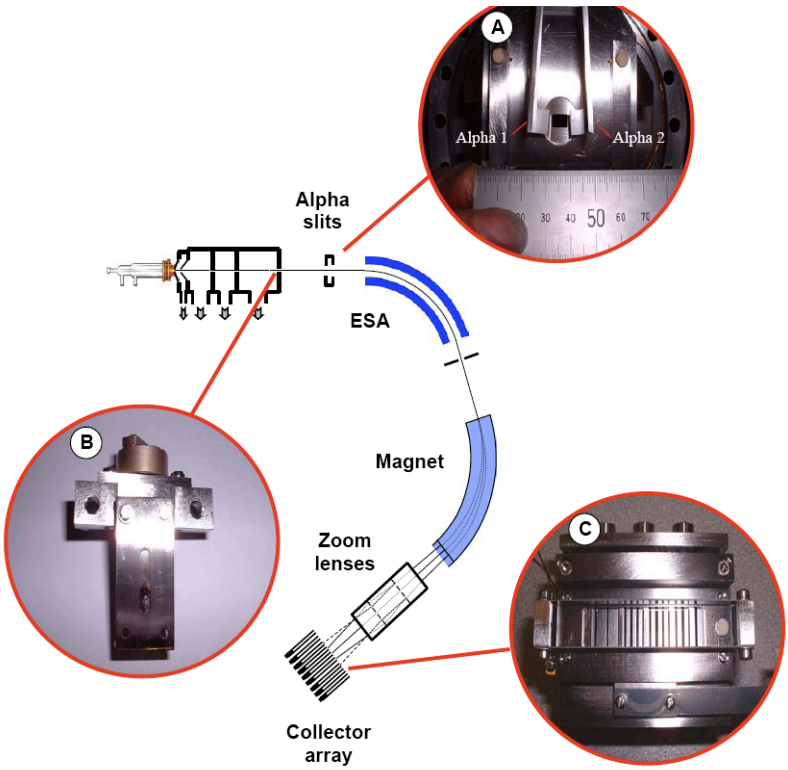

Fig. 2.3: *A) Alpha B) Source, and C) Collector slit photographs and their respective location on a Nu Plasma HR instrument. Adaptd from the NuInstrument ltd. manual.*

Prior to each session the peak resolution was newly defined. The mass resolution (R), which is a measure for the ability to distinguish between two slightly different masses, can be calculated as follows (VanLear and McLafferty, 1969, Vanhaeke and Moens, 2004)

$$R_{95\%} = \frac{M}{\Delta M}$$

where M is the mass (e.g. 28) and ΔM (also called resolving power) is the difference between the mass at 95% of the peak height and 5% of the peak height (Fig. 2.4) . High R-values indicate a better separation of peaks. The mass resolution for silicon isotope measurements has to be at least 2500 (van den Boorn et al., 2006), but mainly values between 3000 and 4000 were reached.

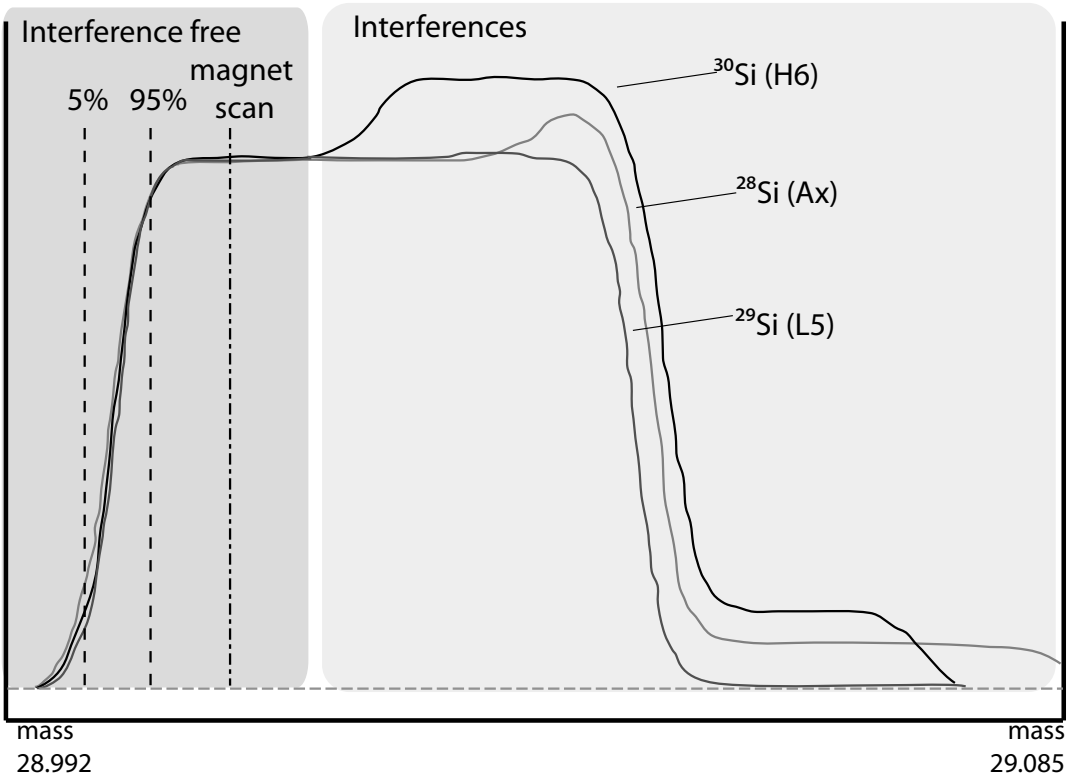

Fig. 2.4: Mass scan during silicon isotope measurement (H6 = ^{30}Si; Ax = ^{29}Si ; L5 = ^{28}Si) showing the separation of the interferences towards the high mass end of the peak. The area shaded in dark grey is the peak area that is almost completely free of interferences, whereas the area shaded in light grey shows the influence by molecular interferences. The dotted line marks the mass (magnet scan), where the measurements are integrated. To define the resolving power the peak intensity at 5% and at 95% of the peak height is required (dashed lined).

2.2.4 Preparation of standards - fusion method

Most of the standards used during the measurements were prepared in Kiel using a NaOH fusion method (after Georg et al., 2006). 10 to 20 mg of the powdered silicate standard were added to 200 mg solid NaOH pellets in a silver crucible. The powder and the NaOH pellets were then put into a furnace and molten at 730°C for exactly 8 min. Subsequently the content of the crucible was diluted in several steps to a volume of approximately 1 Liter. Such high dilution is necessary to keep the sodium concentration as low as possible because otherwise the cation exchange resin would subsequently not be able to adsorb all the sodium. The standard solution was acidified with concentrated HNO_3 to pH 2 to pH 3. The $Si(OH)_4$ concentrations for the standards ranged between 7

to 10ppm. Standards can be stored like this for several years. Thus far no change in the silicon isotopic composition has been detected after 2 years.

2.2.5 Reproducibility of standard and sample measurements

For silicon isotope measurements no certified standard is available. Intercalibration studies (Reynolds et al., 2006; 2007) between different working groups were conducted to obtain reliable data for the main silicon isotope standards (Table 2.4). Long-term measurements of the reference materials IRMM 18, Big Batch and Diatomite in the laboratory of IFM-GEOMAR gave average $\delta^{30}Si$ values of -1.53 ± 0.30‰ ($2\sigma_{sd}$, n = 25), -10.80 ± 0.23‰ ($2\sigma_{sd}$, n=25) respectively, +1.27± 0.29‰ (n=10). For calculation of these values we used the mean isotope standard value obtained at 25, respectively 10 measurement sessions. These values are in good agreement with those obtained by Reynolds et al. (2006; 2007, Tab. 2.4).

Tab. 2.4: Silicon isotope standards with values adapted from an intercalibration study by Reynolds et al. (2006).

Standard	Description	$\delta^{30}Si$ (‰)
NBS 28	*SiO_2*	
IRMM 18	*SiO_2*	*-1.65*
Big Batch	*high fractionated SiO_2*	*-10.48*
Puratronic	*Si (IV) oxide powder*	*-0.51*
Diatomite	*marine biogenic opal*	*+1.26*

The relation between $\delta^{30}Si$ and $\delta^{29}Si$ of the standards follow a mass-dependent fractionation slope of 0.50 close to the expected kinetic isotope fractionation of Si and the value obtained by Reynolds et al. (2006) of 0.51 (Fig. 2.5).

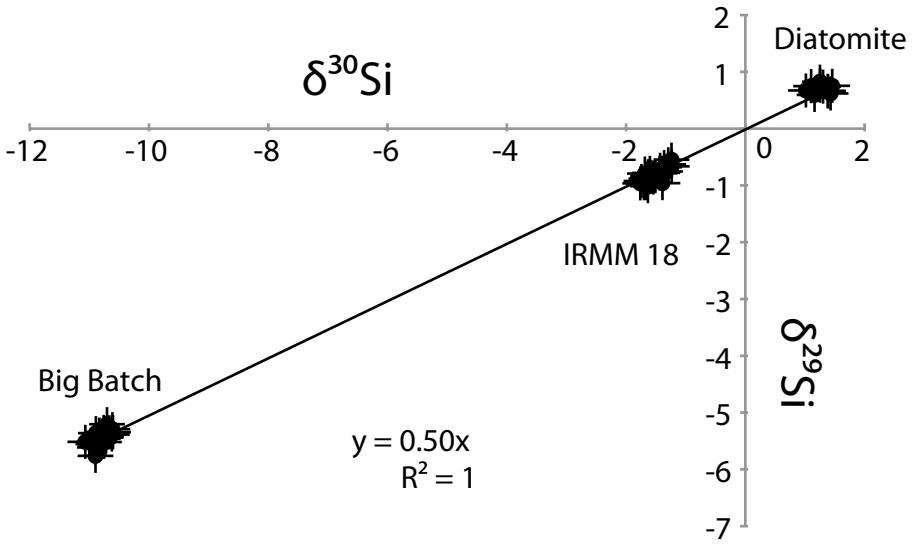

Fig. 2.5: $\delta^{30}Si/\delta^{29}Si$ (in ‰) cross plot for the standards BigBatch, IRMM 18 and Diatomite following a mass-dependent fractionation slope of 0.50, close to the kinetic fractionation value for Si isotopes (0.5092), see also Reynolds et al. (2006).

Replicate measurements of an in-house seawater standard gave a reproducibility of 0.25‰ ($2\sigma_{sd}$, n=12). Samples within the sample-bracketing measurements, which were measured three to five times resulted in an external error of 0.04‰ to outliers of 0.8‰, mostly ranging around 0.2 to 0.3‰. The external error during the sample bracketing method was mainly dependent on the stability of the machine. Repeated measurements of samples on different days mostly resulted in an external reproducibility of 0.01‰ to 0.6‰ (Fig. 2.6), whereas most of the samples show a reproducibility better than 0.3‰.

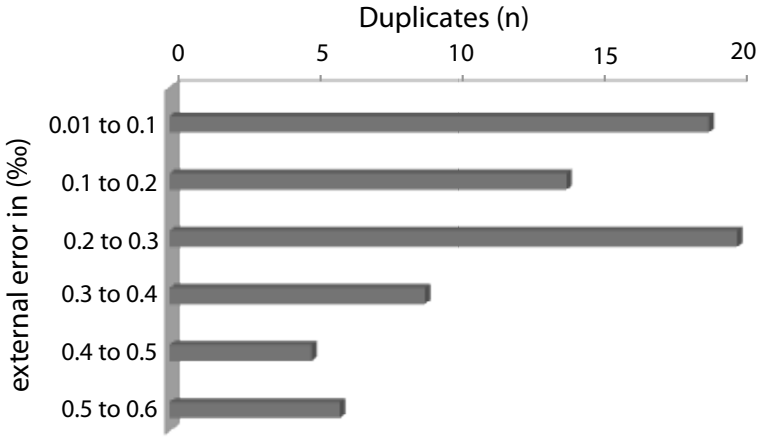

Fig. 2.6: Range of the external reproducibility of duplicate $\delta^{30}Si$ measurements (n) on different days. Most of the duplicate measurements result in an external reproducibility of 0.1‰ to 0.3‰.

Given that the standard material of NBS28 is currently not available, a secondary standard was applied for the sample-standard bracketing method during the silicon isotope measurements. Here IRMM 18 was used, which has been well calibrated against the NBS28. The value that was used to convert from the $\delta^{30}Si$ value normalized to IRMM18 to NBS28 is 1.001637.

2.3 Neodymium Isotopes

2.3.1 Preparation of seawater samples for isotope measurements

For Nd isotope analysis 20L of seawater were collected in previously acid cleaned LDPE cubitainers. The samples were filtered through 0.45µm nitrocellulose acetate filters (Millipore®) within 2 hours after sampling. From each filtered sample an aliquot of 2L was separated for Nd concentration measurements. All samples were acidified to pH 2 with concentrated subboiled hydrochloric acid (0.5ml per Liter). The samples for concentration measurements experienced no further treatment onboard and were stored in previously cleaned PE wide mouth bottles. Already onboard an iron co-precipitation method was applied to the large volume samples for Nd isotope composition analyses to reduce sample size. For this purpose 500µl Iron(III)Chloride solution (~1g Fe(III)Cl/ml in 3M HCl) were added to each acidified 18L sample and after one day of equilibration the samples were adjusted to pH 8 with ammonia (25%, suprapure grade) to co-precipitate the dissolved REEs with the iron hydroxide. After one or two days the supernatant was decanted and the residual FeOOH precipitate was transferred into an acid cleaned 2L PE wide mouth bottle. The samples were then stored for up to several months for further treatment at the home laboratory.

In the laboratory of IFM-GEOMAR the precipitate was then centrifuged in 50ml vials at 2500 rpm for approximately 20min and the supernatant was discarded. This was repeated several times until all seawater was separated from the precipitates. Subsequently the sample was at least rinsed twice with de-ionized water (18.2MΩ) to make sure that major ions such as Na^+ and Cl^- were washed out. The precipitate was re-dissolved in 6M HCl and transferred into 60ml Teflon vials. In several steps the remaining organic compounds in the sample were

destroyed. Therefore 4ml of aqua regia (3:1 mixture of HCl to HNO_3) were assed to the sample and left for at least 24 hour in a closed vial on a hot plate (110°C). Subsequently the sample were dried and re-dissolved in several steps by adding 2ml of 3M and 6M HCl to convert it back into a Cl- form. Finally the sample was dissolved in 2ml 6M HCl prior to Iron separation. To separate the iron from the samples cleaned di-ethyl ether was used. 2ml of the ether were added to each sample and mixed. After separation into the two phases the upper phase, which contained the ether together with the iron was discarded. This step was repeated in total three times until the solution became pale yellow. To separate as much iron as possible is essential to avoid overloading the following cation exchange columns (see also Stichel et al., 2011). After separation of the iron the samples were dried down to make sure that no ether remained and were then dissolved in 1M HCl. REE separation from major element cations and barium was performed using a cation exchange resin (Biorad® AG50W-X12 resin, 200-400 mesh-size, 0.8mL resin bed). The Nd was further purified and separated from the other REEs in a second column chemistry step (Eichrom® Ln Spec, 50-100 mesh-size, 2mL resin bed). The applied column chemistry (Tab. 2.5 & 2.6) followed the methods of Barrat et al. (1996) and Le Fèvre and Pin (2005). In a final step the samples were oxidized by adding 200 µl of a 1:1 mixture of 0.5M HNO_3 and H_2O_2 (30 wt.%) to remove remaining organic components. Before each isotope measurement the concentrations of Nd were checked on the *NuPlasma* MC-ICPMS. Thereby also the content of barium was monitored because many of the samples collected in the upwelling area of Peru showed relatively high barium content.. If the barium content in the sample exceeded 1V the second column chemistry step was repeated to avoid matrix effects in the instrument's plasma.

Tab.2.5: REE collection (AG50W-X12 resin, 200-400 mesh-size, 0.8ml resin bed).

step	volume	chemical
pre-clean	*8 ml*	*6 M HCl*
pre-conditioning	*0.5 ml*	*1 M HCl*
pre-conditioning	*1 ml*	*1 M HCl*
load sample	*0.5 ml*	*1 M HCl*
wash-in	*3 x 0.6 ml*	*1 M HCl*
elute matrix	*0.6 ml*	*3 M HCl*
discard Sr	*5 ml*	*MQ*
change acid	*5 ml*	*2.5 M HNO_3*
elute Ba	*2 x 1ml*	*6 M HNO_3*
collect REE	*9 ml*	*6 M HNO_3*
clean	*6 ml*	*6 M HNO_3*
change acid	*2 x 1ml*	*MQ*
store	*1 ml*	*1 M HCl*

Tab. 2.6: Nd separation (Ln Spec, 50-100 mesh-size, 2ml resin bed).

step	volume	chemical
pre-clean	*8 ml*	*6 M HCl*
pre-conditioning	*0.5 ml*	*0.1 M HCl*
pre-conditioning	*1 ml*	*0.1 M HCl*
load sample	*0.5 ml*	*0.1 M HCl*
wash-in/elute Ba	*0.5 ml*	*0.1 M HCl*
elute LREE	*8 ml*	*0.25 M HCl*
collect Nd	*5 ml*	*0.25 M HNO_3*
clean	*8 ml*	*6 M HNO_3*
pass & store	*1 +1 ml*	*0.3 M HCl*

2.3.2 Neodymium isotope measurements by MC-ICPMS and TIMS

Nd isotope compositions were measured by Multi Collector Inductively Coupled Plasma Mass Spectrometry (MC-ICPMS; *Nu instruments*) or Thermal Ionization Mass Spectrometry (TIMS TRITON; *Thermo Scientific)*. At the beginning of the study the MC-ICPMS was not yet available and therefore measurements were conducted on the TIMS TRITON. As most of the samples collected in the study area showed low Nd concentrations (~5 to 10ng), measurements on the TIMS were difficult or even not possible with the

established methods at the IFM-GEOMAR. For that reason most of the samples were later on measured on the by MC-ICPMS Measured $^{143}Nd/^{144}Nd$ ratios were corrected for instrumental mass bias using $^{146}Nd/^{144}Nd=0.7219$ and an exponential mass fractionation law. All $^{143}Nd/^{144}Nd$ ratios of this study were normalized to the accepted value of the JNdi-1 standard of 0.512115 (Tanaka et al., 2000).

For measurement on the *NuPlasma* MC-ICPMS the purified and dried Nd samples were dissolved in 5% HNO_3 and were measured with an autosampler in automatic mode. Samples containing less than 10ng of Nd were measured on the MC-ICPMS using a manual time resolved mode. Therefore the samples were diluted with 5% HNO_3 to 250µl to 500µl and measured at concentrations ranging from 20 to 30ppb. The integration time for Nd measurement was approximately 2 to 5min.

Table.2. 8: Cup configuration for Nd isotope measurements on the NuPlasma MC-ICPMS.

cup	H6	H5	H4	H3	H2	H1	Ax	L1	L2	L3	L4
mass	-	^{150}Nd	^{148}Nd	^{147}Sm	^{146}Nd	^{145}Nd	^{144}Nd	^{143}Nd	^{142}Nd	^{140}Ce	^{138}Ba
interference mass	-	^{150}Sm	^{148}Sm				^{144}Sm		^{142}Ce		^{138}Ce

For measurements on the TRITON TIMS the dried Nd samples were dissolved in 5µl 1M HCl/0.35 H_3PO_4 and loaded onto a rhenium filament. Samples were measured with a double filament heating method and a beam intensity of 0.5V.

Table. 2.9: Cup configuration for Nd isotope measurements on the Thermo Scientific TRITON TIMS.

cup	H6	H5	H4	H3	H2	H1	C	L1	L2	L3	L4
Mass	-			^{150}Nd	^{147}Sm	^{146}Nd	^{145}Nd	^{144}Nd	^{143}Nd	^{142}Ce	
Interference mass	-			^{150}Sm				^{144}Sm		^{142}Ce	

External reproducibility ($2\sigma_{sd}$) of the Nd isotope measurements ranged between 0.1 ε_{Nd} and 0.8 ε_{Nd} depending on the applied method and sample concentrations. Low concentration measurements, especially in the time

resolved mode showed higher external errors. Duplicate measurements of samples and standards on the MC-ICPMS and on the TIMS resulted in identical isotope compositions within external $2\sigma_{sd}$ reproducibility.

2.3.3 Preparation of seawater samples for concentration measurements (Isotope dilution)

For Nd concentration measurements, 500mL of filtered and acidified seawater were used. The concentrations were determined using an isotope dilution (ID) method (Heuman, 1992 and references therein). A defined amount of a $^{150}Nd/^{144}Nd$ spike artificially enriched in ^{150}Nd was added according to the assumed concentrations and was left for equilibration for one week. The REEs were then separated from disturbing elements following the same method as for the isotope measurements but only using one cation exchange column (Biorad® AG50W-X12 resin, 200-400 mesh-size, 0.8mL resin bed). After column chemistry the samples were oxidized by adding 200 µl of a 1:1 mixture of 0.5M HNO_3 and H_2O_2 (30 wt.%) to reduce disturbing matrix effect of organic compounds during the measurement. The concentration measurements were performed on a *Nu plasma* MC-ICPMS. For several samples replicates were processed. The external reproducibility of the Nd concentration measurements was approximately 2% (1σ). Blank values for isotope and concentration measurements ranged between 1% and 3% of the total sample concentrations and were considered as negligible.

Table. 9: Cup configuration for Nd spike measurements on the Nu plasma MC-ICPMS.

cup	H6	H5	H4	H3	H2	H1	Ax	L1	L2	L3	L4	L5
mass	^{154}Sm	^{152}Sm	^{150}Nd	^{149}Sm	^{148}Nd	^{147}Sm	^{146}Nd	^{145}Nd	^{144}Nd	^{142}Nd	^{140}Ce	^{138}Ba
interference mass	-	-	^{150}Sm	-	^{148}Sm	-	-	-	^{144}Sm	^{142}Ce	-	^{138}Ce

CHAPTER 3

Silicon Isotope Distribution in Waters and Surface Sediments of the Peruvian Coastal Upwelling*

Abstract

We present the first systematic study of the dissolved silicon isotope composition in the water column ($\delta^{30}Si_{Si(OH)4}$) and in diatoms ($\delta^{30}Si_{diatom}$) from the underlying surface sediments in a coastal upwelling region. Upwelled surface waters on the shelf off Peru are mainly fed by southward flowing subsurface waters along the coast, which show a mean $\delta^{30}Si_{Si(OH)4}$ of +1.5‰. The concentration of dissolved silicic acid ($Si(OH)_4$) increases towards the south and with increasing water depth documenting intense remineralisation of particulate biogenic silica ($bSiO_2$) in the water column and in the surface sediments. Surface waters in the realm of intense upwelling between 10°S and 15°S are only weakly fractionated with respect to dissolved Si isotope composition ($\delta^{30}Si_{Si(OH)4}$=+1.7‰), whereas further north and south, where upwelling is less pronounced, surface waters are more strongly fractionated ($\delta^{30}Si_{Si(OH)4}$ up to +2.8‰) due to the higher utilisation of the smaller amounts of available $Si(OH)_4$. The estimated degree of $Si(OH)_4$ utilisation in the surface water along the shelf ranges between 51% and 93%.

The $\delta^{30}Si_{diatom}$ values of picked diatoms in the underlying sediments vary from +0.58‰ to +1.95‰, which is within the order of the expected fractionation between surface waters and diatoms. The fractionation signal produced during formation of the diatoms in the surface water is recorded by $\delta^{30}Si_{diatom}$ values in the underlying sediments. Consistent with the distribution in the surface waters

**This chapter is going to be submitted to Geochimica et Cosmochimica Acta as:*

Ehlert, C., **P. Grasse**, E. Mollier-Vogel, T. Böschen, J. Franz, G. F. de Souza, B. C. Reynolds, L. Stramma, & M. Frank. Silicon Isotope Distribution in Waters and Surface Sediments of the Peruvian Coastal Upwelling.

the diatoms have the lowest $\delta^{30}Si_{diatom}$ values in the main upwelling region. The silicon isotope compositions of bulk biogenic opal b-SiO_2 ($\delta^{30}Si_{bSiO2}$) signatures from the same sediment samples are generally much lower than the $\delta^{30}Si_{diatom}$, indicating a significant contamination of the $bSiO_2$ with biogenic siliceous material other than diatoms, such as sponge spicules. This shift towards much lighter values by up to -1.3‰ for samples with low $bSiO_2$ concentrations potentially biases the interpretation of paleo-$\delta^{30}Si$ records and the reconstruction of past $Si(OH)_4$ utilisation in surface waters.

3.1 Introduction

The Peruvian coastal upwelling region is characterised by extremely high rates of primary productivity (Thiede and Suess, 1983; Berger et al., 1989; Pennington et al., 2006). Persistent easterly trade and alongshore winds produce offshore Ekman transport of surface water, which is replaced by upwelled, nutrient-rich subsurface waters. The main water mass supplying the Peruvian upwelling system are the southward flowing Peru-Chile Countercurrent (PCCC) and the Peru-Chile Undercurrent (PCUC) (Brink et al., 1983), which prevails between 50 m and 150 m water depth (Huyer et al., 1987; Karstensen and Ulloa, 2008). These currents are fed by the eastward flowing high salinity and oxygen enriched waters of the Equatorial Undercurrent (EUC) (Lukas, 1986; Penven et al., 2005; Kessler, 2006) and the Southern Subsurface Countercurrent (SSCC), both originating from the central Pacific (Brink et al., 1983; Toggweiler et al., 1991) (Fig. 3.1a). Near the shelf, the northward flowing Peru Coastal Current (PCoastalC) shows usually a strong seasonality and is strong in September and October (Strub et al., 1998), while it was weaker and showed a strong subsurface component in January 2009 (Czeschel et al., 2011).

Upwelling intensity is generally high during most of the year (Strub et al., 1998; Gunther, 1936), which results in year-round high nutrient concentrations in the surface waters (Pennington et al., 2006) and very high primary productivity, generally dominated by diatoms (Estrada and Blasco 1985; Abrantes et al., 2007). The amount of primary productivity off Peru is so high

that these decomposition processes cause one of the most pronounced Oxygen Minimum Zones (OMZs) of the world's ocean (e.g. Karstensen et al., 2008; Fuenzalida et al., 2009).

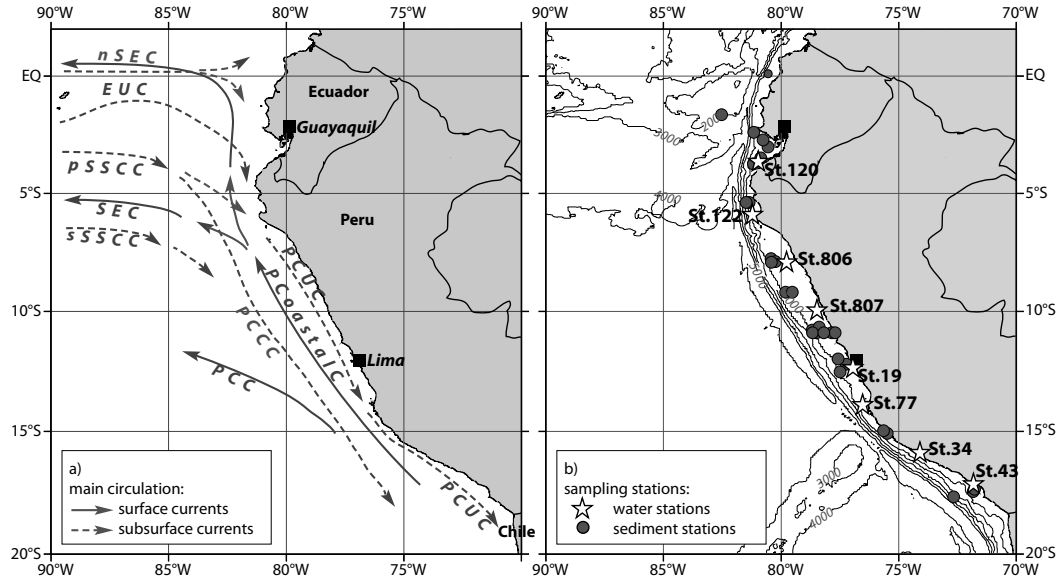

Figure 3.1: Maps showing the a) generalised circulation pathways of currents influencing the near-coastal areas (after Ayon et al., 2008; Kessler, 2006; Penven et al, 2005; and ADCP data according to Czeschel et al., 2011). Surface currents (solid line): SEC South Equatorial Current, nSEC northern South Equatorial Current, PCC Peru-Chile Current, PCoastalC Peru Coastal Current, subsurface currents (dashed line): EUC Equatorial Undercurrent, pSSCC and sSSCC primary and secondary Southern Subsurface Countercurrent, PCUC Peru-Chile Undercurrent, PCCC Peru Chile Countercurrent. b) Location of the CTD stations (white stars with station numbers) and surface sediment stations (grey dots). The bathymetry is given for 0 to 5000 m water depth in 1000 m increments.

From reconstructions based on sedimentary records it has been inferred that most of the changes in bottom water oxygen levels under the coastal upwelling system off Peru have been related to changes in surface water productivity (e.g. DeVries and Schrader, 1981; Schrader, 1992; Rein et al., 2005). So far, it has proven difficult to disentangle the influences of changes in productivity from those caused by changes in circulation and upwelling intensity. The isotopic composition of stable silicon Si (expressed as $\delta^{30}Si$) is a powerful tool to investigate changes of silicic acid ($Si(OH)_4$) utilisation, as well as nutrient dynamics and productivity in the present and past ocean (De La Rocha et al., 1998, Brzezinski et al., 2002; Reynolds et al., 2008). Diatoms take up dissolved ($Si(OH)_4$) to form their opaline frustules (Tréguer et al., 1995),

whereby Si isotopes are fractionated. The lighter isotopes are preferentially incorporated into the diatom frustules and leave the residual surface water enriched in the heavier isotopes (high $\delta^{30}Si$ values). The fractionation factor between seawater and diatoms is about -1.1‰ (De La Rocha et al., 1997; Milligan et al., 2004; Varela et al., 2004; Reynolds et al., 2006; Beucher et al., 2008). In areas of strong upwelling the degree of utilisation and therefore the dissolved $\delta^{30}Si_{Si(OH)4}$ in the surface water is expected to be low due to continuous supply of large amounts of less fractionated $Si(OH)_4$ from subsurface waters. In contrast, in areas of weak upwelling the $Si(OH)_4$ in the surface waters will be almost completely utilised, which means that due to the degree of enrichment $\delta^{30}Si_{Si(OH)4}$ will correspondingly be very high. The $\delta^{30}Si_{Si(OH)4}$ distribution in surface waters therefore directly reflects $Si(OH)_4$ availability (Varela et al., 2004; Cardinal et al., 2005; Reynolds et al., 2006) and thus the amount of newly supplied nutrients with upwelled waters. Changes in $Si(OH)_4$ utilisation by diatoms due to changes in $Si(OH)_4$ supply and upwelling intensity are therefore expected to be reflected by the Si isotope composition of surface water ($\delta^{30}Si_{Si(OH)4}$) and that of the diatoms growing in them ($\delta^{30}Si_{bSiO2}$ for bulk biogenic silica ($bSiO_2$) material and $\delta^{30}Si_{diatom}$ for hand-picked diatoms).

A large fraction of the diatom $bSiO_2$ produced in surface waters re-dissolves in the upper water column because seawater is undersaturated with respect to silicate. On average only about 3% of the $bSiO_2$ produced is ultimately deposited and preserved in the sediment (Tréguer et al., 1995). These remineralisation processes are, however, highly variable and depend on the marine setting. In oligotrophic open ocean gyres 50-100% of the $bSiO_2$ produced in the surface water redissolves in the upper 100m of the water column, whereas in coastal diatom bloom areas preservation rates can be much higher (Nelson and Goering, 1977; Nelson et al., 1995). The dissolution of $bSiO_2$ is strongly influenced by physical parameters, such as temperature and pH (Lewin, 1961), and bacterial activity can lead to higher dissolution rates (Bidle and Azam, 1999; Bidle et al., 2002). A consistent fractionation of Si isotopes during dissolution of $bSiO_2$ of -0.55‰ has been reported (Demarest et al., 2009), which leaves partially-dissolved diatoms with a higher than initial

$\delta^{30}Si$. Ignoring this fractionation effect may result in an overestimation of the level of past $Si(OH)_4$ utilisation in surface waters and an underestimating of the calculated fractionation factor.

In this study, we present new water column profiles of the Si isotope composition of dissolved $Si(OH)_4$ for eight shallow water stations together with isotopic analyses of diatoms extracted from the underlying surface sediments along the Peruvian shelf between the equator and 17.5°S, which covers the major gradients of coastal upwelling intensity. The main goal of this study is to determine the factors controlling the $\delta^{30}Si$ of dissolved $Si(OH)_4$ in the surface waters and how these signatures are recorded by the corresponding sedimentary diatoms as a function of upwelling intensity and diatom productivity. The influence of $Si(OH)_4$ utilisation versus effects of water mass mixing is evaluated including the influence of remineralisation processes on the $\delta^{30}Si_{Si(OH)4}$ distribution, which will serve as a basis for the reliable use of the $\delta^{30}Si_{diatom}$ as a proxy for past upwelling conditions.

3.2 Material and Methods

All samples were collected during cruises M77/1 to 4 with the German RV Meteor between October 2008 and February 2009 in the frame of Collaborative Research Centre (SFB) 754: Climate - Biogeochemistry Interactions in the Tropical Ocean. All sampling stations are located on the Ecuadorian and Peruvian shelf between the equator and 17.5°S (Fig. 3.1b, Table A.1 and A.2).

The water samples for the whole water column, including bottom water, were collected using a rosette with 24 Niskin bottles (10 L each) equipped with a SeaBird CTD. Subsamples for $Si(OH)_4$ concentration measurements were frozen onboard immediately after sampling to be measured at the Max-Planck Institute (MPI) for Marine Microbiology in Bremen, Germany. $Si(OH)_4$ concentrations of frozen samples were compared to selected filtered and acidified (non frozen) seawater samples. Reproducibility between both was within 5 to 10% (no systematic variations). Oxygen concentrations were determined with the O_2-sensor of the CTD and were later calibrated with bottle

data obtained by Winkler titration (Winkler, 1888). $BSiO_2$ in the water column was sampled by filtration through nitrocellulose acetate filters (0.65 µm pore size) at low vacuum pressure (< 200 mbar) on-board and was stored frozen at -20°C. For analysis, the filters with the samples were treated with 25 ml NaOH (0.1 M) in Nalgene bottles and were shaken in a water bath at 85°C for 2h 15 min. After cooling, analysis of the samples was conducted according to the method for determination of inorganic silicate by Hansen and Koroleff (1999).

Seawater samples for $\delta^{30}Si_{SiOH4}$ analysis (500 to 2000 ml) were immediately filtered on board through nitrocellulose acetate filters (0.45 µm pore size), acidified to pH 2 with concentrated Teflon-distilled HCl (1 mL HCl per litre of seawater), and stored in acid cleaned polyethylene bottles.

In the clean laboratory of IFM-GEOMAR Si was separated from the water samples using a brucite-coprecipitation method (following Reynolds et al. (2006), after Karl and Tien (1992)). Given that incomplete precipitation would lead to isotopic fractionation of the Si in the sample, recovery was checked for every sample, and only those with >97% yield were used for isotopic measurements. Depending on the $Si(OH)_4$ concentration of the samples, 10 to 300 mL of previously neutralized seawater was precipitated at pH 10 by adding 1M NaOH (10 µl/ml). The precipitate was dissolved in 6M HCl resulting in a pH of 2-3. Water samples with concentrations of less than 4 µmol/kg $Si(OH)_4$ were preconcentrated through additional precipitation steps applying the same method to ensure that at least 43 nmol Si were processed through ion-exchange chromatography.

The sediment samples were collected using a multicorer. For this study only the uppermost centimetre of each core was used. The content of $bSiO_2$ was measured following DeMaster (1981) and Müller and Schneider (1993). The extraction of diatoms from the sediment samples for Si isotope analyses followed the procedure by Morley et al. (2004). Approximately 300 µg of freeze-dried sediment was treated with concentrated H_2O_2 and HCl to remove organic matter and carbonates and was then wet sieved to extract the 11-32 µm fraction. $BSiO_2$ was separated from detrital material in multiple steps using a sodium polytungstate solution with a density of 2.1-2.2 g/mL. For dissolution of

the diatom frustules the method of Reynolds et al. (2008) was applied and extended by an additional step for oxidation of organic matter. For this purpose, 200 µL concentrated H_2O_2 (suprapure) was added to each sample, which was then dried and redissolved in 0.1 M NaOH. Tests demonstrated that this step does not affect the Si isotope results but significantly increases the stability of the beam during mass spectrometry and improves the reproducibility of the measurements. The Si concentrations in both seawater and diatom samples were measured colorimetrically using a photospectrometer (Hansen and Koroleff, 1999). Al/Si and Ti/Si ratios were measured in aliquots of the dissolved $bSiO_2$ samples prepared for Si isotope analyses using an *Agillent 7500 Series* quadrupole ICPMS at IFM-GEOMAR in Kiel to check for potential contamination by clays (Table A.2).

From selected samples large diatoms were hand-picked to obtain a pure diatom $\delta^{30}Si_{diatom}$ value not influenced by other potentially present $bSiO_2$ phases. These samples were wet sieved through a 63 µm sieve, dried and sieved into different size fractions. Between 100 and 200 individual diatom specimens (non species-specific) were hand-picked from the 125-250 µm fraction, which resulted in concentrations of about 100 to 150 µmol/kg Si after dissolution in 2.5 ml of solution performed with the same method as for the bulk $bSiO_2$.

For Si isotope measurements, all samples were chromatographically purified following the method described by Georg et al. (2006). Si isotope ratios were measured on a *NuPlasma* MC-ICPMS (Nu Instruments) at IFM-GEOMAR, which is equipped with an adjustable source-defining slit set to medium resolution to ensure peak separation of the ^{30}Si peak and molecular interferences. Measurements were carried out with a standard-sample bracketing method (Albarède et al., 2004). All solutions were measured at a Si concentration of 14-21 µmol/kg depending on the performance of the instrument and were introduced into the plasma via a Cetac Aridus II desolvator equipped with a PFA nebulizer at a 60 to 80 µL/min uptake rate. Si isotope compositions are reported in the $\delta^{30}Si$ notation of deviations of the measured $^{30}Si/^{28}Si$ from the international Si standard NBS28 in parts per thousand (‰):

$$\delta^{30}Si = \left[\frac{\left({}^{30}Si/{}^{28}Si \right)_{sample}}{\left({}^{30}Si/{}^{28}Si \right)_{NBS28}} - 1 \right] * 1000$$

Repeated measurements of the reference materials IRMM018 and Big Batch gave average δ^{30}Si values of -1.55 ± 0.28‰ ($2\sigma_{sd}$, n = 38) and -10.80 ± 0.22‰ ($2\sigma_{sd}$, n = 38), respectively, which are in good agreement with values obtained by other laboratories (Reynolds et al., 2007). Samples were measured three to five times within one run, which generally resulted in uncertainties between 0.07 and 0.40‰ ($2\sigma_{sd}$), with one sample having a $2\sigma_{sd}$ of 0.48‰ (Table A.1 and A.2). Replicate measurements of in-house matrix standards for both seawater and diatom samples over longer periods of time gave a reproducibility of 0.25‰ ($2\sigma_{sd}$), which corresponds to all error bars of the Si isotope compositions in the figures.

3.3 Results

3.3.1 Water Stations

3.3.1.1 Subsurface and Bottom Waters

The water column profiles (Fig. 3.2, Table A.1) show a general increase in $Si(OH)_4$ concentrations with water depth. Only at St. 77 the highest concentration (40 µmol/kg) was found at 50m depth and then decreased again to 30 µmol/kg near the bottom of the profile. The subsurface waters (50 to 150 m water depth) flow southward along the shelf. In the northernmost St. 120, the concentration is influenced by the incoming EUC, which has a $Si(OH)_4$ concentration of 15 µmol/kg (red dashed line in Fig. 3.2). Towards the south the $Si(OH)_4$ concentration in this water depth range increases. The highest subsurface $Si(OH)_4$ concentrations are found at St. 19 and St. 77 between 12°S and 14°S (~40 µmol/kg). Further to the south concentrations decrease again (~30 µmol/kg). The $\delta^{30}Si_{Si(OH)4}$ of all water column profiles mirrors the $Si(OH)_4$ concentrations in that it decreases with increasing water depth and $Si(OH)_4$ concentration.

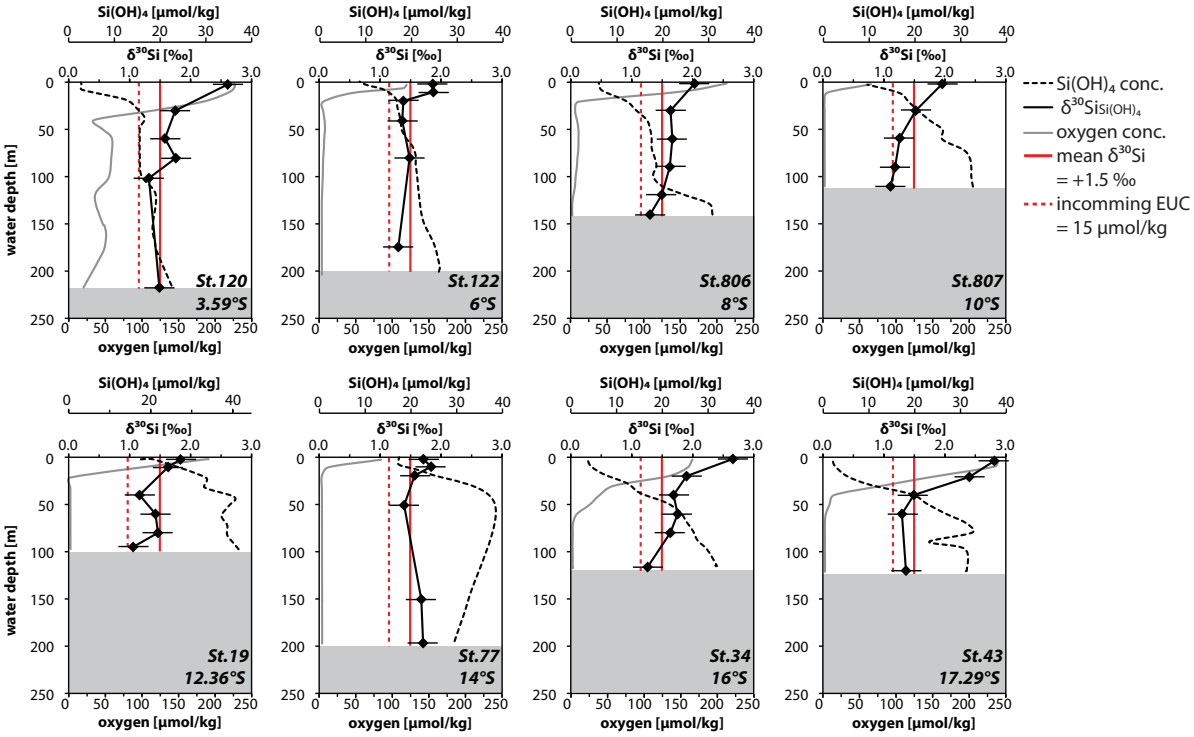

Figure 3.2: Water column profiles for 8 stations along the Ecuadorian and Peruvian shelf from north (top, left) to south (bottom, right) (see Fig. 3.1). The grey shading indicates the bottom. For all stations the $\delta^{30}Si_{Si(OH)4}$ (‰, solid black line) and the $Si(OH)_4$ concentrations (µmol/kg, dashed black line) are shown. The grey solid line indicates the dissolved oxygen concentration (µmol/kg). The solid and dashed red lines mark the mean subsurface $\delta^{30}Si_{Si(OH)4}$ of +1.5‰ (50-150 m water depth of all 8 stations) and the $Si(OH)_4$ concentration of ~15 µmol/kg of the incoming EUC. Please note the slightly different scale for $Si(OH)_4$ concentration for St. 19. Error bars represent 0.25‰ $2\sigma_{sd}$ long-term reproducibility of repeated sample measurements.

The mean $\delta^{30}Si_{Si(OH)4}$ between 50m and 150m water depth, which corresponds to the source depth of the upwelling, is +1.5 ± 0.2‰ ($1\sigma_{sd}$) (marked by the red solid line in Fig. 3.2). At most of the stations the deepest samples represent bottom waters and their $\delta^{30}Si_{Si(OH)4}$ was also found to be near +1.5‰. Only at St. 807 and St. 19 between 10 and 12°S the isotopic composition of the bottom waters is somewhat lower with values of +1.1‰.

3.3.1.2 Surface Waters

In the surface waters the concentration of $Si(OH)_4$ varies widely with latitude and upwelling intensity. The highest concentrations of $Si(OH)_4$ (17.72 µmol/kg, Fig. 3.2, Table A.1) are found close to the coast between 10° to 15°S, where the upwelling is most intense as evidenced by very low sea surface temperatures (SSTs) (Fig. 3.3a). To the north and south of this, the concentrations of $Si(OH)_4$ are lower at minimum values of 2.14 µmol/kg.

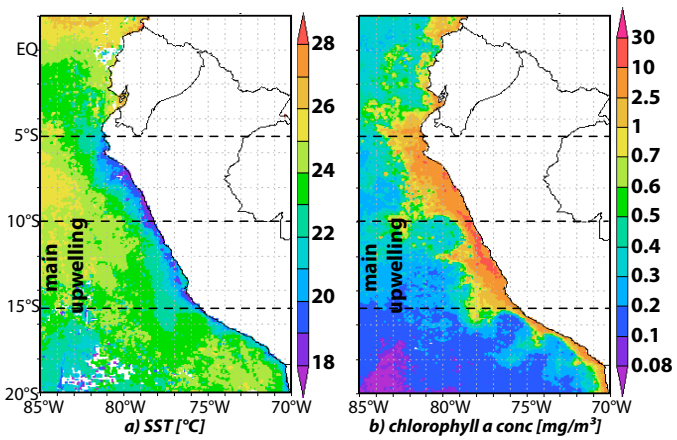

Figure 3.3: Distribution of a) surface water temperature SST (°C) and b) chlorophyll a concentration (mg/m^3) to indicate the area of the strongest upwelling intensity (lowest SST and highest chlorophyll concentration). Data were available from NASA Giovanni (http://disc.sci.gsfc.nasa.gov/giovanni/overview/index.html).

The surface waters show higher $\delta^{30}Si_{Si(OH)4}$ values than the subsurface waters in all profiles, ranging from +1.7‰ to +2.8‰ (Fig. 3.2). The highest $\delta^{30}Si_{Si(OH)4}$ values between +2.6‰ and +2.8‰ were found at the northernmost station (St. 120, 4°S) and at the stations south of 15°S (St. 34, St. 43). Low $\delta^{30}Si_{Si(OH)4}$ in surface waters ranging between +1.7‰ and +2.0‰ were found along the shelf at St. 122, 806, 807, 19 and St. 77 (between 6°S to 15°S), with the latter showing the minimum value. The $\delta^{30}Si_{Si(OH)4}$ values of the surface waters show a clear negative correlation with $Si(OH)_4$ contents (Fig. 3.4, see Tab. A.1). Subsurface water $\delta^{30}Si_{Si(OH)4}$ and $Si(OH)_4$ (marked with the grey shading in Fig. 3.4) show a larger scatter than surface water values.

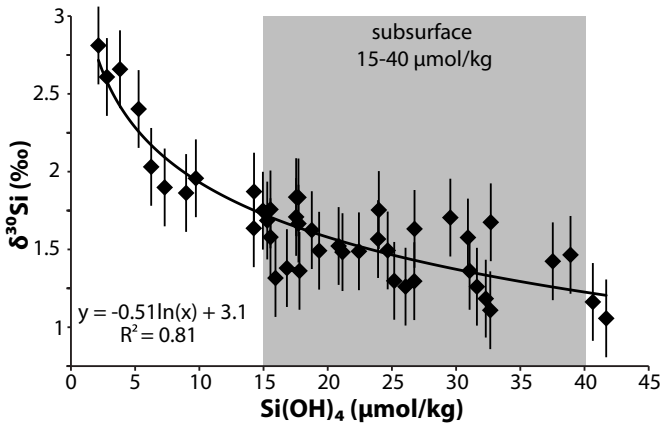

Figure 3.4: Correlation between dissolved $\delta^{30}Si_{Si(OH)4}$ (‰) and $Si(OH)_4$ concentrations (µmol/kg) for all seawater samples. The grey bar indicates the range of subsurface water $Si(OH)_4$ concentrations (50-150m water depth) between 15-40 µmol/kg. Error bars represent 0.25‰ $2\sigma_{(sd)}$ long-term reproducibility of repeated sample measurements.

3.3.2 Surface Sediments

The distribution of $bSiO_2$ concentrations in the surface sediment reflects primary productivity in the surface waters (Fig. 3.3b and 3.5b). The highest

concentrations of up to 21 wt% are found close to the coast between 10 and 15°S. North and south of this area the fraction of $bSiO_2$ in the shelf sediments is much lower and reaches values as low as 0.24 wt% at 3°S. The $\delta^{30}Si_{bSiO2}$ values range between -0.98‰ and +1.07‰, with the highest values found at 15°S (Fig. 3.5a, Table A.2). Along the shelf between 5° and 10°S where the upwelling is weaker and $bSiO_2$ concentrations are lower the values range between +0.3‰ and +0.8‰. Samples (n = 2) from the Gulf of Guayaquil display even lower $\delta^{30}Si_{bSiO2}$ ratios (-0.1‰). The $\delta^{30}Si_{diatom}$ values of the hand-picked diatoms are generally significantly higher than those of the $bSiO_2$ in the same samples with $\delta^{30}Si_{diatom}$ ranging between +0.58‰ to +1.95‰ (Fig. 3.5a, Table A.2). Al/Si and Ti/Si ratios of $bSiO_2$-samples range between 1 to 235 mmol/mol and 31 to 125 µmol/mol (Table A.2).

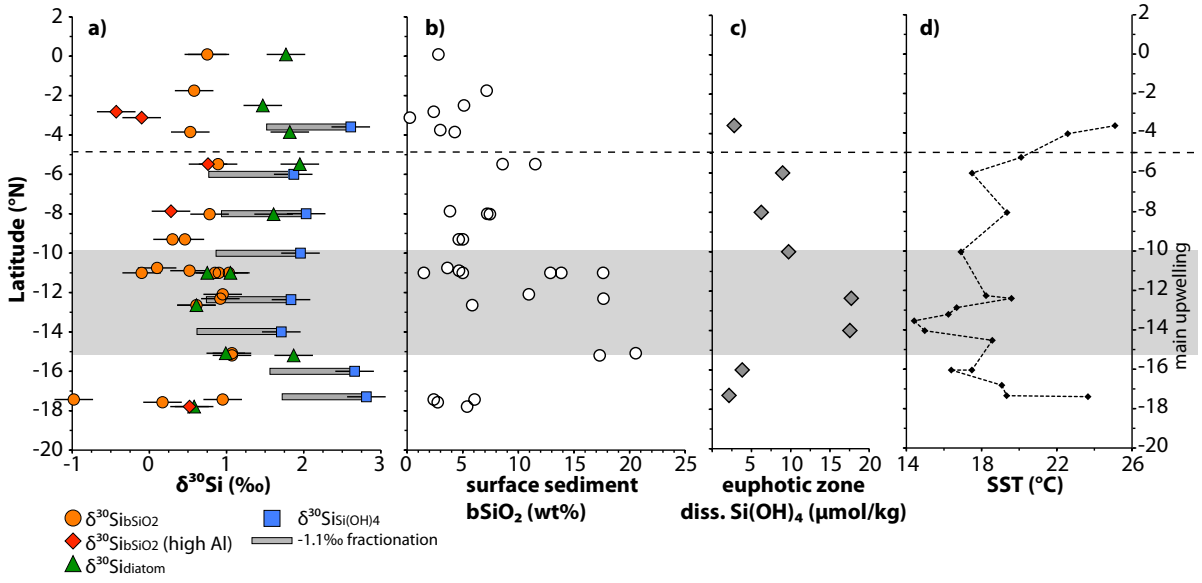

Figure 3.5: Latitudinal distribution of a) $\delta^{30}Si$ in ‰ (orange circles: $bSiO_2$ samples, red diamonds: $bSiO_2$ samples with high Al/Si ratios, green triangles: picked diatoms, blue squares: surface water samples), The horizontal grey bars mark the -1.1‰ for fractionation between water and diatoms, error bars represent 0.25‰ $2\sigma_{(sd)}$ long-term reproducibility of repeated sample measurements, b) surface sediment $bSiO_2$ concentration (wt%), c) surface water $Si(OH)_4$ concentrations (µmol/kg), e) surface water temperature for all shelf stations (°C). The horizontal black dashed line and grey shading indicates the same latitudinal areas as in Fig. 3.3.

3.4 Discussion

3.4.1 Silicon Isotope Distribution in the Water Column

3.4.1.1 Subsurface and Bottom Waters

Upwelling along the Peruvian shelf occurs from the subsurface waters of the PCUC and the PCCC (Fig. 3.1), which mainly originate from the EUC and SSCC (Brink et al., 1983; Penven et al., 2005; Kessler; 2006). During January and February 2009, when the samples were taken, the PCUC was clearly detectable with ADCP along the shelf between 50 to 150 m water depth at 6°S. At 14°S the southward directed PCCC joined the PCUC and they were no longer distinguishable (Czeschel et al., 2011). Subsurface waters between 50 and 150 m, reflecting the main source for the upwelling (Huyer et al., 1987; Karstensen and Ulloa, 2008; Czeschel et al., 2011) are characterized by a mean $\delta^{30}Si_{Si(OH)4}$ signature of +1.5‰, ± 0.2 ($1\sigma_{(sd)}$, Fig. 3.2). The incoming $Si(OH)_4$ concentration at the northerly stations lies around 15 µmol/kg (Fig. 3.2). The $Si(OH)_4$ concentrations within the subsurface waters do increase significantly from 15 to 40 µmol/kg along the southward flowpath, which indicates extensive remineralisation processes occurring both in the water column and most likely also from the shelf sediments. Settling diatoms are (partially) dissolved in the water column, and after sedimentation further dissolution is promoted, by physical parameters (temperature, pressure) and biological activity (Nelson et al., 1995; Dugdale and Wilkerson, 1998). Bacterial activity can also enhance dissolution rates by degrading the organic matrix that protects the diatom frustules (Bidle and Azam, 1999; Bidle et al., 2002). Dissolution of $bSiO_2$ is expected to lead to lower $\delta^{30}Si_{Si(OH)4}$ values in the water column (Demarest et al., 2009). However, it is only in some bottom water samples close to the sediment-water interface (St. 807, 19) where direct indications for dissolution are found ($\delta^{30}Si_{Si(OH)4}$ shows a slight shift to values as low as +1.1‰, Fig. 3.2). A possible explanation for the relatively uniform $\delta^{30}Si_{Si(OH)4}$ of the subsurface waters are efficient vertical water mass mixing due to upwelling, but also horizontal mixing processes and eddy formation, which all together reduce any possible latitudinal effects of remineralisation. Fig. 3.4 shows that the subsurface waters (characterised by $Si(OH)_4$ concentrations

between 15 to 40 µmol/kg) display a much larger scatter than the surface waters, which is an indicator for water mass mixing processes but also dissolution of $bSiO_2$. Upwelled water masses near the coast are transported offshore and downwelled further west. These water masses are mixed again with central Pacific water masses and would thus transport subsurface waters with higher $\delta^{30}Si_{Si(OH)4}$ values back to the shelf. Therefore, a continuous supply of waters with higher $\delta^{30}Si_{Si(OH)4}$ signatures would be mixed with the lower $\delta^{30}Si_{Si(OH)4}$ of the source waters of the upwelling. This would lead to higher $\delta^{30}Si_{Si(OH)4}$ than expected from the southward increasing $Si(OH)_4$ concentrations. In addition, south of 14°S the influence of the PCoastalC is detectable by lower $Si(OH)_4$ concentrations. According to ADCP data of Czeschel et al. (2011) this current flows northward close to the shelf at approximately 50 m to 100 m depth and can thus also influence the isotope signal of the subsurface source waters of the upwelling given that it is derived from subsurface waters of southern origin. North of 14°S the PCoastalC is subducted to a depth of approximately 200 m and therefore does not influence the upwelling source waters any more.

3.4.1.2 Surface Waters

The surface waters along the Peruvian shelf can be separated into different latitudinal regions due to their different physical (SSTs) and biological (chlorophyll a concentration) properties (Fig. 3.3). The high chlorophyll a concentrations are derived from diatom blooms (Bruland et al., 2005), which imply that primary productivity is driven by diatoms. $Si(OH)_4$ concentrations in surface waters of the coastal upwelling area off Peru are high where strong upwelling promotes continuous supply of deeper waters feeding the surface water pool. Conversely, they are lower in those areas where the delivery through upwelling is not as strong and primary productivity utilises the nutrients in the surface water more completely. The $\delta^{30}Si_{Si(OH)4}$ difference between the subsurface source waters and the surface waters above, which reflects the utilisation of $Si(OH)_4$, amounts to only about 0.3‰ within the main upwelling zone between 10°S and 15°S (Fig. 3.2). Along the northern part of the shelf

between 3°S to 8°S the difference is about 0.6‰, and reaches up to 1.2‰ south of 15°S, where upwelling is far less intense (higher SSTs in Fig. 3.3a and 3.5d). The surface water $\delta^{30}Si_{Si(OH)4}$ values directly reflect the availability of $Si(OH)_4$ in the euphotic zone (Fig. 3.5a and c). Higher $Si(OH)_4$ concentrations in the surface water are associated with higher primary productivity (as indicated by the surface water chlorophyll a concentration, Fig. 3.5c and 3.3b) (Bruland et al., 2005), but lower $\delta^{30}Si_{Si(OH)4}$ values (Fig. 3.5a). So, in the surface waters outside of the upwelling region there is a higher degree of utilisation of $Si(OH)_4$ due to phytoplankton productivity, but at the same time $bSiO_2$ productivity is lower (Fig. 3.5a and c). Even within the main upwelling region, nearly continuous re-supply $Si(OH)_4$ to the surface cannot prevent at least a slight Si isotope fractionation of the $Si(OH)_4$ in the surface waters. However, even the maximum difference between surface and deep Si isotope composition of 1.2‰ is still low compared with areas of highly depleted surface $Si(OH)_4$ concentrations, such as in open ocean gyres (Reynolds et al., 2006).

3.4.1.3 Silicon Isotope Fractionation Models

The Si isotope fractionation factor for the formation of diatom silica from seawater assessed by culture experiments is -1.1‰ in $\delta^{30}Si$ (De La Rocha et al., 1997). Two different models can describe the evolution of the $\delta^{30}Si$ composition of surface waters during biologically induced fractionation: a steady-state model, wherein a continuous supply of nutrients causes a dynamic equilibrium of the $Si(OH)_4$ content, and a Rayleigh-type model, in which no additional nutrients are newly supplied to the system (De La Rocha et al., 1997; Cardinal et al., 2005; Reynolds et al., 2006). The two models can be described and approximated by simple equations: Steady-state system:

$$\delta^{30}Si_{Si(OH)_4\,obs} = \delta^{30}Si_{Si(OH)_4\,init} - \varepsilon * (1 - f)$$

$$f = Si(OH)_{4\,obs} / Si(OH)_{4\,init}$$

Under assumed steady state conditions the effective net $bSiO_2$ production (e.g. during one year) is equal to the net $Si(OH)_4$ supply (Fripiat et al., 2011).
Rayleigh-type system:

$$\delta^{30}Si_{Si(OH)_4\,obs} = \delta^{30}Si_{Si(OH)_4\,init} + \varepsilon * (\ln f)$$

$$\delta^{30}Si_{diatom_{inst}} = \delta^{30}Si_{Si(OH)_4\ obs} + \varepsilon$$

$$\delta^{30}Si_{diatom_{acc}} = \delta^{30}Si_{Si(OH)_4\ init} - \varepsilon * (f \ln f / 1 - f)$$

where $\delta^{30}Si_{Si(OH)4\ init}$ is the Si isotope composition of $Si(OH)_4$ in the surface water before biological utilisation starts to fractionate the Si isotopes, $\delta^{30}Si_{Si(OH)4\ obs}$ is the Si isotope composition measured in the surface water, *f* is the depletion factor describing the fraction of the initial $Si(OH)_4$ concentration that remains, ε is the fractionation factor between the $Si(OH)_4$ and the diatoms produced, $\delta^{30}Si_{diatom\ inst}$ is the Si isotope composition of the instantaneously produced diatoms at each time and $\delta^{30}Si_{diatom\ acc}$ is the silicon isotope composition of the diatoms which accumulated and integrate over time.

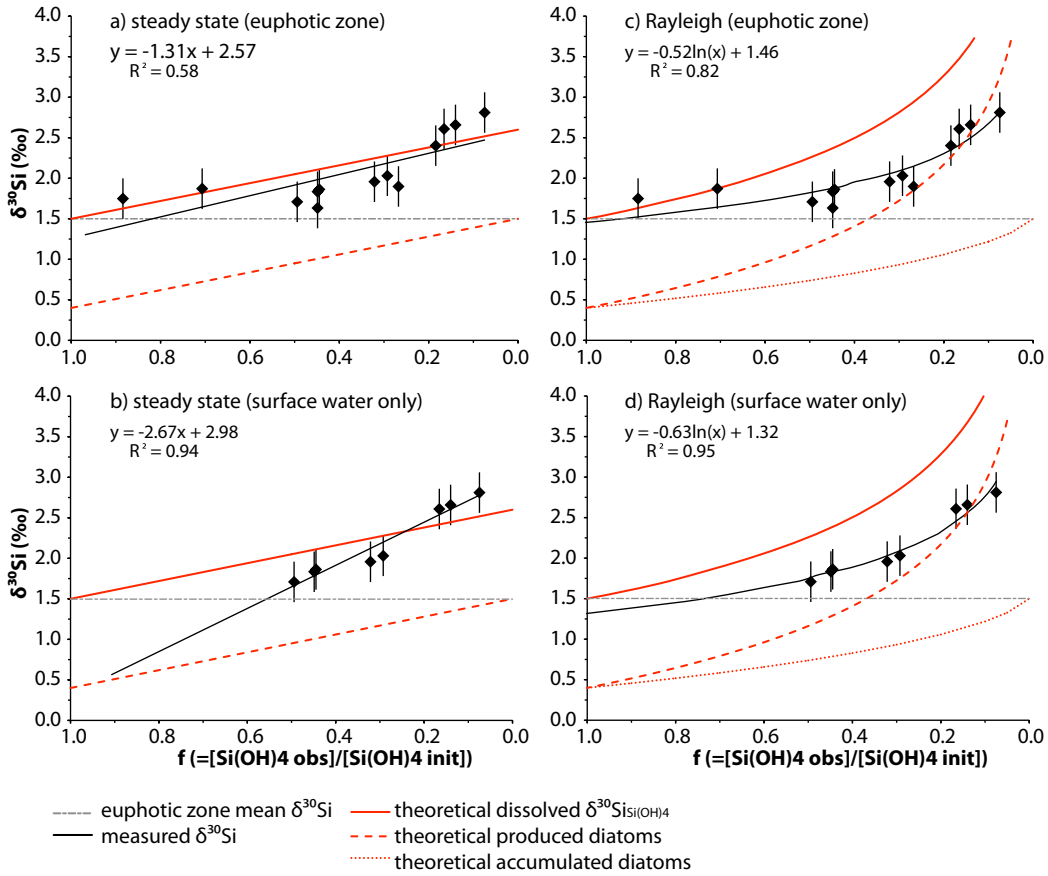

Figure 3.6: $\delta^{30}Si_{Si(OH)4}$ (‰) versus f (remaining $Si(OH)_4$ from the available pool) indicating the fractionation factor for steady state-type (a, b) and Rayleigh-type conditions (c, d, using a logarithmic function) (black curves). The bold red lines in the graphs indicate the fractionation curve of $Si(OH)_4$ for a -1.1‰ fractionation, assuming an initial value of 1.5‰ (grey dashed line), whereas the dashed red line indicates the expected fractionation curve for the produced diatoms as a result of a -1.1‰ fractionation, and the red dotted line indicates the accumulated diatoms under Rayleigh-type conditions. Error bars represent 0.25‰ $2\sigma_{sd}$ long-term reproducibility of repeated sample measurements.

Both models assume a constant fractionation factor. The value of ε is given by the slope of the linear regression between $\delta^{30}Si_{Si(OH)4\ obs}$ and *f* for the steady-state model, and between $\delta^{30}Si_{Si(OH)4\ obs}$ and ln*f* for the Rayleigh-type system model (Fig. 3.6).

Due to the fact, that upwelling is supplied from the subsurface waters, the tightly defined mean $Si(OH)_4$ concentration for the depth between 50 m to 150 m, or bottom water where water depth is less than this, is employed as initial concentration of the upwelling source waters at each station (Table, A.1; Huyer et al., 1987; Karstensen and Ulloa, 2008). These waters show a relatively uniform $\delta^{30}Si$ of +1.5‰, which was defined as the source water signature (Fig. 3.6). Both models were applied for the $\delta^{30}Si_{Si(OH)4}$ from the euphotic zone (defined by the oxycline, which mostly fits also well with the nutricline for $Si(OH)_4$, Fig. 3.2, Fig. 3.6a, c) as well as for surface water samples only (Fig. 3.6b, d). The fractionation factors calculated from our data range between -2.7‰ (steady-state, surface water only) and -0.5‰ (Rayleigh, euphotic zone data) (Fig. 3.6), and thus deviate from the experimentally determined fractionation factor of -1.1‰ (De La Rocha et al., 1997). Applying the steady state model for all measured $\delta^{30}Si_{Si(OH)4}$ from the euphotic zone results in a calculated fractionation factor of -1.3‰, which is very close to the experimentally derived from De La Rocha et al. (1997).

Using all data from the euphotic zone, however, usually results in an underestimation of the fractionation factor due to dissolution of the diatoms (Beucher et al., 2011; Demarest et al., 2011). During dissolution the lighter isotopes are released to the surrounding seawater, which leads to lowers $\delta^{30}Si_{Si(OH)4}$ values and an increase in $Si(OH)_4$ concentration, and consequently to lower calculated utilisation rates. Also, the discrepancies in the calculated fractionation factors are not surprising and arise from the fact that the estimation of the fractionation factor is easily biased by extensive mixing (Reynolds et al., 2006; Fripiat et al., 2011). The steady-state model fits the water data much better. This is a reasonable result for an upwelling area, which is not expected to be a Rayleigh-type system due to the continuous re-supply of upwelled nutrients. The calculated utilisation (for steady state conditions) of available

$Si(OH)_4$ in surface waters on the shelf ranges from about 51% in the main upwelling region to up to 93% further south (utilisation [%] = (1-*f*)*100).

3.4.2 Surface Sediments

The distribution of $bSiO_2$ in surface sediments and surface waters agrees quite well in that the highest concentrations are found at those locations where the upwelling is most intense (Fig. 3.5b). This is also where the $\delta^{30}Si_{Si(OH)4}$ of the surface water indicates the weakest fractionation (Fig. 3.5a). Correspondingly, diatoms deposited in the underlying surface sediments should also have the lowest $\delta^{30}Si$ ratios between 10°S to 15°S. In fact, off Peru, the $\delta^{30}Si_{bSiO2}$ values show no distinct variability (Fig. 3.5), and are mostly isotopically to low when compared to the $\delta^{30}Si_{Si(OH)4}$. Overall, the highest values are found in the area of the strongest upwelling. The concentration of $bSiO_2$ and $\delta^{30}Si_{bSiO2}$ show together a positive trend (Fig. 3.7), which is opposite to the expected correlation in an upwelling area: high $bSiO_2$ concentrations are expected to prevail where the highest delivery of nutrients occurs and where correspondingly only weak Si isotope fractionation occurs. Fractionation processes cannot explain this discrepancy.

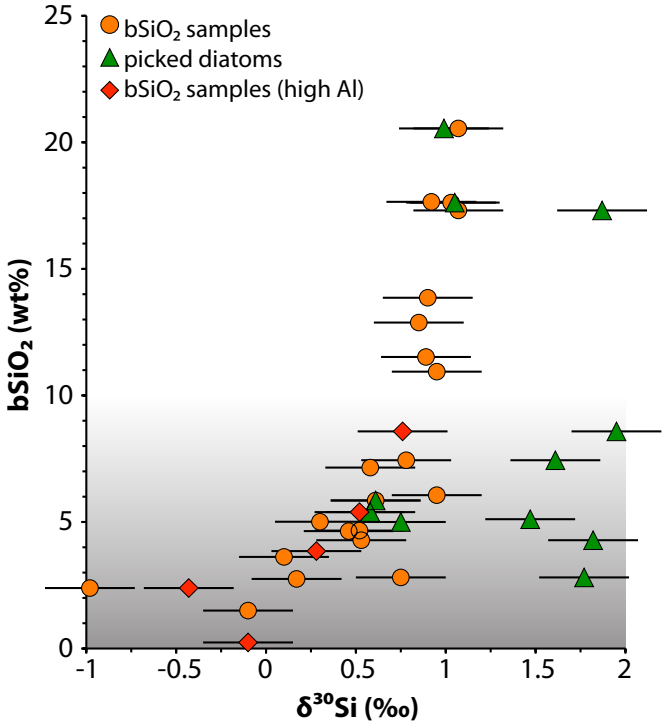

Figure 3.7: Correlation between $bSiO_2$ (wt.%) and $\delta^{30}Si$ (‰) of $bSiO_2$ (orange circles) and of hand-picked diatoms (green triangles) in the surface sediments. The red diamonds mark $bSiO_2$ samples, which have Al/Si ratios >50. The grey shading indicates samples with $bSiO_2$ concentration <10 wt%, which is assumed to be a critical with respect to possible contaminations. Error bars represent 0.25‰ $2\sigma_{sd}$ long-term reproducibility of repeated sample measurements.

Instead, the measured $\delta^{30}Si_{bSiO2}$ may not reflect diatoms alone but may be a mixture of silicate from different sources. The most obvious would be a contamination with clay. If the cleaning process was not sufficient, remaining and (partially) dissolved clays in the sample solution would shift the measured $\delta^{30}Si_{bSiO2}$ towards lighter values (Ding et al., 1996; De La Rocha et al., 2000; Georg et al., 2009). Therefore, Al/Si and Ti/Si ratios were measured for most of the samples in order to exclude significant contributions from such sources (Table A.2). The ratios range between 1 and 235 mmol/mol for Al/Si ratios and between 31 and 125 µmol/mol for Ti/Si ratios. Both elements are present as trace elements in diatom frustules (Ellwood and Hunter, 1999) but more importantly are major elements in clay minerals at much higher concentrations (Al/Si ratios in clays is ~1). It is very difficult to demonstrate complete removal off all clays from the diatoms (Shemesh et al., 1988). If all contamination would arise from clay minerals, Ti and Al should be correlated with each other. However, the poor correlation between Al/Si and Ti/Si ratios (Fig. 3.8a) basically excludes a systematic contamination with clays. The Al content of living diatoms is generally less than 1% (Lewin, 1961; Shemesh et al., 1988; van Bennekom et al., 1989). The concentration of trace metals in the $bSiO_2$ depends on the concentration of the medium they grew from (Ellwood and Hunter, 1999), i.e. higher concentration in the seawater leads to higher concentration in the $bSiO_2$. Additionally, Al can be passively incorporated in $bSiO_2$ immediately after deposition at the sediment–water interface (van Cappellen and Qiu, 1997; Dixit et al., 2001, Ragueneau et al., 2005), leading to an enrichment of Al in the $bSiO_2$, which can alter the interpretation of trace metal measurements.

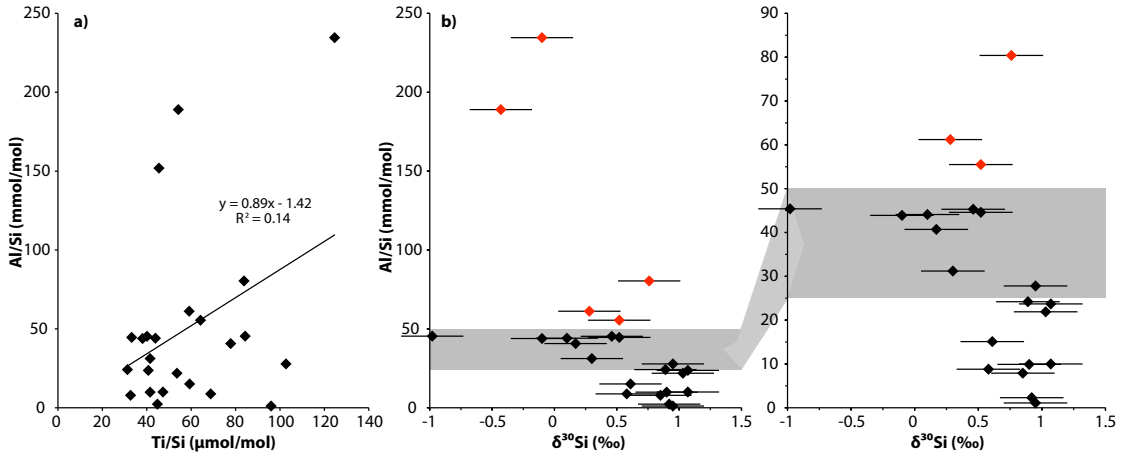

Figure 3.8: a) Ti/Si (µmol/mol) versus Al/Si (mmol/mol) ratios for $bSiO_2$ samples. (Not measured in picked diatoms) b) $\delta^{30}Si_{bSiO2}$ (‰) versus Al/Si ratios (mmol/mol). The grey shading indicates Al/Si ratios between 25 and 50, samples with higher ratios (marked in red) are potentially contaminated with clay material.

Typically, the Al/Si ratio of diatoms in sediments should be between 25 and 50 mmol/mol (Hurd, 1973; van Bennekom et al., 1988), which is one order of magnitude lower than corresponding Al/Si ratios in silicate minerals (Ragueneau et al., 2005). Of the checked $bSiO_2$ samples in this study, most had Al/Si ratios <50, usually much lower. Only five samples had a Al/Si ratio >50 (Fig. 3.8b). These are potentially contaminated with clay mineral-derived silicate, and the respective $\delta^{30}Si_{bSiO2}$ values are excluded from the further interpretation. However, there are several samples, which were considered to be clean (Al/Si <50) and which still revealed very low $\delta^{30}Si_{bSiO2}$ values (Fig. 3.5, 3.7, 3.8). Reason for this must be another contaminant source. For example, siliceous sponge spicules have very light isotope ratios of about -3‰ $\delta^{30}Si$ (Douthitt, 1982; De La Rocha, 2003; Hendry et al., 2010), and radiolarians can be isotopically light as well. A bias to more negative $\delta^{30}Si_{bSiO2}$ ratios due to a contamination with non diatom $bSiO_2$ is the most likely explanation for the overall too low $\delta^{30}Si_{bSiO2}$ values, which is supported by the fact that the highest offset from expected values occurs in those sediments containing the lowest amounts of $bSiO_2$, especially along the northern part of the shelf region (Fig. 3.5 and 3.7). A separation of diatoms from $bSiO_2$ of different origin is not possible with the applied heavy liquid separation method, and sponge spicules and

diatoms do not show a difference in resistivity to dissolution processes during the preparation for Si isotope analyses.

In order to exclude the contamination hypothesis, large diatoms were hand-picked from the same sediment samples. As far as currently known, all diatoms fractionate $Si(OH)_4$ in the same way, independent of species, temperature (De La Rocha et al., 1997) and salinity (Alleman et al., 2005). However, the picked diatom $\delta^{30}Si_{diatom}$ values are significantly different from bulk $\delta^{30}Si_{bSiO2}$ and range from +0.58‰ to +1.95‰ (Fig. 3.5, Table A.2). Different diatom assemblages might represent different times of upwelling season, and can therefore be influenced by different source water signatures. The $bSiO_2$-fraction probably consists mostly of specimens of *Chaetoceros* (resting spores) and *Thalassionema*, the two most abundant species along the Peruvian shelf (Abrantes et al., 2007), which are both indicative of strong upwelling conditions (Schrader and Sorknes, 1991; Abrantes et al., 2007). The large fraction probably mostly contained specimens of *Coscinodiscus*, large-centric diatoms which are especially abundant in tropical-oceanic (low-nutrient) waters or when upwelling is weaker (which would be an explanation for the higher $\delta^{30}Si_{diatom}$ values) (De Vries and Schrader, 1981; Brodie and Kemp, 1994). Sedimentation rates along the Peruvian shelf are highly variable. At 12°S, mostly characterized by strong upwelling it accounts for ca. 0.13 cm/yr (Munoz et al., 2004). On average, the first cm of the sediment, which is always used here, will probably integrate the utilisation signal over ca. 10 years/growing seasons. Within the main upwelling region between 10 to 15°S, where $bSiO_2$ concentrations are highest (Fig. 3.5b), $\delta^{30}Si_{bSiO2}$ and $\delta^{30}Si_{diatom}$ agree very well (Fig. 3.5a). Even if both assemblages reflect different growing seasons, the source water conditions in that area obviously do not change significantly throughout the whole year. Further to the north, especially north of 5°S, there is a general offset of up to 1.3‰ between both sedimentary phases (Fig. 3.5), and the $\delta^{30}Si_{diatom}$ seem to reflect measured surface water $\delta^{30}Si_{Si(OH)4}$ (Fig. 3.5a). Here, $bSiO_2$ concentrations are lowest (Fig. 3.5b), and a potential contamination is most likely. The offset could, however, also be the reflection of the different growing conditions. For the samples north of 5°S having a mean $\delta^{30}Si_{bSiO2}$ of

+0.6‰ this would indicate surface water $\delta^{30}Si_{Si(OH)4}$ of around +1.7‰ (assuming a fractionation between both phases of -1.1‰ (De La Rocha et al., 1997)). This is a very low signature comparable to the values measured in the main upwelling region, but the northerly region does not experience such strong upwelling and nutrient supply (Karstensen and Ulloa, 2008). Another interesting feature are the low $\delta^{30}Si$ values in both $bSiO_2$ and in the picked diatoms south of 15°S, which, except for one $bSiO_2$ sample, do not differ significantly from a value of about +0.6‰. In contrast, the present day surface waters in that area have high $\delta^{30}Si_{Si(OH)4}$ values of about +2.7‰. South of 14°S the northward flowing PCoastalC may have had an influence on the $\delta^{30}Si_{diatom}$ and $\delta^{30}Si_{bSiO2}$ signatures. This current originates in the south, and is characterised by lower $Si(OH)_4$ concentrations. A lighter $\delta^{30}Si_{Si(OH)4}$ signature of this current is possible, although not clearly detectable in the water column (Fig. 3.2), but may have influenced the isotopic signature of the diatoms over a longer time scale. Furthermore, a transport of isotopically lighter diatoms within the PCoastalC is also a possible scenario.

Overall, the $\delta^{30}Si_{diatom}$ samples seem to preserve the utilisation signal much better and more reliably. The $\delta^{30}Si_{diatom}$ data show almost the same distribution pattern as the $\delta^{30}Si_{Si(OH)4}$ in the surface waters. They are low in the main upwelling region, and show much higher values along the northern part of the shelf between 5°S to 10°S. The sedimentary diatoms can be used to reconstruct past-surface water utilisation rates. Therefore, the fractionation factor of -1.1‰ between diatoms and surface water is applied (Fig. 3.9). Hand-picked diatoms, which have $\delta^{30}Si_{diatom}$ values ranging between +0.6‰ and +2.0‰, reflect surface water $\delta^{30}Si_{Si(OH)4}$ values between +1.7‰ and +3.1‰. Under steady state conditions this requires surface water utilisation rates between 50 and ca. 100%. In contrast, the $\delta^{30}Si_{bSiO2}$ range between -1.0‰ and +1.1‰, indicating surface water $\delta^{30}Si_{Si(OH)4}$ values between +0.1‰ and +2.2‰. For these samples, the utilisation rates range between 0 to 70% (Fig. 3.9). That is much lower than the present-day observed one. Such low utilisation rates might occur during different times of the year, but is not very likely that it is a persistent feature.

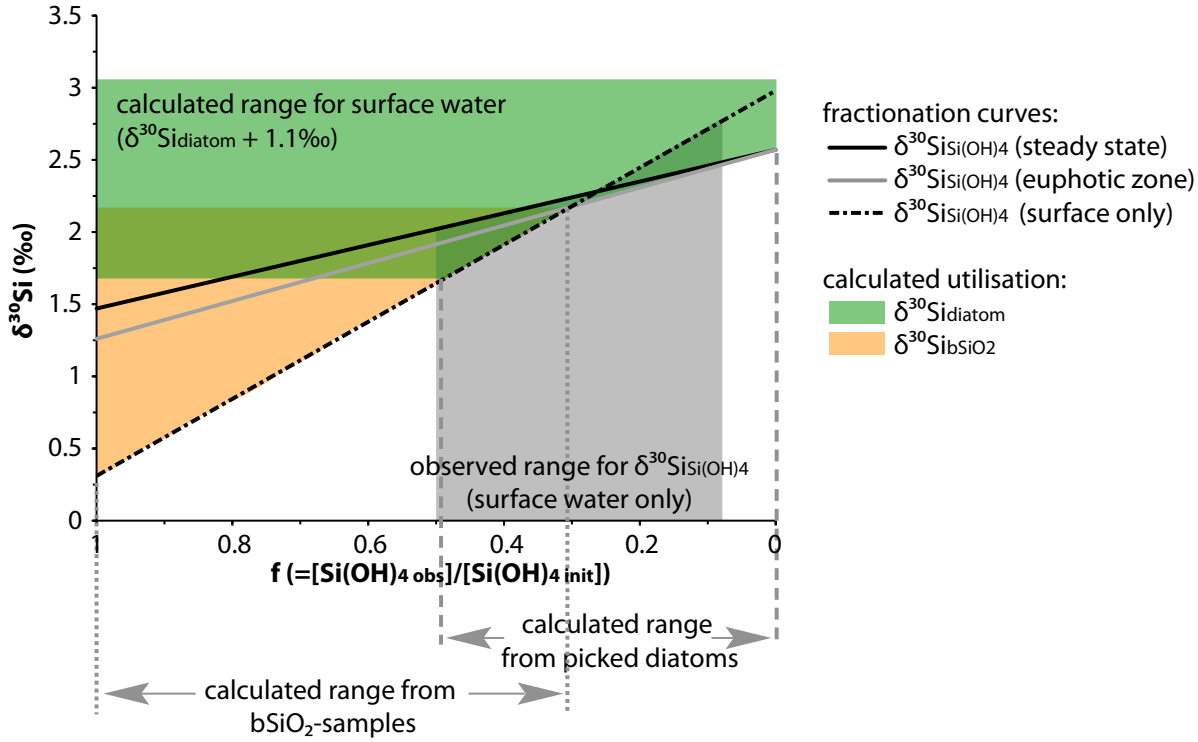

Figure 3.9: $\delta^{30}Si$ (‰) versus f. The curves indicate the fractionation behaviour for steady state-type conditions for surface water for a theoretical fractionation of -1.1‰ (solid black), where the dashed black curve and the solid grey curve indicate the fractionation behaviour for surface water samples only (fractionation factor -2.7‰) and for the euphotic zone (fractionation factor -1.3‰) from measurements in the euphotic zone (see Fig.3. 6a and 3.b). The grey shading indicates the observed range of measurements in the surface water, whereas the green and orange shadings indicate the theoretical surface water conditions calculated from picked diatoms and $bSiO_2$ surface sediment samples (measured $\delta^{30}Si$ + 1.1‰).

Although the actual values indicate a transfer of the surface water signal into the sediment, the picked diatoms integrate the surface water signal over the whole growing season as well as many years, and (partial) dissolution, along-shelf transport, as well as different conditions during single years (e.g. El Niño events) are very likely to influence the deposited signature, which has to be taken into account for interpretations of past upwelling conditions. Even if we assume a higher fractionation of $Si(OH)_4$ in the surface water during El Niño conditions due to diminished upwelling (Feldman, 1984, Fiedler, 2002), this signature is obviously not preserved in these sediments given that the highest $\delta^{30}Si_{Si(OH)4}$ in surface water and the $\delta^{30}Si_{diatom}$ values from hand-picked surface sediment diatoms agree relatively well (Fig.3.5a and 3.9). The reason for this is probably that the majority of the diatoms grow under “normal” conditions, and

that under e.g. El Niño conditions no significant amounts of diatoms are produced at the surface that could transfer the surface water fractionation signal into the underlying sediments.

The general assumption for all paleo-studies using Si isotopes as a paleo-proxy for $Si(OH)_4$ utilisation is that the major fraction of the $bSiO_2$ in the sediment consists of diatoms (De La Rocha et al., 1998; Brzezinski et al., 2002; Beucher et al., 2007; Reynolds et al., 2008). This is probably justified for studies of the Southern Ocean or the Subpolar North Pacific where $bSiO_2$ concentrations are usually higher than 10-20 wt%. However, the surface sediment distribution of $bSiO_2$ off Peru today (Fig. 3.5b) shows strong latitudinal gradients between high and low silica concentrations due to differences in upwelling intensity and nutrient supply. Paleo-studies in this area will focus on questions related to how upwelling intensity changed in the past. During times of overall low upwelling, the concentration of $bSiO_2$ will have also been low in areas where it is high today. In this case, a significant influence of non-diatom $bSiO_2$ cannot be excluded, unless all samples are hand-picked to avoid contamination. Correlations between $bSiO_2$ concentration in the sediment, $\delta^{30}Si_{bSiO2}$, and $\delta^{30}Si_{diatom}$ indicate that off Peru a minimum concentration of 5-10 wt% $bSiO_2$ is necessary to ensure that sufficient amounts of diatoms are present in the sediment to exclude a significant influence of non diatom $bSiO_2$ material.

3.5 Conclusions

Subsurface waters, which feed the coastal upwelling off Peru display a mean $\delta^{30}Si_{Si(OH)4}$ signature of +1.5 ± 0.2‰ all along the Peruvian shelf, whereas the $Si(OH)_4$ concentration increases with latitude towards the south as a function of water mass mixing and the remineralisation of $bSiO_2$ in the water column and in the sediments, as indicated by significant increases in $Si(OH)_4$ concentrations in the bottom waters above the shelf. The $\delta^{30}Si_{Si(OH)4}$ distribution in the surface waters along the Peruvian shelf is controlled by the upwelling intensity, i.e. an interplay between the supply of $Si(OH)_4$ and water mass mixing. In the area of the strongest upwelling and re-supply of $Si(OH)_4$, where

the degree of utilisation of $Si(OH)_4$ is overall low (about 50%), the increase in surface water $\delta^{30}Si_{Si(OH)4}$ compared to the subsurface source waters is small, only 0.2-0.3‰. Higher degrees of $Si(OH)_4$ utilisation (up to 93%) in surface waters outside the main upwelling area result in higher $\delta^{30}Si_{Si(OH)4}$ values of up to 2.8‰, corresponding to a difference of up to 1.2 ‰ from the source water.

The calculation of the fractionation factor ε based on our data gives values between -0.5‰ and -2.7‰ for Rayleigh-type and steady-state system conditions, respectively. This is a large deviation from the experimentally derived value of -1.1‰, which is caused by the strong influence of water mass mixing in this highly dynamic environment. However, all euphotic zone $\delta^{30}Si_{Si(OH)4}$ reveal a fractionation factor of -1.3‰ for steady state conditions, which is very similar to the experimental one, and which also seems realistic given the environmental conditions. Comparison of $\delta^{30}Si_{diatom}$ compositions obtained from hand-picked diatoms from the underlying sediments, which range from 0.58‰ to 1.95‰, shows the same overall distribution as that of $\delta^{30}Si_{Si(OH)4}$. The silicate of these diatoms exhibits lower $\delta^{30}Si_{diatom}$ values in the main upwelling region, where productivity is highest. Along the northern shelf between 5°S to 10°S, where upwelling and productivity are lower, the $\delta^{30}Si_{diatom}$ values are higher.

A comparison between $\delta^{30}Si_{bSiO2}$ signatures obtained from bulk $bSiO_2$ in the sediment, which was extracted applying commonly used methods, and $\delta^{30}Si_{diatom}$ from hand-picked diatoms indicates that in samples with low $bSiO_2$ concentrations a contamination with isotopically lighter siliceous material, such as sponge spicules or radiolarians, occurs. This observation has important implications for the general interpretation of paleo-$\delta^{30}Si$ records at locations with low $bSiO_2$ content and suggests that for sediments containing such low amounts of $bSiO_2$ significant biases of the $\delta^{30}Si$ records can only be excluded if it can be demonstrated that a pure diatom fraction was extracted.

CHAPTER 4

Cycling of Silicic Acid and Nitrate in the Eastern Equatorial Pacific: Insights from Silicon and Nitrogen Isotopes*

Abstract

In this study we present the first direct comparison between dissolved stable silicon ($\delta^{30}Si(OH)_4$) and nitrogen ($\delta^{15}NO_3^-$) isotopes in the upwelling area off Peru to investigate the biogeochemical processes controlling nutrient cycling in one of the globally largest Oxygen Minimum Zones (OMZs). Silicic acid is a key nutrient for diatoms, which dominates the phytoplankton assemblages in upwelling areas. Silicon and nitrogen isotopes in the euphotic zone of the upwelling area are shown to be mainly controlled by biological utilization during which the lighter isotopes are preferentially incorporated into the organic matter. Silicon isotopes are subject to a relatively simple cycling only influenced by utilization and subsequent dissolution of the diatoms. In contrast, there are additional processes exerting control the N isotope composition of nitrate including anoxic ammonium oxidation (anammox) and/or denitrification within the OMZ. Given that the water masses feeding the coastal upwelling cells originate from the suboxic zone, the surface waters near the shelf show low $\delta^{30}Si(OH)_4$ values (2‰) under strong upwelling conditions corresponding to high $\delta^{15}NO_3^-$ values (14‰). During the cruise a large mesoscale eddy moved westward through the study area and clearly influenced the nutrient stable isotope composition, as well as the phytoplankton community.

**A version of this chapter is going to be submitted to Biogeosciences as:*

Patricia Grasse, Evgenia Ryabenko, Jasmin Franz, Claudia Ehlert, Mark A. Altabet, Douglas W. R. Wallace & Martin Frank. Cycling of Silicic Acid and Nitrate in the Eastern Equatorial Pacific:Insights from Silicon and Nitrogen Isotopes

A pronounced silicic acid limitation in the centre of the eddy structure is indicated by high NO_3^-:$Si(OH)^4$ ratios (~15) leading to the highest $\delta^{30}Si(OH)_4$ values (3.7‰) accompanied by high $\delta^{15}NO_3^-$ values (16‰). The results also show that water mass mixing and remineralization processes influence the dissolved nitrogen and silicon isotope composition. Due to grazing of zooplankton a larger fraction of the nitrogen is recycled within the upper water column compared to silicic acid, which is more efficiently transferred to the deep waters. This is indicated by a smaller degree of utilization for nitrate in comparison to silicic acid in the study area. The combination of $\delta^{30}Si(OH)_4$ and $\delta^{15}NO_3^-$ can help to better understand paleo records and to disentangle utlization and N-loss processes.

4.1. Introduction

The upwelling area off Peru is characterized by high primary productivity (Thiede and Suess, 1983; Berger et al., 1989, Pennington et al., 2006) and one of the globally largest Oxygen Minimum Zones (OMZ, Karstensen et al., 2008; Fuenzalida et al., 2009) with oxygen levels below 5µmol/kg between 100 and 500 m water depth (Karstensen et al., 2008). The extent and strength of the OMZ is a function of ventilation and primary productivity in the euphotic zone stimulated by upwelling, and exerts major influence on nutrient cycling. The main water masses supplying the Peruvian upwelling (Fig. 4.1) are the southward flowing Peru-Chile Countercurrent (PCCC) and the Peru-Chile Undercurrent (PCUC). The PCUC is flowing along the shelf between 50 and 150m depth and is the main source for the coastal upwelling (Huyer et al., 1987; Karstensen and Ulloa, 2008). The northward flowing currents are the Peru Chile Countercurrent (POC), the PeruCoastalCurrent (PCoastalCurrent) and the Peru-Chile Current (PCC) at distances of approximately 100 to 300km from the shore (Strub et al., 1998; Penven et al., 2005; Karstensen and Ulloa, 2008). In equatorial regions westward flowing surface currents including the South Equatorial Current (SEC) produce an eastward pressure gradient. This is the force driving the Equatorial Undercurrent (EUC) and the Southern Subsurface Countercurrent (SSCC) to flow eastward along the equator and to supply

oxygen-rich waters to the upwelling area (Brink et al., 1983; Toggweiler et al., 1991; Fiedler and Talley, 2006). In addition, the complex current system off Peru is influenced by mesoscale eddies, which transport shelf waters offshore (Chaigneau et al. 2008).

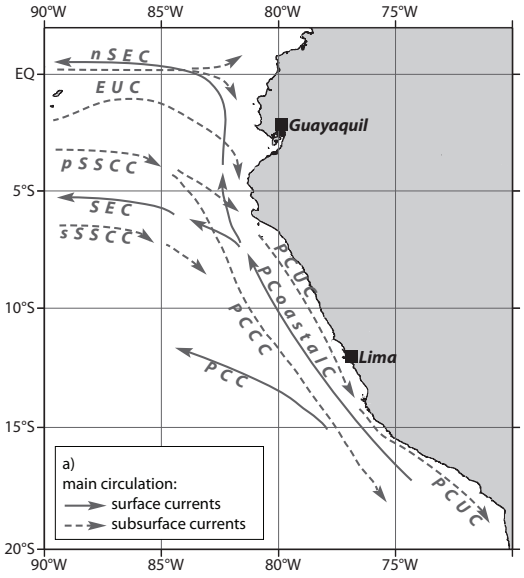

Fig. 4.1: Schematic surface (solid grey lines) and subsurface (dashed grey lines) currents off Peru. (PaC: Panama Current, EUC: Equatorial Undercurrent, pSSCC: primary Southern Subsurface Countercurrent, sSSCC: secondary Southern Subsurface Countercurrent, SEC: South Equatorial Current, PCUC: PeruChile Undercurent, PCC (also called Humboldt current); Peru-Chile current, PCCC: Peru-Chile Countercurrent, POC: Peru Oceanic Current according to Strub et al., 1998: Penven et al., 2005; Kessler et al., 2006; Ayon et al., 2008; Karstensen and Ulloa, 2008; and ADCP data according to Czeschel et al., 2011).

The dominant phytoplankton species in the upwelling region are diatoms (Estrada & Blasco, 1985; Abrantes, 2007), which require silicic acid for the formation of their biogenic opal shells (Lewin, 1961) and which contribute with up to 45% of the total oceanic production (Mann, 1999). Thus diatoms are also important for carbon sequestration to the deep ocean (Allen et al., 2005; Smetacek, 1985) although the present day Peruvian upwelling area is considered a source rather than a sink of CO_2 (Friedrich et al., 2008). Due to the upwelling of subsurface waters the shelf regions show generally show high phosphate, silicic acid and iron concentrations (Bruland et al., 2005) inducing high productivity. In contrast, the offshore waters are rather characterized by high nutrient, low chlorophyll (HNLC) conditions (Thomas, 1979, Strickland et al., 1969, Minas and Minas 1992). In general, HNLC regions tend to become Si limited due to grazing pressure by zooplankton and therefore enhanced regeneration of N over Si (Dugdale & Wilkerson, 1998) which is also called the silicate pump (Dugdale et al., 1995). Both the biogenic silicate (bSi) dissolution and nitrogen recycling depend on a number of factors, including water

temperature, nutrient conditions, particle sizes, and zooplankton grazing (Ragueneau et al., 2000, Jiang et al. 2003 and references therein). The phytoplankton uses both, new and recycled nitrogen in the form of different N-species including nitrate (NO_3^-), nitrite (NO_2^-) and ammonia (NH_4^+) to balance their uptake of $Si(OH)_4$, whereas uptake of ammonia have the lowest energetic expenses. Diatoms normally incorporate NO_3^- and $Si(OH)_4$ in a 1:1 ratio (Ragueneau et al., 2000), but stress, such as iron limitation can lead to an enhanced uptake of $Si(OH)_4$ compared to nitrate resulting in thicker frustules of the diatoms (Hutchins and Bruland, 1998; Takeda, 1998; Franck et al., 2000). The ratio of nitrate to silicic acid can be applied as an indicator for silicic acid and nitrate limitation such that NO_3^-: $Si(OH)_4$ below one already causes stress for the diatoms (Conley and Malone 1992; Wilkerson and Dugdale, 1996).

Silicon and Nitrogen isotopes are powerful tools to investigate biological processes and nutrient cycling. They can be used as indicators for utilization processes because the lighter isotopes are preferentially incorporated into the organisms (e.g. DeNiro and Epstein, 1981; De LaRocha et al., 1997). Silicic acid is fractionated during incorporation into diatoms with a fractionation factor of -1.1‰ (De La Rocha et al., 1997), which leaves the surrounding seawater enriched in heavy isotopes. Nitrate utilization by organism causes a fractionation of 3 to 6 ‰ per trophy level (DeNiro and Epstein, 1981; Minagawa and Wada, 1984), which means that primary producers are isotopically depleted compared to the surrounding seawater. In OMZs, however, a range of other processes occur that influence the nitrogen isotope composition. Low oxygen concentrations (2 to 10 µmol/l) induce N-loss processes, such as denitrification ($NO_3^-\rightarrow NO_2^-\rightarrow NO\rightarrow N_2O\rightarrow N_2$) and/or the more direct anammox process ($NH_4+NO_2^-\rightarrow N_2$; Codispodi, 2007; Lam et al., 2009). While these N-loss processes increase the $\delta^{15}NO_3^-$ of seawater by approximately 20‰ to 30‰, nitrite oxidation leads to a lowering of the $\delta^{15}NO_3^-$ values in the water column (Brandes et al., 1998; Voss et al., 2001; Pantoja et al., 2002, Casciotti et al., 2009).

Silicic acid and nitrate are important nutrients within the marine biogeochemical cycles, which is why it is crucial to understand the interplay of

the factors controlling the $Si(OH)_4$ and NO_3^- budgets and the supply of these nutrients to the euphotic zone including primary productivity, remineralization processes and water mass mixing. In order to investigate these factors we analyzed nutrient concentrations and the stable isotope composition of dissolved $Si(OH)_4$ and NO_3^- in the water column along a section perpendicular to the coast line at 10°S in the Eastern Equatorial Pacific.

4. 2 Material & Methods

All samples were collected during cruises M77-3 with the German RV Meteor between December 2008 and January 2009 in the frame of the Collaborative Research Centre (SFB) 754: Climate – Biogeochemistry Interactions in the Tropical Ocean. Seawater samples were collected along a transect at 10°S approximately perpendicular to the Peruvian Coast (Fig. 4.2, Table A.4).

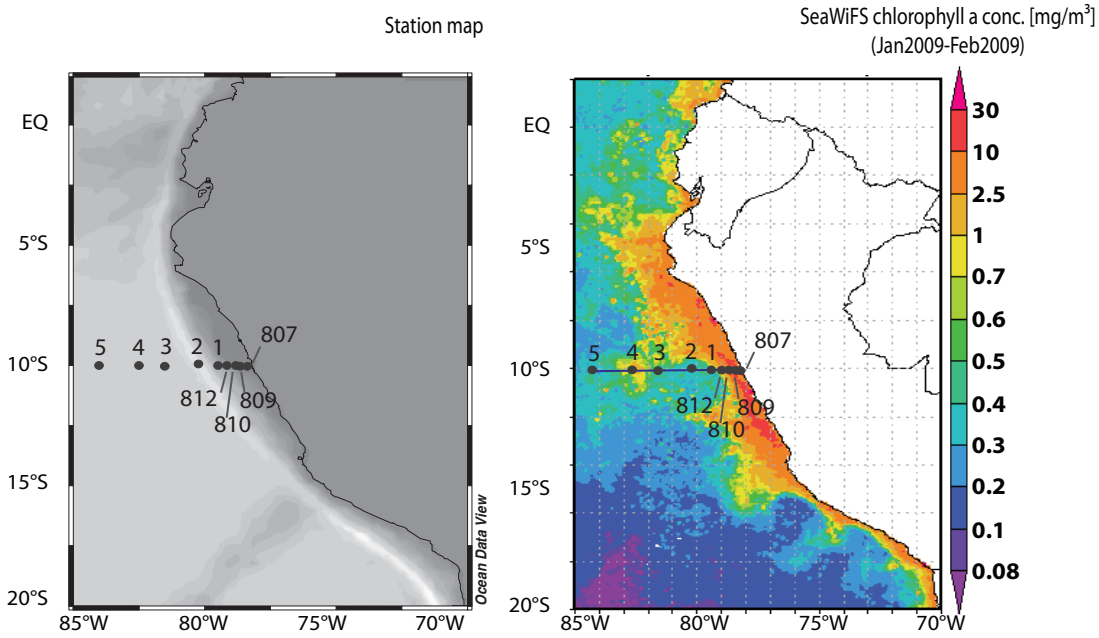

Fig. 4.2: Sampling locations and bathymetry (left) and chlorophyll a concentrations (mg/m^3, right) off the Peruvian shelf. Chlorophyll concentrations were obtained from the NASA Giovanni website (http://disc.sci.gsfc.nasa.gov/giovanni/overview/index.html) for January and February 2009. For stations 1 and 3 no silicon isotope measurements were carried out.

Seawater samples for analysis of silicon isotope, nitrogen isotope, nutrient and oxygen concentration measurements were collected using a Seabird CTD

Rosette System equipped with oxygen sensors. Samples for nutrient measurements were frozen (-20°C) on board immediately after sampling and measured in the laboratory of the Max-Planck Institute (MPI) for Marine Microbiology in Bremen, Germany. Nutrient concentrations were measured following (Grasshoff et al., 1999). $Si(OH)_4$ concentrations of frozen samples were compared to filtered and acidified (non frozen) samples and the reproducibility ranged between 5 and 10%. Oxygen concentrations were determined with the O_2-sensor of the CTD and were later calibrated with bottle data obtained by Winkler titration (Winkler, 1888). Seawater samples for silicon isotope measurements were immediately filtered on board through nitrocellulose acetate filters (0.45µm pore size) and were than acidified with HCl to pH 2. At GEOMAR Si was separated from the samples using a brucite-coprecipitation method (Reynolds et al., 2006; after Karl and Tien, 1992). Only samples with yields >97% were accepted for isotopic measurements given that incomplete precipitation would lead to isotopic fractionation of the Si in the samples. For Si isotope measurements, samples were purified following the method by Georg et al. (2006) and measured on a *NuPlasma* MC-ICPMS (Nu instruments) at GEOMAR (for a detailed description see chapter 3). Concentration measurements of particulate organic carbon (POC), particulate organic nitrogen, particulate organic phosphate, biogenic silicate (bSi), dissolved organic nitrogen (DON) and dissolved organic phosphate (DOP) were adapted from Franz et al. (2011).

The isotopic composition of dissolved NO_3^- was measured using Cd-reduction to NO_2^- followed by reaction with azide to produce N_2O (McIlvin and Altabet, 2005). NaCl was added to ensure consistent quantitative yields (Ryabenko et al, 2009). Samples were analyzed in both Germany (GEOMAR) and the USA (SMAST) using a purge-trap isotope ratio mass spectrometer (PT-IRMS) system.

Si and N isotope compositions are reported in the δ notations representing the deviations of the isotope ratios of the samples from that of a reference standard in parts per thousand (‰):

$$\delta^{30}Si/\delta^{15}N = \left(\frac{R_{sample}}{R_{std}}\right) * 1000$$

R_{sample} represents the ratio of the measured heavy isotope against the light isotope ($^{30}Si/^{28}Si$, respectively $^{15}N/^{14}N$), whereas R_{std} denotes the isotope ratio of the reference standard. For silicon isotopes the NBS28 standard is used, whereas nitrogen isotopes are given relative to the N isotope ratio of air. Repeated Measurements of in-house standards and samples over longer periods of time gave a reproducibility of 0.3‰ ($2\sigma_{sd}$) for silicon isotope measurements and 0.2‰ ($2\sigma_{sd}$) for nitrogen isotope measurements.

4.3 Results

4.3.1.Hydrographic Setting of the Study Area

During the time of sampling in January 2009 a large anticyclonic coastal Eddy was observed to move westward in the study area (Fig 4.2). The eddy structure showed high chlorophyll a concentrations (~ 2.5 to 20 mg/m^{-2}) in its periphery and low chlorophyll concentrations in its centre (~ 0.3 to 0.5 mg/m^{-2}). The inner diameter of the eddy structure amounted to approximately 300 km and elevated chlorophyll concentrations of the outer filament were detected to a longitude of 82°W corresponding to the location of station 3, whereas station 2 was located within the centre of the eddy with low chlorophyll concentrations. The lower sea surface temperature at station 3 (Fig. 4.3) also indicates the influence of upwelled shelf waters transported offshore by the eddy structure.

The sampling locations (St. 807, 809 and 810) on the shelf were strongly influenced by upwelled waters indicated by low sea surface temperatures (Fig 4.3). Upwelled water masses on the shelf are mainly derives from the southward flowing PCUC, which is the main source for the upwelling on the shelf from a depth of 50m to 150m (Brink et al., 1983, Fig. 4.2).

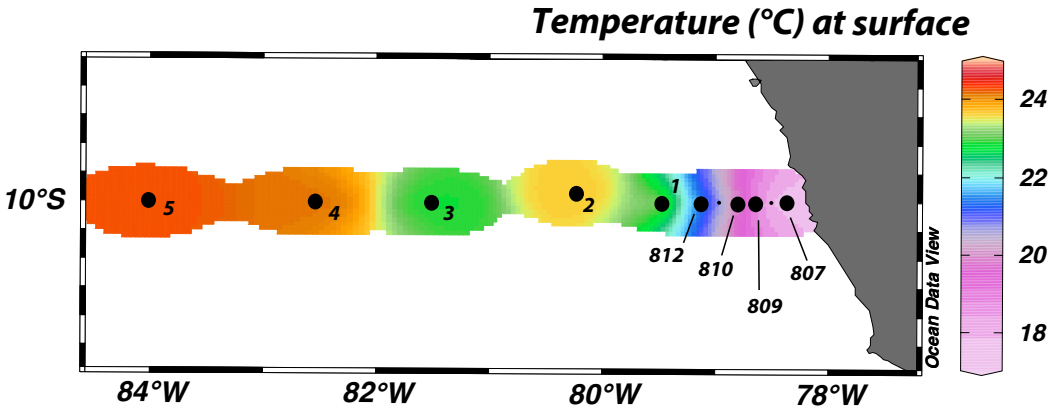

Fig. 4.3: Sea surface temperature (°C) along the 10°S transect reflecting upwelling intensity and water mass mixing.

Surface, subsurface and intermediate water masses along the 10° transect are influenced by currents from the south, as well as from the north as shown in Fig. 4.2 and Fig. 4.4. Unfortunately no ADCP data are available for the 10°S transect. The velocity distribution along the 14°S transect was, however, recorded in February 2009 during Meteor cruise M77-4 (Czeschel et al., 2011). At approximately 76°W the PCoastalC, a water mass originating from the south was detectable at depths of 100m to 200m. Between 76°W and 78°W the PCCC flowed south at depths of up to 500m. Another very prominent feature is the PCC, also called Humboldt Current (HC) at approximately 80°W, which originates in the south and is characterized by a pronouncedly strong velocity at the surface.

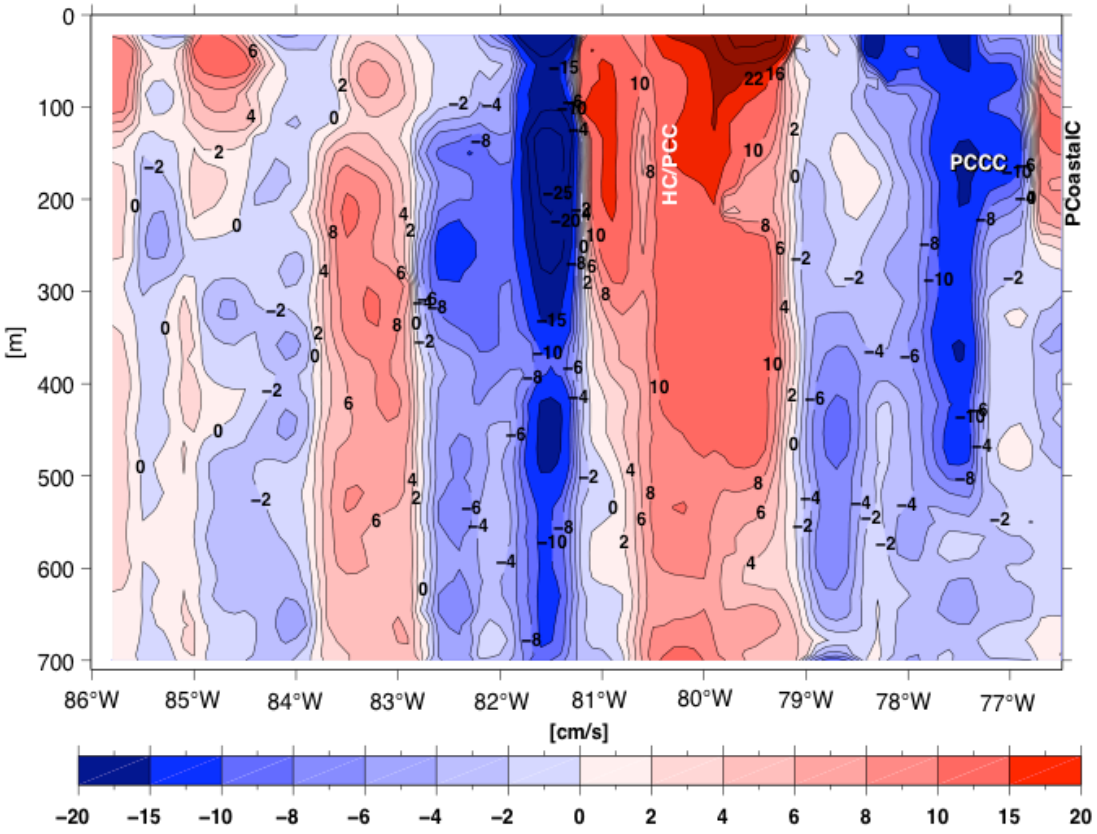

Fig. 4.4: Meridional velocity distribution (in cm s -1; positive northward along 14°S Transect (from Czeschel et al., 2011).

4.3.2 Distribution of $\delta^{30}Si(OH)_4$, $\delta^{15}NO_3^-$, Nutrient and Oxygen Concentrations along the 10°S Transect

Samples for $\delta^{30}Si(OH)_4$ and $\delta^{15}NO_3^-$, as well as nutrients were analyzed within the upper 500m of the water column along the 10°S transect. The silicic acid concentrations range from 0.4 µmol/kg in surface samples to 77 µmol/kg at depth (Fig. 4.5a) with $\delta^{30}Si(OH)_4$ from 1.1‰ to 3.7‰. The highest $\delta^{30}Si(OH)_4$ (3.7 ‰) is observed in surface water at station 2 (80°13'W) with silicic acid concentrations of 0.4 µmol/kg. Extremely high silicic acid concentrations within the OMZ of up to 30 µmol/kg are observed above the shelf (St.807), which correspond to low $\delta^{30}Si(OH)_4$ values (1.1‰).

Nitrate concentrations range from 2 to 52 µmol/kg with $\delta^{15}NO_3^-$ ranging form 3‰ to 25‰. The lowest nitrate concentrations are found in surface waters and on the shelf at approximately 70 to 100m depth (2 to 7 µmol/kg). Low nitrate concentrations are associated to the highest $\delta^{15}NO_3^-$ values of up to

25‰. Besides the shelf region and surface waters extremely high $\delta^{15}NO_3^-$ values (11‰ to 16‰) were also be observed at station 5 (83°5'W) at 150m depth and at stations 1 and 3 (79°28'W, respectively 81°30'W) at 300m depth. Within the oxycline at 80°13'W (St. 2, center of the eddy) extremely low $\delta^{15}NO_3^-$ values as low as 3‰ to 5‰ were measured at 60 to 80 depth (Fig. 4.5c &d).

The oxycline varied between 20 and 90m, whereby the shallowest oxycline was observed at station 807 on the shelf and the deepest one at St. 2. Below the oxycline oxygen concentrations are essentially always below 10µmol/kg (Fig. 4.5e).

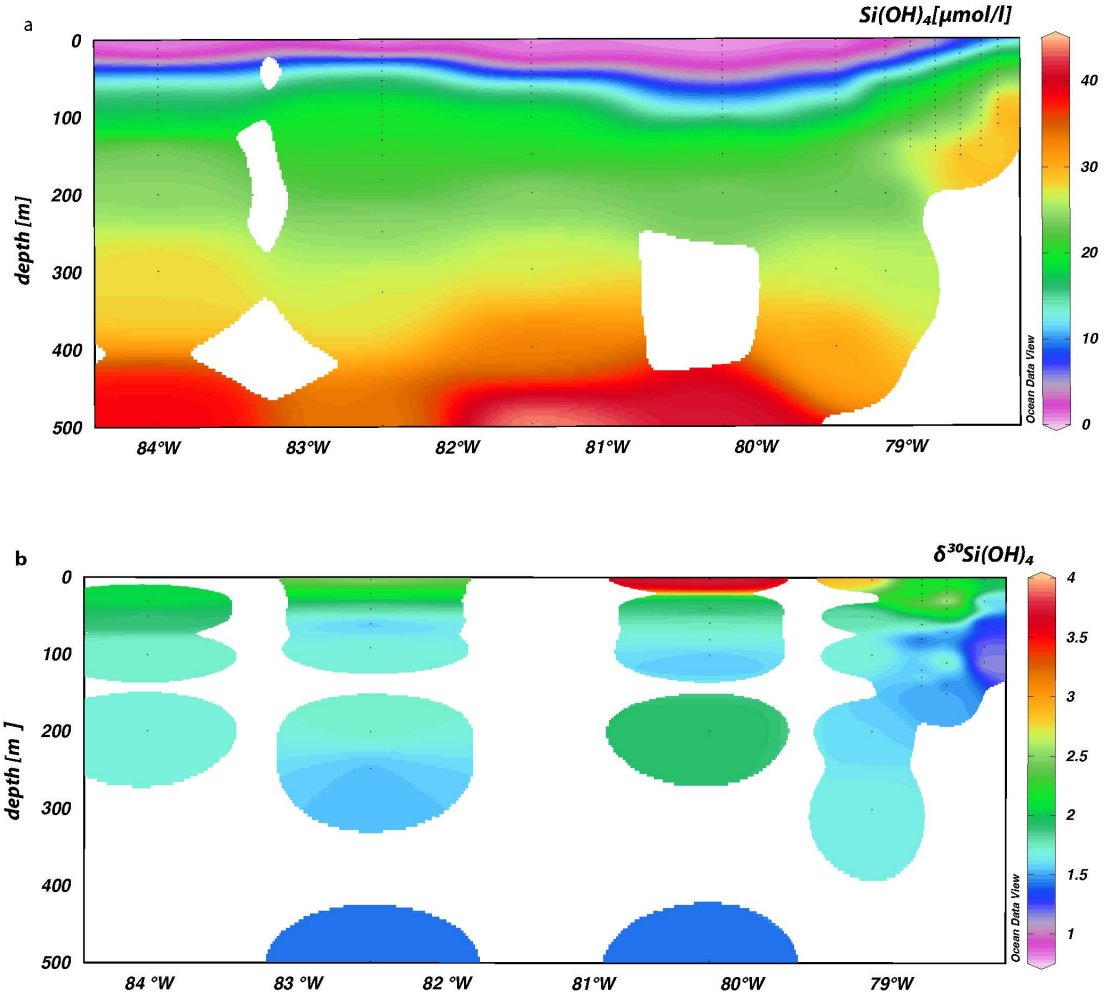

Fig. 4.5: Distribution of silcic acid concentrations (a), $\delta^{30}Si(OH)_4$ in ‰ (b), nitrate concentrations (c), $\delta^{15}NO_3^-$ in ‰ (d) and oxygen concentration (e) along the 10° transect.

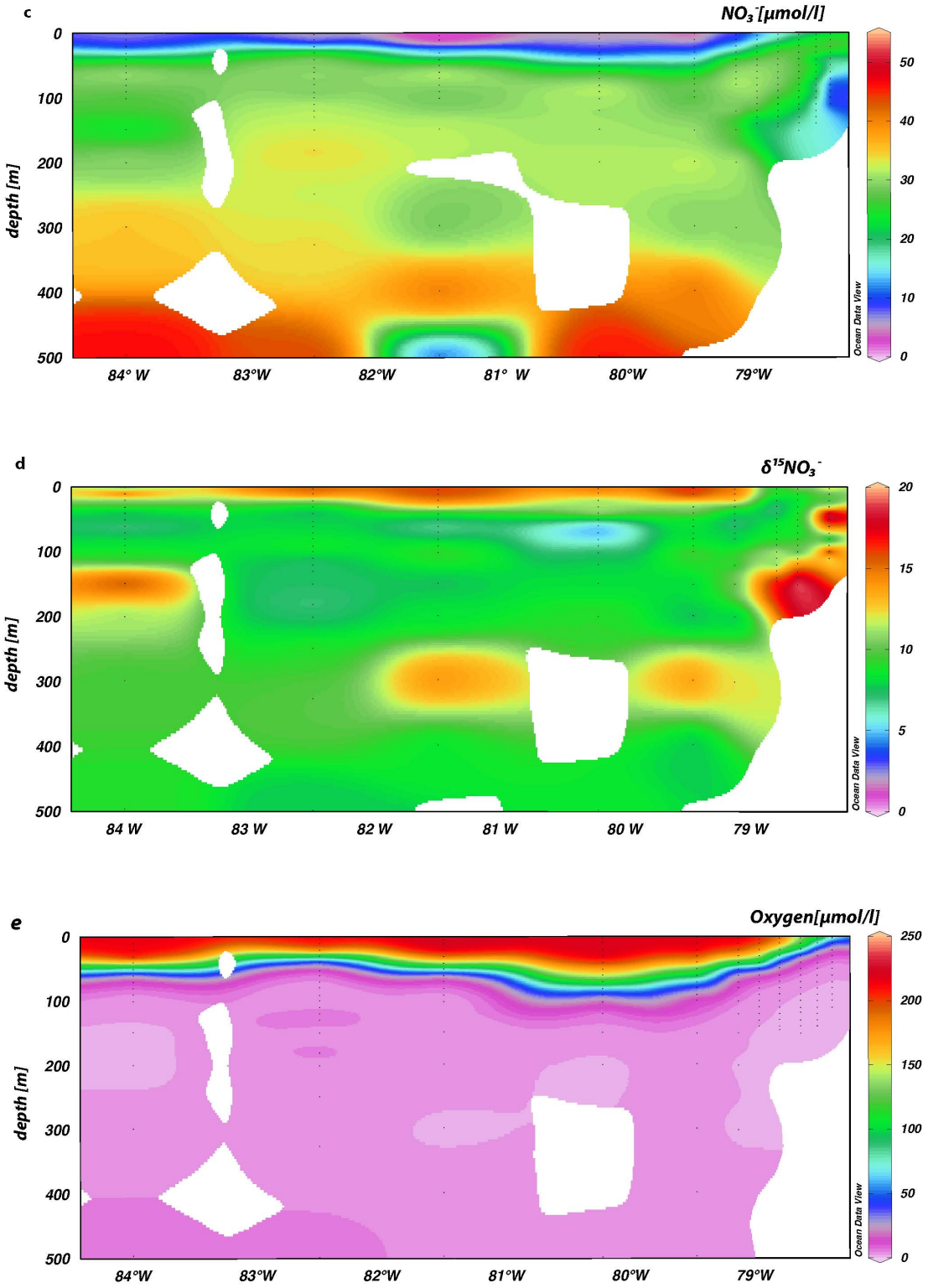

Fig. 4.5: Distribution of silcic acid concentrations (a), $\delta^{30}Si(OH)_4$ in ‰ (b), nitrate concentrations (c), $\delta^{15}NO_3^-$ in ‰ (d) and oxygen concentration (e) along the 10° transect.

4.3.2.1 Surface Waters along the 10°S Transect

The highest silicic acid concentrations in surface waters (10 µmol/kg) occurred above the shelf at approximately 78°W. With distance from the shelf the $Si(OH)_4$ continuously decreased to less than 1 µmol/kg. The highest nitrate concentrations were also measured on the shelf (21 µmol/kg). Generally nitrate concentrations were also diminished in the offshore samples, but the continuous decrease only reflects that of dissolved silicate until 79°30'W and then changes at low concentrations (2 to 7 µmol/kg) (Fig 4.6b).

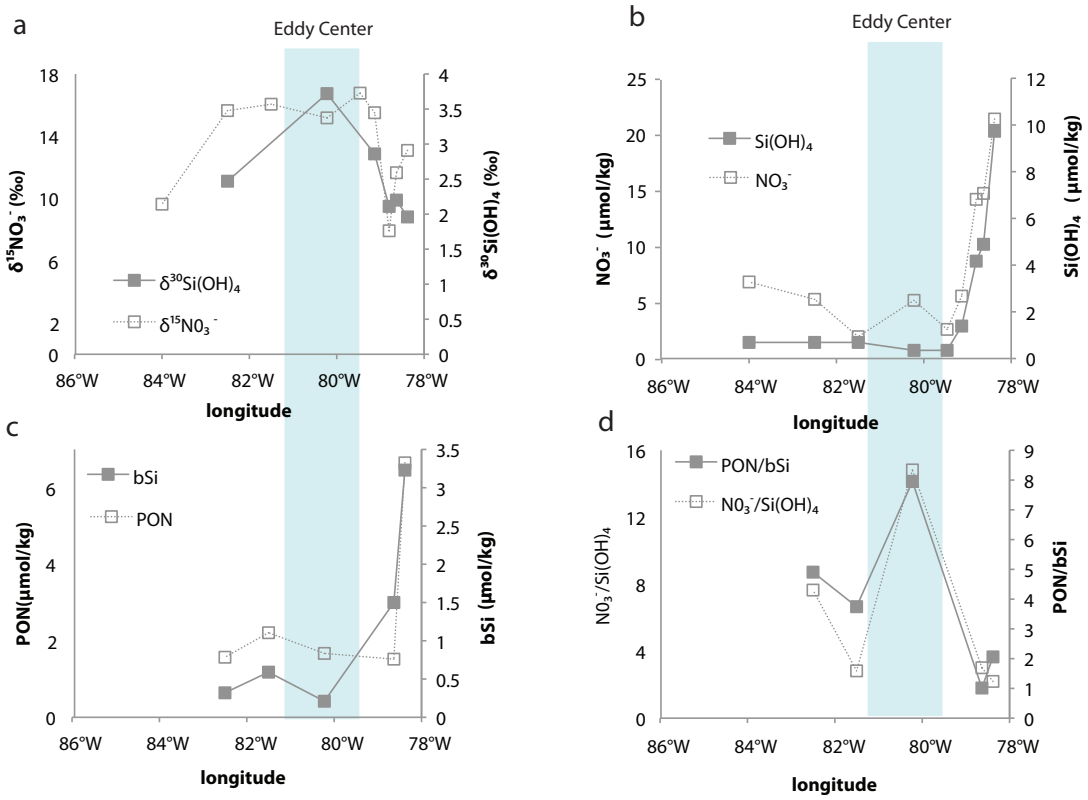

Fig. 4.6:a) Surface distribution of silicon and nitrogen isotope data, b) silicic acid and nitrate concentrations, c) biogenic silicate (bSi) and particulate organic nitrogen (PON) concentrations and d) the ratio of dissolved nitrate to silicate together with the ratios of the particulate phases (PON/bSI). The blue shaded area indicates the inner centre of an eddy structure (see also Fig. 4.1). PON and bSi is adapted from Franz et al. (2011).

On the shelf at approximately 78°W the lowest $\delta^{30}Si(OH)_4$ values (~2‰) occurred together with high $\delta^{15}NO_3^-$ (14‰). The highest $\delta^{30}Si(OH)_4$ value in in surface waters (3.7‰) corresponds to a very low bSi concentration (0.2 µmnol/kg) and the highest $NO_3^-/Si(OH)_4$ values (Fig. 4.6a &d). In Fig 4.6 the

location of the centre of the eddy is marked (Station 2), which is characterized by high $\delta^{30}Si(OH)_4$ (3.7‰) and $\delta^{15}NO_3^-$ (16‰) together with high PON to bSi ratios. At station 3 the PON/bSI ratios decrease to approximately 4, whereas at the shelf stations (St. 807 and St. 810) the ratios is between1 and 2 corresponding to low $NO_3^-/Si(OH)_4$ of 3 to 4.

4.3.2.2. Dissolution and N-loss processes within the OMZ

Within the OMZ at oxygen concentration below 5µmol/kg the lightest $\delta^{30}Si(OH)_4$ (1.1‰) values are observed at the highest silicic acid concentrations (33 µmol/kg), whereas low concentrations (~16 µmol/kg) show a larger range of $\delta^{30}Si(OH)_4$ signatures between 1.5‰ to 2.5‰. The relationship of the two parameters shows a rather weak correlation with r^2=0.29 (Fig. 4.7). Comparison between $\delta^{15}NO_3^-$ and nitrate (r^2=0.41) shows the highest $\delta^{15}NO_3^-$ (25‰) corresponding to very low nitrate concentrations (1.7 µmol/kg) and vice versa. A few samples show diminished Nitrate concentrations (< 10 µmol/kg), which are reflected by moderate fractionated waters (<14‰).

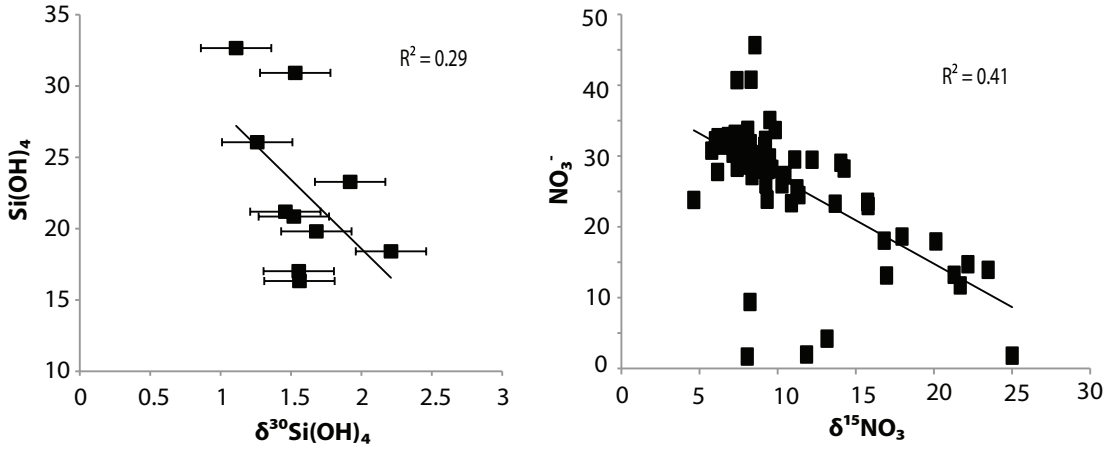

Fig. 4.7: $\delta^{30}Si(OH)_4$ (‰) versus silicic acid concentrations (left) and $\delta^{15}NO_3^-$ (‰) versus nitrate concentrations (right) for sample locations within the OMZ at oxygen concentrations below 5µmol/kg. Nutrient concentrations are in µmol/kg. Error bars are given in 2σ, for nitrate isotope samples the external error is smaller than the symbol size.

4.4 Discussion

4.4.1 Nutrient Utilization in Surface Waters

With distance from the shelf the silicic acid and nitrate concentrations in surface samples decrease systematically (Fig. 4.6a) which is not always directly reflected by their stable isotope compositions, as demonstrated in previous studies (e.g. Altabet and Francois, 1994, Reynolds et al., 2006; Ehlert 2011). This is explained by water mass mixing processes and/or other processes than utilization influencing the surface water isotope compositions. In general the isotope composition in seawater is enriched in heavy isotopes due to "preferred" incorporation of light isotopes into the organisms leading to higher $\delta^{30}Si(OH)_4$ and $\delta^{15}NO_3^-$ values. The silicon and nitrate isotope composition in seawater can only be directly compared on the shelf (St. 807, 809 and 810) where diatoms dominate the phytoplankton assemblages and are the main nitrate consumers (Parker et al., 2011), whereas further offshore the nitrate is also utilizated by non-siliceous organisms (Franz et al., 2011).

The lowest $\delta^{30}Si(OH)_4$ values (2‰) in surface waters are observed on the shelf corresponding to enhanced upwelling of silicic acid and therefore low utilization of the available silicic acid pool, as also shown by Ehlert et al. (2011). These signatures correlate to relatively high $\delta^{15}NO_3^-$ values (13‰, Fig. 4.6a), mainly because the water masses feeding the upwelling cells originate from the suboxic zone, where the nitrogen isotope signal is influenced by denitrification and/or anammox processes resulting in an increase of the $\delta^{15}NO_3^-$ signatures (e. g. Casciotti, 2009). Surface waters (between 50 to 100m depth) at St. 807 are clearly influenced by intense upwelling (Fig. 4.3) and show a mean $\delta^{15}NO_3^-$ values of 17‰ within the suboxic zone due to N-loss processes (Fig 4.5c & d). The surface waters at this station show even lower $\delta^{15}NO_3^-$ signatures than the subsurface source waters. Given that the isotopic fractionation of nitrate due to utilization ranges between 3‰ to 6‰ (e.g. DeNiro and Ebstein, 1981) a $\delta^{15}NO_3^-$ of approximately 20‰ would have been expected. Additionally also the nitrate concentrations in surface waters are higher, than in the subsurface (Fig. 4.5c). One possible explanation is that the surface waters mixed with water masses carrying a lower $\delta^{15}NO_3^-$ (8‰), such asthe PCC or the PCCC further away from

the coast (Fig. 4.4). This would be in agreement with the silicon isotope signature of the PCC and the PCCC, which show also a lower $\delta^{30}Si(OH)_4$ 1.5‰. However, intense remineralization of PON may also contribute to the isotope signature given that nitrate is more efficient recycled (up to 70%) in the mixed layer than silicic acid at proportions of approximately 50% (Dugdale & Wilkerson, 1998, Demarest et al., 2011). A study by Demarest et al. (2011) showed that up to 70% of nitrate that is taken up by phytoplankton is already regenerated in the euphotic zone rather than being supplied by upwelling waters. This is also supported by the high nitrate concentrations found in surface waters on the shelf despite that the PCUC, the source for the upwelling is characterized by generally low nitrate concentrations (Fig. 4.6b).

The highest $\delta^{30}Si(OH)_4$ values (3.7‰) in surface waters correlate to the highest NO_3^-:$Si(OH)_4$ ratios(~ 15) at 80°W in the centre of the mesoscale eddy (St. 2, Fig. 4.6a and 4.6d), which is most likely causes by a deepening of the thermocline. Ratios >1 already cause stress for diatoms (Conley and Malone, 1992), which is also reflected by the very low concentrations of particulate biogenic silicate (Fig. 4.6c). Highly depleted silicic acid concentrations at this station may also originate from northward flowing currents, such as the HC (also called PCC, Fig. 4.4), which it flowed along the high productivity area of the Chilean Coast before reaching the study area (Daneri et al., 2000). In general the NO_3^-:$Si(OH)_4$ ratios in equatorial upwelled source waters are below 2 (Wilkerson and Dugdale, 1996), which is also supported by the data of this study (Fig. 4.6d). At stations 3 and 4, which are characterized by slightly higher bSi and PON concentrations, relatively low $\delta^{30}Si(OH)_4$ values (2.5‰) and high $\delta^{15}NO_3^-$ (16‰) most likely reflect the isotope composition of surface waters on the shelf transported offshore and thereby getting enriched in their isotopic signal due to utilization (Fig. 4.6a &c).

For samples within the euphotic zone we calculated the fractionation factors for silicon and nitrogen isotopes (Fig. 4.8). In order to do this a source concentration for both systems was defined to calculate *f*, which is defined as the remaining fraction of the available pool of both nutrients. For better illustration we converted *f* to the percentage of utilization (1-*f* in %). Assuming a

source concentration in a system as dynamic as the Peruvian upwelling is challenging and associated with some uncertainties but it appeared most appropriate to use the concentrations of the upwelling source waters on the shelf. These waters were either transported westward by currents or within the eddy structure. Consequently these values should be reliable for most of the stations. Even though this is a very simplified attempt in regard to the complex water mass structure of the area. Given that nitrate is respired within the OMZ on the shelf, due to denitrification and anammox processes, the NO_3^- concentration of the source water has to be estimated from the observed NO_3^- concentration minus the observed phosphate concentration in its Redfield ration. The so-called Nitrogen deficit, also N* is defined as $NO_3^- - 16*PO_4$ (Gruber and Sarmiento, 1997). The source concentration of nitrate calculated from N* is most likely overestimated due to high phosphate fluxes on the shelf (Noffke et al., 2012), which would influence the calculations in the way that utilization factors are underestimated and the calculated fractionation factor is slightly biased.

The best model fit to the silicon isotope data is achieved by using a Rayleigh-type model leading to a fractionation factor of -0.4‰ and an initial source $\delta^{30}Si(OH)_4$ of 1.3‰ (for equations see Chapter 2). The nitrate isotope data are better explained by a steady state model with a fractionation factor of 18.4‰ and an initial source of 16.3‰ (Fig. 4.8). Whereas the fractionation factor for the incorporation of silicon into diatom valves from dissolved silicic acid is around -1.1‰ (De La Rocha et al., 1997), the average fractionation for nitrate is generally assumed to be -3 to -6% (DeNiro and Epstein 1981) and therefore the calculated fractionation factors are either underestimated in terms of silicic acid or overestimated for nitrate utilization. The underestimation of the silcic acid fractionation factor could be a result of dissolution processes within the euphotic zone. This would lower the dissolved $\delta^{30}Si(OH)_4$ and therefore the estimated fractionation factor, as already speculated by Beucher et al. (2011). The extremely high estimated fractionation factor for nitrate is clearly biased by the N-loss processes on the shelf and the alteration of the $\delta^{15}NO_3^-$ signal in the surface waters during offshore advection. Interestingly, the $\delta^{30}Si(OH)_4$ data

rather follow a Rayleigh-type model, which indicates nearly no new input of silicic acid into the pool, whereas the $\delta^{15}NO_3^-$ appears to be closer to a steady state system due to intense remineralization and therefore input of nitrate into the euphotic zone. The comparison of the utilization of $Si(OH)_4$ and NO_3 in the euphotic zone (Fig. 4.8) shows that nitrate is always less utilized than silicic acid, which could be a result of the intense recycling and lower degree of utilization from upwelled water (Demarest et al., 2011).

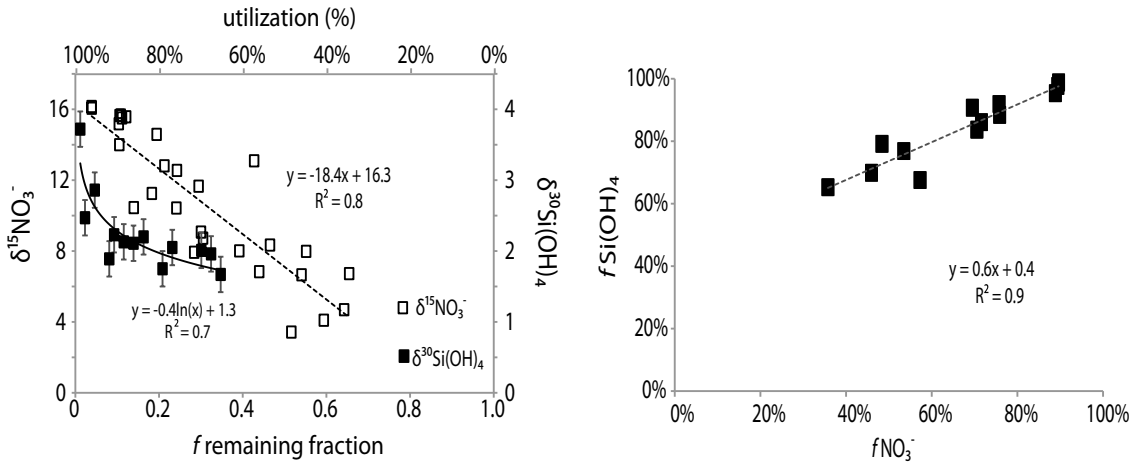

Fig. 4.8: Stable isotope composition against the remaining fraction of nitrate and silicic acid in the pool, respectively the utilization of the available pool (1-f in %) for samples within the euphotic zone. For silicon isotopes the best fit was obtained by a Rayleigh-type model model, whereas for the nitrate isotope data a steady state model appears more appropriate (left). Comparison of the degree of utilization of the available nutrient pool for silicic acid and nitrate for samples within the euphotic zone (right).

In general the offshore surface waters along the 10°S transect appear to be rather limited by the availability of silicic acid than by nitrate, as may be expected given that the N-loss occur within the suboxic zone (Fig. 4.7). No limitation in nitrate is most likely also the result of more efficient recycling of nitrate than of silicic acid (Dugdale and Wilkerson, 1998, Parker et al., 2011, Demarest et al., 2011). Furthermore silicic acid is transported to the deep ocean more efficiently. Dugdale et al. (1995) described this effect as the silicate pump and described the Eastern Equatorial Pacific as a HNLSLC (High nitrate, low silcic acid, low chlorophyll area). In general, high nutrient, low chlorophyll areas (HNLC) are controlled either by limitation of essential micronutrients, such as

iron (Bruland et al., 2001) or by grazing pressure of meso-and/or microzooplankton (Minas et al., 1986; Cullen et al., 1992).

4.4.2 Processes affecting the stable Si and N isotope composition within the OMZ

In general, the dissolution of $bSiO_2$ is highly influenced by physical parameters, such as temperature and pH (Lewin, 1961, Natori et al., 2006), but bacterial activity as it in the OMZ could lead to higher dissolution rates (Bidle and Azam, 1999; Bidle et al., 2002). Therefore we had a closer look at the silicon isotope distribution within the OMZ. The lowest $\delta^{30}Si(OH)_4$ values were measured above the shelf corresponding to high $Si(OH)_4$ concentrations (Fig. 4.6c & d). Given that the Si fluxes from the sediments on the shelf are extremely high (3600 $mmol/m^{-2}$ yr^{-1}, pers. communications A. Noffke) compared to for example fluxes around 400mm $mmol/m^{-2}$ yr^{-1} in the eastern south Atlantic. This is most likely a consequence of dissolution effects of bSi, which would lead to decreased $\delta^{30}Si(OH)_4$ values in the water column (Demarest et al. 2009). This is supported by the high bSi content on the shelf within the OMZ, where no active diatoms are present (Franz et al., 2011). This indicates efficient recycling of silicate on the shelf and in general in the upper water column as was already proposed by Nelson and Goering (1977) and Demarest et al. (2011). Fig. 4.7 shows only a weak correlation between $\delta^{30}Si(OH)_4$ and the silicic acid concentrations, but the silicon isotope signal may be also affected by mixing processes. In addition, the dissolution of diatom valves will lead to lower $\delta^{30}Si(OH)_4$ values with a fractionation factor of +0.5‰, which is low and differences are not easy to detect considering the external reproducibility of 0.3‰ by additional water mass. Nevertheless the lowest $\delta^{30}Si(OH)_4$ values (1.1‰) correspond to high $Si(OH)_4$ concentrations.

The lowest nitrate concentrations are found above the shelf (Fig. 4.5c & d) reflecting the highest $\delta^{15}NO_3^-$ values of 25‰. Nitrate isotopes within the OMZ are increased due to denitrification and anammox processes, which have fractionation factors ranging from 22 to 30‰ (Brandes et al., 1998; Voss et al., 2001). Even though N-loss processes occur within the OMZ, nitrate concentrations in surface water are never limited indicating again an efficient

recycling. For a better understanding of remineralization and dissolution processes within the OMZ, a comprehensive data set of particulate material and its isotopic composition together with the dissolved would be required.

4.5 Conclusions

In this study the first direct comparison between the stable isotope composition of Si in dissolved silicate ($\delta^{30}Si(OH)_4$) and N in dissolved nitrate ($\delta^{15}NO_3^-$) was carried out to better understand the biogeochemical cycling of silicic acid and nitrate in the Peruvian Upwelling area. Samples were taken along a 10°S transect perpendicular to the Peruvian coast, which was characterized by strong upwelling and therefore nutrient-rich surface waters nearshore and nutrient-depleted water further offshore. During strong upwelling near the shelf, low $\delta^{30}Si(OH)_4$ signatures (2‰) correspond to rather high $\delta^{15}NO_3^-$ (14‰), because the source waters are influenced by dissolution processes of bSi and N-loss processes within the OMZ. Even though nitrate concentrations are diminished within the OMZ and used by more phytoplankton species than silicic acid, the limiting macro nutrient further offshore was most $Si(OH)_4$. The direct comparison also showed that surface waters are strongly influenced by water mass advection and it has to be taken into account that nitrate is more efficiently recycled within the upper water column than $Si(OH)_4$ due to zooplankton grazing pressure, which may also have an influence on the isotopic signal. Within distance from the shelf the silicic acid and nitrate concentrations constantly decreased, which was not directly mirrored by the isotope compositions and demonstrates significant influence of water mass mixing, like admixture with the PCC and the PcoastalC from the south or the PCCC from the north. Additionally the study area was influenced by a large mesoscale eddy, which transports nutrients offshore and therefore stimulated phytoplankton growth at its edges, whereas the centre of the eddy was characterized by low chlorophyll concentrations. The surface waters in the centre of the eddy were characterized by low chlorophyll concentrations, strongly depleted in silicate and nitrate and therefore highly fractionated in $\delta^{30}Si(OH)_4$ (3.7‰) and $\delta^{15}NO_3^-$ (16‰). Eddies such as the one observed are

recurrent features that may have a major influence on the distribution and dynamics of nutrients and the stable isotope composition in surface waters of upwelling regions.

Chapter 5

Silicon Isotope Distribution in the Eastern Equatorial Pacific*

Abstract

The distribution of the silicon isotope composition of dissolved silicic acid ($\delta^{30}Si(OH)_4$) was analyzed in the water column of the Eastern Equatorial Pacific (EEP), where one of the globally largest Oxygen Minimum Zones (OMZs) is located. Samples were collected at 7 stations along two meridional sections at 85°50'W and 82°00'W off the Ecuadorian and Peruvian coast. Surface samples show a large range in isotope composition ($\delta^{30}Si(OH)_4$ from 2.3‰ to 4.4‰) with the highest measured values at the southernmost station, which also revealed the most depleted silicic acid concentrations (0.2µmol/kg). Calculated fractionation factors (ε) according to a Rayleigh-type and a steady state model are highly variable depending on the assumed source of the silicic acid. We compared models for silicic acid originating from upwelling sources near the coast and from transport via surface currents to the sampling locations. The best fit to the data was achieved for a Rayleigh-type model assuming advection of silicic acid via surface currents. The calculated fractionation factor of -0.8‰ is close to the fractionation factor derived from culture experiments (ε = -1.1‰). The large range in $\delta^{30}Si(OH)_4$ in the upper water column and within the OMZ with oxygen concentrations below 10µmol/kg most likely reflects dissolution processes of biogenic silicate rather than advection and mixing of different water masses. Intermediate water masses in the study area are largely invariant and show a mean $\delta^{30}Si(OH)_4$ of 1.4‰ ranging from 1.1‰ to 1.9‰. Deep water masses below 2000m are around 1.1‰ (n=7), ranging from 0.9‰ to 1.4‰ and are slightly lighter in $\delta^{30}Si(OH)_4$ compared to a study in the EEP at 140°W.

**This chapter is a manuscript in preparation*

Deep water masses in the study area, as well as in the north and south Pacific show no clear correlation between silicic acid concentrations or distinct water masses and $\delta^{30}Si(OH)_4$. This implies that the distribution of distinct $\delta^{30}Si(OH)_4$ signatures in deep waters of the Pacific are a consequence of a combination of the relatively sluggish deep water circulation and remineralization processes.

5.1 Introduction

The Silicon isotope composition of dissolved silicic acid ($\delta^{30}Si(OH)_4$) is an important tool for the investigation of the biogeochemical cycle of silicon. Silicic acid ($Si(OH)_4$) is besides nitrate (NO_3^-) and phosphate (PO_4^{3-}) a major nutrient for diatoms, which require $Si(OH)_4$ to build up their frustules (Lewin, 1961). $\delta^{30}Si(OH)_4$ not only helps to understand the biogeochemical cycling of Si in today's ocean and, through its incorporation into diatom frustules, is also an important proxy for the reconstruction of silicic acid utilization in the past (De La Rocha et al., 1998; Reynolds et al., 2008; Pichevin et al., 2009; Ehlert, 2011).

The main factor controlling $\delta^{30}Si(OH)_4$ in surface waters is silicate utilization. Diatoms preferentially incorporate the lighter Si isotopes into their frustules thereby leaving seawater enriched in the heavy isotopes. According to two culture studies the fractionation factor (ε) between seawater and diatoms is -1.1‰ and no dependence of temperature, species and pCO_2 has been observed so far (De LaRocha et al. 1997; Milligan et al., 2004). Apart from utilization $\delta^{30}Si(OH)_4$ is influenced by mixing of surface water masses and remineralization of the diatom opal, whereby the lighter $\delta^{30}Si(OH)_4$ of the frustules is released back into seawater (Reynolds et la., 2006; Fripiat et al., 2011). Culture experiments by (Demarest et al., 2009) demonstrated that isotopic fractionation with a fractionation factor of +0.55‰ occurs during partial dissolution of diatom biogenic silicate (bSi), whereby the lighter Si isotopes are released to seawater. These processes have a significant effect on the $\delta^{30}Si(OH)_4$ in seawater, in particular in near surface waters given that most of the biogenic silicate (bSi) formed in the euphotic zone is already remineralized in the uppermost water column and on average only 3% of the bSi production is buried on the sea floor (Tréguer et al., 1995). The dissolution of $bSiO_2$ is strongly influenced by physical parameters, such as temperature and pH

(Lewin, 1961), but bacterial activity can lead to higher dissolution rates (Bidle and Azam, 1999; Bidle et al., 2002) and therefore OMZ with high bacterial activities could enhance the dissolution processes.

Several studies have shown that the $\delta^{30}Si(OH)_4$ signatures of deep water masses are characterized by distinct silicon isotope signatures (e.g. Cardinal et al., 2005; Reynolds et al., 2006; Beucher et al., 2008), even though model data suggested that no variation of the $\delta^{30}Si(OH)_4$ in deep waters is expected (Wischmeyer et al., 2003). A study by Reynolds et al. (2006) in the North Pacific revealed low $\delta^{30}Si(OH)_4$ signatures for Lower Circumpolar Deep Water (0.8‰) and North Pacific Deep Water (0.6‰), whereas Antarctic Bottom Water in the Southern Ocean has values near 1.2‰ (Cardinal et al., 2005). The observed variation in silicon isotopes seems to be in contrasts with the deep water distribution of the stable nitrogen isotope composition of nitrogen dissolved nitrate ($\delta^{15}NO_3^-$) in deep water basins, which is essentially invariant (Sigman et al., 2000; 2009). A satisfying explanation for this difference is still missing.

In the following study, we will focus on the influence of low oxygen concentrations due to degradation of organic matter on the silicic acid concentrations and the silicon isotope distribution. Furthermore the silicon isotope distribution of deep water is targeted to better understand deep water circulation and the processes influencing the silicon isotope distribution.

5.2 Material & Methods

All samples were collected during cruises M77-3 and M77-4 with the German RV Meteor in the frame of the Collaborative Research Centre (SFB) 754: Climate – Biogeochemistry Interactions in the Tropical Ocean between December 2008 and January 2009. Seawater samples were collected along two meridional sections at 85°50'W and 82°00'W off the Ecuadorian and Peruvian coasts between the equator and 14°S (Fig. 5.1, Table A.4).

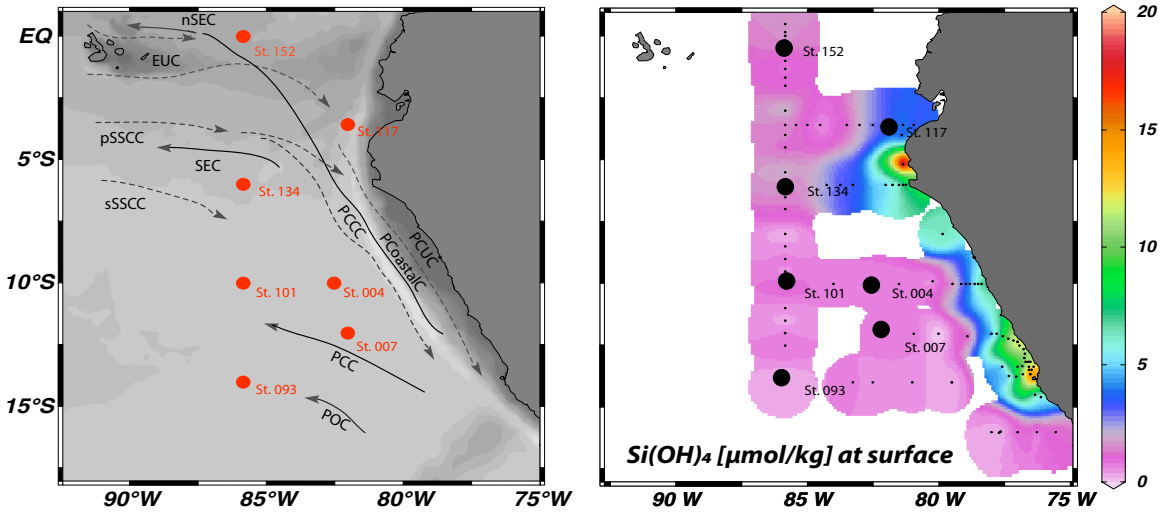

Fig. 5.1: Left: Station map of sampling locations and schematic surface (solid grey lines) and subsurface currents (dashed grey lines) off Equator and Peru according to Strub et al., 1998; Penven et al., 2005; Kessler, 2006; Ayon et al., 2008; Karstensen and Ulloa, 2008; and ADCP data according to Czeschel et al., 2011 (nSEC: northern South Equatorial Current, EUC: Equatorial Undercurrent, SEC: South Equatorial Current, pSSCC: primary Southern Subsurface Countercurrent, sSSCC: secondary Southern Subsurface Countercurrent, PCUC: Peru Chile Undercurrent, PCC: Peru Chile Current, PCCC: Peru Chile Countercurrent, POC: Peru Oceanic Current). Right: $Si(OH)_4$ concentrations in surface waters in µmol/kg determined on samples from RV Meteor cruises M77-3 and M77-4 together with sampling locations.

Seawater samples for analysis of silicon isotope, nutrient and oxygen concentration measurements were collected using a Seabird CTD Rosette System equipped with an oxygen sensor was attached. Nutrient concentrations were measured following (Grasshoff et al., 1999). Oxygen concentrations were determined with the O_2-sensor from the CTD and were later calibrated with the bottle data obtained by Winkler titration (Winkler, 1888). Seawater samples for silicon isotope measurements were immediately filtered on board through nitrocellulose acetate filters (0.45µm pore size) and were then acidified with distilled concentrated HCl to pH 2. At IFM-GEOMAR the silicon was separated from the samples using a brucite-coprecipitation method (Reynolds et al., 2006; after Karl and Thien, 1992). Depending on the Si concentration between 5 and 300 ml of seawater were used. Only samples with a yield >97% were used for isotopic measurements given that incomplete precipitation leads to fractionation of the Si in the sample. Samples with silicic acid concentrations below 10 µmol/L were preconcentrated through additional precipitation steps applying the same method (for detailed description see chapter 2). The precipitate was

redissolved in HCl (pH 2) and approximately 1% v/v of 1M NaOH were added. Per precipitation step only approximately 10% of the magnesium contained in the samples is precipitated, which allows to significantly reducing the magnesium content in the sample solution (see also Reynolds et al., 2006).

For Si isotope measurements the samples were purified following the method by Georg et al. (2006) and measured on a *NuPlasma* MC-ICPMS (Nu instruments) at the IFM-GEOMAR. The MC-ICPMS is equipped with an adjustable source-defining slit set to medium resolution to ensure separation of the ^{30}Si peak from molecular interferences. Measurements were carried out with a standard-sample bracketing method (Albarède et al., 2004). All solutions were measured at a Si concentration of 14 to 21 µmol/kg depending on the performance of the instrument and were introduced into the plasma via a Cetac Aridus II desolvator equipped with a PFA nebulizer with an uptake rate of 60 to 80 µL/min.

Si isotope compositions are reported in the δ notation using the reference standard NBS28 in parts per thousand ($\delta^{30}Si=((R_{sample}/R_{standard})-1)*1000$), where R_{sample} is the $^{30}Si/^{28}Si$ ratio of the sample and $R_{standard}$ is the $^{30}Si/^{28}Si$ ratio of the standard. External reproducibility is given as 2σ standard deviations either from the sample-bracketing method (2sd) or as external reproducibility of n repeated sample measurements (2σ standard error of the mean ($2\sigma_{SEM}$, Table A.4). The external errors ranging from mostly from 0.1‰ and 0.3‰, only two samples showed a worse reproducibility of 0.4‰, respectively 0.5‰. Long term measurements of the reference materials IRMM018 and Big Batch gave average $\delta^{30}Si$ values of -1.53 ± 0.30‰ ($2\sigma_{sd}$, n=25) and -10.80 ± 0.23‰ ($2\sigma_{sd}$ n=25), respectively, which are in agreement with values obtained by other laboratories (Reynolds et al., 2007). The standard errors are representing the mean obtained during 25 sessions. All error bars given in the figures are $2\sigma_{SEM}$ of the samples.

5.3. Results

5.3.1 Study Area and Hydrographic Setting

Persistent easterly trade and alongshore winds produce offshore Ekman transport of surface waters, which are replaced by upwelling of nutrient-rich subsurface waters on the shelf (Fig. 5.1b). The main source water masses for the Peruvian upwelling are the southward flowing Peru-Chile Countercurrent (PCCC) and the Peru-Chile Undercurrent (PCUC, Brink et al., 1983). Surface waters of the sampling locations are mainly influenced by currents from the south or currents that are transported from the shelf offshore, such as the Peru Oceanic Current (POC), the Peru Coastal Current (PCoastalC) or the Peru Chile Current (PCC) (Fig. 5.1, Strub et al., 1998; Penven et al., 2005; Karstensen and Ulloa, 2008). These currents are the driving force for the Equatorial Undercurrent (EUC) and the Southern Subsurface Countercurrent (SSCC) to flow eastward along the equator thereby supplying oxygen-rich waters to the upwelling area (Brink et al., 1983; Toggweiler et al., 1991; Fiedler and Talley, 2006). During austral summer 2009, when the samples for this study were taken, the EUC encountered the west coast of South America at approximately 0°N to 1°N at a core depth of 90m (Czeschel et al., 2011), almost exactly at the location of station 152.

Surface water masses show a large scatter in salinity. Due to higher precipitation rates in the north (St.152), the salinity is low (33.6 PSU) compared to the south (St.93) with salinities around (35.5 PSU) At a water depth of 120m to 170m m the T-S diagram (Fig. 2) clearly shows the admixture of Subantarctic Water (SAAW) at St. 93 characterized by a salinity minimum (33.8 PSU) and transported to the EEP from the south (Silva et al., 2009). St. 007, which is also located in the southern part of the study area still shows admixture of SAAW albeit much weaker. The intermediate waters (IW) between approximately 200 and 1500m water depth waters mainly consist of three water masses (Bostock et al., 2010 and references therein): North Pacific Intermediate Water (NPIW), Antarctic Intermediate Water (AAIW) and the Equatorial Pacific Intermediate Water (EqPIW) with potential densities ranging between 26.8 and 27.1. NPIW and AAIW are not clearly distinguishable in their TS properties, but NPIW

shows higher silicic acid concentrations between 50 and 130 µmol/kg compared to AAIW, which is characterized by concentrations between 5 to 80 µmol/kg (Bostock et al., 2010). The densest water mass in the Pacific basin is Lower Circumpolar Deep Water (LCDW; Wijffels et al., 1996), which is formed in the Southern Ocean and then flows north along different pathways. Through internal mixing processes LCDW is transformed into North Pacific Deep Water (NPDW), which is again modified by admixture of Upper Circumpolar Deep Water (UCDW) near the Hawaiian Islands. From there NPDW broadly flows southward along the continental slope of Central and South America and contributes to the mixture of deep water masses off Peru (Wijffels et al., 1996; Kawabe and Fujio, 2010). For the distinction of deep water masses temperature-salinity characteristics are ambiguous because NPDW and LCDW are very similar both in salinity and temperature. But NPDW is can be easily distinguished on the basis of its significantly higher silicate concentrations and lower oxygen concentrations than those of LCDW.

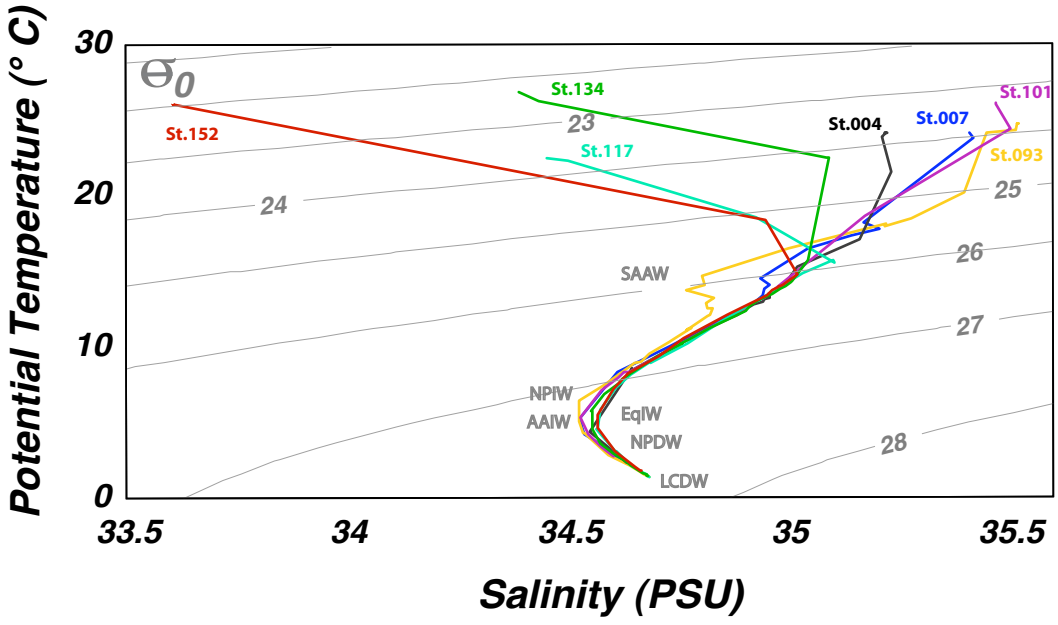

Fig.5.2: T-S diagram with potential density isolines (σ_θ) for the 7 stations and potential water masses in the study area according to Johnson and Tool (1993), Bostock et al. (2010), and Amakawa et al. (2009). LCDW: Lower Circumpolar Deep Water (σ_θ=0.85, Sal. 34.7), NPDW: North Pacific Deep Water (27.6<σ_θ>27.8, 1°C<T_{pot}>1.8°C:3-5, 34.6<Sal.>34.7), NPIW: North Pacific Intermediate Water (σ_θ=26.8, $T_{pot.}$:6.4, 33.9<Sal>34.1), AAIW: Antarctic Intermediate Water (σ_θ=27.1, 3<T_{pot}5, 34.3<Sal.>34.5), EqIW: Equatorial Intermediate Water (σ_θ=27.3, 34.5<Sal>34.6), SAAW: Subantarctic Water (σ_θ=25.7, Tpot. 1.3°C, Sal. 33.8).

5.3.2 Distribution of Silicon Isotope Compositions and Silicic Acid Concentrations

The dissolved silicic acid concentrations increase at all stations from low concentrations in the surface waters (0.22 µmol/kg) to high concentrations (153 µmol/kg) in the deep waters (Fig. 5.3, Table A.4). This pattern is generally reflected by the corresponding silicon isotope compositions in a way that the highest $\delta^{30}Si(OH)_4$ values are found in the surface waters ranging from 2.3‰ to 4.4‰. The highest $\delta^{30}Si(OH)_4$ values of 3.0‰ and 4.4‰ are found at stations 7 and 93 in the south of the study area. Surface samples north of 10°S are homogeneous in their $\delta^{30}Si(OH)_4$ signatures ranging between 2.3‰ and 2.5‰, corresponding to silcic acid concentrations ranging from 0.7 µmol/kg to 2.7 µmol/kg. Depending on mixed layer depth samples from below 10 to 20m meters water depth are already less fractionated ($\delta^{30}Si$= ~2‰). The. $Si(OH)_4$ concentrations between the silicic acid nutricline (located at water depths between 30m and 150m) and 200m water depth of all stations ranges from 13µmol/kg to 28µmol/kg, respectively. The corresponding $\delta^{30}Si(OH)_4$ values are between 1.2‰ and 1.9‰ with a mean of 1.6‰ (n=20), whereby the silicon isotope distribution do not always reflect the silicic acid concentration patterns. The silicon isotope composition within the OMZ (Oxygen concentration below 10 µmol/kg) falls between 1.2‰ and 1.9‰ (n=19) with a mean of 1.6‰. The extent of the OMZ ranges between 50 and 300m depth to 370 to 500m depth (Fig. 5.3) and varies as a function of latitude and of proximity to the coastal upwelling centers. The range of the silicon isotope compositions in the intermediate water masses ($26.8 \leq \sigma_\theta \geq 27.3$) between 1.1‰ to 1.9‰ with a mean of 1.4‰ (n=14) is similar to that of the OMZ but is characterized by higher $Si(OH)_4$ concentrations (between 16 µmol/kg and 42 µmol/kg µmol/kg).

Deep water $Si(OH)_4$ concentrations are consistently increasing to a depth of approximately 2000m and below remains essentially stable at values around 140µmol/kg with slightly lower concentration at southernmost station 93 (130µmol/kg). This is accompanied by the lowest $\delta^{30}Si(OH)_4$ value (0.9 ± 0.2‰) observed in this study at a water depth of 4000m, whereas a station further north (St.134, 6°S) shows a $\delta^{30}Si(OH)_4$ of 1.4 ± 0.1‰ at 3500m depth (Fig. 5.3).

In general, the $\delta^{30}Si(OH)_4$ signature of seawater below 2000m shows low values between 0.9‰ and 1.4‰ with a mean of 1.1‰ (n=7).

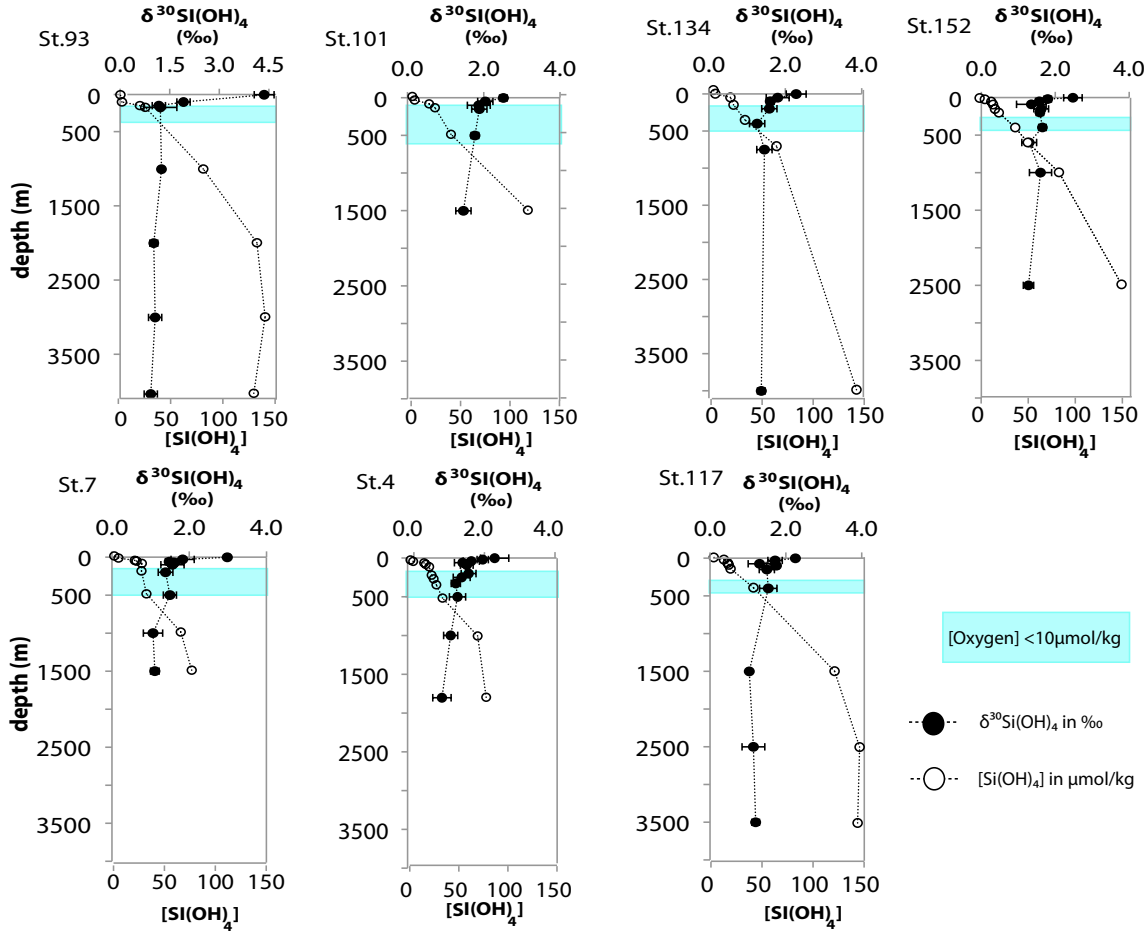

Fig. 5.3: $\delta^{30}Si(OH)_4$ (filled circles) and silicic acid concentrations in µmol/kg (open circles) against water depth. The upper 4 stations reflect the section along 85°50'W and lower 3 stations represent the section along 82°00'W *with the southernmost stations on the left and northern stations on the right. The blue box indicates the extent of the OMZ with oxygen concentrations below 10 µmol/kg. Please, note the different scale for* $\delta^{30}Si(OH)_4$ at station 93.

There is a general decrease of $\delta^{30}Si(OH)_4$ with increasing silicic acid concentrations (Fig. 5.4). At high silicic acid concentrations >50 µmol/kg the low $\delta^{30}Si(OH)_4$ values are not clearly distinguishable any more outside external reproducibility (Fig 5.4a). The intermediate and deep waters of the study area, for which $1/Si(OH)_4$ is <0.03 (>33 µmol/kg) (Fig. 5.4b), still tend to show slightly higher $\delta^{30}Si(OH)_4$ at lower concentrations indicating distinguishable water mass signatures in $\delta^{30}Si(OH)_4$. The red stars indicate possible mixing end members as observed in the north and central Pacific (Reynolds et al., 2006; de Souza,

2011). The $\delta^{30}Si(OH)_4$ data of Reynolds et al. (2006) show very low values (0.6‰) for NPDW and for LCDW (0.8‰), whereas the observed data in this study are higher (Fig. 5.4b).

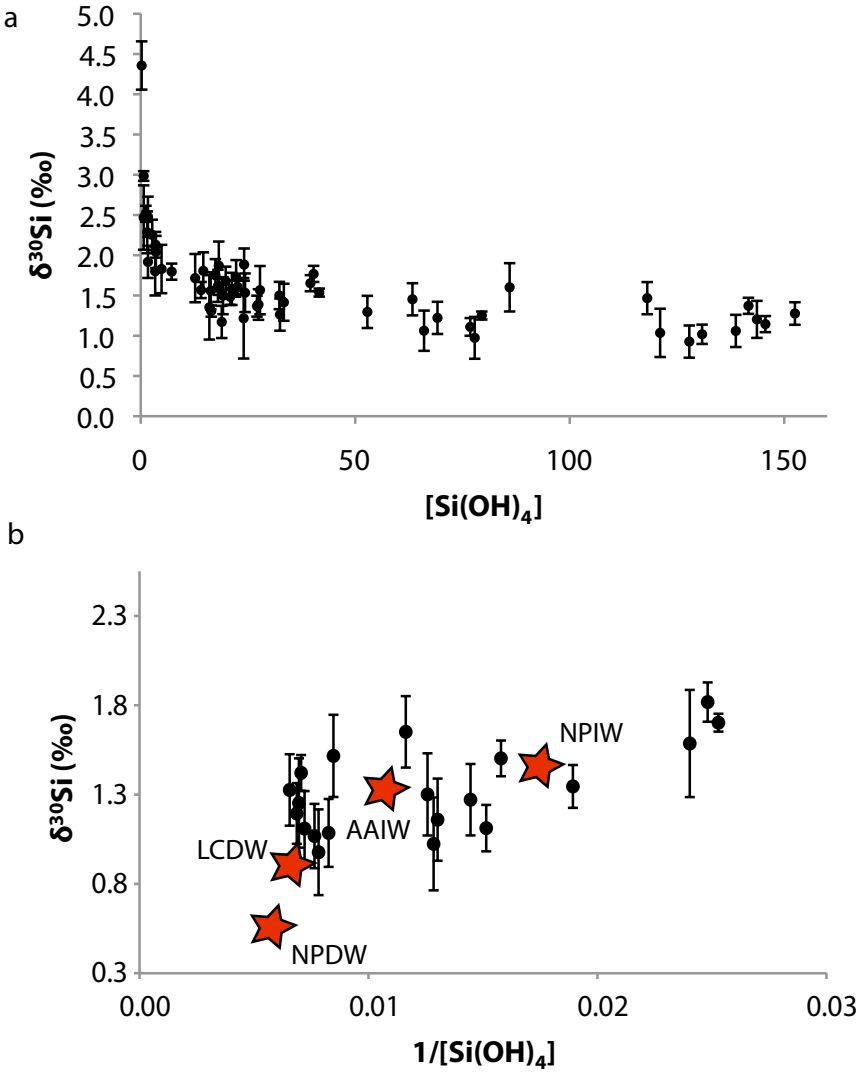

Fig. 5.4: Silicon isotope composition against silicic acid concentrations (a) and against 1/[Si(OH)₄] (b) for the intermediate and deep water masses with 1/Si(OH)₄ below 0.03 The data for deep and intermediate water masses of the study area including possible mixing end members (red stars) from the North Pacific (Reynolds et al., 2006) and for AAIW from the Central South Pacific (de Souza 2011).

5.4 Discussion

5.4.1. Surface Utilization of Silicic Acid and Modeling of the Silicon Isotope Fractionation

The $\delta^{30}Si(OH)_4$ in surface waters of the study area ranges from 2.3‰ to 4.4‰ with the highest values occurring at the southernmost stations (St. 93 and St. 7). The dissolved silicon in the surface waters is fractionated during utilization of silicic acid mainly by diatoms with an assumed fractionation factor of -1.1‰ (De LaRocha et al., 1997). The value of 4.4‰ at the surface of St. 93 is the highest measured $\delta^{30}Si(OH)_4$ observed so far for seawater and corresponds to highly depleted $Si(OH)_4$ concentrations (0.2µmol/kg). Station 93 is clearly influenced by the POC (Fig.5.1), a water mass originating from the south. The silicic acid concentration of the POC gets strongly depleted while flowing along the high productivity areas off the Chilean Coast (Daneri et al., 2000). For comparison, Reynolds et al. (2006) observed the highest $\delta^{30}Si(OH)_4$ of 3.2‰ in oligotrophic surface waters of the subtropical gyre in the North Pacific corresponding to a higher silicic acid concentration of 0.6µmol/kg.

But not only utilization, also water mass mixing can influence the $\delta^{30}Si(OH)_4$ signature in surface waters. Two fundamentally different model approaches can thus be applied to describe the evolution of the $\delta^{30}Si(OH)_4$ signature of surface waters during biologically induced fractionation at a particular location. The first is a steady-state model, wherein a continuous supply of nutrients results in a dynamic equilibrium of the $Si(OH)_4$ content in the water body under investigation, whereas in a Rayleigh-type model, no additional nutrients are newly supplied to the system (Mariotti et al., 1981; De La Rocha et al., 1997; Cardinal et al., 2005; Reynolds et al., 2006). Both models assume a constant fractionation factor ε. The value of ε is given by the slope of the linear regression between $\delta^{30}Si(OH)_{4obs}$ and f for the steady-state model, and between $\delta^{30}Si(OH)_{4\ obs}$ and $\ln f$ for the Rayleigh-type model (Fig. 5.5). A detailed description of the models can be found in Chapter 1 and 3. To determine the fractionation factor ε an initial concentration has to be assumed to calculate the remaining fraction f of the available silicic acid pool. In a highly dynamic system,

such the Peruvian Upwelling this is quite challenging as the source waters can either have been influenced by upwelling from the subsurface or by silicic acid concentrations transported to the location by surface currents (see Fig. 5.1). The remaining fraction *f* is calculated using following equation

$$f = \frac{[Si(OH)_4]_{observed}}{[Si(OH)_4]_{initial}}$$

where $Si(OH)_{4obs.}$ is the silicic acid concentration measured in the surface water and $Si(OH)_{4initial}$ is the concentration of the source. In order to compare the influence of upwelling, versus supply by surface currents two different initial concentrations were assumed to calculate *f* (Fig. 5.5*)*. For the initial $Si(OH)_4$ induced by upwelling *f* was calculated by dividing $Si(OH)_{4\ obs.}$ in surface water by $Si(OH)_4$ from the nutricline. As an initial silicic acid concentration advected to the study by surface currents area we assumed 3.35 µmol/kg, given that this is the average surface silicic acid concentration at the shelf edge (Fig. 5.1), from where persistent easterly trade winds and Ekman transport drive surface currents offshore.

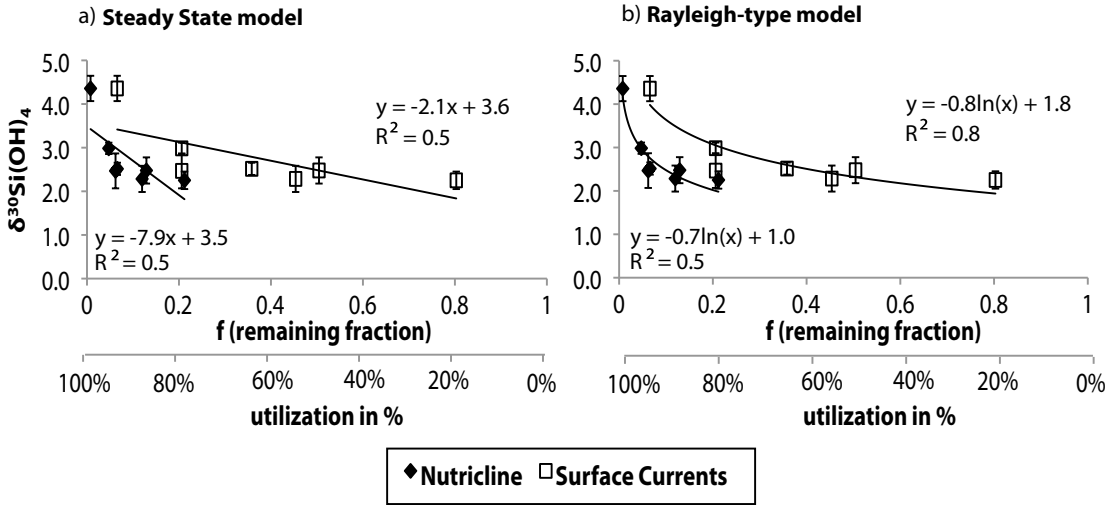

Fig. 5.5: Calculations of silicon isotope fractionation for the samples of this study using a (a) steady state model, and a (b) Rayleigh-type model, whereby $\delta^{30}Si_{Si(OH)4}$ of the surface samples is plotted against f (remaining $Si(OH)_4$ from the available pool). For the $Si(OH)_4$ concentration of the source we assumed either that the silicic acid concentrations were transported to the sampling location by upwelling of ($Si(OH)_4$) from the nutricline (filled diamonds) or the initial concentration transported to the stations by surface currents originating on the shelf with an initial concentration of 3.35µmol/kg (open squares).

For an advection of silicic acid from the nutricline the calculated utilization of silicic acid from the available pool is ranging between 80% and 100%, whereas the utilization calculated by advection from surface currents show lower utilization rates down to 20%. The best fit is achieved by the Rayleigh-type model for the advection of $Si(OH)_4$ from surface currents resulting in a fractionation factor of -0.8‰ close the fractionation factor assessed by culture studies (De La Rocha et al., 1997), whereas the worst fit and an extremely high fractionation factor (-7.9‰) is calculated assuming a steady state system with upwelled $Si(OH)_4$ from the nutricline. Both models and the assumptions of different initial $Si(OH)_4$ concentrations can only provide rough estimates of the fractionation factor due to the complexity of water mass structure in the study area. A study by Ehlert (2011) along the Peruvian shelf, which is characterized by strong coastal upwelling, estimated a fractionation factor between -0.6‰ (steady state) and -2.7‰ (Rayleigh-type) and is thus, as expected, closer to the theoretical value for the steady state approach, whereas stations further offshore, like in this study rather correspond to a Raleigh-type model with less input of new nutrients.

5.4.2 Water Mass Mixing and Dissolution Processes Influencing $\delta^{30}Si(OH)_4$

The estimation of the modelled fractionation factors can also be biased by dissolution and remineralization processes within the source waters given that fractionation in the models only occurs through uptake (Beucher et al., 2011). A study at 140°W in the EEP showed that up to 52% of the biogenic silica production is already redissolved in the upper 300m (Demarest et al., 2011; Beucher et al., 2011). This is expected to result in lighter $\delta^{30}Si(OH)_4$ signatures (Demarest et al., 2009). In our study the $\delta^{30}Si(OH)_4$ signature of waters below the mixed layer rapidly decreases to values between 1.2‰ and 1.9‰ within in the upper 200m water depth (Fig. 5.2). This large variation can either be explained by a dissolution effect or be the result of mixing with different water masses. Station 152 near the equator, which is clearly influenced by the incoming EUC at a depth of 90m, shows a $\delta^{30}Si(OH)_4$ of 1.4‰, which is within error identical to the value observed by Beucher et al. (2008) for the EUC (1.5‰) at 140°W. In contrast to the $\delta^{30}Si(OH)_4$ distribution at 140°W (Beucher et

al., 2008) this value is not distinctly different from other water masses at similar water depths and therefore rather reflect dissolution processes. The SAAW influence at Station 93 (Fig. 5.2) is reflected by slightly lower $\delta^{30}Si(OH)_4$ of 1.2‰ at 150, respectively 170m water depth. Given that this water mass consists of subducted former surface waters from the south (Silva et al., 2009), a higher $\delta^{30}Si(OH)_4$, signature would be expected unless this water mass has been influenced by dissolution processes on its way north.

The OMZ in the study area with oxygen concentrations below 10 µmol/kg extends to water depths of up to several hundred meters (Fig. 5.3). The anoxic waters may have a significant effect on biogenic opal dissolution processes given that enhanced bacterial activity can lead to higher dissolution rates (Bidle and Azam, 1999, Bidle et al., 2002, Demarest et al., 2011). Therefore the $\delta^{30}Si(OH)_4$ signatures within water masses with oxygen concentrations below 10µmol/kg were compared with higher oxygen levels. This comparison shows that the OMZ is characterized by $\delta^{30}Si(OH)_4$ signatures between 1.2‰, to 1.9‰ and does not show significantly lighter $\delta^{30}Si(OH)_4$ values compared with better oxygenated waters at similar water depths (Fig. 5.3).

The intermediate waters show $\delta^{30}Si(OH)_4$ signatures between 1.1‰ and 1.9‰ with a mean of 1.4 (n=14) but different water masses are not unambiguously distinguishable (Fig. 5.4b). Some water mass signatures are comparable to data observed for NPIW (Reynolds et al., 2006) and for AAIW (de Souza et al., 2011), but the data cannot be explained by simple mixing between these two water masses. The $\delta^{30}Si(OH)_4$ distribution in subsurface and intermediate water masses in the study area is obviously affected by both intense remineralization processes and water mass mixing. For a better understanding and distinction of these factors influencing the $\delta^{30}Si(OH)_4$ distribution in these water masses a detailed data set of the concentrations, as well the isotopic composition of particulate biogenic opal of the same samples would be necessary.

5.4.3. Mixing of Deep Water Masses

Deep water masses below 2000m water depth reveal a range of $\delta^{30}Si(OH)_4$ between 0.9‰ and 1.4‰, whereby the lowest value is observed at the southernmost station St.93 at 4000m depth and the highest values is found further north at St.134 at 3500m depth. Given that LCDW does not spread into all areas of the Pacific (Johnson and Toole, 1993), admixture of NPDW is expected to influence the $\delta^{30}Si(OH)_4$ distribution. The advection of NPDW is indicated by higher silicic acid concentrations at the northernmost stations, but is not supported by the silicon isotope distribution in deep waters of the study area, which are highest in the northern part (Fig. 5.4b). The $\delta^{30}Si(OH)_4$ data of Reynolds et al. (2006) show very low values (0.6‰) for NPDW and for LCDW (0.8‰), whereas the observed data in this study are higher (Fig. 5.4b).

A compilation of available silicon isotope data for the Pacific Ocean and adjacent seas for water depths below 2000m show a wide range of silicon isotope data (Fig. 5.7, De La Rocha et al., 2000, Cardinal et al., 2005, Reynolds et al., 2006, Beucher et al., 2008, Cao et al., 2012). The silicon isotope data show a large scatter ranging from 0.6‰ to 1.5‰ and no clear trend with respect to the silicic acid concentration. Even in regard of relatively high external errors (up to 0.3‰) for the silicon isotope measurement values are distinguishable. The lowest $\delta^{30}Si(OH)_4$ values (0.6‰) were observed in the North Pacific at silicic acid concentrations of 150µmol/kg (Reynolds et al., 2006). The highest $\delta^{30}Si(OH)_4$ values (1.5‰) are found in the Southern Ocean, south of Australia corresponding to concentrations of 80µmol/kg (Cardinal et al., 2005). The mean $\delta^{30}Si(OH)_4$ value (1.2‰) of the deep northern stations 152 (Equator), 117 (4°S) and 134 (6°S) is indistinguishable from the data reported by Beucher et al. (2008) for the EEP at 140°W (1.3‰), whereas the southernmost station 93 of our study shows a lighter $\delta^{30}Si(OH)_4$ value (0.9‰) at lower silicic acid concentrations. As also demonstrated in Fig. 5.4c, the deep water distribution of $\delta^{30}Si(OH)_4$ and $Si(OH)_4$ concentrations in the study area, as well as overall in the Pacific Ocean can not be explained by a simple mixture of LCDW and NPDW.

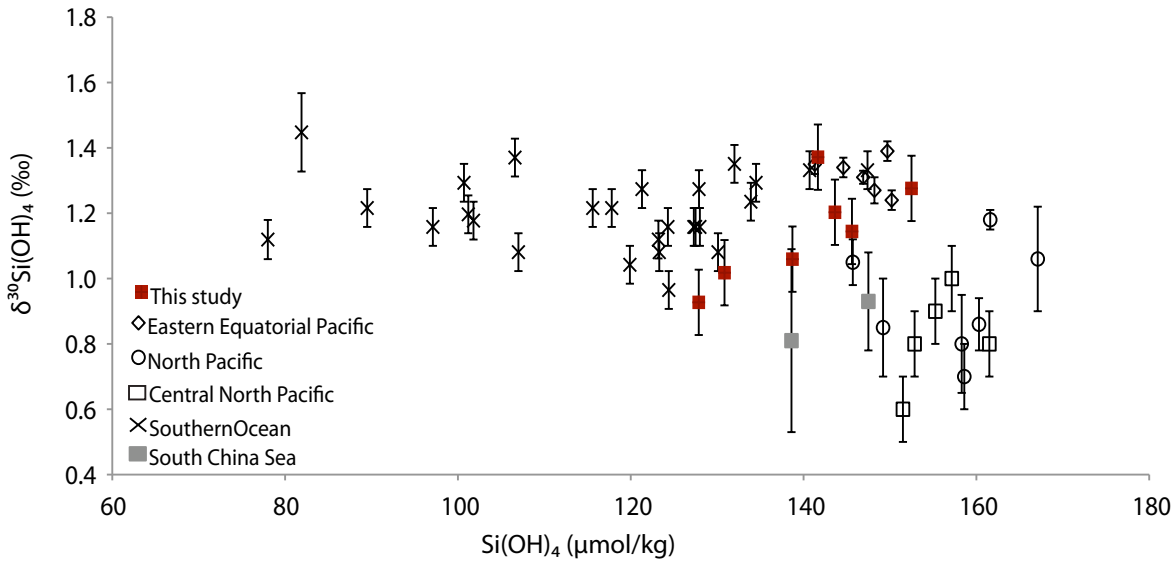

Fig. 5.7: $\delta^{30}Si_{Si(OH)4}$ against silicic acid concentration (µmol/kg) for samples collected below 2000m water depth in the Eastern Equatorial Pacific at 140°W (open diamonds, Beucher et al., 2008), North Pacific (open circles, Reynolds et al., 2006), Central North Pacific (open squares; De La Rocha et al., 2000), the Southern Ocean, south of Australia (crosses, Cardinal et al., 2005) he South China Sea (grey squares, Cao et al., 2012) and this study from the Eastern Equatorial Pacific (red squares).

The variability in silicon isotope data seems to be in contrast to the distribution of the stable nitrogen isotope composition of dissolved nitrate ($\delta^{15}NO_3^-$), which shows similar values near 5‰ in deep waters of all ocean basins (Sigman et al., 2009). However, in deep water off the Peruvian and Ecuadorian coast also $\delta^{15}NO_3^-$ shows small but significant variations ranging between 5‰ and 7‰ below 2000m water depth (Ryabenko et al., 2011). Even though this variation is small compared to the fractionation factors occurring during N speciation processes (up to 38‰, Casciotti et al., 2009) a close comparison of the nitrogen and silicon isotope distributions in deep water would contribute to a better understanding of both systems. In view of the different fractionation factors, the relatively large difference between $\delta^{30}Si(OH)_4$ and $\delta^{15}NO_3^-$ of global deep waters may result from different intensities of remineralization. Remineralization processes in the deep North Atlantic and the deep North Pacific along the deep branch of the global conveyor belt are 6.4 times higher for silicic acid by accumulation of diatom opal through dissolution than for nitrate by the degradation of organic matter. In general the North Pacific and the Southern

Ocean are the predominant regions for opal dissolution (Sarmiento et al., 2007). Given that fractionation during partial dissolution of biogenic opal should lower the $\delta^{30}Si(OH)_4$ values of ambient seawater (Demarest et al., 2009), the deep water $\delta^{30}Si(OH)_4$ is expected to show a larger variability than those of $\delta^{15}NO_3^-$. Very low $\delta^{30}Si(OH)_4$ (≤1.0‰) occur in the Northern Pacific (Reynolds et al. 2006), the South China Sea (Cao et al., 2012) and the Eastern Equatorial Pacific (this study, 1.1‰), which are either characterized by high productivity, mainly of diatoms, or by high $Si(OH)_4$ concentrations as a consequence of opal dissolution (Sarmiento et al., 2007). Higher $\delta^{30}Si(OH)_4$ values (1.3‰) in the Central Eastern Pacific (Beucher et al., 2008, de Souza et al., 2011) of lower primary productivity in the surface ocean and therefore less burial of opal to the bottom. A study by de Souza et al. (2012) in the Atlantic Oceanic basin showed a quasi-conservative mixing for dissolved $Si(OH)_4$ of North Atlantic Deep Water and Antarctic Bottom Water. This is not supported by this study as we cannot see a clear water mass mixing of LCDW and NPDW. This is most likely the result of remineralization of biogenic opal in high productivity areas like the Upwelling area of Peru and a more sluggish circulation of Pacific deep water. Therefore the deep water signal of $\delta^{30}Si(OH)_4$ is most likely a result of the combination of water mass advection and remineralization processes, but in order to better understand the processes influencing silicon isotope composition in deep water masses of the Pacific ocean a more comprehensive data set would be required.

5.5 Conclusion

The distribution of the dissolved silicon isotope composition of silicic acid ($\delta^{30}Si(OH)_4$), as well as of the $Si(OH)_4$ concentration were analyzed in the EEP along two meridional sections between 100 to 1000 km off the Ecuadorian and Peruvian coast from the equator to 14°S. Surface waters in the study area, in particular in its southern part are strongly depleted in silicic acid concentrations, which leads to highly fractionated Si in the surface waters reaching $\delta^{30}Si(OH)_4$ of up to 4.4‰. This is most likely a function of northward advection of highly Si-depleted surface water masses into the study area. The calculated fractionation factor of ε=-0.8‰, assuming an advection of surface currents, is close to the

fractionation factor derived from culture experiment. Different subsurface and intermediate water masses cannot be clearly distinguished in their $\delta^{30}Si(OH)_4$ signatures given that the factors mainly controlling the Si isotope distribution are different intensities of dissolution of bSi and not the mixing of distinct water masses. No clear correlation between $\delta^{30}Si(OH)_4$ and suboxic or anoxic waters of the OMZ can be observed in the study area and dissolution processes are apparently mainly a function of water depth. This needs to be studied in more detail to reach firmer conclusions on the importance of oxygen levels, respectively the enhanced bacterial activity in suboxic waters. The data obtained in this study for water masses below 2000m showed lower $\delta^{30}Si(OH)_4$ (1.1‰) compared to the Central Pacific (1.3‰) and higher values compared to the North Pacific (0.7‰). A compilation of the data, which is available for the Pacific ocean show a large scatter ranging from 0.6‰ to 1.5‰ and no clear trend with respect to the silicic acid concentration or distinct water masses. Thus it is suggested that the distribution of distinct $\delta^{30}Si(OH)_4$ signatures in deep waters of the Pacific are a consequence of a combination of the relatively sluggish deep water circulation and remineralization processes.

CHAPTER 6

Neodymium Isotopes and Concentrations in the Eastern Equatorial Pacific: Water Mass Advection Versus Particle Exchange*

Abstract

The radiogenic isotope composition of the Rare Earth Element (REE) neodymium (Nd) is a powerful water mass proxy for present and past ocean circulation. The processes controlling the Nd bugdet of the global ocean are not quantitatively understood and in particular source and sink mechanisms are still under debate.

In this study we present the first full water column data set of dissolved Nd isotope compositions and Nd concentrations for the Eastern Equatorial Pacific (EEP), where one of the globally largest Oxygen Minimum Zones (OMZ) is located. This region is of particular interest for understanding the biogeochemical cycling of REEs because anoxic conditions may lead to release of REEs from the shelf, whereas high particle densities and fluxes potentially remove the REEs from the water column. Data were obtained between 1°40'N and 16°S along a nearshore and an offshore transect. Near surface zonal current bands, such as the Equatorial Undercurrent (EUC) and the Subsurface Countercurrent (SSCC), which are supplying oxygen-rich water to the OMZ are characterized by radiogenic Nd isotope signatures (ε_{Nd} = -2). Surface waters in the northernmost part of the study area are even more radiogenic (ε_{Nd} = +3), most likely due to release of Nd from volcanogenic material.

**This chapter is submitted to Earth and Planetary Sciences Letter as:*

Patricia Grasse, Torben Stichel, Roland Stumpf, Lothar Stramma, and Martin Frank. The Distribution of Neodymium Isotopes and Concentrations in the Eastern Equatorial Pacific: Water Mass Advection Versus Particle Exchange

Deep and bottom waters at the southernmost offshore station (14°S) are clearly controlled by advection of water masses with less radiogenic signatures (ε_{Nd} = -7) originating from the Southern Ocean. Towards the equator, however, the deep waters show a clear trend towards more radiogenic values of up to ε_{Nd}= -2. The northernmost station located in the Panama basin shows highly radiogenic Nd isotope signatures in the entire water column, which indicates that particle scavenging, downward transport and release processes play an important role. This is supported by relatively low Nd concentrations in deep waters (3000m to 6000m) in the EEP (20 pmol/kg) compared to locations in the Northern and Central Pacific (40-60 pmol/kg), which suggests enhanced removal of Nd in the EEP.

6.1 Introduction

6.1.1. Nd Isotopes

The radiogenic isotope composition of the Rare Earth Element (REE) neodymium (Nd) is a powerful water mass tracer for the present and past ocean due to its intermediate oceanic residence time (360 to 1900 years) and the fact that it is independent of biological fractionation processes (Piepgras at al., 1979; Jeandel et al., 1995; Frank, 2002; Tachikawa et al., 2003; Arsouze et al., 2007, 2009).

The Nd isotope composition ($^{143}Nd/^{144}Nd$, expressed as ε_{Nd}, which corresponds to the deviation of the measured $^{143}Nd/^{144}Nd$ of the samples from CHUR (Chondritic Uniform Reservoir with $^{143}Nd/^{144}Nd$=0.512638, Jacobsen and Wasserburg, 1980) in parts per 10,000: $\varepsilon_{Nd} = [(^{143}Nd/^{144}Nd_{sample}/^{143}Nd/^{144}Nd_{Chur})-1]*10.000$) of water masses is primarily controlled by the isotopic composition of the surrounding landmasses at their origin. Weathering of young mantle-derived rocks surrounding the Pacific Ocean leads to more radiogenic values compared to the Atlantic Ocean with its margin predominantly composed of old continental crust. In addition water masses from the northern Pacific and from the Southern Ocean are clearly labeled by distinct isotopic fingerprints. North Pacific water masses, such as North Pacific Deep Water (NPDW) and North Pacific Intermediate Water (NPIW) show more radiogenic values (ε_{Nd} = -3 to ε_{Nd} = -5,

Piepgras and Jacobsen, 1988; Amakawa et al., 2004; 2009) compared to water masses originating from the Southern Ocean (ε_{Nd} = -8 to ε_{Nd} = -9, Piepgras and Wasserburg, 1982; Stichel et al., 2011). The exact input mechanisms and the influence of weathering processes on the Nd isotope composition and Nd concentration of seawater are not yet fully understood but it has become clear that besides eolian and riverine inputs (Goldstein et al., 1984; Goldstein & Jacobsen, 1988; Elderfield et al., 1989; Henry et al., 1994; Sholkovitz et al., 1999) also processes at the continent-seawater interface, so called "boundary exchange" must play an important role or may even dominate the inputs (Lacan & Jeandel, 2005; Arsouze et al., 2007; 2009). In contrast, the contribution of Nd to the ocean via hydrothermal inputs has been suggested to be negligible. In fact, hydrothermal vents rather have to be considered a sink of REEs in the global ocean budget together with particle scavenging processes (German et al., 1990; Klinkhammer et al., 1983; Halliday et al., 1992). The importance of particle scavenging and release processes is most notably documented by the nutrient-like vertical distribution of the concentrations of most REEs (e.g. Elderfield and Greaves, 1982). At the same time numerous studies have demonstrated that Nd isotopes clearly label particular water masses that can be followed across entire ocean basins. This phenomenon has been named the "Nd paradox" (Jeandel et al., 1995; Tachikawa et al., 1999; Siddall et al., 2008). To better understand the processes influencing the isotope composition as well as the concentration gradients in the ocean, several modeling studies were conducted (Tachikawa et al., 2003; Arsouze et al., 2007; 2009; Jones et al., 2008; Siddall et al., 2008; Oka et al., 2009). Although inclusion of boundary exchange processes has improved the modeled isotope and concentration distributions it still seems that there are additional sources and sinks of Nd. To resolve these uncertainties a comprehensive data set for the global distribution of Nd isotope compositions, as well as Nd concentrations is required for the global ocean, a goal that is currently being pursued by the international GEOTRACES program. Since 1980 a large number of dissolved Nd isotope data from the Atlantic Ocean have been published but data from the Pacific Ocean are scarce (Piepgras and Wasserburg, 1982; Piepgras and Jacobsen,

1988; Amakawa et al., 2000, 2004, 2009, Vance et al., 2004; Lacan & Jeandel, 2001; Shimizu et al., 1994) and as yet no dissolved Nd isotope or Nd concentration data are available for the Eastern Equatorial Pacific (EEP).

6.1.2. Currents and water masses of the Eastern Tropical Pacific

The general oceanography of EEP is governed by intense upwelling and northward flowing surface currents, such as the Peru Oceanic Current (POC), the Peru Coastal Current (PCoastalC) and the Peru Chile Current (PCC), which can be found approximately 100 to 300 km offshore (Fig. 6.1a). These water masses originate in subantarctic regions (Strub et al., 1998, Penven et al., 2005, Karstensen and Ulloa, 2008).

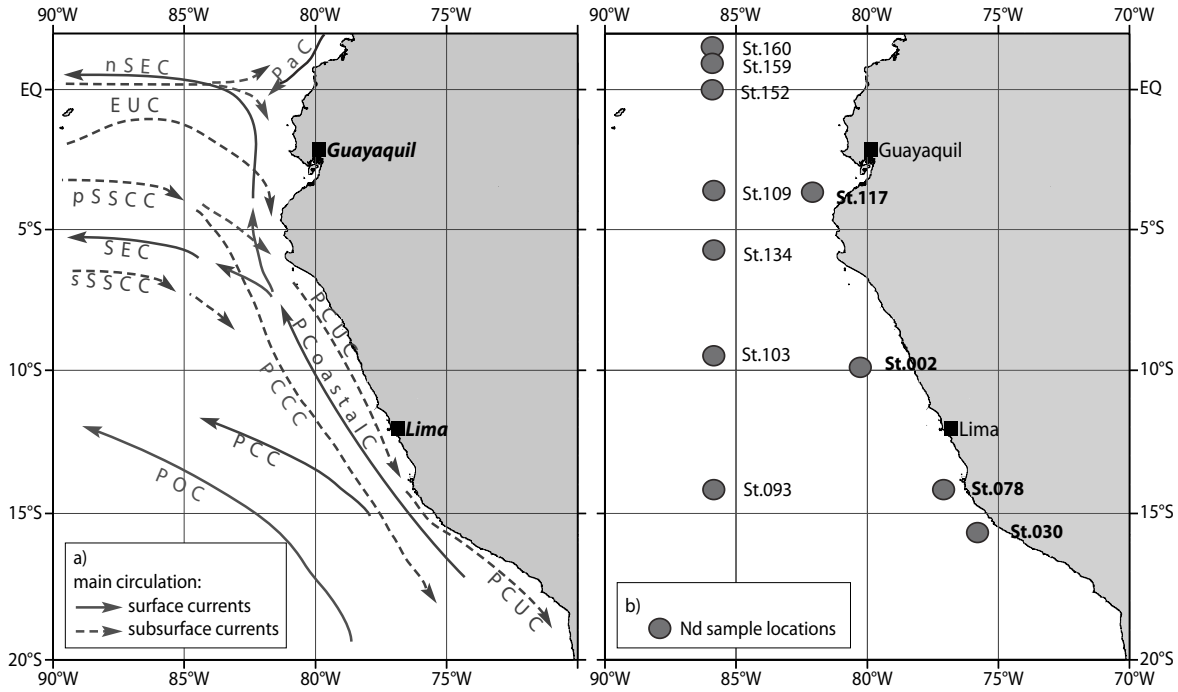

Fig. 6.1: (a) Schematic surface (solid grey lines) and subsurface (dashed grey lines) currents off Peru; and (b) sampling locations for Nd isotopes and concentrations during R/V Meteor cruises M77-3 and M77-4 (PaC: Panama Current, EUC: Equatorial Undercurrent, pSSCC: primary Southern Subsurface Contercurrent, sSSCC: secondary Southern Subsurface Countercurrent, SEC: South Equatorial Current, PCUC: Peru Chile Undercurrent, PCC: Peru Chile Current, PCCC: Peru Chile Countercurrent, POC: Peru Oceanic Current (after Strub et al., 1998; Penven et al., 2005; Kessler, 2006; Ayon et al., 2008; Karstensen and Ulloa, 2008; and ADCP data according to Czeschel et al., 2011).

The Subantarctic Water (SAAW) which is transported to the EEP also from the south is a low salinity surface water mass which is subducted towards the equator to depth around 100m to 200m (Fig. 6.2, Silva et al., 2009). Persistent

easterly trade and alongshore winds produce offshore Ekman transport of surface waters, which causes the upwelling of nutrient-rich subsurface water to the euphotic zone (Brink et al., 1983). In equatorial regions westward flowing surface currents, such as the South Equatorial Current (SEC) produce an eastward pressure gradient. This force drives the Equatorial Undercurrent (EUC) and the Southern Subsurface Countercurrent (SSCC) to flow eastward along the equator and supply oxygen-rich waters to the upwelling area (Brink et al., 1983; Toggweiler et al., 1991; Fiedler and Talley, 2006). During austral summer 2009, when the samples for this study were taken, the EUC encountered the western coast of South America at approximately 0°N to 1°N at a core depth of 90m (Czeschel et al., 2011). Together with the primary Southern Subsurface Countercurrent (pSSCC) and the secondary Southern Subsurface Countercurrent (sSSCC) these currents are feeding the Peru Chile Undercurrent (PCUC) and account for up to 30% of its volume (Montes et al., 2010). The PCUC is the source water mass of the coastal upwelling and flows southward along the shelf at approximately 50m to 150m water depth (Huyer et al., 1987, Penven et al., 2005, Karstensen and Ulloa, 2008).

The intermediate waters between 200 and 1500m water depth show a complex water mass structure. Eastern Pacific intermediate waters mainly consist of three water masses (Fig.6.2, Bostock et al., 2010 and references therein): North Pacific Intermediate Water (NPIW), Antarctic Intermediate Water (AAIW) and the Equatorial Pacific Intermediate water (EqPIW). AAIW is primarily formed in the southeast Pacific, just off the coast of southern Chile where it is subducted and flows northward to a latitude of approximately 20°S (Talley, 1999; Kawabe and Fujio, 2010). NPIW is formed in the northwestern subtropical gyre along the Kuroshio and Oyashio Front (Talley, 1993) and is generally characterized by lower oxygen concentrations (<150 µmol/kg) than its Southern hemisphere counterpart, the AAIW (200 to 300 µmol/kg; Bostock et al., 2010).

Unlike the Atlantic Ocean, the Pacific Ocean has no high-latitude northern source of deep water. The densest water mass in the Pacific basin is the Lower Circumpolar Deep Water (LCDW; Wijffels et al., 1996). The LCDW

transforms into North Pacific Deep Water (NPDW), which is again modified by admixture of Upper Circumpolar Deep Water (UCDW) near the Hawaiian Islands. From there NPDW broadly flows southward along the continental slope of Central and South America and contributes to the mixture of deep water masses off Peru (Wijffels et al., 1996; Kawabe and Fujio, 2010). For the distinction of deep water masses temperature-salinity characteristics are ambiguous because NPDW and LCDW are very similar both in salinity and temperature (Fig. 6.2). But NPDW is can be easily distinguished by significantly higher silicate concentrations and lower oxygen concentrations than LCDW.

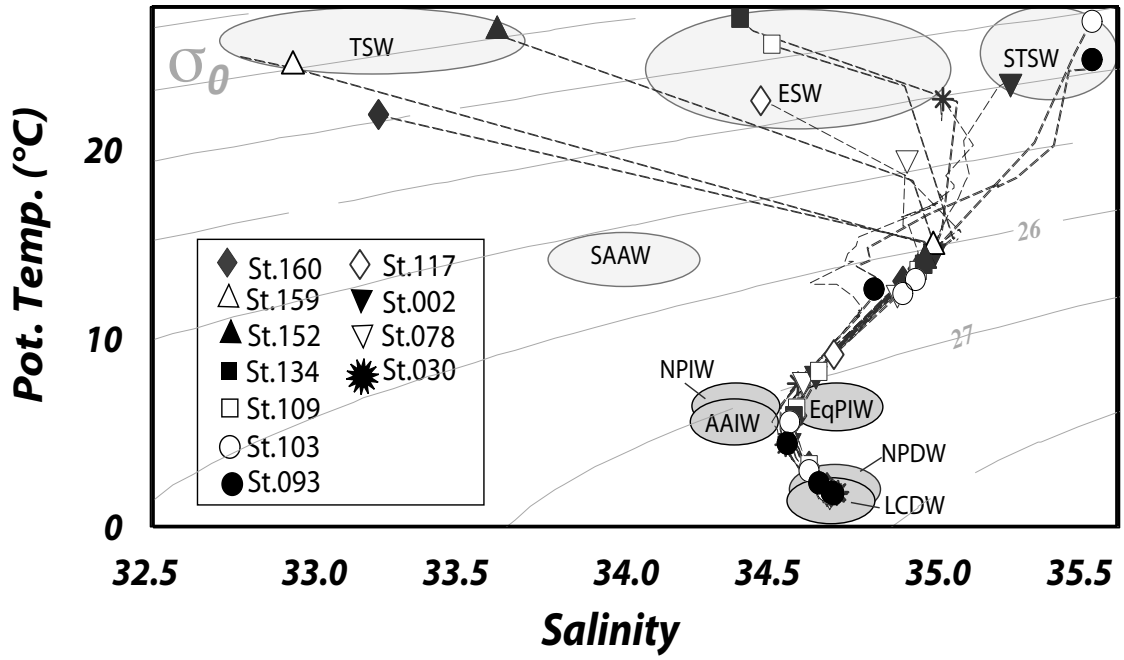

Fig. 6.2: T-S diagram with potential density (σ_θ) for the 11 stations of this study. Offshore stations are listed in the left column and nearshore stations in the right column of the inset legend: TSW: Tropical Surface Water, ESW: Equatorial Surface Water, STSW: Subtropical Surface Water, SAAW: Subantarctic Water, EqPIW: Equatorial Intermediate Water, NPIW: North Pacific Intermediate Water, AAIW: Antartic Intermediate Water, NPDW: North Pacific Deep Water, LCDW: Lower Circumpolar Deep Water are marked according to Wijffels et al. (1996), Johnson and Toole (1993), Fiedler and Talley (2006) and Silva et al. (2009), see also Table. A.5.

6.2. Material & Methods

The Samples were collected in the EEP between December 2008 and February 2009 aboard the German research vessel Meteor (M77/3 & M77/4) as

part of the German-led Collaborative Research Centre “SFB 754” (Biochemistry Interactions in the Tropical Ocean, www.sfb754.de). The samples were taken at 7 stations along a longitudinal offshore section at 85°50’W between 1°40’N and 14°S and at 4 nearshore stations at distances between 100km and 200km from the coast between 3°35’S and 16°S (Fig. 6.1b). Seawater samples for analyses of Nd concentrations and isotope compositions were collected using a Seabird CTD Rosette System equipped with an O_2-sensor. Nutrient concentrations were measured following (Grasshoff et al., 1999). Oxygen concentrations were determined with the O_2-sensor of the CTD and were later calibrated with bottle data obtained by Winkler titration (Winkler, 1888).

For Nd isotope analysis 20L of seawater were collected in previously acid cleaned LDPE cubitainers. The samples were filtered through 0.45µm nitrocellulose acetate filters (Millipore®) within 2 hours after sampling. From each filtered sample an aliquot of 2L was separated for Nd concentration measurements. All samples were acidified to pH 2with concentrated quartzglas distilled hydrochloric acid (0.5ml per Liter). On board 500µl Iron(III)Chloride solution (~1g Fe(III)Cl/ml in 3M HCl) were added to each 20L sample and after one day of equilibration the samples were adjusted to pH 8 with ammonium hydroxide (25%, suprapure grade) to co-precipitate the dissolved REEs with the iron hydroxide. At IFM-GEOMAR (Kiel, Germany) REE separation from major element cations was performed using a cation exchange resin (Biorad® AG50W-X12 resin, 200-400µm mesh-size, 0.8mL resin bed). The Nd was further purified in a second column chemistry step (Eichchrom® Ln Spec, 50-100µm mesh-size, 2mL resin bed). The applied column chemistry followed the methods of Barrat et al. (1996) and Le Fèvre and Pin (2005).

Nd isotope measurements were carried out on a *Nu plasma* MC-ICPMS as well as on a *Thermo Scientific* TIMS TRITON. Measured $^{143}Nd/^{144}Nd$ ratios were corrected for mass fractionation to $^{146}Nd/^{144}Nd=0.7219$. All measured $^{143}Nd/^{144}Nd$ ratios of this study were normalized to the accepted value of the JNdi-1 standard of 0.512115 (Tanaka et al., 2000).

Samples containing less than 10ng of Nd were measured on the MC-ICPMS using a manual time resolved mode. External reproducibility (2σ) of the

Nd isotope measurements ranged between 0.1 ε_{Nd} and 0.8 ε_{Nd} depending on the applied method and sample concentrations (Table A.6). Duplicate measurements of samples and standards on the MC-ICPMS and on the TIMS resulted in identical isotope compositions within the external 2σ reproducibilities.

For Nd concentration measurements, 500mL of filtered and acidified seawater were used. The concentrations were determined using an isotope dilution (ID) method (Heuman, 1992 and references therein). A defined amount of $^{150}Nd/^{149}Sm$ spike was added according to the assumed concentrations and was left for equilibration for one week. REEs were then separated from disturbing elements following the same method as for the isotope measurements but only using one cation exchange column (Biorad® AG50W-X12 resin, 200-400µm mesh-size, 0.8mL resin bed). The external reproducibility of the Nd concentration measurements was approximately 2% (1σ). Blank values for isotope and concentration measurements ranged between 1% and 3% of the sample concentration and were considered as negligible.

6.3. Results

6.3.1. Vertical Distribution of Nd isotope Composition and Concentration

In Fig. 6.3 the profiles of dissolved Nd concentrations and Nd isotope compositions for the offshore and nearshore transect are compared (see also Table A.6). All stations show a general increase in Nd concentrations from the surface towards greater depth, ranging from from 4.8 pmol/kg in surface waters to 24.1 pmol/kg in deep water samples. However, the increase is not always linear. Station 109 has nearly constant Nd concentrations around 8 pmol/kg in the upper 1500m rising to 22 pmol/kg at the bottom. The northernmost station (St. 160) has a maximum concentration of 28.2 pmol/kg at 800m water depth. The southernmost station (St. 30) close to the Peruvian coast shows an abrupt increase from 8 pmol/kg to 20 pmol/kg at a depth of 1000m. Below that depth only a minor increase in Nd concentration was found down to about 5500m. Some stations (109, 117, 134) show higher concentrations in the surface waters than in subsurface waters. Stations 152 and 159 (Table A.6, data not shown in

Fig. 6.3) show an increased concentration at 90m (11 pmol/kg), respectively 100m (20 pmol/kg) compared to similar depths in other profiles (~6 pmol/kg). The Nd isotope composition shows a wide range within the depth profiles of single stations overall ranging from ε_{Nd} = -7 to ε_{Nd} = +2.7. The mean Nd isotope composition of intermediate water masses between 200m and 1500m water depth ranges from ε_{Nd} = -4 (14°S) to ε_{Nd} = -1.6 (1°40'N) with no obvious differences

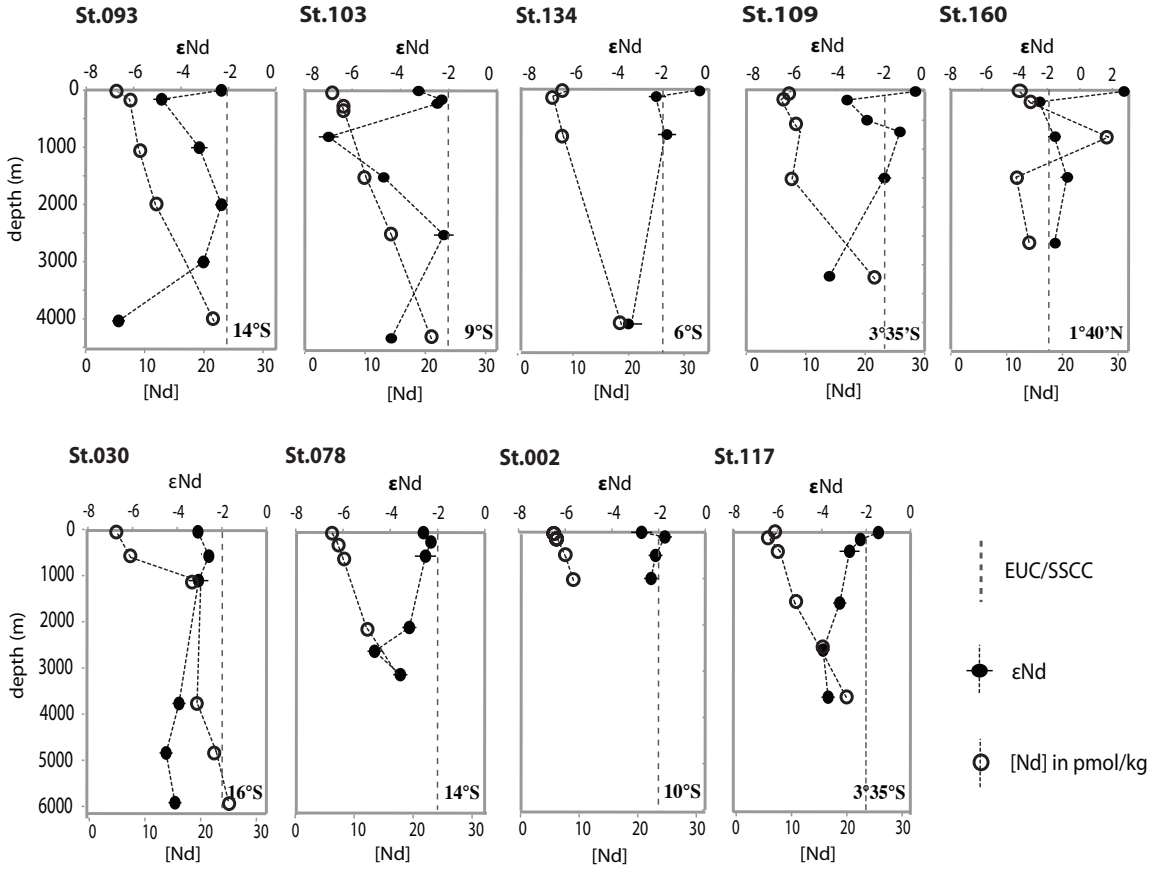

Fig. 6.3: Nd isotope composition (ε_{Nd}, filled black circles) and Nd concentrations in pmol/kg (open circles) of 9 stations. Offshore stations along the 85°50'W are shown in the upper part of the graph. Nearshore stations (100km to 200km off the coast) are shown in the lower part. Stations 152 and 159, for which only two water depths were sampled are not shown. The dashed grey line indicates the isotope signature of the EUC/SSCC encountered from station 152, 159 and 134. Please note the different scale for the ε_{Nd} values at station 160.

between offshore and nearshore samples. During austral summer 2009, when the samples for this study were taken, the EUC encountered the western coast of South America at approximately 0°N to 1°N at a core depth of 90m and then continued its flow southward. The presence of the SSCC, another subsurface

water mass originating from the Central Pacific was observed between 5°S and 6°20'S with core depths of 100m to 200m and 400m to 500m, respectively (Czeschel et al., 2011). According to ADCP data (Czeschel et al. 2011) and oxygen concentrations of station 152 (85°50'W/Equator) and station 159 (85°50'W/1°20'W) are closest to those of the EUC at approximately 100m water depth and show ε_{Nd} = -1.8 (10.5 pmol/kg) and ε_{Nd} = -2.2 (19.6 pmol/kg), respectively (Table A.6, data not shown on Fig. 6.3). A water sample within the SSCC (St.134, 100m) shows an ε_{Nd} value of -2.2 (6.3 pmol/kg). The average ε_{Nd} value of these water masses originating in the Central Pacific is about ε_{Nd} = -2.0 (Fig. 6.3, dashed grey line). In relation to the radiogenic isotope signature of these zonal current bands (EUC/SSCC), the southern stations, in particular on the offshore transect show less radiogenic Nd isotope signatures compared to stations in the south.

6.3.2 Lateral Distribution of Nd Isotopes and Concentrations in Surface and Deep Water Samples

Fig. 6.4 shows the variations of dissolved Nd isotope compositions and Nd concentrations together with hydrographic and nutrient data for surface and deep water samples (lowermost sample approximately 50m above ground, only stations 93 and station 117 were sampled at 500m above the ground) for each station along the offshore and nearshore section between 16°S and 1°40'N. The surface waters (Fig. 6.2, Fig. 6.4) are subdevided into 3 zones from south to north with following decreasing salinity: Subtropical water (STSW), Equatorial Surface Water (ESW) and Tropical Surface Water (TSW). The Nd isotope composition of surface waters becomes systematically more radiogenic towards the equator ranging from ε_{Nd} = -3.3 to ε_{Nd} = +2.7. The corresponding Nd concentrations increase from 5 pmol/kg at the southernmost stations (Station 30 and Station 93) to 12 pmol/kg at the northern end of the section (St. 160). Higher Nd concentrations are accompanied by increased silicic acid concentrations. Towards the equator the surface waters are less saline compared to the south. Offshore and nearshore surface waters show similar Nd

isotope compositions and Nd concentrations, whereas the nearshore surface waters are characterized by lower surface temperatures (Fig. 6.4a).

Towards the north and similar to the surface water distribution, the Nd isotope composition of deep water samples becomes systematically more radiogenic ranging from ε_{Nd} = -6.6 at 14°S to ε_{Nd} = -1.6 at 1°40'N (Fig. 6.4b). The nearshore stations south of 14°S (ε_{Nd} = -4) show more radiogenic values compared to the offshore stations (ε_{Nd} = -6) mirroring lower oxygen concentrations. The highest potential temperature is observed in the north. The lowest Nd concentration (14 pmol/kg) in deep water samples close to the bottom is observed at the northernmost station, whereas Nd concentrations at the southern stations are approximatly 20 pmol/kg.

6.4. Discussion

6.4.1 Controls of Nd Isotopes and Concentrations in Surface and Subsurface Water Masses

Surface waters in the study area of the EEP show a systematic trend towards more radiogenic ε_{Nd} values and higher Nd concentrations from south to north (Fig. 6.4a). This pattern is reflected by the hydrographic data given that continuously decreasing salinities are observed towards the equator (Fig. 6.4) due to enhanced rainfall (Wooster, 1959). The northernmost water masses represent the TSW range from ε_{Nd} = +0.6 to +2.7 and are sourced, among others, by the Panama Current (PaC), which is advected from the north (Fig. 6.1, Fig. 6.4a). The Nd isotope composition of the PaC most likely originates from exchange with either volcanogenic particles in the water column or highly radiogenic shelf sediments along Central America (ε_{Nd} = +2 to +6, Jeandel et al., 2007). Tachikawa et al. (2004) and Lacan and Jeandel (2005) proposed that exchange between dissolved and particulate phases significantly contributes to the dissolved isotopic signal of a water mass.

ESW from offshore stations shows a characteristic Nd isotope composition of approximately ε_{Nd} = -0.3. The nearshore station at 3°35'S with its distinct Nd isotope signature of ε_{Nd} = -1.5 is either more influenced by surface currents originating in the south or by upwelled waters which have received

their isotopic fingerprints from the shelf margin. Surface waters south of 8°S show higher salinities and are generally referred to STSW, which is characterized by isotope signatures between ε_{Nd} = -3.3 and ε_{Nd} = -2.3. These water masses are clearly influenced by less radiogenic surface currents, such as the POC, PCC and the SEC (Fig. 6.1a) which originate in the south and are transported westward due to persistent easterly trade winds.

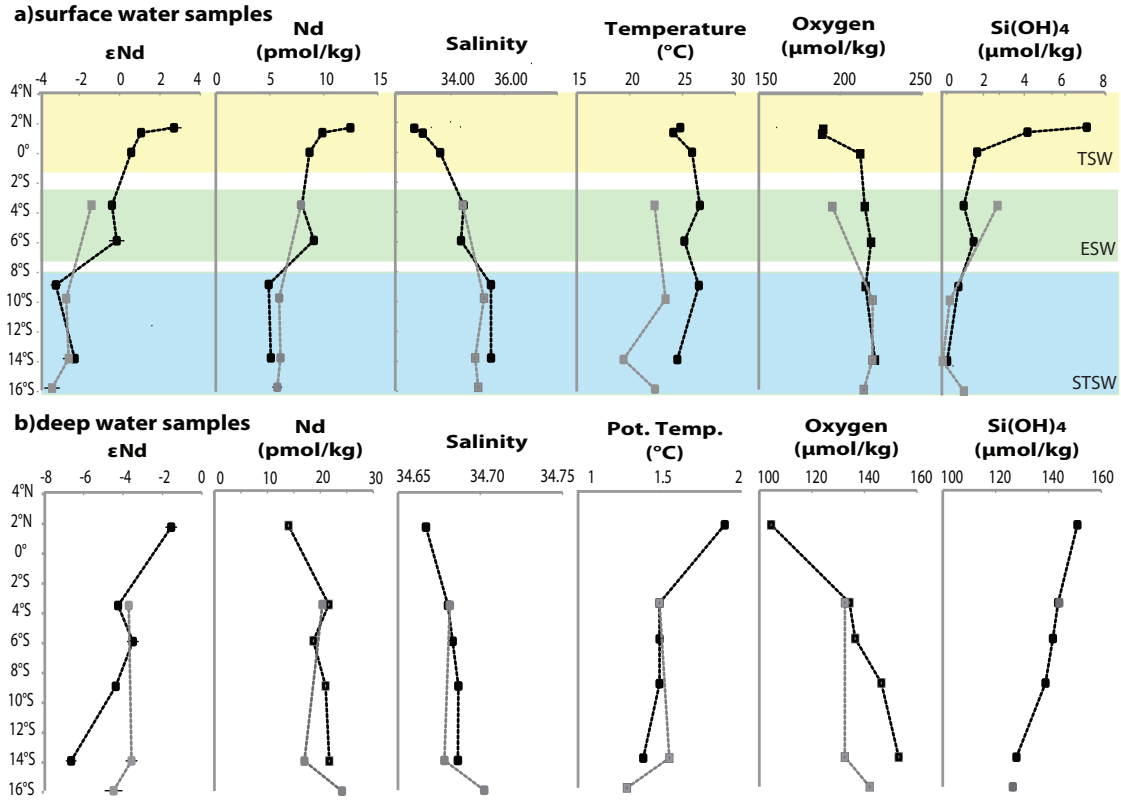

Fig. 6.4: For each station the surface water (a) and deep water (b) ε_{Nd}, Nd concentration (pmol/kg), salinity (PSU), potential temperature (°C), oxygen and silicic acid concentration (µmol/kg) are plotted against latitude. The black line marks the 85°50'W transect, the grey line marks the nearshore transect. Color shaded areas in the upper plot represent the different surface water masses (TSW: Tropical Surface Water; ESW: Equatorial Surface Water; STSW: Subtropical Surface Water). All deep water samples were sampled below 3000m, only the northernmost station (St. 160) was sampled at 2600m water depth.

Surface waters in the north show more than twice the Nd concentrations (12 pmol/kg) compared to surface waters in the south (5 pmol/kg, Fig. 6.4a). Lower Nd concentrations in the south are most likely the result of Nd-depleted westward flowing water masses, such as the POC and PCC originating on the shelf. In particular between 10°S and 15°S, the coastal upwelling on the shelf

and therefore productivity are most intense (Chavez and Barber 1987; Chavez and Messié 2009), which goes along with high biogenic particle density. This particle density causes enhanced scavenging of dissolved Nd. Furthermore the low dissolved Nd concentrations correlate well with low silicic acid concentrations (Fig. 6.4a). As diatoms are dominating the phytoplankton in upwelling areas (Estrada and Blasco 1985), it is most likely that Nd is scavenged by the large surfaces of the diatoms. In the Atlantic sector of the Southern Ocean a similar explanation for the strong correlation between Nd and silicic acid concentration has been proposed by Stichel et al. (2011). During the cruise in February 2009 the core of the EUC, which could be identified due to ADCP data and elevated oxygen concentrations (~90µmol) was found immediately north of the equator at water depths between 80m and 100m (Czeschel et al., 2011). Hydrographic parameters at station 152 and 159 at 85°50'W at the equator are closest to those of the EUC at approximately 100m water depth and show ε_{Nd} = -1.8 and ε_{Nd} = -2.2, respectively. These values are in good agreement with data from Lacan and Jeandel (2001) which obtained ε_{Nd} = -1.6 for the core of the EUC at 140°W. They suggested that this water mass obtains its radiogenic signature, when the AAIW passes the Papua New Guinea Slope, which consists of easily weatherable island arc rocks, before flows eastward. Nd concentrations of the EUC (St. 152 and 159) are two to three times higher (11 pmol/kg; respectively 20 pmol/kg) compared to similar depths at other stations (~6 pmol/kg). This agrees with investigation by Slemons et al. (2010) and Kaupp et al. (2011) who also reported elevated dissolved iron and aluminum concentrations in the EUC, most likely caused by sediment resuspension and particle release processes in the source area of the zonal current band near Papua New Guinea, which was also shown to be a source of dissolved REEs (Sholkovitz et al., 1999) The SSCC, another subsurface water mass originating from the Central Pacific influencing the intermediate depth waters of the study area, was observed between 5°S and 6°20'S with core depths of 100m to 200m and 400m to 500m, respectively. The SSCC (St.134, 100m) shows a ε_{Nd} = -2.2, similar to the EUC. These zonal current bands are feeding the PCUC, the main source water mass for the upwelling, with up to

30% of its volume (Montes et al., 2010). Therefore the PCUC should accordingly be influenced by this radiogenic isotope composition. The hydrographic data, characterized by a salinity minimum in the subsurface for St. 93 and St. 30 show a clear influence of SAAW, which originates in the south (Fig. 6.2). No water sample was taken from exactly the depth where the peak of the salinity minimum was located. Only Station 93 shows a less radiogenic signature (ε_{Nd} = -4.8) at a depth of 160m, which corresponds to the lower part of the salinity minimum.

In summary, highly radiogenic surface and subsurface water masses of the EEP are not only a result of advection of water masses from the Central Pacific with their radiogenic isotope signature but also local sources, such as the Central American Coast seem to play an important role for the surface water Nd isotopic signature. This is clearly indicated by the highly radiogenic Nd isotope compositions of the water masses transported to the study area by the Panama Current (Fig. 6.1a).

6.4.2 Intermediate water masses

Intermediate water masses between 200 and 1500m depth show a relatively wide range in their isotopic composition (Offshore: ε_{Nd} = -4 (14°S) to ε_{Nd} = -1.6 (1°40'N); Nearshore: from ε_{Nd} = -3.2 (16°S) to ε_{Nd} =-2.7 (3°35'N)). Intermediate water masses of all stations between 200m and 1500m depth show a mean ε_{Nd} = -2.8. For a mixture of NPIW (ε_{Nd} = - 3.4 to ε_{Nd} = - 2.7; Amakawa et al. 2004, 2009) and AAIW (ε_{Nd} = -6.0 to ε_{Nd} = -7.0; Stichel et al., 2011) the intermediate water Nd isotope compositions are too radiogenic. This is consistent with the study of Bostock et al. (2010) who suggested that a mixture of AAIW and NPIW does not directly form the EqPIW. This is supported for example by radiocarbon data which indicate an influence by lateral advection of an older deeper water mass. Station 103 shows a quite unradiogenic Nd isotope composition (ε_{Nd} = -7) at 800m, which is suggesting an admixture of a southern water mass, most likely AAIW, which is transported westward with the subtropical gyre. However this is not clearly supported by the hydrographic data. The Nd profiles show relatively heterogeneous isotope

compositions and cannot always be explained by mixtures of specific water masses, which is due to the fact that the EEP is a highly dynamic system, in which also mesoscale eddies play an important role for the vertical and horizontal mixing processes (Chaigneau et al., 2008).

This is also reflected by Station 160, which shows a peak Nd concentration (30 pmol/kg) at 800m depth (Fig. 6.3). Such concentration peaks may be explained by intrusions of water masses that obtained their high Nd concentrations on the shelf before being transported offshore. Rickli et al. (2009) found a similar concentration peak in the Bay of Biscay accompanied by an increased dissolved iron concentration that was also ascribed to such an intrusion (Laës et al., 2003). Elevated dissolved iron concentration in the water column can derive from water masses that have been in contact with shelf sediments as iron is readily dissolved and released from sub-oxic or anoxic sediments, such as those on the Peruvian shelf (Landing and Bruland, 1987; Bruland et al., 2005).

6.4.3 Deep and Bottom Waters

Deep and bottom water samples show the least radiogenic neodymium isotope signatures (ε_{Nd} = -6.6) at the southernmost station at 85°50'W with a clear trend to more radiogenic values in the north (ε_{Nd} = -1.6, Fig. 6.4b). The deep water masses along the offshore transect in the south are less radiogenic and coincide with higher oxygen and lower silicic acid concentrations indicating a larger proportion of LCDW (ε_{Nd} = -8.5, Stichel et al., 2011) compared to the nearshore water masses. Given that LCDW does not spread into all areas of the Pacific (Johnson and Toole, 1993), admixture of NPDW is also expected (ε_{Nd} = -3.8, Piepgras and Jacobsen, 1988). In order to calculate the fractions of water masses of northern and southern origin contributing to the deep water in the EEP we assumed simple mixing of NPDW with LCDW, which is described by the following equation:

$$\varepsilon Nd_{Mix} = \left(\frac{(\varepsilon Nd_1 * [Nd]_1 * f) + (\varepsilon Nd_2 * [Nd]_2 * (1-f))}{[Nd]_1 * f + [Nd]_2 * (1-f)} - 1 \right)$$

εNd_{mix} is the isotope composition of the mixed water mass. εNd_1 and εNd_2 represent the isotope composition of the two endmembers, $[Nd]_1$ and $[Nd]_2$ are the corresponding concentrations and *f* the percentage of the respective endmember.

For the mixing line (Fig. 6.5) we applied Nd isotope and concentration data from Piepgras and Jacobsen (1988) for NPDW at 24°25'N and 141°85'E and from Stichel et al. (2011) for LCDW (57°37'S, 60°50'W).

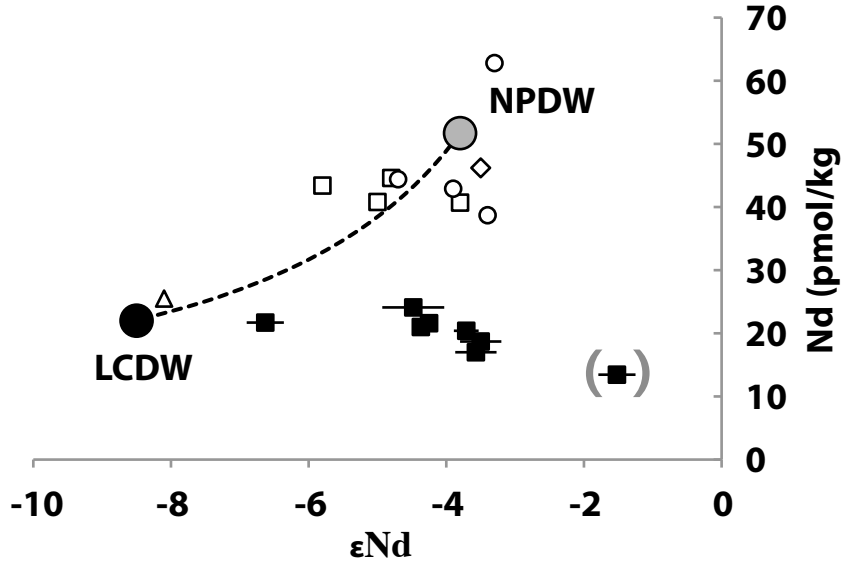

Fig. 6.5: The plot shows the mixing line (dashed line) between LCDW (black dot) and NPDW (grey dot) for Nd concentration (pmol/kg) against Nd isotope composition (ε_{Nd}). Black squares indicate deep water samples in the study area (below 3000m, only the northernmost station 160 (in brackets) is sampled at 2600m). Open symbols indicate water samples below 3000m water depth from the North and Central Pacific Ocean according to published data (Piepgras and Wasserburg, 1982 (open triangle); Amakawa et al., 2009 (open squares), Piepgras and Jacobsen, 1988 (open circles), Vance et al., 2004 (open diamond)). Endmember values for Nd isotope signatures and Nd concentrations of NPDW and LCDW are taken from (Piepgras and Jacobsen (1988); εNd = -3.8, [Nd]= 51.7 pmol/kg), Stichel et al., (2011); εNd = -8.5, [Nd]= 25.3 pmol/kg).

It is clear that this is an oversimplification but given the similarity of various water profiles in the respective source areas, the choice of these numbers is justified to achieve first order estimates.

The measured Nd isotope ratios and concentrations in the deep waters of the EEP are not in good agreement with the mixing line between the NPDW and LCDW (Fig. 6.5). Dissolved Nd concentrations in EEP deep waters are obviously depleted; respectively the Nd isotope compositions are too

radiogenic. So far no other water profiles from the Pacific Ocean have shown concentrations in deep waters similarly low to those obtained in this study. Nd concentrations in deep waters (below 3000m) of the North and Central Pacific generally show concentrations of 40 to 60 µmol/kg (Vance et al., 2004; Piepgras and Wasserburg, 1982; Piepgras and Jacobsen, 1988; Amakawa et al., 2009), which is more than twice as high as in the EEP. One possible explanation for the diminished concentration is efficient scavenging of dissolved Nd by particles. Due to intense upwelling of nutrient rich subsurface waters the EEP is characterized by high primary productivity (Pennington et al., 2006) and therefore high particle densities. The sinking biogenic particles will adsorb the dissolved Nd and, as already mentioned, it is particularly the large phytoplankton species such as diatoms, which dominate the biogenic particles in the study area (Estrada and Blasco, 1985). In support of this, a modeling study by Arsouze et al. (2009) suggested that particle size and the resulting sinking velocity will have a significant influence on the dissolved Nd concentration as well as the Nd isotope composition in the deep water.

At the same time, deep water masses at the northernmost station (St. 160, Fig. 6.3) are highly radiogenic in their Nd isotope composition, even at a depth of 1500m (ε_{Nd} = -0.8), respectively 2600m (ε_{Nd} = -1.6). These radiogenic values in the north are similar to data obtained from a ferromangenese crust that incorporated its isotopic signature from bottom waters at approximately 14°N off the Mexican coast (ε_{Nd} = -2.5, Frank et al., 1999). One possible explanation for the radiogenic Nd isotope signatures in the deep waters is intense exchange processes with the nearby continental margin, which is characterized by highly radiogenic Nd isotope values in this area (ε_{Nd} = ~ +10, Jeandel et al., 2007). Many authors have suggested that boundary exchange processes with continental margins play an important, if not the dominant role for the dissolved Nd isotope composition of seawater (Lacan & Jeandel, 2005; Arsouze et al., 2007, 2009), but also exchange processes with deep-sea sediments may exert some influence.

Another possible explanation is vertical transport of particles with radiogenic isotope signatures from surface waters to the deep ocean. Surface

waters in the northern part of the study area are characterized by highly radiogenic values of ε_{Nd} = 0 to ε_{Nd} = +3, which have probably been controlled by partial dissolution of particles. When these particles sink to the bottom and keep releasing Nd, this will also influence the dissolved Nd isotope signal of the deep waters. Vertical processes can thus explain the radiogenic Nd isotope values of deep water masses at the northern stations but not their diminished concentrations. Our data clearly suggest that not only exchange but also net removal of Nd in the EEP water column must occur during the scavenging processes for example by biogenic particles. The removal can be considered very efficient given that the anoxic sediments underlying the OMZ off Peru are expected to represent an additional source of REEs (Elderfield and Sholkovitz, 1987; Haley et al., 2004) and other redox-sensitive metals, such as iron (Landing and Bruland, 1987; Bruland et al., 2005). The above combined effects best explain why the deep water masses in the Eastern Pacific Basin do not fit on a hypothetical mixing line between LCDW and NPDW (Fig. 6.5).

The general agreement of the Nd isotope distribution with that of the major water masses supports the applicability of Nd as a proxy for present and past ocean circulation. Zonal surface and subsurface currents, which transport oxygen-rich water to the upwelling area, are clearly traceable by their specific radiogenic Nd isotope compositions. By extracting the Nd isotope composition of past water masses involved in the Peruvian upwelling this information can be used to reconstruct the import of oxygen-rich waters to the shelf regions and therefore to determine changes in the strength of the OMZ caused by changes in advective supply of oxygen. However, the results of our study also demonstrate that in areas with high particle fluxes and prevalence of easily weatherable phases, such as volcanogenic particles, the dissolved Nd isotope signal of the waters can be influenced. This has to be taken into account for the interpretation of paleo records in shelf regions, as well as for the reconstruction of deep water mass mixing.

6.5. Conclusions

This study presents the first full water column distributions of dissolved Nd isotopes and Nd concentrations in the EEP. Zonal current bands from the Central Pacific providing oxygen-rich water masses are clearly traceable by distinctly radiogenic Nd isotope compositions (ε_{Nd} = -2), which can be used to reconstruct the evolution of advective import of oxygen-rich water masses into the coastal upwelling system and the OMZ off Peru. More radiogenic Nd isotope signatures in the northern part of the study area indicate the advection of Central Pacific Water masses into intermediate water depths of the EEP. The deep water Nd isotope signatures in all profiles reflect the mixture between sources in the Southern Ocean and the North Pacific except the northernmost station from the Panama Basin.

There is, however, also clear evidence for non-conservative effects. Surface water masses show a trend towards more radiogenic values in the north coupled to higher Nd concentrations, which is obviously caused by particle exchange. Deep and bottom waters in the northern part of the study area are significantly depleted in their Nd concentration and at the same time show more radiogenic isotopic signatures than expected from mixing between NPDW and LPDW. To explain these observations dissolved Nd must be scavenged resulting in a net removal from the water column, most likely by sinking biogenic particles despite that the anoxic sediments off Peru have to be considered an additional source for REEs and other redox-sensitive metals. At the same time, some of the scavenged Nd must be released to the deep and bottom waters, which is documented by highly radiogenic Nd isotope compositions in the entire water column in the northern part of the study area. Alternatively, these radiogenic Nd isotope signatures can also be explained by transport of volcanic particles from surface waters to the deep ocean, where partial dissolution and release of radiogenic Nd occurs. In addition, exchange processes with the shelf sediments at the Peruvian margin may also contribute to the observed dissolved Nd isotope distribution.

7. Conclusions and Outlook

7.1 General Conclusions

The main goal of this study was to characterize the Si and Nd isotope composition of water masses, in particular the currents supplying oxygen-rich water to the OMZ of the Eastern Equatorial Pacific and to better understand the processes controlling biogeochemical cycling in the highly productivity upwelling area off Ecuador and Peru. These processes are the key factors controlling the oxygen content and the extent of the OMZ.

The first direct comparison between the dissolved Si isotope composition ($\delta^{30}Si(OH)_4$) in the water column along the Peruvian shelf with isotopic analyzes of hand-picked diatoms ($\delta^{30}Si_{diatom}$), respectively biogenic silicate ($\delta^{30}Si_{bSiO2}$) extracted from the underlying surface sediments. Upwelled surface waters on the shelf off Peru are mainly fed by southward flowing subsurface waters along the coast, which show a mean $\delta^{30}Si_{Si(OH)4}$ of 1.5‰. The concentration of dissolved silicic acid ($Si(OH)_4$) increases towards the south and with increasing water depth documenting intense remineralization of particulate biogenic silica ($bSiO_2$) in the water column and in the sediment. In the area of the strongest upwelling and re-supply of $Si(OH)_4$, where the degree of utilization of $Si(OH)_4$ is overall low (about 50%), the increase in surface water $\delta^{30}Si_{Si(OH)4}$ compared to the subsurface source waters is small, only 0.2 to 0.3‰. Higher degrees of $Si(OH)_4$ utilization (up to 93%) in surface waters outside the main upwelling area result in higher $\delta^{30}Si_{Si(OH)4}$ values of up to 2.8‰, corresponding to a difference of up to 1.2 ‰ from the source water. It is demonstrated that the silicon isotopes are a reliable proxy for silicic acid utilization but a direct comparison to $\delta^{30}Si_{bSiO2}$ signatures obtained from bulk $bSiO_2$ in the sediment, and $\delta^{30}Si_{diatom}$ from hand-picked diatoms indicates that in sediment samples with low $bSiO_2$ concentrations a contamination with isotopically lighter siliceous material occurs, which may influence the interpretation of paleo records.

In the 4th chapter a direct comparison of $\delta^{30}Si_{Si(OH)4}$ to the distribution of of dissolved nitrate isotopes ($\delta^{15}NO_3^-$) is presented along a 10°Stransect perpendicular to the coast. During strong upwelling near the shelf, low

$\delta^{30}Si(OH)_4$ signatures (2‰) correspond to rather high $\delta^{15}NO_3^-$ (14‰), because the source waters are influenced by dissolution processes of $bSiO_2$ and N-loss under suboxic conditions due to denitrification and/or anammox processes. Even though nitrate concentrations are diminished within the OMZ and used by more phytoplankton species than silicic acid, the limiting macro nutrient further offshore was most $Si(OH)_4$. The direct comparison also showed that surface waters are strongly influenced by water mass advection and it has to be taken into account that nitrate is more efficiently recycled within the upper water column than silicic acid due to zooplankton grazing pressure, which may also have an influence on the isotopic signal. During the time of sampling the study area was influenced by a large mesoscale eddy, which transported nutrients offshore and therefore stimulated phytoplankton growth at its edges. The surface waters in the centre of the eddy in contrast were characterized by low chlorophyll concentrations, strongly depleted in $Si(OH)_4$ and NO_3^- and therefore highly fractionated in $\delta^{30}Si(OH)_4$ (3.7‰) and $\delta^{15}NO_3^-$ (16‰). Eddies such as the one observed are recurrent features that have a major influence on the distribution and dynamics of nutrients and the stable isotope composition in surface waters of upwelling regions. The differences in the stable isotope distributions have to be taken into account for the interpretation of paleo records given that the nitrate isotope composition is rather influenced by denitrification and/or anammox processes than by utilization.

Furthermore a characterization of deep water masses in the study area was conducted. Previous studies showed that different deep water masses show distinct silicon isotope values. The data obtained in this study for water masses below 2000m showed lower $\delta^{30}Si(OH)_4$ (1.1‰) compared to the Central Pacific (1.3‰) and higher values compared to the North Pacific (0.7‰). A compilation of the data, which is available for the Pacific ocean show a large scatter ranging from 0.6‰ to 1.5‰ and no clear trend with respect to the silicic acid concentration or distinct water masses. Thus it is suggested that the distribution of distinct $\delta^{30}Si(OH)_4$ signatures in deep waters of the Pacific are a consequence of a combination of the relatively sluggish deep water circulation

and remineralization processes. A larger data set has to be obtained to fully understand the processes influencing the Si isotope signature.

The Nd isotope composition in deep and bottom waters in the northern part of the study area are significantly depleted in their Nd concentration and at the same time show more radiogenic isotopic signatures than expected from mixing between NPDW LPDW. This is supported by relatively low Nd concentrations in deep waters (3000m to 6000m) in the EEP (20 pmol/kg) compared to locations in the Northern and Central Pacific (40-60 pmol/kg), which suggests enhanced removal of Nd in the EEP. To explain these observations dissolved Nd must be scavenged efficiently resulting in a net removal from the water column, most likely adsorbed to sinking biogenic particles despite that the anoxic sediments off Peru have to be considered an additional source for REEs and other redox-sensitive metals. At the same time, some of the scavenged Nd must be released again to the deep and bottom waters, which is documented by highly radiogenic Nd isotope compositions in the entire water column in the northern part of the study area. Alternatively, these radiogenic Nd isotope signatures can also be explained by transport of volcanic particles from surface waters to the deep ocean, where partial dissolution and release of radiogenic Nd occurs. This is also documented by the highly radiogenic values in surface waters in the northern part of the study (ε_{Nd} = +3). In addition, exchange processes with the shelf sediments at the Peruvian margin may also contribute to the observed dissolved Nd isotope distribution. Near surface zonal current bands, such as the Equatorial Undercurrent (EUC) and the Subsurface Countercurrent (SSCC), which supply oxygen-rich water to the OMZ are characterized by radiogenic Nd isotope signatures (ε_{Nd} = -2). As these currents partly feed the Peru-Chile Undercurrent (PCUC), which is the main subsurface source water mass for the upwelling, this information can be used as a proxy indicator for the current regime of the past that controlled the upwelling intensity.

In this study I presented the first Si and Nd isotope composition obtained in an upwelling region. Furthermore the first direct comprehensive comparison of dissolved $\delta^{30}Si(OH)_4$ data from the water column with measurements on bulk

biogenic opal ($\delta^{30}Si_{bSiO2}$) and from handpicked diatoms ($\delta^{30}Si_{diatom}$) from the underlying surface sediments were made. These are new findings, which have local, as well as general implications for the interpretation of present and past distributions of Si and Nd isotopes in terms of nutrient utilization and paleocirculation.

7.2 Outlook

The Peruvian upwelling area is a high productivity region, which leads to one of the globally largest OMZs in the world. Upwelling intensity and remineralization of nutrients are directly driving the primary productivity above the OMZ. Therefore it is of great interest to better understand the factors controlling the nutrient concentrations. The $\delta^{30}Si(OH)_4$ in subsurface waters and within the OMZ of the study area showed that the factors mainly controlling the Si isotope distribution are different intensities of dissolution of bSi and not the mixing of distinct water masses. Nevertheless no clear correlation between $\delta^{30}Si(OH)_4$ and suboxic or anoxic waters of the OMZ can be observed in the study area. Dissolution processes are apparently mainly a function of water depth, but bacterial activities, which especially occur within the OMZ can enhance the bSi dissolution rates. Remineralization processes needs to be studied in more detail to reach firmer conclusions on the importance for oxygen levels. For a better understand of the remineralization of organic matter and the dissolution of $bSiO_2$ it would be necessary to analyze the silicon isotopes, as well as nitrogen isotopes in the particulate phases.

The distribution of Nd concentrations in deep water masses of the EEP showed unexpectedly low Nd concentrations and rather radiogenic Nd isotope compositions, indicating that scavenging and release processes in this area have a major impact on the Nd budget. Further studies, especially the analysis of particulate phases could lead to a better understanding of the processes influencing the Nd isotope composition as well the Nd concentrations. For both, the radiogenic Nd as well as the stable Si isotopes it would be of great interest to obtain detailed information of the isotope distribution in and released from

pore waters given that exchange with shelf sediments plays a major role in controlling the Si, as well as the Nd budget.

A major part of this thesis was to establish the silicon isotope measurements at IFM-GEOMAR in Kiel. At the beginning many problems had to be solved in terms of ion exchange chromatography and in particular the achievement of the required analytical precision and accuracy. Future work has to be carried out to improve the measurements and the external reproducibility. This will allow to resolve the relatively small fractionation factors during utilization and the dissolution processes of silicon isotopes, as well as the small differences in deep water masses.

References

Abrantes, F., Lopes, C., Mix, A., & Pisias, N. (2007). Diatoms in Southeast Pacific surface sediments reflect environmental properties. *Quaternary Science Reviews*, *26*, 155-169

Albarède, F., Telouk, P., Blichert-Toft, J., Boyet, M., Agranier, A., & Nelson, B. (2004). Precise and accurate isotopic measurements using multiple-collector ICPMS1. *Geochimica et Cosmochimica Acta*, *68*(12), 2725-2744

Alleman, L. Y., Cardinal, D., Cocquyt, C., Plisnier, P.-D., Descy, J.-P., Kimirei, I., Sinyinza, D., et al. (2005). Silicon Isotopic Fractionation in Lake Tanganyika and Its Main Tributaries. *Journal of Great Lakes Research*. *31*(4), 509-519

Allen, J. T., Brown, L., Sanders, R., Moore, C. M., Mustard, A., Fielding, S., Lucas, M., et al. (2005). Diatom carbon export enhanced by silicate upwelling in the northeast Atlantic. *Nature*. *437*, 728-732.

Altabet, M. A., & Francois, R. (1994). Sedimentary nitrogen isotopic ratio as a recorder for surface ocean utilization, *Global biogeochemical Cycles. 8* (1), 103-116.

Amakawa, H., Alibo, D. S., and Nozaki, Y., (2000). Nd isotopic composition and REE pattern in the surface waters of the eastern Indian Ocean and its adjacent seas. *Geochimica et Cosmochimica Acta. 64* (10), 1715-1727

Amakawa, H., Nozaki, Y., Alibo, D. S., Zhang, J., Fukugawa, K., & Nagai, H., (2004). Neodymium isotopic variations in Northwest Pacific waters. *Geochimica et Cosmochimica Acta*. *68* (4), 715-727

Amakawa, H., Sasaki, K., & Ebihara, M., (2009). Nd isotopic composition in the central North Pacific. *Geochimica et Cosmochimica Acta*. *73*, 4705-4719

Arsouze, T., Dutay, J., Lacan, F., & Jeandel, C., (2007). Modeling the neodymium isotopic composition with a global ocean circulation model. *Chemical Geologie*, *239*, 165-177

Arsouze, T., Dutay, J.-C., Lacan, F., and Jeandel, C., (2009). Reconstructing the Nd oceanic cycle using a coupled dynamical – biogeochemical model. *Biogeosciences. 6*, 2829-2846

Ayon, P., Criales-Hernandez, M., Schwamborn, R., and Hirche, H. (2008). Zooplankton research off Peru: A review. *Progress In Oceanography*. *79*, 238-255

Barrat, J. A., Keller, F., Amossé, J., Taylor, R. N., Nesbitt, R. W., Hirata, T., (1996). Determination of Rare Earth Elements in Sixteen Silicate

Reference Samples By Icp-Ms After Tm Addition and Ion Exchange Separation. *Geostand. Geoanal. Res. 20*, 133-139

Berger W. H., Smetacek V. S., and Wefer G. (1989). *Productivity of the Ocean: Present and Past*. John Wiley & Sons, Berlin, p. 471

Beucher, C. P., Brzezinski, M. A., & Jones, J. (2011). Mechanisms controlling silicon isotope distribution in the Eastern Equatorial Pacific. *Geochimica et Cosmochimica Acta*, 75, 4286-4294

Beucher, C. P., Brzezinski, M. A., and Crosta, X. (2007). Silicic Acid dynamics in the glacial sub-Antartic: Implications for the silicic acid leakage hypothesis. *Global Biogeochemical Cycles*, 21 (3), GB3015, doi: 10.1029/2006GB002746

Beucher, C., Brzezinski, M. A., & Jones, J. (2008). Sources and biological fractionation of Silicon isotopes in the Eastern Equatorial Pacific. *Geochimica et Cosmochimica Acta*, *72*, 3063-3073

Bidle, K. D. and Azam, F. (1999). Accelerated dissolution of diatom silica by marine bacterial assembledges. *Nature*, 397, 508-512

Bidle, K. D., Manganelli, M., & Azam, F. (2002). Regulation of oceanic silicon and carbon preservation by temperature control on bacteria. *Science 298*, 1980-1983

Bostock, H. C., Opdyke, B. N., & Williams, M. J. M. (2010). Characterising the intermediate depth waters of the Pacific Ocean using $\delta^{13}C$ and other geochemical tracers. *Deep Sea Research Part I: Oceanographic Research Papers*, *57*, 847-859

Brainard, R. E. and McLain, D. R. (1987). Seasonal and Interannual Subsurface Temperature Variability off Peru, 1952-1984, In: the Peruvian Anchoveta and ist Upwelling Ecosystem: three Decades of Change, edited by Pauly, D. and Tsukayama. ICLARM Studies and Reviews

Brandes, J. A., Devol, A. H., Yoshinari, T., Jayakumar, D. A., Naqvi, W.A. (1998). Isotopic composition of nitrate in the central Arabian Sea and eastern tropical North Pacific: A tracer for mixing and nitrogen cycles. *Limnology and Oceanography*, 43 (7), 1680-1689

Brink, K., Halpern, D., Huyer, A., & Smith, R. L. (1983). The physical environment of the Peruvian upwelling system. *Progress In Oceanography*, *12*, 285-305

Brodie, I., & Kemp, A. E. S. (1994). Variation in biogenic and detrital fluxes and formation of laminae in late Quaternary sediments from the Peruvian coastal upwelling zone. *Marine Geology*, *116*, 385-398.

Broecker, W.S., (1991). The great ocean conveyor belt. *Oceanography.* 4, 79-89

Broecker, W.S., Peng, T.H., (1982). Tracers in the Sea. *Eldigio Press*, New York.

Bruland, K., Rue, E., Smith, G., & Ditullio, G. (2005). Iron, macronutrients and diatom blooms in the Peru upwelling regime: brown and blue waters of Peru. *Marine Chemistry*, *93*, 81-103.

Bruland, K., W., Rue, E. L., Smith, G. J. (2001). Iron and macronutrients in California coastal upwelling regimes: Implications for diatom blooms. *Limnology and Oceanography* 46(7), 1661-1674

Brzezinski, M. A., Pride, C. J., Franck, V. M., Sigman, D. M., Sarmiento, J. L., Matsumoto, K., Gruber, N., et al. (2002). A switch from $Si(OH)_4$ to NO_3^- depletion in the glacial Southern Ocean. *Geophysical Research Letters*, *29*(12), 1-4. doi:10.1029/2001GL014349

Cardinal, D., Alleman, L. Y., Dehairs, F., Savoye, N., Trull, T. W., & André, L. (2005). Relevance of silicon isotopes to Si-nutrient utilization and Si-source assessment in Antarctic waters. *Global Biogeochemical Cycles*. *19*(2), 1-13. doi:10.1029/ 2004GB002364

Carr, M.-E., P. T. Strub, A. C. Thomas, and J. L. Blanco (2002), Evolution of 1996–1999 La Niña and El Niño conditions off the western coast of South America: A remote sensing perspective, *Journal of Geophysical Research 107*(C12), 3236, doi:10.1029/2001JC001183.

Casciotti, K. L. (2009a). Inverse fractionation during bacterial nitrite oxidation. *Geochimica and Cosmochimica Acta.* 73. 2061-2076

Casciotti, K. L. and McLLvin, M. R. (2009b). Isotopic analysis of nitrate and nitrite from reference mixtures and application to Eastern Tropical North Pacific waters. *Marine Chemistry.* 107, 184-201

Chaigneau, A., Gizolme, A., & Grados, C. (2008). Mesoscale eddies off Peru in altimeter records: Identification algorithms and eddy spatio-temporal patterns. *Progress In Oceanography*, *79*, 106-119

Chavez, F. P., and Barber, R. T., (1987). An estimate of new production in the equatorial Pacific. *Deep-Sea Research. 34*(7), 1229-1243

Chavez, F. P. (1989). Size distribution of Phytoplankton in the Central and Eastern Tropical Pacific. *Global Biogeochemical Cycles*, 3 (1), 27-35

Chavez, F. P., and Messié, M., (2009). A comparison of Eastern Boundary Upwelling Ecosystems. *Progress in Oceanography. 83*, 80-96.

Codispoti, L. A. (2007). An oceanic fixed nitrogen sink exceeding 400 Tg N a−1 vs. the concept of homeostasis in the fixed-nitrogen inventory. *Biogeosciences*, *4*, 233-253

Conley, D. J., & Malone, T. C. (1992). Annual cycle of dissolved silicate in Chesapeake Bay: Implications for the production and fate of phytoplankton biomass. *Marine Ecology Progress Series*. *81*, 121-128

Correa-Ramirez, M. A.,Hormazábal, S. and Yuraz, G. (2007). Mesoscale Eddies and high chlorophyll concentrations off ventral Chile (29°-39°S), L12604, doi:10.1029/2007GL029541

Cullen, J. J., Lewis, M. R., Davis, C. O., & Barber, R. T. (1992). Photosynthetic Characteristics and Estimated Growth Rates Indicate Grazing Is the Proximate Control of Primary Production in the Equatorial Pacific. *Journal of Geophysical Research*, *97*(C1), 639-654. doi:10.1029/91JC01320

Czeschel, R., Stramma, L., Schwarzkopf, F. U., S, B., Funk, A., & Karstensen, J. (2011). Mid-depth circulation of the eastern tropical South Pacific and its link to the oxygen minimum zone. *Journal of Geophysical Research*, *116*. CO1015. doi:10.1029/2010JC006565

Daneri, G., Dellarossa, V., Quinones, R., Jacob, B., Montero, P., & Ulloa, O. (2000). Primary production and community respiration in the Humboldt Current System off Chile and associated oceanic areas. *Marine Ecology Progress Series*, *197*, 41-49

De La Rocha, C., Brzezinski, M. A., & Deniro, M. (1997). Fractionation of silicon isotopes by marine diatoms during biogenic silica formation. *Geochimica et Cosmochimica Acta*. *61*(23), 5051-5056

De La Rocha, C. L., Brzezinski, M. A., De Niro, M. J., & Shemesh, A. (1998). Silicon-isotope composition of diatoms as an indicator of past oceanic change. *Nature*. *395*, 680-683

De La Rocha, C. L., Brzezinski, M. A., & De Niro, M. J. (2000). A first look at the distribution of the stable isotopes of silicon in natural waters. *Geochimica et Cosmochimica Acta*. *64*(14), 2467-2477

De La Rocha, C. L. (2003). Silicon isotope fractionation by marine sponges and the reconstruction of the silicon isotope composition of ancient deep water. *Geology*, *31*, 423-426

De Souza, Gregory (2011). The marine biogeochemical cycle of silicon: insights from silicon stable isotopes. *Dissertation*, ETH Zürich

De Souza, G., Reynolds, B., Rickli, J., Frank, M., Saito, M. Gerringa, L. J. A., Bourdon, B. (2012). Southern Ocean control of silicon stable isotope distribution in the deep Atlantic. *Global Biogeochemical Cycles*. submitted.

De Vries, T. J., & Schrader, H. (1981). Variations of upwelling/oceanic conditions during the latest Pleistocene through Holocene off the central Peruvian coast: a diatom record. *Marine Micropaleontology*, *6*, 157-167.

Demarest, M. S., Brzezinski, M. a, & Beucher, C. P. (2009). Fractionation of silicon isotopes during biogenic silica dissolution. *Geochimica et Cosmochimica Acta*, *73*, 5572-5583

Demarest, M. S., Brzezinski, M. A., Nelson, D. M., Krause, J. W., Jones, J. L., Beucher, C. P. (2011). Net biogenic silica production and nitrate regeneration determine the strength of the silica pump in the Eastern Equatorial Pacific. *Deep-Sea Research II*, 58, 462-476

DeMaster, D. J. (1981). The supply and accumulation of silica in the marine environment. *Geochimica et Cosmochimica Acta*, *45*(10), 1715-1732.

DeNiro, M. and Ebstein, S. (1981) Influence of diet on the distribution of nitrogen isotopes in animals, *Geochimica et Cosmochimica Acta. 45 (3), 341-351*

Deutsch, C., Brix, H., Ito, T., Frenzel, H., Thompson, L. (2011). Climate-Forced Variability of Ocean Hypoxia. *Science*. 333, 336-338

Dixit, S., van Cappellen, P., & van Bennekom, A. J. (2001). Processes controlling solubility of biogenic silica and pore water build-up of silicic acid in marine sediments. *Marine Chemistry*. *73*, 333-352.

Douthitt, C. B. (1982). The geochemistry of the stable isotopes of silicon. *Geochimica et Cosmochimica Acta*. *46*(8), 1449-1458

Dugdale, R. C., & Wilkerson, F. P. (1998). Silicate regulation of new production in the equatorial Pacific upwelling. *Nature*. *391*, 270-273.

Dugdale, R. C., Wilkerson, F., & Minas, H. (1995). The role of a silicate pump in driving new production. *Deep Sea Research Part I: Oceanographic Research Papers*, *42*(5), 697-719

Ehlert, C. (2011). Late quaternary changes in silicate utilization and upwelling intensity off Peru: insights from silicon and neodymium isotopes *Dissertation*, Christian-Albrecht University of Kiel, Germany

Elderfield, H., & Sholkovitz, E., (1987). Rare earth elements in the pore waters of reducing nearshore sediments. *Earth and Planetary Sciences Letter. 82*, 280-288.

Elderfield, H., and Greaves, M. J., (1982). The rare earth elements in seawater. *Nature*. *296*, 214-219

Elderfield, H., Upstill-Goddard, R., and Sholkovitz, E., (1989). The rare earth elements in rivers, estuaries, and coastal seas and their significance to the composition of ocean waters. *Geochimica and Cosmochimica Acta*. *54*, 971-991

Ellwood, M. J., & Hunter, K. A. (1999). Determination of the Zn/Si ratio in diatom opal: a method for the separation, cleaning and dissolution of diatoms. *Marine Chemistry*, *66*(3-4), 149-160

Estrada M., and Blasco D. (1985). Phytoplankton assemblages in coastal upwelling areas. In C. Bas, R. Margalef, & P. Rubies (Eds.), *Simposio Internacional Sobre Las Areas de Afloramiento Mas Importantes del Oeste Africano (Cabo Blanco y Benguela).* Instituto de Investigaciones Pesqueras, Barcelona, pp. 379-402.

Feldman, G., Clark, D., & Halpern, D. (1984). Satellite Color Observations of phytoplankton distribution in the Eastern Equatorial Pacific during the 1982-1983 El Nino. *Science*, *226*, 1069-1071

Fiedler, P. C. (2002). Environmental change in the Eastern tropical Pacific Ocean: review of ENSO and decadal variability. *Marine Ecological Process Series*, *224*, 265-283

Fiedler, P., & Talley, L. (2006). Hydrography of the eastern tropical Pacific: A review. *Progress In Oceanography*, *69*, 143-180

Franck, V.M., Brzezinski, M. A., Coale, K.H., Nelson, D. M. (2000). Iron and silicic aid concentrations regulate Si uptake north and south of the Polar Frontal Zone in the Pacific Sector of the Southern Ocean. *Deep Sea Research II*, 47, 3315-3558

Frank, M. (2002). Radiogenic isotopes: Tracers of past ocean circulation and erosional input. *Reviews of Geophysics 40*, 1001, 38PP, doi:10.1029/2000RG00094

Frank, M., Reynolds, B. C., & O'Nions, R. K., (1999). Nd and Pb isotopes in Atlantic and Pacific water masses before and after closure of the Panama gateway. *Geology, 27*, 1147-1150

Franz, J., Krahmann, G., Lavik, G., Grasse, P., Dittmar, P., Riebesell, U. (2011). Dynamics and stoichiometry of nutrients and phytoplankton in waters influenced by the oxygen minimum zone in the eastern tropical Pacific. *Deep-Sea Research II. in press*

Friedrich, G., Ledesma, J., Ulloa, O., Chavez, F. P. (2008). Air-Sea carbon dioxide fluxes in the coastal southeastern tropical Pacific. *Progress in Oceanography*, 79, 156-166

Fripiat, F., Cavagna, A.-J., Savoye, N., Dehairs, F., André, L., & Cardinal, D. (2011). Isotopic constraints on the Si-biogeochemical cycle of the Antarctic Zone in the Kerguelen area (KEOPS). *Marine Chemistry*. *123*(1-4), 11-22

Fuenzalida, R., Schneider, W., Garcés-Vargas, J., Bravo, L., & Lange, C. B. (2009). Vertical and horizontal extension of the oxygen minimum zone in the eastern South Pacific Ocean. *Deep-Sea Research*, *56*(16), 1027-1038

Ganachaud et al., (2011). Observed and expected changes to the tropical Pacific Ocean. Published in: Bell JD, Johnson JE and Hobday AJ (eds),

Vulnerability of Tropical Pacific Fisheries and Aquaculture to Climate Change. Secretariat of the Pacific Community, Noumea, New Caledonia.

Georg, R. B., Reynolds, B., Frank, M., & Halliday, A. (2006). New sample preparation techniques for the determination of Si isotopic compositions using MC-ICPMS. *Chemical Geology*, *235*(1-2), 95-104

German, C. R., Klinkhammer, G. P., Edmond, J. M., Mitra, A., and Elderfield, H., (1990). Hydrothermal scavenging of rare-earth elements in the ocean. *Nature*. *345*, 516-518.

Goldstein, S. J., and Jacobsen, S. B., (1988). REE in the Great Whale River estuary, northwest Quebec. *Earth and Planetary Science Letter. 88*(3-4), 241-252

Goldstein, S., O'Nions, R. K., and Hamilton, P., (1984). A Sm-Nd isotopic study of atmospheric dusts and particulates from major river systems. *Earth and Planetary Science Letter*, *70*. 221-236.

Goméz, F., Claustre, H., Raimbault, P. and Soissi, S. (2007). Two High-Nutrient Low-Chlorophyll phytoplankton assembledges: the tropical central Pacific and the offshore Perú-Chile Current. *Biogeosciences*, 4, 1101-1103

Grasshoff, K., Kremlin, K. Erhardt, M. (1999). *Methods for seawater analysis – third completely revised and extended version*. Wiley VHC, New York, p. 600.

Gruber, N., Sarmiento, J. L. (1979) Global pattern of marine nitrogen fixation and denitrification. *Global Biogeochemical Cycles*, 11 (2), 235-266

Gunther, E. R. (1936). A report on oceanographic investigations in the Peru Coastal Current. *Discovery Report*, *13*, 107-276.

Haley, B.A., Klinkhammer, G.P., and McManus, J., (2004). Rare earth elements in pore waters of marine sediments. *Geochimica and Cosmochimica Acta*. *68*, 1265-1279.

Halliday, N., Davidson, P., Holden, P., Owen, M., Olivarez, M., (1992). Metalliferous sediments and the scavenging residence time of Nd near hydrothermal vents. *Geophysical Research Letters 19*(8), 761-764.

Hansen, K. R., and Koroleff, F. (1999). Determination of nutrients. In K. Grasshoff, K. Kremling, M. Ehlert (Eds.), in *Methods of seawater analysis* (3rd ed.). Verlag Chemie, Weinheim, 159-228

Garcia, H. E., R. A. Locarnini, T. P. Boyer and J. I. Antonov (2010). *World Ocean Atlas 2009, Volume 4: Nutrients (phosphate, nitrate, silicate)*. NOAA Atlas NESDIS 71. U.S. Government Printing Office, Washington DC.

Hendry, K. R., Georg, R. B., Rickaby, R. E. M., Robinson, L. F., & Halliday, A. N. (2010). Deep ocean nutrients during the Last Glacial Maximum

deduced from sponge silicon isotopic compositions. *Earth and Planetary Science Letters*, *292*(3-4), 290-300

Henry, F., Jeandel, C., Dupré, B., Minster, J.-F.(1994). Particulate and dissolved Nd in the western Mediterranean Sea: Sources, fate and budget. *Marine Chemistry. 45*(4), 283-305

Heumann, K. G., (1992). Isotope dilution mass spectrometry (IDMS) of the elements. *Mass Spectrometry Reviews. 11*, 41-67

Hormazabal, S., Núñez, S., Arcas, D., Espindola, F., Yures, G. (2004) Mesoscale eddies and pelagic fishery off central Chile (33°-40°S), *Gayana (Concepc.)*, 68, (2), 291-296

Hurd, D. C. (1973). Interactions of biogenic opal, sediment and seawater in the Central Equatorial Pacific. *Geochimica et Cosmochimica Acta*. *37*(10), 2257-2282

Hutchins, D. A. and Bruland, K. W. (1998). Iron-limitated diatom growth and Si:N uptake ratios in a coastal upwelling regime. Nature, 393, 561-563

Huyer, A., Smith, R. L., & Paluszkiewicz, T. (1987). Coastal Upwelling off Peru During Normal and El Niño Times, 1981–1984. *Journal of Geophysical Research*, *92*(C13), 297-307. doi:10.1029/JC092iC13p14297

Jacobsen, S. B., and Wasserburg, G. J., (1980). Sm-Nd isotopic evolution of chondrites. *Earth and Planetary Science Letter*. *50*, 139-155

Jeandel, C., Arsouze, T., Lacan, F., Techine, P., Dutay, J., (2007). Isotopic Nd compositions and concentrations of the lithogenic inputs into the ocean: A compilation, with an emphasis on the margins. *Chemical Geologie 239*, 156-164

Jeandel, C., Bishop, J. K., and Zindler, A., (1995). Exchange of neodymium and its isotopes between seawater and small and large particles in the Sargasso Sea. *Geochimica and Cosmochimica Acta*. *59*(3), 535-547

Jiang, M.-S., Chai, F., Dugdale, R. C., Wilkerson, F. P., Peng, T.-H., Barber, R. T. (2003). A nitrate and silicate budbet in the equatorial Pacific Ocean: a coupled physical-biological model study. *Deep Sea Research II*. 50, 2971-2996

Johnson, G., and Toole, J. (1993). Flow of deep and bottom waters in the Pacific at 10°N. *Deep Sea Research Part I: Oceanographic Research Papers*, *40*(2), 371-394

Jones, K. M., Khatiwala, S. P., Goldstein, S. L., Hemming, S. R., van de Flierdt, T., (2008). Modeling the distribution of Nd isotopes in the oceans using an ocean general circulation model. *Earth and Planetary Science Letter 272*(3-4), 610-619.

Karl, D. M., and Michaels, A. F. (2001). Nitrogen Cycle. *Encyclopedia of OceanSciences. 1st edition.* Elsevier ltd, .pp 1876-1884.

Karl, D. M., and Tien, G. (1992). MAGIC: A sensitive and precise method for measuring dissolved phosphorus in aquatic environments. *Limnology and Oceanography*, 37(1), 105-16

Karstensen, J., & Ulloa, O. (2008). The Peru-Chile Current System. *Encyclopedia of Ocean Sciences 2nd edition online*.

Karstensen, J., Stramma, L., & Visbeck, M. (2008). Oxygen minimum zones in the eastern tropical Atlantic and Pacific oceans. *Progress In Oceanography*, *77*(4), 331-350

Kaupp, L. J., Measures, C. I., Selph, K. E., & Mackenzie, F. T., (2011). The distribution of dissolved Fe and Al in the upper waters of the Eastern Equatorial Pacific. *Deep-Sea Res Pt. II*. *58*, 296-310. Elsevier.

Kawabe, M., and Fujio, S. (2010). Pacific ocean circulation based on observation. *Journal of Oceanography*, *66*, 389-403. doi:10.1007/s10872-010-0034-8

Keeling, R. F., Körtzinger, A., and Gruber, N.(2010). Ocean Deoxygenation in a Warming World. *Annual Review of Marine Sciences*, 2, 199-229

Kessler, W. (2006). The circulation of the eastern tropical Pacific: A review. *Progress In Oceanography*, *69*, 181-217

Klinkhammer, G. P., Elderfield, H., Hudson, A., (1983). Rare earth elements in seawater near hydrothermal vents. *Nature. 305*, 185-187.

Lacan, F., and Jeandel, C., (2001). Tracing Papua New Guinea imprint on the central Equatorial Pacific Ocean using neodymium isotopic compositions and Rare Earth Element patterns. *Earth Planet. Sci. Lett. 186*, 497-512.

Lacan, F. and Jeandel, C. (2005) Acquisition of the neodymium isotopic composition of the North Atlantic Deep Water. Geochemistry Geophysics Geosystems, 6(12). Q12008, doi:10.1029/2005GC000956

Lacan, F., and Jeandel, C., (2005). Neodymium isotopes as a new tool for quantifying exchange fluxes at the continent–ocean interface. *Earth Planet. Sci. Lett. 232*(3-4), 245-257.

Laës, A., Blain, S., Laan, P., Achterberg, E. P., Sarthou, G., de Baar, H. J. W., (2003). Deep dissolved iron profiles in the eastern North Atlantic in relation to water masses. *Geophys. Res. Lett. 30*, 1902, doi:10.1029/2003GL017902

Lam, P., Lavik, G., Jensen, M. M., van de Vossenberg, J., Schmid, M., Woebken, D., Gutiérrez, D., et al. (2009). Revising the nitrogen cycle in the Peruvian oxygen minimum zone. *Proceedings of the National*

Academy of Sciences of the United States of America, *106*(12), 4752-7. doi:10.1073/pnas.0812444106

Landing, W., and Bruland, K., (1987). The contrasting biogeochemistry of iron and manganese in the Pacific Ocean. *Geochimimica and Cosmochimica Acta*, *51*, 29-43.

Le Fèvre, B., and Pin, C., (2005). A straightforward separation scheme for concomitant Lu–Hf and Sm–Nd isotope ratio and isotope dilution analysis. *Analytical Chimical Acta*, *543*, 209-221.

Leth, O., and J. F. Middleton (2004), A mechanism for enhanced upwelling off central Chile: Eddy advection, *Journal of Geophysical Research*,*109*, C12020, doi:10.1029/2003JC002129.

Lewin, J. (1961). The dissolution of silica from diatom walls. *Geochimica et Cosmochimica Acta*, *21*(3-4), 182-198. doi:10.1016/S0016-7037(61)80054-9

Lukas, R. (1986). The termination of the Equatorial Undercurrent in the eastern Pacific. *Progress In Oceanography*, *16*(2), 63-90. doi:10.1016/0079-6611(86)90007-8

Mann, D. G. (1999), The species concept in diatoms: *Phycologia*, 38 (6), pp. 437-495

Mariotti, A., Germon, J. C., Hubert, P., Kaiser, P., Letolle, R., Tardieux, A., & Tardieux, P. (1981). Experimental determination of nitrogen kinetic isotope fractionation: some principles; illustration for the denitrification and nitrification processes. *Plant and Soil*, *62*, 413-430.

Marshall, H. G. (1970). Phytoplankton in Tropical Surfcae Waters between the coast of Ecuador and the gulf of Panama. Journal of Washington Academic Sciences, 60 (1), 18-21

Martin, E. E., and Scher, H. D. (2004). Preservation of seawater Sr and Nd isotopes in fossil fish teeth: bad news and good news. *Earth and Planetary Science Letters*. 220, 25-39

McGregor, H. V., Gagan, M. K., McCulloch, M. T., Hodge, E., Mortimer, G. (2008). Mid-Holocene variability in the marine 14C reservoir age for northern coastal Papua New Guinea. *Quarternary Geochronology*, 3, 213-225

McIlvin, M., R. and Altabet, M. A. (2005). chemical Conversion of Nitrate and Nitrite to nitrous Oxid for Nitrogen and Oxygen Isotopic Analysis in Freshwater and Seawater. Analytical Chemistry, 77, 5589-5595

Milligan, A. J., Varela, D. E., Brzezinski, M. A., & Morel, F. M. M. (2004). Dynamics of silicon metabolism and silicon isotopic discrimination in a

marine diatom as a function of pCO2. *Limnology and Oceanography*, *49*(2), 322-329. doi:10.4319/lo.2004.49.2.0322

Minagawa, M., & Wada, E. (1984). Stepwise enrichment of ^{15}N along food chains : Further evidence and the relation between d^{15}N and animal age. *Geochimica et Cosmochimica Acta*. *48*, 1135-1140

Minagawa, M., & Wada, E. (1986). Nitrogen Isotope ratios of the red tide organisms in the East China Sea: A Characterization of biological nitrogen fixation. *Marine Chemistry*, *19*, 245-259.

Minas, H.J., and Minas, M. (1992). Net community production in "High Nutrient-Low Chlorophyll" waters of the tropical and Antarctic Oceans: grazing versus iron hypothesis. *Oceanologica Acta*, 15, 145-162.

Minas, H.J., Minas, M., Packard, T.T., (1986). Productivity in upwelling areas deduced from hydrographic and chemical fields. *Limnology and Oceanography*. 31, 1182-1206.

Mollier-Vogel, E., Ryabenko, E., Philippe, M., Wallace, D., Altabet, M. A., Schneider, R. (2011). Nitrogen isotope gradients off Peru and Ecuador related to upwelling, productivity, nutrient uptake and oxygen deficiency. *Deep Sea Research II submitted*

Montes, I., Colas, F., Capet, X., Schneider, W., (2010). On the pathways of the equatorial subsurface currents in the eastern equatorial Pacific and their contributions to the Peru-Chile Undercurrent. *Journal of Geophysical Research. 115*, 1-16. C09003, 18PP, doi: 10.1029/2009JC005710

Morales, C. E., Hormazábal, S. E., Blanco, J. L. (1999). Interannual variability in the mesoscale distribution of the depth of the upper boundary of the oxygen minimum layer off northern Chile (18–24S): Implications for the pelagic system and biogeochemical cycling. Jo*urnal of Marine Research*. 57, 909-932

Morley, D. W., Leng, M. J., Mackay, A. W., Sloane, H. J., Rioual, P., & Battarbee, R. W. (2004). Cleaning of lake sediment samples for diatom oxygen isotope analysis. *Journal of Paleolimnology*. *31*(3), 391-401

Müller, P. J., & Schneider, R. (1993). An automated leaching method for the determination of opal in sediments and particulate matter. *Deep-Sea Research*. *40*(3), 425-444

Natori, Y., Haneda, A., Suzuki, Y. (2006). Vertical and seasonal differences in biogenic silica dissolution in natual seawater in Surunga Bay, Japan: Effects of temperature and organic matter. *Marine Chemistry*. 102, 230-241

Nelson, D. M., and Goering, J. J. (1977). Near-surface silica dissolution in the upwelling region off northwest Africa. *Deep-Sea Research*. *24*(1), 65-73

Nelson, D. M., Tréguer, P., Brzezinski, M. A., Leynaert, A., & Quéguiner, B. (1995). Production and dissolution of biogenic silica in the ocean: Revised global estimates, comparison with regional data and relationship to biogenic sedimentation. *Global Biogeochemical Cycles*. *9*(3), 359-372.

Noffke, A., Hensen, C., Sommmer, S., Scholz, F., Bohlen, L., Mosch, T., Graco, M, Wallmann, K. (2012). Benthic Iron and Phosphorus Fluxes across the Peruvian Oxygen Minimum Zone, *Limnology and Oceanography submitted*

Oka, A., Hasumi, H., Obata, H., Gamo, T., and Yamanaka, Y., (2009). Study on vertical profiles of rare earth elements by using an ocean general circulation model. *Global Biogeochemical Cycles. 23*, GB4025, doi: 10.1029/2008GB003353.

Pantoja, S., Repeta, D. J., Sachs, J. P., and Sigman, D. M. (2002). Stable isotope constraints on the nitrogen cycle of the Mediterranean Sea water column. *Deep Sea Research Part I: Oceanographic Research Papers*, *49*, 1609-1621. doi:10.1016/S0967-0637(02)00066-3

Parker, A. E., Wilkerson, F. P., Dugdale, R. C., Marchi, A., M., Hogue, V. E., Landry, M., R., Taylor, A., G. (2011). Spatial patterns of nitrogen uptake and phytoplankton in the equatorial upwelling zone (110°W-140°W) during 2004 and 2005. Deep-Sea Research II, 58, 417-433

Pennington, J. T., Mahoney, K., Kuwahara, V. S., Kolber, D. D., Calienes, R., & Chavez, F. P. (2006). Primary production in the eastern tropical Pacific: A review. *Progress In Oceanography*, *69*(2-4), 285-317

Penven, P., Echevin, V., Pasapera, J., Colas, F., and Tam, J. (2005). Average circulation, seasonal cycle, and mesoscale dynamics of the Peru Current System: A modeling approach. *Journal of Geophysical Research*, *110*. doi:10.1029/2005JC002945

Pichevin, L. E., Reynolds, B. C., Ganeshram, R. S., Cacho, I., Pena, L., Keefe, K., & Ellam, R. M. (2009). Enhanced carbon pump inferred from relaxation of nutrient limitation in the glacial ocean. *Nature*. *459*, 1-4

Piepgras, D. J., Wasserburg, G. J., & Dasch, E. J., (1979). The isotopic composition of Nd in different water masses. *Earth and Planetary Science Letters. 45*, 223-236

Piepgras, D. J., and Wasserburg, G. J., (1982). Isotopic composition of neodymium in waters from the drake passage. *Science*. *217*, 207-217

Piepgras, D. J., and Jacobsen, S. B., (1988). The isotopic composition of neodymium in the North Pacific. *Geochimica et Cosmochimica Acta*. *52*, 1373-1381

Quigg, A., Finkel, Z. V., Irwin, A. J., Rosenthal, Y., Ho, T.-Y., Reinfelder, J. R., Schofield, O., et al. (2003). The evolutionary inheritance of elemental stoichiometry in marine phytoplankton. *Nature*. *425*, 291-294

Ragueneau, O., Tréguer, P., Leynaert, A., Anderson, R. F., Brzezinski, M. A., DeMaster, D. J., Dugdale, R. C., et al. (2000). A review of the Si cycle in the modern ocean: recent progress and missing gaps in the application of biogenic opal as a paleoproductivity proxy. *Global and Planetary Change*, *26*, 317-365

Rahmstorf, S., 2002. Ocean circulation and climate during the past 120 000 years. *Nature*, 419, 207-214.

Rein, B., Lückge, A., Reinhardt, L., Sirocko, F., Wolf, A., & Dullo, W.-C. (2005). El Niño variability off Peru during the last 20,000 years. *Paleoceanography*, *20*(4), 1-18. doi:10.1029/2004PA001099

Reynolds, B., Frank, M., & Halliday, A. (2006). Silicon isotope fractionation during nutrient utilization in the North Pacific. *Earth and Planetary Science Letters*, *244*, 431-443. doi:10.1016/j.epsl.2006.02.002

Reynolds, B. C., Aggarwal, J., André, L., Baxter, D. C., Beucher, C. P., Brzezinski, M. A., Engström, E., et al. (2007). An inter-laboratory comparison of Si isotope reference materials. *Journal of Analytical Atomic Spectrometry*, *22*(5), 561-568. doi:10.1039/b616755a

Reynolds, B. C., Frank, M., & Halliday, A. N. (2008). Evidence for a major change in silicon cycling in the subarctic North Pacific at 2.73 Ma. *Paleoceanography*, *23*, PA4216. doi:10.1029/2007PA001563

Reynolds, B. C. (2011). Silicon isotopes as tracers of terrestrial processes. In: M. Baskaran (ed.) *Handbook of Environmental Isotope Geochemistry*, Advances .in Isotope Geochemistry, 87–104. Springer, Berlin

Rickli, J., Frank, M., & Halliday, A. N., (2009). The hafnium–neodymium isotopic composition of Atlantic seawater. *Earth and Planetary Science Letter 280*, 118-127.

Rojas de Mendiola, B. (1981). Seasonal phytoplankton distribution along the Peru coast. In F. Richards (Ed.), *Coastal Upwelling* (pp. 345-356). Washington, D.C.: American Geophysical Union.

Rosman, K. J. R. and P. D. P. Taylor (1998). Isotopic compositions of the elements 1997. *Pure and Applied Chemistry,* 70: 217–235.

Round, F. E., Crawford, R. M., Mann, D. G. (1990). The diatoms. Cambridge University Press. 1st edition

Ryabenko, E. (2011). Nitrogen Isotopes in the Atlantic and Pacific Oxygen Minimum Zones. *Dissertation, Christian-Albrechts Universität zu Kiel*

Ryabenko, E., Altabet, M. A, Wallace, D. W. R. (2009). Effect of chloride on the chemical conversion of nitrate to nitrous oxide for $\delta^{15}N$ analysis. *Limnology and Oceanography: Methods*, 7, 545-552

Sarmiento, J. L., and N. Gruber (2006). *Ocean Biogeochemical Dynamics*. Princeton University Press, Princeton. Alheit and Bernal, 1993

Sarmiento, J. L., Simeon, J., Gnanadesikan, A., Gruber, N., Key, R. M., & Schlitzer, R. (2007). Deep ocean biogeochemistry of silicic acid and nitrate. *Global Biogeochemical Cycles*, *21*, GB1S90. doi:10.1029/2006GB002720

Schlitzer, R. (2009). Ocean Data View, http://odv.awi.de.

Schrader, H., and Sorknes, R. (1991). Peruvian coastal upwelling: Late Quaternary productivity changes revealed by diatoms. *Marine Geology*, *97*, 233-249

Schrader, H. (1992). Coastal upwelling and atmospheric CO2 changes over the last 400,000 years: Peru. *Marine Geology*, *107*(4), 239-248

Shemesh, A., Mortlock, R. A., Smith, R. J., & Froelich, P. N. (1988). Determination of Ge/Si in marine siliceous microfossils: Separation, cleaning and dissolution of diatoms and radiolaria. *Marine Chemistry*, *25*(4), 305-323

Shimizu, H., Tachikawa, K., Masuda, A., Nozaki, Y., (1994). Cerium and neodymium isotope ratios and REE patterns in seawater from the North Pacific Ocean. *Geochimica et Cosmochimica Acta*. *58*, 323-333.

Sholkovitz, E.R., Elderfield, H., Szymczak, R., Casey, K., (1999). Island weathering: river sources of rare earth elements to the Western Pacific Ocean. *Marine Chemistry. 68*, 39-57.

Siddall, M., Khatiwala, S., van de Flierdt, T., Jones, K., Goldstein, S., Hemming, S., et al., (2008). Towards explaining the Nd paradox using reversible scavenging in an ocean general circulation model. *Earth and Planetary Science Letters. 274*, 448-461

Sigman, D. M., DiFiore, P., J., Hain, M. P., Deutsch, C., Wang, Y., Karl, D. M., Knapp, A., N., Lehmann, M. F., Pantoja, S. (2009). The dual isotopes of deep nitrate as a constraint on the cycle and budget of oceanic fixed nitrogen. Deep-Sea Research I, 56, 1419-1439

Sigman, D. M., Mccorkle, D. C., Francois, R., & Fischer, G. (2000). The d15N of nitrate in the Southern Ocean : Nitrogen cycling and the circulation in the ocean interior, *105*(C8), 599-614.

Silva, N., Rojas, N., & Fedele, A. (2009). Water masses in the Humboldt Current System: Properties, distribution, and the nitrate deficit as a chemical water mass tracer for Equatorial Subsurface Water off Chile.

Deep Sea Research Part II: Topical Studies in Oceanography, *56*, 1004-1020

Slemons, L. O., Murray, J. W., Resing, J., Paul, B., Dutrieux, P., 2010. Western Pacific coastal sources of iron, manganese, and aluminum to the Equatorial Undercurrent. *Global Biogeochemical Cycles 24*, GB3024, doi: 10.1029/2009GB003693.

Smetacek, V. S. (1985). Role of sinking in diatom life-history cycles: ecological, evolutionary and geological significance. *Marine Biology*, *84*, 239-251

Stichel, T. (2011). Tracing water masses and continental wethering by neodymium and hafnium isotopes in the Atlantic sector of the Southern Ocean. *Dissertation, Christian-Albrecht University of Kiel, Germany*

Stichel, T., Frank, M., Rickli, J., and Haley, B. A., (2011). The hafnium and neodymium isotope composition of seawater in the Atlantic sector of the Southern Ocean. *Earth and Planetary Science Letters* submitted.

Stramma, L., and England, M. (1999). On the water masss and mean circulation of the South atlantic Ocean. Journal of Geophysical Research, 104, C9, 1999JC900139.

Stramma, L., Schmidtko, S., Levin, L. A., & Johnson, G. C. (2010). Ocean oxygen minima expansions and their biological impacts. *Deep Sea Research Part I: Oceanographic Research Papers*. *57*, 587-595.

Stramma, L., E.D. Prince, S. Schmidtko, J. Luo, J.P. Hoolihan, M. Visbeck, D.W.R. Wallace, P. Brandt, und A. Körtzinger (2011): Expansion of oxygen minimum zones may reduce available habitat for tropical pelagic fishes. *Nature Climate Change*. 2, 33-37

Strickland, J. D. H., Holm-Hansen, O., Eppley, R. W., Linn, R. J. (1969). The use of a Deep Tank in Plankton Ecology. I. Studies of the growth and composition of Phytoplankton Crops at Low Nutrient Levels. *Limnology and Oceanography*. 14 (1), 23-34

Strub, P. T., Mesias, J. M., Montecino, V., Rutlland, J., & Salinas, S. (1998). Coastal Ocean Circulation off western South America. In A. R. Robinson & K. H. Brink (Eds.), *The Sea, vol. 11* (pp. 273-314). Holboken, N. J.: John Wiley.

Tachikawa, K., Athias, V., & Jeandel, C., (2003). Neodymium budget in the modern ocean and paleo-oceanographic implications. *Journal of Geophysical Research 108*, 3254, doi:10.1029/1999JC000285

Tachikawa, K., Jeandel, C., and Roy-Barman, M., (1999). A new approach to the Nd residence time in the ocean: the role of atmospheric inputs. *Earth and Planetary Science Letter. 170*(4), 433-446

Tachikawa, K., Roy-Barman, M., Michard, Thouron, D., Yeghicheyan, D., & Jeandel, C., (2004). Neodymium isotopes in the Mediterranean Sea: comparison between seawater and sediment signals1. *Geochimica et Cosmochimica Acta*. *68*(14), 3095-3106.

Takeda, S. (1998). Influence of iron availability on nutrient consumption ratio in oceanic waters. *Nature*, 393, 774-777

Talley, L., (1993). Distribution and Formation of North Pacific Intermediate Water. *Journal of Physical Oceanography, 23*, 517-538

Talley, L., (1999). Some aspects of ocean heat transport by shallow, intermediate and deep overturning circulation. In: Clark Webb, Keigwin (Eds.). *Mechanisms of Global Climate change at Millenial Time Scales, Geophysical Monograph Series*. 112, American Geophysical Union, 1-22

Tanaka, T., Togashi, S., Kamioka, H., Amakawa, H., Kagami, H., Hamamoto, T., Yuhara, M., et al., (2000). JNdi-1: a neodymium isotopic reference in consistency with LaJolla neodymium. *Chem. Geol. 168*, 279-281

Thiede J., and Suess E. (1983). *Coastal Upwelling: Its Sediment Record*. Plenum Publishing Corporation, New York, p. 610

Thomas, W. H. (1979). Anomalous nutrient-chlorophyll interrelationships in the offshore eastern tropical Pacific Ocean. *Journal of Marine Research*, 37, 327-335

Toggweiler, J. R., Dixon, K., & Broecker, W. S. (1991). The Peru Upwelling and the Ventilation of the South Pacific Thermocline. *Journal of Geophysical Research*, *96*(C11), 467-497. doi:10.1029/91JC02063

Tréguer, P., Nelson, D. M., Van Bennekom, A. J., DeMaster, D. J., Leynaert, A., & Quéguiner, B. (1995). The silica balance in the world ocean: a reestimate. *Science*, *268*, 375-9

van Bennekom, A. J., Jansen, J. H. F., van der Gaast, S. J., van Iperen, J. M., & Pieters, J. (1989). Aluminium-rich opal: an intermediate in the preservation of biogenic silica in the Zaire (Congo) deep-sea fan. *Deep-Sea Research*, *36*(2), 173-190

van Cappellen, P., & Qiu, L. (1997). Biogenic silica dissolution in sediments of the Southern Ocean. I. Solubility. *Deep-Sea Research*, *44*(5), 1109-1128

van de Flierdt, T, Robinson, L.F., Adkins, J. F. (2010). Deep Sea Corals as a recorder for the neodymium isotopic composition of seawater. *Geochimica et Chosmochimica Acta*. 74(21), 6014-6032

van den Boorn, S. H. J. M., Vroon, P. Z., van Belle, C. C., van der Wagt, B., Schwieters, J., & van Bergen, M. J. (2006). Determination of silicon isotope ratios in silicate materials by high-resolution MC-ICP-MS using a

sodium hydroxide sample digestion method. *Journal of Analytical Atomic Spectrometry*, *21*(8), 734. doi:10.1039/b600933f

Vance, D., Scrivner, A. E., Beney, P., Staubwasser, M., Henderson, G. M., & Slowey, N. C., (2004). The use of foraminifera as a record of the past neodymium isotope composition of seawater. *Paleoceanography*. *19*, PA2009, doi:10.1029/2003PA000957

Vanhaecke, F., and Moens, L. (2004). Overcoming spectral overlap in isotopic analysis via single- and multi-collector ICP-mass spectrometry. *Analytical and Bioanalytical Chemistry*, *378*(2), 232-240. doi:10.1007/s00216-003-2175-8

VanLear, G. E., & McLafferty, F. W. (1969). Biochemical Aspects of High-Resolution Mass Spectrometry. *Annual Rev. Biochemical*, *38*, 289-322.

Vaquer-Sunyer, R. and Duarte, C. M. (2008). Thresholds of hypoxia for marine biodiversity. *PNAS*,105 (40), 15452-15457

Varela, D. E., Pride, C. J., and Brzezinski, M. A. (2004). Biological fractionation of silicon isotopes in Southern Ocean surface waters. *Global Biogeochemical Cycles*, *18*(1), 1-8

Voss, M., Dippner, J. W., and Montoya, J. P. (2001). Nitrogen isotope patterns in the oxygen-deficient waters of the Eastern Tropical North Pacific Ocean. *Deep Sea Research Part I: Oceanographic Research Papers*, *48*, 1905-1921

Wijffels, S., Toole, J., Bryden, H., Fine, R., Jenkins, W., & Bullister, J. (1996). The water masses and circulation at 10°N in the Pacific. *Deep Sea Research Part I: Oceanographic Research Papers*, *43*(4), 501-544

Wilkerson, F. P., & Dugdale, R. C. (1996). Silicate versus nitrate limitation in the equatorial Pacific estimated from satellite-derived sea-surface temperatures. *Advances in Space Research*, *18*(7), 81-89. doi:10.1016/0273-1177(95)00951-5

Wille, M., Sutton, J., Ellwood, M. J., Sambridge, M., Maher, W. A., Eggins, S., & Kelly, M. (2010). Silicon isotopic fractionation in marine sponges: A new model for understanding silicon isotopic variations in sponges. *Earth and Planetary Science Letters*, *292*(3-4), 281-289

Winkler, L. W. (1888). Die Bestimmung des im Wasser gelösten Sauerstoffs. *Berichte der Deutschen Chemischen Gesellschaft*, 21, 2843-2855

Wischmeyer, A. G., De La Rocha, C. L., Meier-Reimer, E.-, Wolf-Gladrow, D. A. (2003). Control mechanisms for the oceanic distribution of silicon isotopes. *Global Biogeochemical Cycles*, *17*(3), 1-12

Wooster , W. S. (1959) Oceanography observations in the Panama Bight, “Askoy” expedition, 194. *Bull. Am. Mus, Nat. Hist*., 118, 113-151

Zabel., M, Dahmke, A., Schukz, H. D. (1998). Regional distribution of diffusive phosphate and silicate fluxes trough the sediment-water interface: the eastern Atlantic. *Deep-Sea Research I*, 45, 277-300

Appendix

Tab. A.1: Seawater oxygen and $Si(OH)_4$ concentrations and $\delta^{30}Si_{Si(OH)4}$ data from the RV Meteor cruises M77/3 and 4, collected in January and February 2009. $2\sigma_{(sd)}$ represents the external reproducibilities of repeated sample measurements.

Station	Latitude	Longitude	water depth [m]	Oxygen [µmol/kg]	$Si(OH)_4$ [µmol/kg]	$\delta^{30}Si$ [‰]	$2\sigma_{(sd)}$
120	3° 35.4' S	80° 57.0' W	2.4	227.86	2.80	2.61	0.28
			4.7	227.77	2.87	-	-
			10.1	221.53	2.99	-	-
			20.5	185.57	12.40	-	-
			30.1	116.71	14.95	1.75	0.15
			40.2	35.13	16.62	-	-
			49.9	46.38	15.60	-	-
			59.6	59.16	15.54	1.58	0.07
			80.4	58.31	15.54	1.76	0.11
			101.6	54.49	15.93	1.32	0.33
			120.7	35.87	18.98	-	-
			151.2	47.16	18.37	-	-
			151.6	48.93	18.39	-	-
			160.3	51.28	18.29	-	-
			170.3	50.32	18.79	-	-
			180.4	46.76	19.18	-	-
			217.4	20.29	22.43	1.49	0.29
122	6° 00.0' S	81° 15.6' W	1.9	118.82	8.97	1.86	0.09
			5.7	113.89	10.62	-	-
			10.5	46.24	14.26	1.87	0.19
			19.9	5.11	16.82	1.38	0.18
			30.2	5.11	17.21	-	-
			40.8	7.09	17.80	1.36	0.24
			51.7	7.18	18.00	-	-
			60.6	6.23	18.88	-	-
			69.7	5.94	20.36	-	-
			80.2	4.90	21.15	1.48	0.14
			90.5	4.64	21.15	-	-
			100.4	4.37	21.44	-	-
			125.5	3.13	21.93	-	-
			150.0	3.17	22.81	-	-
			174.5	3.12	25.18	1.30	0.18
			198.1	3.13	26.36	-	-
			203.2	3.20	26.16	-	-
806	8° 00.0' S	79° 50.4' W	1.5	212.83	6.25	2.03	0.22
			9.7	155.43	6.95	-	-
			20.8	10.72	12.16	-	-
			30.2	6.10	14.24	1.64	0.28
			41.0	8.73	16.68	-	-
			50.2	10.56	17.37	-	-
			60.4	10.59	17.72	1.67	0.20
			70.6	10.43	17.72	-	-

Table A.1: continued

Station	Latitude	Longitude	water depth [m]	Oxygen [µmol/kg]	$Si(OH)_4$ [µmol/kg]	$\delta^{30}Si$ [‰]	$2\sigma_{(sd)}$
806	8° 00.0' S	79° 50.4' W	81.2	9.09	18.41	-	-
			90.2	8.39	18.76	1.62	0.28
			100.2	6.70	18.07	-	-
			110.3	5.85	19.80	-	-
			120.0	3.59	24.67	1.49	0.21
			129.7	2.02	30.23	-	-
			141.0	2.12	30.92	1.58	0.35
807	10° 00.0' S	78° 22.8' W	2.0	65.53	9.73	1.96	0.11
			10.8	6.00	16.68	-	-
			20.5	1.84	18.76	-	-
			29.8	1.90	20.85	1.52	0.20
			39.9	1.89	23.28	-	-
			49.6	1.91	26.06	-	-
			60.2	1.97	26.06	1.26	0.18
			70.9	1.96	30.58	-	-
			79.7	1.96	31.97	-	-
			90.1	2.03	32.31	1.18	0.16
			99.5	2.05	32.31	-	-
			110.0	2.00	32.66	1.11	0.16
19	12° 21.6' S	77° 00.0' W	2.3	191.39	17.72	1.83	0.23
			2.7	184.47	21.20	-	-
			10.4	2.08	-	1.63	0.20
			21.7	1.84	33.70	-	-
			32.0	1.84	33.36	-	-
			39.9	2.01	-	1.16	0.20
			42.2	1.86	40.65	-	-
			51.7	1.87	39.26	-	-
			60.2	1.98	-	1.42	0.19
			62.1	1.93	37.53	-	-
			72.1	1.97	38.91	-	-
			79.5	2.02	-	1.47	0.16
			82.4	1.94	38.91	-	-
			92.0	2.02	40.65	-	-
			97.5	2.04	41.69	1.06	0.17
77	14° 00.0' S	76° 30.6' W	2.0	83.46	17.54	1.71	0.31
			10.0	12.00	17.54	1.84	0.26
			19.2	2.64	23.92	1.57	0.29
			50.8	2.70	-	1.36	0.34
			51.2	2.72	38.28	-	-
			150.4	2.91	32.70	1.68	0.29
			196.7	2.97	29.55	1.71	0.29
34	16° 00.0' S	74° 10.8' W	2.1	165.82	3.82	2.66	0.48
			11.1	158.44	4.52	-	-
			20.0	132.15	7.30	1.90	0.30
			29.9	58.64	12.51	-	-
			40.1	38.72	15.29	1.69	0.40
			50.1	25.27	20.85	-	-
			60.2	7.72	23.98	1.75	0.22
			70.6	2.53	25.37	-	-

Table A.1: continued

Station	Latitude	Longitude	water depth [m]	Oxygen [µmol/kg]	$Si(OH)_4$ [µmol/kg]	$\delta^{30}Si$ [‰]	$2\sigma_{(sd)}$
77	14° 00.0' S	76° 30.6' W	80.1	2.42	26.76	1.63	0.18
34	16° 00.0' S	74° 10.8' W	90.4	2.12	27.80	-	-
			100.1	2.16	29.88	-	-
			116.9	2.35	31.62	1.26	0.22
			117.3	2.32	31.97	-	-
43	17° 18.0' S	71° 54.0'W	3.9	238.46	2.14	2.81	0.33
			9.9	234.36	2.60	-	-
			20.8	149.15	5.27	2.40	0.16
			30.1	81.91	10.36	-	-
			40.0	15.15	19.33	1.49	0.18
			50.0	8.54	22.57	-	-
			60.7	3.21	26.74	1.30	0.28
			70.3	2.17	31.01	-	-
			80.5	2.14	32.40	-	-
			90.3	2.15	23.07	-	-
			97.8	2.18	30.80	-	-
			121.0	2.28	31.23	-	-
			121.3	2.23	31.05	1.36	0.25

Table.A.2: $BSiO_2$ concentrations and $\delta^{30}Si$ data for bulk $bSiO_2$ and hand-picked diatoms from surface samples collected on Meteor cruises M77/1 and 2, collected in November and December 2008 ***(Chapter 3, data from Claudia Ehlert).***

Station	Latitude	Longitude	Depth [m]	$bSiO_2$ [wt%]	$\delta^{30}Si_{bSiO2}$ [‰]	$2\sigma_{(sd)}$	Al/Si [mmol/mol]	Ti/Si [µmol/mol]	$\delta^{30}Si_{diatom}$ [‰]	$2\sigma_{(sd)}$
M77/2-076	00° 05.5' N	80° 33.4' W	290	2.81	0.75	0.29	9	69	1.77	0.10
M77/2-067	01° 45.1' S	82° 37.5' W	2075	7.15	0.58	0.09				
M77/2-062	02° 30.0' S	81° 14.7' W	1678	5.11					1.47	0.23
M77/2-071	02° 50.0' S	80° 50.7' W	100	2.39	-0.43	0.29	189	54		
M77/2-070	03° 07.0' S	80° 38.8' W	59	0.24	-0.1	0.13	235	125		
M77/2-060	03° 51.1' S	81° 15.5' W	701	4.28	0.53	0.22			1.82	0.40
M77/2-052	05° 29.0' S	81° 27.0' W	1252	8.58	0.76	0.10	80	84	1.95	0.13
M77/2-053	05° 28.9' S	81° 34.0' W	2607	11.52	0.89	0.21	24	31		
M77/2-047	07° 52.0' S	80° 31.4' W	625	3.85	0.28	0.19	61	59		
M77/2-050	08° 01.0' S	80° 30.1' W	1013	7.44	0.78	0.25			1.61	0.17
M77/2-028	09° 17.7' S	79° 53.9' W	1105	5.01	0.3	0.10	31	42		
M77/2-029	09° 17.7' S	79° 37.1' W	437	4.64	0.46	0.29	45	40		
M77/2-026	10° 45.1' S	78° 28.4' W	424	3.62	0.1	0.14	44	44		
M77/2-022	10° 53.2' S	78° 46.4' W	1923	4.66	0.52	0.10	45	33		
M77/1-450	11° 00.0' S	78° 10.0' W	319	13.86	0.9	0.17	10	42		
M77/1-460	11° 00.0' S	78° 35.2' W	1245	1.50	-0.1	0.29	44	38		
M77/1-462	11° 00.0' S	78° 44.7' W	2020	5.00					0.75	0.05
M77/1-469	11° 00.1' S	77° 56.6' W	145	17.62	1.03	0.15	22	54	1.05	0.38
M77/1-543	11° 00.0' S	77° 47.4' W	77	12.88	0.85	0.15	8	33		
M77/2-005	12° 05.7' S	77° 40.1`W	214	10.94	0.95	0.10	1	96		
M77/1-620	12° 18.6' S	77° 19.2' W	150	17.65	0.92	0.18	2	45		
M77/1-623	12° 38.2' S	77° 34.6' W	1085	5.85	0.61	0.13	15	59	0.61	0.20
M77/2-002	15° 04.8' S	75° 44.0`W	290	20.55	1.07	0.22	10	47	0.99	0.15
M77/1-420	15° 11.4' S	75° 34.9' W	516	17.31	1.07	0.13	24	41	1.87	0.10
M77/1-396	17° 26.0' S	71° 51.4' W	299	6.06	0.95	0.29	28	103		
M77/1-403	17° 26.0' S	71° 51.4' W	296	2.39	-0.98	0.21	45	84		
M77/1-407	17° 34.4' S	71° 56.0' W	788	2.75	0.17	0.15	41	78		
M77/1-411	17° 47.2' S	72° 44.7' W	2167	5.39	0.52	0.16	56	64	0.58	0.25

Table. A.3: Stable Isotope data for silicon and nitrate isotope (data for $^{15}NO_3$- from Evgenia Ryabenko) as well as hydrographic parameters and nutrient concentrations from the RV Meteor cruises M77/3 and 4, collected in January and February 2009. $2\sigma_{(sd)}$ represents the external reproducibility of repeated sample measurements. The external error ($2\sigma_{(sd)}$) for $\delta^{15}NO_3$- is 0.2‰. Particulate organic Nitrate (PON) and biogenic silicate data (bSi) is adapted from (Franz et al., 2011) **Chapter 4.**

	depth	$\delta^{30}Si(OH)_4$	2sd	$\delta^{15}NO_3^-$	Temp.	Salinity	Oxygen	Nitrate	Nitrtite	Phosphate	NH_4	$Si(OH)_4$	PON	bSi
	m	[‰]		[‰]	[°C]		[umol/kg]	[umol/kg]	[umol/kg]	[umol/kg]	[umol/kg]	[umol/kg]	[umol/kg]	[umol/kg]
St. 807	109	1.1	0.2	8.1	13.65	34.97	2.0	1.7	10.5	3.3	0.3	32.7	NaN	NaN
10°S/78°23'W	99	NaN	NaN	25.0	13.65	34.97	2.1	1.8	10.7	3.3	0.3	32.3	0.4	0.7
max. 111m	90	1.2	0.2	11.8	13.64	34.97	2.0	2.0	10.6	3.3	0.5	32.3	2.3	NaN
	79	NaN	NaN	NaN	13.65	34.97	2.0	1.9	10.8	3.3	0.4	32.0	NaN	NaN
	71	NaN	NaN	13.2	13.65	34.97	2.0	4.2	11.5	3.2	0.4	30.6	NaN	NaN
	60	1.3	0.2	17.0	13.69	34.97	2.0	13.1	10.8	3.0	0.6	26.1	1.9	0.6
	49	NaN	NaN	21.7	13.75	34.98	1.9	11.7	11.4	3.0	0.1	26.1	1.6	0.7
	40	NaN	NaN	23.5	13.97	34.99	1.9	13.9	11.8	3.0	0.8	23.3	0.5	0.2
	30	1.5	0.2	9.3	14.21	35.00	1.9	23.8	5.2	2.9	0.2	20.9	1.2	0.6
	20	NaN	NaN	8.6	14.36	35.00	1.8	29.3	1.7	2.8	0.6	18.8	1.1	0.5
	11	NaN	NaN	9.6	15.17	35.05	6.0	28.3	2.7	2.9	0.8	16.7	2.7	1.3
	2	2.0	0.1	13.1	16.38	35.00	65.5	21.4	1.8	2.9	1.4	9.7	6.6	3.3
St.809	150	1.5	0.3	21.3	13.21	34.95	2.1	13.2	7.3	3.2	0.4	30.9	1.2	0.5
10°S/78°38'W	139	1.4	0.1	22.2	13.24	34.95	2.0	14.7	7.2	3.2	0.8	30.6	NaN	NaN
max. 149m	130	NaN	NaN	18.0	13.35	34.95	2.1	18.6	6.7	3.1	0.3	27.5	NaN	NaN
	117	NaN	NaN	15.8	13.48	34.97	2.0	22.9	5.8	2.9	0.5	24.7	NaN	0.5
	110	1.8	0.2	11.2	13.56	34.97	2.0	25.4	3.8	2.8	0.4	23.6	NaN	NaN
	99	NaN	NaN	6.2	13.64	34.97	2.0	27.8	2.6	2.9	0.7	22.6	1.0	0.5
	89	NaN	NaN	10.5	13.73	34.98	1.9	27.3	2.5	2.8	1.0	22.2	NaN	NaN
	80	NaN	NaN	8.9	13.78	34.98	1.9	28.1	2.3	2.9	0.9	21.9	NaN	NaN
	70	1.5	0.2	7.4	13.92	34.99	1.9	28.3	2.0	2.9	1.0	21.2	1.1	0.5
	60	NaN	NaN	8.2	14.02	34.99	2.0	28.7	1.9	2.8	0.8	20.9	NaN	NaN
	50	2.1	0.2	8.3	14.15	34.99	1.8	28.7	1.7	2.8	0.6	20.2	NaN	NaN
	40	2.2	0.1	8.6	14.55	35.01	1.8	28.4	2.1	2.9	1.2	18.4	1.2	0.6
	30	2.8	0.1	8.2	15.39	35.04	5.6	29.5	1.1	2.9	0.7	15.6	NaN	NaN
	19	2.5	0.1	8.0	16.38	35.06	84.7	27.6	1.1	2.7	0.9	12.5	1.5	0.4
	11	2.1	0.2	8.3	18.33	35.17	150.9	23.3	1.4	2.3	1.1	7.0	NaN	NaN
	2	2.2	0.3	11.7	18.90	28.78	144.4	14.7	0.8	1.5	1.0	4.9	1.5	1.5

Table A.3 continued	depth m	$\delta^{30}Si(OH)_4$ (‰)	2sd	$\delta^{15}NO_3^-$ (‰)	Temp. (°C)	Salinity	Oxygen (umol/kg)	Nitrate (umol/kg)	Nitrtite (umol/kg)	Phosphate (umol/kg)	NH_4 (umol/kg)	$Si(OH)_4$ (umol/kg)	PON (umol/kg)	bSi (umol/kg)
St.810	145			20.1	13.18	34.94	2.0	17.9	7.1	2.6	0.0	27.8	NaN	NaN
10°S/78°48'W	140	1.4	0.3	16.8	13.18	34.94	2.1	18.1	7.1	2.7	0.3	28.1	NaN	NaN
max. 151m	129	1.7	0.2	11.4	13.27	34.95	2.1	24.5	4.4	2.6	0.2	24.7	NaN	NaN
	120	1.5	0.2	4.6	13.32	34.95	2.1	23.8	5.1	2.6	0.2	24.7	NaN	NaN
	110	NaN	NaN	10.9	13.38	34.96	2.0	23.3	5.3	2.6	0.2	25.0	NaN	NaN
	100	NaN	NaN	13.7	13.44	34.96	2.1	23.3	5.4	2.6	0.1	24.3	NaN	NaN
	89	NaN	NaN	9.2	13.68	34.98	2.0	29.7	1.6	2.6	0.0	21.5	NaN	NaN
	79	1.4	0.2	8.3	13.82	34.99	1.9	30.3	1.2	2.5	0.2	20.9	NaN	NaN
	69	NaN	NaN	8.3	14.05	34.99	1.9	30.3	1.1	2.4	0.2	19.8	NaN	NaN
	60	1.8	0.1	8.8	14.34	35.01	1.9	29.8	1.4	2.5	0.0	19.1	NaN	NaN
	49	NaN	NaN	7.8	14.52	35.01	1.8	30.2	1.1	2.6	0.2	18.1	NaN	NaN
	40	NaN	NaN	5.8	14.73	35.01	2.1	30.8	0.6	2.6	0.2	17.4	NaN	NaN
	29	2.4	0.1	5.4	15.71	35.05	30.5	30.8	0.4	2.5	0.3	12.5	NaN	NaN
	20	2.0	0.2	6.7	16.78	35.14	156.3	27.0	0.6	2.2	0.3	9.0	NaN	NaN
	10	2.2	0.2	8.7	18.06	35.16	194.7	15.3	1.2	1.4	1.7	2.8	NaN	NaN
	2	2.1	0.1	7.9	20.04	35.14	208.4	14.2	0.9	1.3	0.8	4.2	NaN	NaN
St.812	301	1.7	0.2	12.2	11.78	34.86	2.2	29.5	2.6	2.7	0.7	26.1	NaN	NaN
10°S/79°08'W	199	1.6	0.2	7.3	12.89	34.93	2.0	31.7	0.2	2.6	0.4	22.6	NaN	NaN
max. 331m	149	NaN	NaN	9.5	13.20	34.95	2.0	29.8	1.4	2.6	0.5	23.3	NaN	NaN
	120	NaN	NaN	8.1	13.41	34.96	3.6	33.7	0.1	2.5	0.8	20.5	NaN	NaN
	100	1.7	0.2		13.65	34.98	3.7						NaN	NaN
	79	NaN	NaN	6.8	13.81	34.99	3.6	32.8	0.0	2.5	0.6	18.8	NaN	NaN
	70	NaN	NaN	8.2	13.91	34.99	3.2	31.8	0.0	2.4	0.5	18.8	NaN	NaN
	60	NaN	NaN	6.0	14.20	35.00	2.0	32.2	0.1	2.5	0.5	18.4	NaN	NaN
	51	1.8	0.1	6.9	14.59	35.00	13.7	30.5	0.1	2.5	0.5	14.3	NaN	NaN
	41	NaN	NaN	6.9	16.54	35.07	104.1	28.5	0.2	2.3	0.6	9.4	NaN	NaN
	30	NaN	NaN	9.1	19.01	35.30	199.7	15.0	1.1	1.5	2.1	3.8	NaN	NaN
	20	NaN	NaN	14.6	20.54	35.35	216.6	9.7	0.3	1.0	2.4	1.7	NaN	NaN
	10	NaN	NaN	15.6	21.39	35.14	222.4	6.1	0.3	1.0	1.9	1.0	NaN	NaN
	3	2.9	0.3	15.5	21.85	35.13	225.0	5.6	0.2	0.9	1.5	1.4	NaN	NaN

Table A.3 continued	depth m	$\delta^{30}Si(OH)_4$ (‰)	2sd	$\delta^{15}NO_3^-$ (‰)	Temp. (°C)	Salinity	Oxygen (umol/kg)	Nitrate (umol/kg)	Nitrtite (umol/kg)	Phosphat (umol/kg)	NH_4 (umol/kg)	$Si(OH)_4$ (umol/kg)	PON (umol/kg)	bSi (umol/kg)
St.1	1584	NaN	NaN	5.9	2.93	34.61	81.7	45.8	0.0	3.1	0.4	76.8	NaN	NaN
10°S/79°28'W	1287	NaN	NaN	6.0	3.49	34.58	71.0	47.1	0.0	3.2	0.7	69.2	NaN	NaN
max. 1662m	1089	NaN	NaN	6.1	4.10	34.57	60.2	48.2	0.0	3.4	0.4	66.0	NaN	NaN
	991	NaN	NaN	6.3	4.47	34.55	51.6	49.0	0.0	3.4	1.5	65.3	NaN	NaN
	891	NaN	NaN	6.5	4.89	34.55	40.6	49.8	0.0	3.5	0.6	65.7	NaN	NaN
	793	NaN	NaN	6.5	5.42	34.55	28.0	51.0	0.0	3.5	0.7	61.9	NaN	NaN
	694	NaN	NaN	6.6	5.99	34.56	14.8	51.6	0.0	3.4	0.6	56.7	NaN	NaN
	596	NaN	NaN	7.2	6.84	34.58	8.2	50.5	0.0	3.5	0.5	47.6	NaN	NaN
	397	NaN	NaN	7.4	9.55	34.71	3.5	40.7	0.0	3.0	0.9	30.6	NaN	NaN
	297	NaN	NaN	14.0	11.16	34.81	2.3	29.1	3.9	2.8	0.8	26.4	NaN	NaN
	198	NaN	NaN	7.3	12.41	34.90	3.4	32.1	0.0	2.5	0.6	22.9	NaN	NaN
	150	NaN	NaN	7.8	13.05	34.94	4.0	30.8	0.1	2.6	0.4	21.9	NaN	NaN
	99	NaN	NaN	10.3	13.94	34.94	3.4	26.0	0.2	2.8	0.7	18.1	NaN	NaN
	90	NaN	NaN	8.7	14.15	34.93	13.1	27.5	0.1	2.8	0.6	16.0	NaN	NaN
	79	NaN	NaN	8.4	14.73	34.97	29.6	28.3	0.1	2.7	0.6	13.2	NaN	NaN
	70	NaN	NaN	8.0	15.24	34.97	66.0	27.1	0.1	2.5	0.9	10.8	NaN	NaN
	60	NaN	NaN	8.6	16.85	35.11	128.8	21.2	1.0	2.0	1.5	7.3	NaN	NaN
	50	NaN	NaN	7.9	18.09	35.14	139.1	18.0	1.1	1.8	2.7	6.3	NaN	NaN
	39	NaN	NaN	10.9	19.35	35.30	198.4	11.9	0.6	1.4	2.8	3.5	NaN	NaN
	30	NaN	NaN	11.2	20.39	35.16	211.0	9.8	0.5	1.2	4.5	2.4	NaN	NaN
	20	NaN	NaN		21.77	35.10	226.7	5.3	0.2	0.9	1.8	1.4	NaN	NaN
	10	NaN	NaN	16.7	23.21	35.18	219.6	2.7	0.1	0.6	1.0	0.4	NaN	NaN
	1	NaN	NaN	16.8	23.34	35.19	219.0	2.6	0.1	0.6	1.8	0.4	NaN	NaN

Table A.3 continued	depth m	$\delta^{30}Si(OH)_4$ (‰)	2sd	$\delta^{15}NO_3^-$ (‰)	Temp. (°C)	Salinity	Oxygen (umol/kg)	Nitrate (umol/kg)	Nitrate (umol/kg)	Phosphat (umol/kg)	NH_4 (umol/kg)	$Si(OH)_4$ (umol/kg)	PON (umol/kg)	bSi (umol/kg)
St.2	498	1.4	0.4	8.5	8.16	34.63	3.3	45.7	0.0	3.3	0.6	41.0	0.7	0.3
9°55'S/80°13'W	199	1.9	0.2	9.2	12.54	34.91	2.0	31.4	0.1	2.7	0.5	23.3	0.6	0.4
max. 6296	148	NaN	NaN	8.2	13.16	34.94	2.6	30.6	0.0	2.5	0.6	21.2	1.0	0.3
	119	NaN	NaN	8.0	13.85	34.99	1.8	30.4	0.0	2.5	0.4	19.5	NaN	NaN
	101	1.6	0.9	7.7	14.60	35.01	4.6	30.2	0.0	2.5	0.5	17.0	0.8	0.4
	91	NaN	NaN	6.7	15.85	35.05	20.1	32.7	0.1	2.3	0.9	11.8	NaN	NaN
	81	1.7	0.4	4.7	16.59	35.07	56.9	32.1	0.1	2.4	0.8	10.4	NaN	NaN
	70	NaN	NaN	4.1	17.40	35.10	124.3	29.7	0.1	2.3	0.6	8.7	NaN	NaN
	59	1.8	0.2	3.4	18.28	35.12	160.7	25.8	0.1	1.8	0.6	6.3	1.1	0.3
	50	NaN	NaN	6.8	18.63	35.13	172.1	22.0	0.8	1.8	1.0	3.8	NaN	NaN
	40	1.9	0.2	12.6	19.64	35.12	212.1	12.1	1.3	1.3	3.8	2.4	NaN	NaN
	30	NaN	NaN	11.3	20.43	35.12	224.7	9.1	0.4	1.1	3.4	1.4	NaN	NaN
	20	NaN	NaN	10.5	23.27	35.22	221.9	7.0	0.3	0.9	1.2	0.7	2.4	0.4
	9	NaN	NaN	14.0	23.61	35.26	220.2	5.3	0.1	0.7	0.4	0.4	NaN	NaN
	2	3.7	0.1	15.2	23.60	35.26	219.8	5.2	0.1	0.7	0.8	0.4	1.7	0.2
St.3	496	NaN	NaN		7.98	34.63	3.4	10.7	0.0	0.9	0.1	44.1	0.6	NaN
10°/81°30'W	397	NaN	NaN	8.3	9.38	34.70	2.6	40.8	0.0	3.1	0.9	33.0	NaN	NaN
max. 4713	297	NaN	NaN	14.3	11.44	34.83	2.2	28.2	4.1	2.8	0.6	26.8	NaN	NaN
	198	NaN	NaN	8.2	12.59	34.91	2.5	NaN	NaN	NaN	0.0	24.0	0.7	0.3
	148	NaN	NaN	7.5	13.19	34.95	2.2	31.7	0.0	2.6	0.8	20.5	NaN	NaN
	100	NaN	NaN	9.6	13.73	34.97	1.9	28.2	0.6	2.6	1.1	19.8	1.2	0.3
	90	NaN	NaN	9.4	14.07	34.98	1.8	28.0	0.4	2.6	0.7	18.8	NaN	NaN
	80	NaN	NaN	7.7	14.45	35.00	3.4	29.6	0.2	2.6	0.7	17.0	NaN	NaN
	70	NaN	NaN	6.4	14.89	35.01	2.1	31.5	0.1	2.6	0.5	15.6	0.9	0.2
	60	NaN	NaN	6.2	15.77	35.06	4.3	32.7	0.4	2.5	0.5	14.2	NaN	NaN
	50	NaN	NaN	6.5	17.22	35.10	62.7	30.8	0.9	2.6	2.0	9.4	NaN	NaN
	41	NaN	NaN	8.0	18.49	35.20	162.1	19.6	1.4	1.8	3.1	4.9	1.5	0.4
	30	NaN	NaN	12.8	20.73	35.30	207.2	10.6	0.7	1.2	3.1	2.1	NaN	NaN
	20	NaN	NaN	15.4	22.77	35.13	225.1	NaN	NaN	NaN	NaN	0.7	1.3	0.3
	11	NaN	NaN	16.2	22.83	35.12	224.1	1.9	0.1	0.7	1.0	0.7	NaN	NaN
	4	NaN	NaN	16.1	22.84	35.12	224.8	2.0	0.1	0.7	1.1	0.7	2.2	0.6

Table A.3 continued	depth m	$\delta^{30}Si(OH)_4$ (‰)	2sd	$\delta^{15}NO_3^-$ (‰)	Temp. (°C)	Salinity	Oxygen (umol/kg)	Nitrate (umol/kg)	Nitrate (umol/kg)	Phosphat (umol/kg)	NH_4 (umol/kg)	$Si(OH)_4$ (umol/kg)	PON (umol/kg)	bSi (umol/kg)
St.4	498	NaN	NaN	9.9	8.64	34.65	6.6	43.9	0.0	3.0	0.2	33.4	0.8	NaN
10°S/82°30'W	326	1.5	0.2	9.2	11.02	34.81	2.3	33.7	0.8	2.8	0.2	27.1	NaN	NaN
max. 4444m	248	1.7	0.2	7.3	11.85	34.86	2.2	32.3	0.5	2.6	0.3	24.3	NaN	NaN
	200	NaN	NaN	6.7	12.42	34.90	4.4	NaN	NaN	NaN	NaN	NaN	1.0	NaN
	180	NaN	NaN	7.3	12.57	34.91	5.2	33.9	0.0	2.5	0.2	21.5	0.9	0.1
	149	NaN	NaN	7.5	12.86	34.92	3.8	33.1	0.0	2.5	0.3	21.2	NaN	NaN
	130	NaN	NaN	6.9	13.04	34.94	4.5	31.2	0.0	2.5	0.4	21.2	1.0	0.2
	119	NaN	NaN	6.9	13.13	34.95	7.5	32.2	0.0	2.5	0.4	19.5	NaN	NaN
	110	NaN	NaN	8.8	13.28	34.96	4.4	32.2	0.0	2.5	0.2	19.1	NaN	NaN
	99	1.7	0.2	9.2	13.42	34.96	2.2	28.5	0.6	2.5	0.3	20.5	NaN	NaN
	91	NaN	NaN		13.50	34.96	2.1	28.9	0.2	2.6	0.3	19.8	0.9	0.2
	79	NaN	NaN	8.7	13.69	34.97	2.4	28.6	0.0	2.6	0.3	19.1	NaN	NaN
	70	NaN	NaN	7.9	13.97	34.99	2.4	30.0	0.1	2.5	0.3	17.4	NaN	NaN
	60	1.6	0.0	7.9	14.32	35.00	2.4	29.7	0.1	2.5	0.4	16.3	0.9	0.3
	53	NaN	NaN	7.8	14.75	35.01	3.0	29.5	0.1	2.6	0.5	16.7	NaN	NaN
	40	1.8	0.2	6.8	15.28	35.02	10.6	30.7	0.3	2.5	0.6	14.6	NaN	NaN
	30	NaN	NaN	7.4	17.11	35.16	79.6	27.5	1.2	2.4	1.2	11.1	1.4	0.2
	20	2.1	0.2	10.4	21.55	35.23	206.8	12.1	0.6	1.2	1.8	3.5	NaN	NaN
	10	NaN	NaN	15.7	23.87	35.21	213.1	5.4	0.1	0.7	1.0	0.7	NaN	NaN
	2	2.5	0.2	15.7	24.10	35.22	213.8	5.3	0.1	0.7	0.7	0.7	1.6	0.3

Table A.3 continued	depth m	$\delta^{30}Si(OH)_4$ (‰)	2sd	$\delta^{15}NO_3^-$ (‰)	Temp. (°C)	Salinity	Oxygen (umol/kg)	Nitrate (umol/kg)	Nitrate (umol/kg)	Phosphat (umol/kg)	NH_4 (umol/kg)	$Si(OH)_4$ (umol/kg)	PON (umol/kg)	bSi (umol/kg)
St.5	496	NaN	NaN	9.0	8.06	34.61	6.8	46.2	0.0	3.3	0.2	38.2	NaN	NaN
10°S/83°53'W	298	NaN	NaN	9.5	11.10	34.82	2.5	35.1	0.0	2.7	0.3	27.8	NaN	NaN
max. 4537m	199	1.7	0.2	11.1	12.08	34.87	2.2	29.5	0.7	2.6	0.3	24.3	NaN	NaN
	148	NaN	NaN	15.8	12.60	34.89	2.1	23.5	1.9	2.7	0.3	23.6	NaN	NaN
	100	1.7	0.2	9.2	13.60	34.93	1.9	26.0	0.1	2.7	0.3	18.4	NaN	NaN
	90	NaN	NaN	8.4	13.82	34.93	2.0	27.2	0.1	2.6	0.2	17.4	NaN	NaN
	80	NaN	NaN	8.1	14.06	34.94	6.5	28.5	0.1	2.7	0.2	16.0	NaN	NaN
	71	NaN	NaN	7.1	14.51	34.98	3.8	30.3	0.1	2.6	0.2	16.0	NaN	NaN
	60	NaN	NaN	6.3	15.20	35.00	7.2	31.1	0.1	2.6	0.4	14.6	NaN	NaN
	50	1.9	0.1	8.1	16.30	35.06	61.7	28.5	0.6	2.4	0.4	12.2	NaN	NaN
	40	NaN	NaN	6.5	19.06	35.21	164.0	24.9	1.2	2.2	0.8	9.4	NaN	NaN
	31	2.1	0.5	9.3	21.64	35.37	233.7	14.3	0.6	1.3	1.0	4.2	NaN	NaN
	20	NaN	NaN	10.2	24.11	35.45	215.5	8.7	0.3	0.8	0.8	1.4	NaN	NaN
	10	NaN	NaN	16.3	24.15	35.43	214.9	7.0	0.2	0.7	0.5	0.7	NaN	NaN
	1	NaN	NaN	9.6	24.23	35.44	214.5	6.8	0.2	0.7	1.8	0.7	NaN	NaN

Tab. A.4: Sampling locations in the Eastern Equatorial Pacific with silicon isotope data, nutrient concentrations, as well as salinity, potential temperature and potential density. External errors are given in 2 σ standard deviation for repeated measurements during the sample-bracketing method (2sd), as well as for n duplicate measurements on different days given as $2\sigma_{SEM}$ ***(Chapter 5)***

	Depth (m)	$\delta^{30}Si$ ‰	2sd	n	$2\sigma_{SEM}$	Pot. Temp (°C)	Pot. Density (kg/m3)	Salinity (PSS)	$Si(OH)_4$ (µmol/kg)	PO_4- (µmol/kg)	NO_3- (µmol/kg)	Oxygen (µmol/kg)
M77-3	1802	1.0	0.2	2	0.3	2.37	27.65	34.64	77.85	2.89	44.59	92.63
St.004	999	1.2	0.2	1		4.38	27.39	34.55	69.17	3.27	49.13	52.65
10°S/82°30'W	502	1.4	0.2	1		8.59	26.91	34.65	33.36	3.01	43.87	6.61
4444m depth	328	1.4	0.1	1		10.98	26.63	34.81	27.1	2.82	33.67	2.31
	250	1.5	0.2	1		11.82	26.52	34.86	24.32	2.61	32.28	2.19
	201	1.7	0.2	1		12.4	26.43	34.90	22.24	2.57	33.77	4.24
	92	1.7	0.2	1		13.49	26.23	34.96	19.81	2.59	28.89	2.05
	60	1.6	0.2	1		14.31	26.12	35.00	16.33	2.52	29.73	2.37
	41	1.8	0.2	1		15.27	25.93	35.02	14.59	2.54	30.7	10.56
	21	2.1	0.2	1		21.54	24.53	35.23	3.47	1.23	12.07	206.78
	2	2.5	0.2	2	0.4	24.1	23.78	35.22	0.69	0.68	5.28	213.81
M77-3	1499	1.1	0.1	1		2.95	27.57	34.60	76.81	3.24	46.39	78
St.007	999	1.1	0.3	1		4.27	27.39	34.54	66.04	3.32	48.69	53.22
12°S/81°W	499	1.5	0.2	1		8.38	26.91	34.62	32.32	3.28	44.73	7.83
4749m depth	199	1.4	0.2	1		12.5	26.41	34.90	27.45	2.95	14.83	2.06
	100	1.6	0.1	2	0.3	13.41	26.27	34.95	27.8	2.93	5.58	1.94
	70	1.6	0.1	1		14.09	26.14	34.70	22.58	2.96	14.4	2.39
	60	1.5	0.1	1		14.55	26.02	34.94	20.85	2.95	18.99	4.26
	30	1.8	0.1	2	0.3	17.8	25.48	35.21	4.86	1.53	11.35	219.23
	2	3.0	0.1	2	0.1	24.15	23.91	35.42	0.69	0.85	6.54	215.17
M77-4	4036	0.9	0.2	2	0.1	1.44	27.76	34.69	127.87	2.52	35.5	153.06
St.093	3004	1.1	0.2	1		1.59	27.74	34.67	138.71	2.66	37.58	132.76
14°S/85°50'W	2003	1.0	0.3	2	0.1	2.17	27.67	34.64	130.85	2.87	39.65	105.82
4579m depth	1007	1.3	0.2	4	0.1	4.31	27.39	34.54	79.5	3.19	44.08	57.98
	174	1.2	0.2	2	0.5	12.55	26.35	34.83	24	2.74	18	2.94
	150	1.2	0.2	1		13.23	26.22	34.83	18.89	2.68	21.15	18.27
	101	1.9	0.2	2	0.1	16.51	25.63	35.00	1.69	1.06	9.06	194.84
	3	4.4	0.3	2	0.1	24.72	23.82	35.52	0.22	0.53	3.72	221.17

Table: A.4 continued	Depth (m)	$\delta^{30}Si$ ‰	2sd	n	$2\sigma_{SEM}$	Pot. Temp (°C)	Pot. Density (kg/m3)	Salinity (PSS)	$Si(OH)_4$ (µmol/kg)	PO_4- (µmol/kg)	NO_3- (µmol/kg)	Oxygen (µmol/kg)
M77-4	1503	1.5	0.2	2	0.1	2.77	27.57	34.61	118.06	2.98	41.42	89.22
St.101	502	1.8	0.1	1		8.33	26.93	34.63	40.3	NaN	NaN	4.65
10°S/85°50'W	152	1.9	0.2	1		12.7	26.39	34.91	24.1	NaN	NaN	5.32
4420m depth	101	1.9	0.1	2	0.3	13.76	25.25	34.97	18.2	2.38	27.64	6.06
	50	2.0	0.2	1		18.62	25.25	35.18	3.54	1.19	11.61	168.45
	3	2.5	0.1	2	0.1	26.06	23.37	35.47	1.2	0.45	3.63	215.54
M77-4	3501	1.2	0.3	2	0.2	1.52	27.75	34.68	143.63	2.64	36.5	132.62
St. 117	2501	1.1	0.1	2	0.1	1.75	27.73	34.67	145.6	2.75	37.88	116.68
3°35'W/82°W	1501	1.0	0.3	1		3.09	27.57	34.61	121.07	2.99	40.64	79.61
4085m depth	401	1.5	0.1	2	0.1	9.06	26.87	34.69	41.61	2.9	38.86	6.05
	151	1.5	0.2	2	0.2	13.63	26.29	34.96	19.18	1.97	26.95	47.08
	100	1.8	0.2	1		14.19	26.14	34.99	17.41	1.98	27.25	43.19
	75	1.3	0.1	2	0.1	14.48	26.1	35.01	16.43	1.93	26.36	50.2
	31	1.7	0.3	1		15.71	25.89	35.10	12.69	1.62	21.84	77.01
	2	2.3	0.1	2	0.2	22.53	23.66	34.46	2.69	0.74	7.67	195.24
M77-4	4002	1.4	0.1	1		1.5	27.76	34.68	141.66	2.66	37.39	136.49
St.134	751	1.5	0.2	1		5.77	27.23	34.56	63.34	3.21	44.43	34.78
6°S/85°50'W	400	1.3	0.2	2	0.1	9.43	26.82	34.71	32.46	2.77	32.66	3.21
4103m depth	199	1.6	0.2	1		12.77	26.38	34.92	21.25	2.35	31.38	7.43
	100	1.6	0.1	1		13.83	26.21	34.98	18.2	2.09	28.82	28.77
	51	1.8	0.1	2	0.3	15.73	25.85	35.05	3.37	0.96	10.52	41.6
	2	2.3	0.1	2	0.3	26.9	22.3	34.39	1.52	0.39	4.18	218.81
M77-4	2500	1.3	0.3	2	0.1	1.88	27.71	34.67	152.49	2.84	38.37	106.01
St.152	999	1.6	0.1	2	0.3	4.68	27.37	34.58	85.99	3.06	41.23	62.58
Equator/85°50'W	598	1.3	0.2	1		7.23	27.08	34.61	52.83	3	40.64	26.4
2906m depth	398	1.7	0.1	2	0.1	9.42	26.82	34.71	39.55	2.83	37.39	7.57
	199	1.6	0.2	1		12.76	26.37	34.90	22.13	2.12	28.92	39.49
	150	1.6	0.2	1		13.74	26.22	34.96	18	1.86	24.79	62.26
	90	1.4	0.3	2	0.4	14.03	26.17	34.98	16	NaN	NaN	87.72
	51	1.6	0.1	1		14.75	26.05	35.02	14.06	1.54	20.56	92.41
	20	1.8	0.1	1		18.36	25.15	34.96	7.22	1.22	15.15	139.21
	3	2.5	0.2	2	0.3	26.06	21.94	33.61	1.69	0.49	4.27	212.23

Tab. A.5: Abbreviations and hydrographic characteristics of water masses in the study area

	Water Mass	Pot. Temp. (°C)	Salinity (PSU)	Pot. Density (kg/m^3)	$Si(OH)_4$ (µmol/kg)	Oxygen (µmol/kg)	References
AAIW	Antarctic Intermediate Water	3-5	34.3-34.5	27.1	5-80	200-300	Bostock et al. 2010
EqPIW	Equatorial Pacific Intermediate Water	−−	34.5-34.6	27.3	20-115	0-125	Bostock et al. 2010
ESW	Equatorial Surface Water	<25	>34	−−	−−	−−	Fiedler & Talley 2006
LCDW	Lower Circumpolar Deep Water	0.85	34.7	−−	~130	~200	Johnson & Toole 1993
NPDW	North Pacific Deep Water	1.0-1.8	34.6-34.7	27.6-27.8	−−	−−	Amakawa et al. 2009
NPIW	North Pacific Intermediate Water	6.4	33.9-34.1	26.8	50-130	0-150	Bostock et al. 2010
SAAW	Subantarctic Water	11.5	33.8	25.7	5	4-6	Silva et al. 2009
STSW	Subtropical Surface Water	−−	>35	−−	−−	−−	Fiedler & Talley 2006
TSW	Tropical Surface Water	25	<34	−−	−−	−−	Fiedler & Talley 2006

Tab. A.6: Nd sample locations with depth, isotope composition of Nd (ε_{Nd}), Nd concentrations, potential temperature, potential density, salinity, silicic acid and oxygen concentrations.

	Depth (m)	εNd	2sd	Nd (pmol/kg)	Pot. Temperatur (°C)	Pot. Density (kg/m^3)	Salinity (PSU)	$Si(OH)_4$ (µmol/kg)	Oxygen (µmol/kg)
St.2	991	-2.3	0.1	8.9	4.49	27.38	34.55	0	49.5
10°S/80°W	498	-2.1	0.1	7.6	8.11	26.97	34.63	41.0	3.3
6296m depth	101	-1.7	0.3	6.2	13.02	26.34	35.01	17.0	4.6
	2	-2.7	0.3	5.8	14.79	25.99	35.26	0.4	219.8
St.30	5494	-4.5	0.5	24.1	1.31	27.78	34.70	126.5	142.0
16°S/75°33'W	4571	-4.9	0.5	22.1	1.36	27.78	34.70	121.3	141.9
6165m depth	3549	-4.3	0.5	18.9	1.51	27.76	34.69	134.5	124.4
	1011	-3.4	0.4	19.5	4.28	27.39	34.53	68.5	53.8
	501	-2.9	0.5	7.8	7.28	27.04	34.57	37.5	15.9
	3	-3.4	0.4	5.6	22.57	24.09	35.04	1.0	215.5
St.78	2986	-3.6	0.3	17.0	1.55	27.75	34.68	n.a	132.6
14°S/77°03'W	2498	-4.7	0.3	14.5	1.70	27.73	34.67	n.a	131.7
3026m depth	1999	-3.2	0.3	11.8	2.15	27.67	34.64	n.a	103.4
	498	-2.5	0.4	7.7	7.74	26.99	34.59	n.a	9.1
	199	-2.3	0.4	6.8	12.37	26.44	34.89	n.a	3.0
	2	-2.6	0.4	5.9	19.54	24.83	34.93	n.a	219.5
St.93	4036	-6.6	0.3	21.7	1.44	27.76	34.69	127.9	153.1
14°S/85°50'W	3004	-3.1	0.3	16.9	1.60	27.74	34.68	138.7	132.8
4579m depth	2003	-2.3	0.3	11.8	2.16	27.67	34.64	130.9	105.8
	1007	-3.2	0.4	8.9	4.32	27.39	34.54	79.5	58.0
	161	-4.8	0.4	7.4	12.52	26.34	34.82	23.7	2.9
	3	-2.3	0.2	5.0	24.72	23.82	35.52	0.2	221.2
St.103	4292	-4.4	0.1	21.0	1.45	27.76	34.69	138.7	146.5
9°S/85°50'W	2501	-2.2	0.4	14.4	1.74	27.73	34.67	147.6	118.3
4251m depth	1501	-4.7	0.1	10.2	2.85	27.58	34.61	121.6	83.2
	800	-7.0	0.4	8.0	5.48	27.26	34.55	66.4	34.0
	221	-2.5	0.3	6.1	12.31	26.46	34.91	21.7	33.6
	152	-2.3	0.1	6.1	13.06	26.34	34.95	21.5	10.4
	2	-3.3	0.3	4.8	26.75	23.19	35.52	0.8	215.5
St.109	3201	-4.3	0.1	21.6	1.54	27.75	34.68	143.6	134.3
3°35'S/85°50'W	1501	-1.8	0.3	8.1	3.13	27.56	34.61	118.1	80.0
3261 m depth	701	-1.1	0.2	9.4	6.22	27.19	34.57	61.0	22.1
	499	-2.6	0.1	8.1	8.13	26.97	34.64	46.1	8.6
	151	-3.5	0.2	6.3	13.50	26.26	34.96	19.6	46.4
	2	-0.4	0.1	7.9	25.40	22.83	34.49	1.0	215.0
St.117	3453	-3.7	0.2	20.4	1.53	27.75	34.68	144.1	132.6
3°35'S/82°00'W	2473	-3.9	0.2	15.9	1.76	27.73	34.67	145.6	116.7
4084m depth	1487	-3.2	0.8	11.1	3.09	27.57	34.61	121.1	79.6
	398	-2.8	0.1	8.4	9.06	26.87	34.69	41.6	6.1
	150	-2.3	0.1	6.6	13.62	26.24	34.96	19.2	47.1
	2	-1.5	0.2	7.8	22.53	23.66	34.46	2.7	195.2
St.134	3942	-3.5	0.3	18.7	1.50	27.76	34.68	141.7	136.5
6°00'S/85°50'W	745	-1.7	0.4	8.1	5.77	27.23	34.56	63.3	34.8
4113m depth	99	-2.2	0.4	6.3	13.83	26.21	34.98	18.2	28.8
	2	-0.2	0.4	9.0	26.90	22.30	34.39	1.5	218.8

Table A.6 continued	Depth (m)	εNd	2sd	Nd (pmol/kg)	Pot. Temperatur (°C)	Pot. Density (kg/m^3)	Salinity (PSU)	$Si(OH)_4$ (µmol/kg)	Oxygen (µmol/kg)
St.152	90	-1.8	0.1	10.5	14.01	26.17	34.98	15.7	87.7
O°/85°50'W	3	0.6	0.1	8.6	26.06	21.97	33.61	1.7	212.2
2907m depth									
St.159	99	-2.2	0.4	19.6	14.03	26.17	34.98	15.3	92.4
1°20'N/85°50'W	52	-1.8	0.3	5.9	14.72	26.04	35.01	13.7	94.7
2977m depth	1	1.1	0.1	9.8	24.33	22.00	32.95	4.2	189.0
St.160	2607	-1.6	0.3	14.0	1.87	27.72	34.67	150.9	104.5
1°40'N/85°50'W	1488	-0.8	0.4	11.7	3.04	27.57	34.61	122.3	78.2
2607m depth	795	-1.6	0.4	28.2	5.81	27.24	34.57	67.3	43.9
	199	-2.5	0.4	14.2	12.99	26.33	34.91	20.8	51.8
	4	2.7	0.4	12.4	25.01	21.55	32.63	7.1	189.7